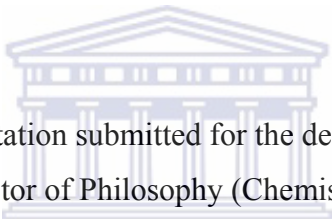


**Development of polyaniline nanotube electrocatalysts and sensor
devices for phenolic-pollutants**

by

Michael John Klink



Dissertation submitted for the degree of
Doctor of Philosophy (Chemistry)

UNIVERSITY *of the*
WEST At the CAPE

University of the Western Cape

University of the Western Cape, Chemistry Department
Bellville, South Africa

Supervisor

Prof. E. I. Iwuoha

Co-Supervisor

Dr. P.G. L. Baker

March 2007

Declaration

“I declare that **Development of polyaniline nanotube electrocatalysts and sensor devices for phenolic-pollutants** is my own work and that all sources quoted have been indicated and acknowledged by means of references.”



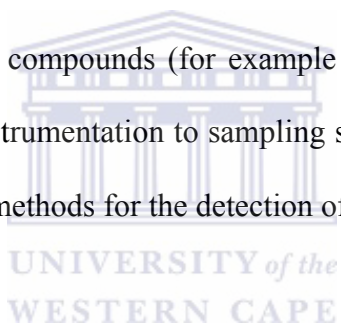
Michael John Klink

Signed:

Date:

Abstract

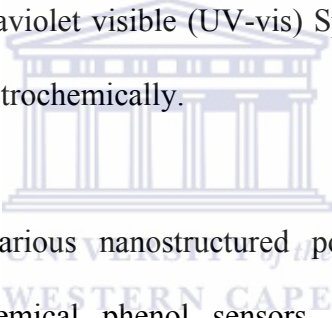
As a source of life water is one of the most precious commodities for all living organisms. Water resources are reported to be declining in numbers or the amount of water present and the existing ones are being polluted as a result of negligent human activities and intense industrialisation. Thus, there is an ever-increasing demand to monitor the quality of potable and waste water in our surroundings in real time. The nature of pollution and the extreme threat to human and aquatic life caused by organic pollutants, especially aromatic compounds (for example phenolic compounds), and the fact that it is difficult to get instrumentation to sampling sites, have led to research being conducted on developing new methods for the detection of organic pollutants in water.



This study has been directed towards the preparation of novel electroactive nanostructured (nanophase) polyanilines which included: polyaniline anthracene sulfonic acid (PANI-ASA), polyaniline phenanthrene sulfonic acid (PANI-PSA), poly(*ortho*-methoxyaniline) anthracene sulfonic acid (POMA-ASA), poly(*ortho*-methoxyaniline) phenanthrene sulfonic acid (POMA-PSA), poly(2,5 dimethoxyaniline) anthracene sulfonic acid (PDMA-ASA) and poly(2,5 dimethoxyaniline) phenanthrene sulfonic acid (PDMA-PSA). The polyanilines were used to develop chemical sensor (chemosensor) for the detection of certain Environmental Protection Agency's (EPA) priority phenols.

Nanophase structures of the following polyanilines were successfully evaluated which includes: nanotubes or nanofibres of PANI-ASA and PANI-PSA with diameters between 50 – 100 nm, nanomicelles and nanosheets of POMA-ASA and POMA-PSA respectively, with radii in the 100 to 300 nm range, nanowires of PDMA-ASA with diameter between 200 – 300 nm and nanowires of PDMA-PSA with observed diameters between 50 and 100 nm.

The polyanilines were characterised instrumentally using Fourier Transform Infrared (FT-IR) Spectroscopy, Ultraviolet visible (UV-vis) Spectroscopy, Scanning Electron Microscopy (SEM) and electrochemically.



For the first time the various nanostructured polyanilines were used in the development of electrochemical phenol sensors. The following phenols were determined: Phenol (Ph), 4-Chlorophenol (4-CP), 4-Nitrophenol (4-NP), 2,4-Dinitrophenol (2,4-DNP), 2,4,6-Trichlorophenol (2,4,6-TCP), 4-Chloro-3-methylphenol (4-C3MP), 2,4-Dichlorophenol (2,4-DCP), 2,6 Dinitro-4-methylphenol (2,6-DN4MP), 2,4-Dimethylphenol (2,4-DMP) and Pentachlorophenol (PCP). The sensitivity values of the sensor for phenols range from 13.7 mA/M for Pt/PDMA-PSA to 28 mA/M for Pt/POMA-PSA. The detection limit of the sensor for phenols range from 2.09×10^{-3} M for Pt/PDMA-PSA to 6.18×10^{-4} M for Pt/POMA-PSA. These values are within the same range of guideline level concentrations of phenols in water when biosensors are used.

The study provides a new technology that can be applied in the real time determination of phenols. If further developed and commercialised, this will be a useful instrument for environmental detection and monitoring of phenols and can be adapted for producing electrochemical reactors for phenol remediation.



Acknowledgements

I thank **God** for helping me through this period of my life

I wish to thank the following people and institutions for their assistance with this project:

I take this opportunity with deep sense of gratitude to record my sincere thanks to my research promoters **Prof. Emmanuel Iwuoha** and **Dr. Priscilla Baker** for their keen interest, valuable guidance, drive towards perfection and constructive criticism during the course of this investigation.

Dr. Richard White for his belief in me and persuasion to do this study. Vernon Somerset and Neil Benjamin for sharing ideas, advice or just having a laugh. I wish to thank the Chemistry Department (both academic and technical staff), my labmates in the Sensor Research Laboratory (UWC) for their willing co-operation extended to me through various stages of this work, The Electronic Microscopy Units at UCT and UWC for instrumental analysis and The National Research Foundation (NRF) for funding.

It will be an injustice if I did not mention my friends and family both in Cape Town and Napier whose support helped me to take up challenges and improve.

I would like to give full credit to my parents (Gustava and the late Michael) and brothers and sisters for every achievement I have made in my life.

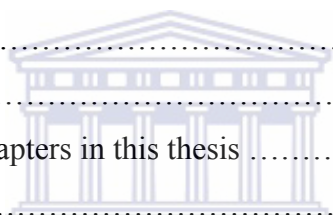
Last but not least, I gratefully acknowledge the help and support of my wife Shirene and daughters Melanie and Shandr e.

Table of Contents

Declaration	i
Abstract	ii
Acknowledgements	v
Table of contents	vi
List of Figures	xi
List of Tables	xviii
Abbreviations and Acronyms	xix

Chapter 1: Introduction

1.1 Rationale and Motivation for the dissertation	4
1.2 Objectives	8
1.3 Methodology	9
1.4 Synthesis	9
1.5 Characterisation	10
1.6 Application	10
1.7 Outline of the remaining chapters in this thesis	10
1.8 References	13



UNIVERSITY of the
West of Scotland

Chapter 2: Literature Review

2.1 Introduction	17
2.2 Polymers	18
2.3 Properties that make polymers conduct electrically	19
2.4 Electronics of Electrically Conducting Polymers (ECPs)	20
2.5 Conductivity of Electrically Conducting Polymers (ECPs)	21
2.6 Doping of Electrically Conducting Polymers	22
2.6.1 Classification of dopants	23
2.7 Synthesis of Electrically Conducting Polymers	24
2.8 Types of Electrically Conducting Polymers	25
2.9 Polyaniline (PANI) as ECP	26
2.10 PANI derivatives Poly(<i>ortho</i> -methoxyaniline) [POMA] and Poly(2,5 dimethoxyaniline) [PDMA] as ECPs	31
2.11 Doping of Electrically Conducting PANI and derivatives	32
2.12 Conducting polymer nanostructures	35
2.13 Electro-catalysts	36
2.14 Development of electro-catalysts	37
2.15 Sensors and Sensor devices	38
2.15.1 The need for Chemical Sensors	38
2.15.2 Chemical Sensor	39

2.15.3	Components of Chemical Sensors	40
2.15.3.1	Transducer	40
2.15.3.2	Receptors	41
2.16	What is the characteristics of an ideal sensor?	43
2.17	Film Deposition	44
2.18	Types of Chemical Sensors	45
2.18.1	Electrochemical Sensors	45
2.18.2	Optical Sensors	45
2.18.3	Mass Sensitive (Piezoelectric) Sensors	45
2.18.4	Heat Sensitive Sensors	45
2.18.5	Biosensors	46
2.19	The Kinetics of Enzyme Catalysis	47
2.19.1	Determination of V_{max} and K_M by changing of the substrate concentration	53
2.20	Phenolic pollutants in the environment	56
2.21	Treatment and reactions of phenol	56
2.22	Traditional analytical methods for phenol detection	59
2.23	Electrochemical Phenol Sensors	61
2.24	Electrochemical Methods and Techniques	66
2.24.1	Voltammetric Techniques	67
2.24.1.1	Cyclic Voltammetry	67
2.24.1.2	Square Wave Voltammetry	80
2.24.1.3	Differential Pulse Voltammetry	83
2.25	Conclusions	87
2.26	References	89

Chapter 3: Preparation of dopants and conducting nanostructured polyanilines

3.1	Introduction	96
3.2	Synthesis of the dopants: Anthracene Sulfonic Acid (ASA) and	
3.3	Phenanthrene Sulfonic Acid (PSA)	97
3.3.1	Chemicals	97
3.3.2	Synthesis of Anthracene sulphonic acid and phenanthrene sulphonic acid	97
3.4	The Preparation of Polyaniline (PANI), Poly(<i>ortho</i> -methoxyaniline) (POMA) and Poly(2,5 dimethoxyaniline) (PDMA) with Anthracene Sulphonic Acid (ASA) and Phenanthrene Sulphonic Acid (PSA)	98
3.4.1	Chemicals	98
3.4.2	Synthesis of polyaniline/Anthracene sulfonic acid nano-structures and polyaniline/Phenanthrene sulfonic acid nanostructures	99
3.4.3	Synthesis of poly(<i>ortho</i> -methoxyaniline)/Anthracene sulfonic acid nanostructures and poly(<i>ortho</i> -methoxyaniline)/Phenanthrene sulfonic acid nanostructures	99
3.4.4	Synthesis of poly(2,5 dimethoxyaniline)/Anthracene sulfonic acid nanostructures and poly(2,5 dimethoxyaniline)/Phenanthrene sulfonic acid nanostructures	100
3.5	Results and Discussion	103
3.6	Conclusions	105

Chapter 4: Characterisation of the dopants and the conducting nanostructured polyanilines

4.1	Introduction	109
4.2	Experimental	110
4.2.1	Fourier Transform Infrared Spectroscopy (FT-IR)	110
4.2.2	Ultraviolet visible Spectroscopy (UV-vis)	110
4.2.3	Scanning Electron Microscopy (SEM)	111
4.2.4	Electrochemical measurements	111
4.3	Characterisation results and discussion	112
4.3.1	Fourier Transform Infrared Spectroscopy (FT-IR)	112
4.3.2	Ultraviolet visible Spectroscopy (UV-vis)	118
4.3.3	Scanning Electron Microscopy (SEM)	121
4.3.4	Electrochemical characterisation	124
4.3.4.1	Cyclic Voltammetry (CV) characterisation of the polymers on platinum (Pt) electrode	124
4.3.4.2	Kinetic studies of the different polymers on Pt electrode in 1 M HCl	131
4.4	Conclusion	134
4.5	References	135

Chapter 5: The Catalytic, Electro-catalytic and Redox Mediator Effects of Nanostructured PANI-ASA and PANI-PSA Modified Electrodes as Phenol (and phenol derivatives) Sensors

5.1	Introduction	139
5.2	Method	140
5.2.1	Chemicals	140
5.2.2	Construction of Phenol (derivative) Chemical sensor	140
5.2.3	Determination of Phenol and Phenol derivatives	141
5.2.4	Experimental conditions	142
5.3	Results and discussion	144
5.3.1	The potentials of the modified electrodes	144
5.3.2	Electrochemical behaviour of the Pt/PANI-ASA electrode	145
5.3.3	The difference in potential shifts of Pt/PANI-ASA and Pt/PANI-PSA electrodes with phenol (derivatives) addition	146
5.3.4	Electrochemical behaviour of Phenol (Ph) at the Pt/PANI-ASA and Pt/PANI-PSA electrodes	147
5.3.5	Electrochemical behaviour of 4-ChloroPhenol (4-CP) at the Pt/PANI-ASA and Pt/PANI-PSA electrodes	149
5.3.6	Electrochemical behaviour of 4-Nitrophenol (4-NP) at the Pt/PANI-ASA and Pt/PANI-PSA electrodes	150
5.3.7	Calibration curves of the Pt/PANI-PSA chemosensors for Phenol (derivatives)	152

5.3.8	Pt/PANI-PSA chemosensor kinetic parameters for phenol (derivatives) detection	153
5.4	Conclusions	155
5.5	References	156

Chapter 6: The Catalytic, Electro-catalytic and Redox Mediator Effects of Nanostructured POMA-ASA and POMA-PSA Modified Electrodes as Phenol (and phenol derivatives) Sensors

6.1	Introduction	158
6.2	Methods	158
6.3	Results and discussion	159
6.3.1	Electrochemical behaviour of the Pt/PANI-ASA electrode	159
6.3.2	The shift in formal potentials (ΔE°) of Pt/POMA-ASA and Pt/POMA-PSA electrodes with phenol (derivatives)	160
6.3.3	Electrochemical behaviour of Phenol (Ph) at the Pt/POMA-ASA and Pt/POMA-PSA electrodes	161
6.3.4	Electrochemical behaviour of 4-ChloroPhenol (4-CP) at the Pt/POMA-ASA and Pt/POMA-PSA electrodes	163
6.3.5	Electrochemical behaviour of 4-Nitrophenol (4-NP) at the Pt/POMA-ASA and Pt/POMA-PSA electrodes	164
6.3.6	Calibration curves of the Pt/POMA-ASA and Pt/POMA-PSA chemosensors for Phenol (derivatives)	166
6.3.7	Chemosensor Kinetic Parameters for Phenol (derivative) detection	170
6.4	Conclusions	173
6.5	References	174

Chapter 7: The Catalytic, Electro-catalytic and Redox Mediator Effects of Nanostructured PDMA-ASA and PDMA-PSA Modified Electrodes as Phenol (and phenol derivatives) Sensors

7.1	Introduction	176
7.2	Methods	176
7.3	Results and discussion	177
7.3.1	Electrochemical behaviour of the Pt/PDMA-ASA electrode	177
7.3.2	The shift in potentials of Pt/PDMA-ASA and Pt/PDMA-PSA electrodes with phenol (derivatives)	179
7.3.3	Electrochemical behaviour of Phenol (Ph) at the Pt/PDMA-ASA and Pt/PDMA-PSA electrodes	180
7.3.4	Electrochemical behaviour of 4-ChloroPhenol (4-CP) at the Pt/PDMA-ASA and Pt/PDMA-PSA electrodes	182

7.3.5	Electrochemical behaviour of 4-Nitrophenol (4-NP) at the Pt/PDMA-ASA and Pt/PDMA-PSA electrodes	184
7.3.6	Calibration curves of the Pt/POMA-ASA and Pt/POMA-PSA chemosensors for Phenol (derivatives)	186
7.3.7	Chemosensor Kinetic Parameters for Phenol (derivative) detection	190
7.3.8	Conclusions	193
7.4	References	195

Chapter 8: General discussions, recommendations and future work

8.1	Introduction	197
8.2	The preparation of dopants and conducting nanostructured polyanilines	198
8.3	The characterisation of the dopants and the conducting polyaniline nanomaterials	199
8.4	The electro-catalytic and redox mediator effects of PANI-ASA and PANI-PSA modified Pt electrodes as phenol (and phenol derivatives) sensors	200
8.5	The electro-catalytic and redox mediator effects of POMA-ASA and POMA-PSA modified Pt electrodes as phenol (and phenol derivatives) sensors	201
8.6	The electro-catalytic and redox mediator effects of PDMA-ASA and PDMA-PSA modified Pt electrodes as phenol (and phenol derivatives) sensors	202
8.7	The comparison of the Pt polymers as redox mediators for phenol (and phenol derivatives) sensors	203
8.8	Recommendations for future work	205
8.9	Output from this thesis	205
8.9.1	Contributions at conferences	205
8.9.2	Papers published	206
8.9.2	Papers prepared for publication	207
	Appendix A	208

List of Figures

Figure 1.1:	A schematic representation of a Pt/Polymer electrochemical Phenol chemical sensor	7
Figure 2.1:	Chemical structures of polyethylene and polyaniline.....	19
Figure 2.2:	Band structure in an electronically conducting polymer.....	20
Figure 2.3:	Positively charged defects on poly(p-phenylene) A: polaron B: bipolaron	22
Figure 2.4:	Chemical structures of some conjugated polymers.....	25
Figure 2.5:	Chemical structure of polyaniline.....	26
Figure 2.6:	Mechanism of chemical oxidation of polyaniline.....	27
Figure 2.7:	Different oxidation states of polyaniline by Green and Woodhead.....	28
Figure 2.8:	Electrochemical polymerisation of aniline.....	30
Figure: 2.9:	Electrosynthesis of a PANI film in HCl (1 M) on a Pt electrode surface	30
Figure 2.10:	Chemical structures of (a) poly(<i>ortho</i> -methoxyaniline) and (b) poly(2,5 dimethoxyaniline)	31
Figure 2.11:	Doping and undoping of polyaniline (HM = any protonic acid).....	33
Figure 2.12:	Electrosynthesis of PANI/PVS film in HCl (1 M) on a Pt electrode surface	35
Figure 2.13:	Schematic representation of a chemical sensor using a redox mediator...	39
Figure 2.14:	Different types of transducers in a chemical sensor.....	41
Figure 2.15:	Graph of reaction velocity, V , as a function of the substrate concentration, $[S]$, for an enzyme that obeys Michaelis-Menten kinetics	48

Figure 2.16:	A graph of $1/V$ versus $1/[S]$. The slope is K_M/V_{\max} , the y-intercept is $1/V_{\max}$, and the x-intercept is $1/K_M$	54
Figure 2.17:	An Eadie-Hofstee plot of $V/[S]$ versus V , to obtain V_{\max} at $(V/[S]) = 0$ and K_M from the slope of the line.....	55
Figure 2.18:	The general reaction pathways of phenol oxidation.....	57
Figure 2.19:	Structures of some EPA priority phenols.....	60
Figure 2.20:	A typical cyclic voltammogram exhibited by a species which undergoes a electrochemistry reduction at $E^{\circ'} = 0.00$ V.....	68
Figure 2.21:	A Randles-Sevcik plot of I_p against $v^{1/2}$	74
Figure 2.22:	A typical cyclic voltammogram for an irreversible electrochemical process.....	75
Figure 2.23:	Qualitative behaviour of the cyclic voltammograms for a reduction process having features of: a) reversibility; b) quasi-reversibility; c) irreversibility. $A = 0.5$; $E^{\circ'} = 0.00$ V, $T = 25$ °C.....	78
Figure 2.24:	Potential-time perturbation on Osteryoung Square Wave Voltammetry	81
Figure 2.25:	Typical Osteryoung Square Wave voltammogram.....	82
Figure 2.26:	Potential-time pulses in Differential Pulse Voltammetry (DPV)	84
Figure 2.27:	A typical voltammogram in Differential Pulse Voltammetry (DPV).....	85
Figure 3.1:	Schematic representation of the synthesis and incorporation of anthracene sulphonic acid (ASA) in the polymerisation of 2,5 dimethoxyaniline (DMA)	101
Figure 3.2:	Schematic representation of the synthesis and incorporation of phenanthrene sulphonic acid (PSA) in the polymerisation of 2,5 dimethoxyaniline (DMA).....	102
Figure 3.3:	SEM micrograph of Polyaniline (PANI) doped with phenanthrene sulfonic acid (PSA)	103
Figure 3.4:	SEM micrograph of Poly(2,5 dimethoxyaniline) (PDMA) doped with phenanthrene sulfonic acid (PSA)	104

Figure 3.5:	SEM micrograph of Poly(<i>ortho</i> -methoxyaniline) (POMA) doped with phenanthrene sulfonic acid (PSA).....	105
Figure 4.1:	FT-IR spectra of Anthracene sulfonic acid (ASA) and Phenanthrene sulfonic (PSA) acid.....	113
Figure 4.2:	FT-IR spectra of PANI-PSA and PANI-ASA.....	114
Figure 4.3:	FT-IR spectra of POMA-ASA and POMA-PSA.....	116
Figure 4.4:	FT-IR spectra of PDMA-ASA and PDMA-PSA.....	116
Figure 4.5:	UV-visible absorption spectra of the conducting polymers, PANI-ASA and PANI-PSA dissolved in dimethyl sulfoxide (DMSO)	118
Figure 4.6:	UV-visible absorption spectra of the conducting polymers, POMA-ASA, POMA-PSA and POMA-HCl dissolved in DMSO.....	119
Figure 4.7:	UV-visible absorption spectra of the conducting polymers, PDMA-ASA, PDMA-PSA and PDMA-HCl dissolved in DMSO	120
Figure 4.8:	SEM images of PDMA-ASA and PDMA-PSA at different magnifications	122
Figure 4.9:	SEM images of POMA-ASA and POMA-PSA at different magnifications	122
Figure 4.10:	SEM images of PANI-ASA and PANI-PSA at different magnifications	123
Figure 4.11:	Multi-scan cyclic voltammograms (CV) of Pt/PANI-ASA in 1 M HCl at 25 °C	124
Figure 4.12:	Multi-scan cyclic voltammograms (CV) of Pt/PANI-PSA in 1 M HCl at 25°C.....	126
Figure 4.13:	Multi-scan cyclic voltammograms (CV) of Pt/POMA-ASA in 1 M HCl at 25 °C.....	127
Figure 4.14:	Multi-scan cyclic voltammograms (CV) of Pt/POMA-PSA in 1 M HCl at 25°C.....	128

Figure 4.15:	Multi-scan cyclic voltammograms (CV) of Pt/PDMA-ASA in 1 M HCl at 25 °C	129
Figure 4.16:	Multi-scan cyclic voltammograms (CV) of Pt/PDMA-PSA in 1 M HCl at 25 °C	130
Figure 5.1:	The formal potentials (E°) of the different Pt/Polymer modified electrodes in 1 M HCl before the addition of the phenol (derivatives)	144
Figure 5.2:	Characterisation of Pt/PANI-ASA on Pt- electrode in 1 M HCl at scan rates 2, 5, 10, 20, 30, and 40 mV/s	145
Figure 5.3:	The shift in formal potentials (ΔE°) of the different Pt/PANI-Dopant modified electrodes in 1 M HCl before and after the addition of 20 μ L of phenol (derivatives)	146
Figure 5.4:	Differential pulse voltammograms of Pt/PANI-PSA chemosensor responses to 0, 30, 40, 50 and 70 μ L addition of Phenol (0.002 M) in 1 M HCl (1 ml) at a scan rate of 10 mV/s and a frequency of 5 Hz	147
Figure 5.5:	Differential pulse voltammograms of Pt/PANI-ASA chemosensor responses to 0, 30, 40, 50 and 70 μ L addition of Phenol (0.002 M) in 1 M HCl (1 ml) at a scan rate of 10 mV/s and a frequency of 5 Hz.....	148
Figure 5.6:	Differential pulse voltammograms of Pt/PANI-PSA chemosensor responses to 0, 30, 40, 50 and 70 μ L addition of 4-CP (0.002 M) in 1 M HCl (1 ml) at a scan rate of 10 mV/s and a frequency of 5 Hz	149
Figure 5.7:	Square wave voltammograms of Pt/PANI-ASA chemosensor responses to 0, 30, 40, 50 and 70 μ L addition of 4-CP (0.002 M) in 1 M HCl (1 ml) at a scan rate of 10 mV/s and a frequency of 5 Hz	150
Figure 5.8:	Differential pulse voltammograms of Pt/PANI-PSA chemosensor responses to 0, 30, 40, 50 and 70 μ L addition of 4-NP (0.002 M) in 1 M HCl (1 ml) at a scan rate of 10 mV/s and a frequency of 5 Hz	151
Figure 5.9:	Square wave voltammograms of Pt/PANI-ASA chemosensor responses to 0, 30, 40, 50 and 70 μ L addition of 4-NP (0.002 M) in 1 M HCl (1 ml) at a scan rate of 10 mV/s and a frequency of 5 Hz	151

Figure 5.10:	Calibration curves of the Pt/PANI-PSA modified electrode for Ph, 2,4-DCP, PCP and 4-C3MP.....	152
Figure 5.11:	Calibration curve of the Pt/PANI-PSA modified electrode for 2,4-DMP, 2,4,6-TCP and 2,6-DN4MP	154
Figure 6.1:	Characterisation of Pt/POMA-ASA on Pt- electrode in 1M HCl at scanrates 5, 10, 20, 30, 40 and 50 mV/s.....	159
Figure 6.2:	The shift in formal potentials (ΔE°) of the different Pt/POMA-dopant modified electrodes in 1 M HCl before and after the addition of the phenol (derivatives)	160
Figure 6.3:	Differential pulse voltammograms of Pt/POMA-ASA chemosenser responses to 0, 30, 40, 50 and 70 μ L addition of Phenol (0.002 M) in 1 M HCl (1 mL) at a scan rate of 10 mV/s and a frequency of 5 Hz	161
Figure 6.4:	Differential pulse voltammograms of Pt/POMA-PSA chemosenser responses to 0, 30, 40, 50 and 70 μ L addition of Phenol (0.002 M) in 1 M HCl (1 mL) at a scan rate of 10 mV/s and a frequency of 5 Hz	162
Figure 6.5:	Differential pulse voltammograms of Pt/POMA-ASA chemosensor responses to 0, 30, 40, 50 and 70 μ L addition of 4-CP (0.002 M) in 1 M HCl (1 mL) at a scan rate of 10 mV/s and a frequency of 5 Hz	163
Figure 6.6:	Differential pulse voltammograms of Pt/POMA-PSA chemosensor responses to 0, 30, 40, 50 and 70 μ L addition of 4-CP (0.002 M) in 1 M HCl (1 mL) at a scan rate of 10 mV/s and a frequency of 5 Hz	164
Figure 6.7:	Differential pulse voltammograms of Pt/POMA-ASA chemosensor responses to 0, 30, 40, 50 and 70 μ L addition of 4-NP (0.002 M) in 1 M HCl (1 mL) at a scanrate of 10 mV/s and a frequency of 5 Hz	165
Figure 6.8:	Differential pulse voltammograms of Pt/POMA-PSA chemosensor responses to 0, 30, 40, 50 and 70 μ L addition of 4-NP (0.002 M) in 1 M HCl (1 mL) at a scan rate of 10 mV/s and a frequency of 5 Hz	165
Figure 6.9:	Calibration curves of the Pt/POMA-ASA modified electrode for Ph, 4-CP and 4-NP.....	167

Figure 6.10:	Calibration curves of the Pt/POMA-ASA modified electrode for 2.4-DCP and 2.4.6-TCP.....	167
Figure 6.11:	Calibration curves of the Pt/POMA-ASA modified electrode for 2.4- DNP, 2.4.-DMP, PCP and 4-C3MP and 2.6-DN4MP	168
Figure 6.12:	Calibration curves of the Pt/POMA-PSA modified electrode for Ph, 4-CP and 4-NP	169
Figure 6.13:	Calibration curves of the Pt/POMA-PSA modified electrode for 2.4-DCP, 2.4-DNP, 2.4.6-TCP, PCP and 4-C3MP	170
Figure 6.14:	Reaction scheme outlining the role of the POMA-PSA as a redox mediator in the oxidation of phenol for the Pt/POMA-PSA chemosensor	172
Figure 7.1:	Characterisation of PDMA-ASA on Pt electrode in 1 M HCl at scan rates 10, 20, 30, 40 and 40 mV/s	177
Figure 7.2:	Characterisation of PDMA-ASA on Pt electrode in 1 M HCl at a scan rate of 20 mV/s	178
Figure 7.3:	The shift in formal potentials (ΔE°) with Pt/PDMA-ASA modified electrodes in 1 M HCl before and after 20 μ L addition of the phenol (derivatives)	179
Figure 7.4:	Differential pulse voltammograms of Pt/PDMA-ASA chemosensor responses to 0, 30, 40, 50 and 70 μ L addition of Phenol (0.002 M) in 1 M HCl (1mL) at a scan rate of 10 mV/s and a frequency of 5 Hz	181
Figure 7.5:	Differential pulse voltammograms of Pt/PDMA-PSA chemosensor responses to 0, 30, 40, 50, 60 and 70 μ L addition of Phenol (0.002 M) in 1 M HCl (1mL) at a scan rate of 10 mV/s and a frequency of 5 Hz	182
Figure 7.6:	Differential pulse voltammograms of Pt/PDMA-ASA chemosensor responses to 0, 10, 20, 30, 40, 50 and 60 μ L of 4-CP (0.002 M) in 1 M HCl (1 mL) at a scan rate of 10 mV/s and a frequency of 5 Hz	183
Figure 7.7:	Differential pulse voltammograms of Pt/PDMA-PSA chemosensor responses to 0, 10, 20, 30, 40, 50, 60 and 70 μ L of 4-CP (0.002 M) in 1 M HCl (1 mL) at a scan rate of 10 mV/s and a frequency of 5 Hz	184

Figure 7.8:	Differential pulse voltammograms of Pt/PDMA-ASA chemosensor responses to 0, 10, 20, 30, 40 and 50 μL of 4-NP (0.002 M) in 1 M HCl (1 mL) at a scan rate of 10 mV/s and a frequency of 5 Hz	185
Figure 7.9:	Square wave voltammograms of Pt/PDMA-PSA chemosensor responses to 0, 10, 20, 30, 50, 60 and 70 μL of 4-NP (0.002 M) in 1 M HCl (1mL) at a scan rate of 10 mV/s and a frequency of 5 Hz	185
Figure 7.10:	Calibration curves of the Pt/PDMA-ASA modified electrode for Ph, 4-CP and 4-NP	187
Figure 7.11:	Calibration curves of the Pt/PDMA-ASA modified electrode for 2.4-DNP, 2.4-DMP and 4-C3MP	187
Figure 7.12:	Calibration curves of the Pt/PDMA-ASA modified electrode for 2.4-DCP, PCP and 2.6-DN4MP	188
Figure 7.13:	Calibration curves of the Pt/PDMA-PSA modified electrode for 4-CP, 2.4-DCP, 2.4-DNP, 2.4-DMP and 2.4.6-TCP	189
Figure 7.14:	Calibration curves of the Pt/PDMA-PSA modified electrode for 2.4-DCP, PCP and 2.6-DN4MP	189
Figure 7.15:	Reaction scheme outlining the role of the PDMA-PSA as a redox mediator in the oxidation of phenol for the Pt/PDMA-PSA chemosensor	192

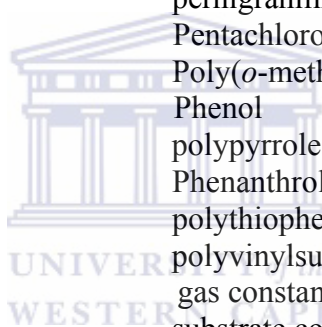
List of Tables

Table 4.1:	Kinetic parameters of the conducting nanostructured polyanilines	133
Table 5.1:	Parameters for differential pulse voltammetry (DPV) experiments	143
Table 5.2:	Parameters for square wave voltammetry experiments	143
Table 5.3:	Instrumental parameters for cyclic voltammetry (CV) experiments	143
Table 5.4:	Kinetic parameters of the Pt/PANI-PSA chemosensor for various phenols	153
Table 6.1:	Kinetic parameters of the Pt/POMA-PSA chemosensor for various phenols	171
Table 7.1:	Kinetic parameters of the Pt/POMA-PSA chemosensor for various phenols	191
Table A1:	Catalytic currents (A) versus concentrations (M) of the Pt/PANI-ASA modified electrode for phenol (derivatives)	208
Table A2:	Catalytic currents (A) versus concentrations (M) of the Pt/PANI-PSA modified electrode for phenol (derivatives)	209
Table A3:	Catalytic currents (A) versus concentrations (M) of the Pt/POMA-ASA modified electrode for phenol (derivatives)	210
Table A4:	Catalytic currents (A) versus concentrations (M) of the Pt/POMA-PSA modified electrode for phenol (derivatives)	211
Table A5:	Catalytic currents (A) versus concentrations (M) of the Pt/PDMA-ASA modified electrode for phenol (derivatives)	212
Table A6:	Catalytic currents (A) versus concentrations (M) of the Pt/PDMA-PSA modified electrode for phenol (derivatives)	213

Abbreviations and Acronyms

A	area of electrode
APS	Ammonium persulfate
ASA	Anthracene Sulphonic Acid
AMEL7050, BAS 100W, BAS 50W	Bioanalytical Systems
c_{analyte}	bulk concentration
CSA	camphor sulphonic acid
CV	Cyclic Voltammetry
4-CP	4-Chlorophenol
4-C3MP	4-Chloro-3-methylphenol
D_e	the diffusion coefficient
DBSA	dodecyl benzenesulphonic acid
DMA	2,5 dimethoxyaniline
DNA	Deoxyribonucleic Acid
2,4-DCP	2,4-Dichlorophenol
2,4-DMP	2,4-Dimethylphenol
2,6-DN4MP	2,6 Dinitro-4-methylphenol
2,4-DNP	2,4-Dinitrophenol
DPV	Differential Pulse Voltammetry
E	enzyme
E_i	initial potential
E_λ	switch potential
E^θ	standard electrode potential
$E^{o'}$	formal electrode potential
E_p	peak potential
$E_{p,a}$	anodic peak potential
$E_{p,c}$	cathodic peak potential
$E_{p/2}$	half-peak potential
ΔE_p	separation peak potential
ΔE_{pulse}	the pulse amplitude
E_T	total enzyme concentration
ECPs	Electrically Conducting Polymers
EM	emeraldine state
EM^{*+}	emeraldine radical cation
ES	enzyme-substrate complex
EPA	Environmental Protection Agency
EU	European Countries
F	Faraday constant
FT-IR	Infrared Spectroscopy
$I_{p,c}$	cathodic reaction
$I_{p(\text{forward})}$	forward current
$I_{p(\text{reverse})}$	reverse current
$I_{p,a}$	current for the anodic reaction

$I_{p/2}$	half peak current
I_p	peak current
k	rate constant
k^0	standard rate constant
K_M	Michaelis-Menten constant
LE	leucoemeraldine state LE
LM^{*+}	leucoemeraldineradical cation
MAC	Maximum Admissable Concentration
n-doping	negative doping
n	number of electrons transferred
4-NP	4-Nitrophenol
OMA	<i>o</i> -methoxyaniline
P	product
PA	polyacetylene
PANI	Polyaniline
PDMA	Poly(2,5 dimethoxyaniline)
p-doping	Positive doping
PE	pernigraniline state
PCP	Pentachlorophenol
POMA	Poly(<i>o</i> -methoxyaniline)
Ph	Phenol
PPY	polypyrrole
PSA	Phenanthroline Sulfonic acid
PT	polythiophene
PVS	polyvinylsulphonate
R	gas constant
[S]	substrate concentration
SEM	Scanning Electron Microscopy
SCE	saturated calomel electrode
SWV	Square Wave Voltammetry
T	temperature
TOC	total organic carbons
2,4,6-TCP	2,4,6-Trichlorophenol
US	United States
UV-vis	Ultraviolet Spectroscopy
ν	scan rate
V	rate of catalysis
V_{max}	maximal rate
$\nu_{forward}$	forward scan rate
$\nu_{reverse}$	reverse scan rate
WHO	The World Health Organisation
α	transfer coefficient
Ψ	complex mathematical function
Γ^*	the surface concentration



Chapter 1

Introduction

An “*Overview of the National Water Conservation and Water Demand Strategy for South Africa*” concluded that South Africa is a water-stressed country. Water resources are limited and in global terms, scarce. The sustained growth in human population, economic development and the urgent need to supply water services to millions of people without essential services in South Africa, has led to an increasing demand for water. Being largely an arid country, South Africa is fast approaching the limits of its available water supply, threatened in terms of both quantity and quality. To compound the problem the average rainfall is less than half of the world’s average rainfall and it is spread unevenly across the country, resulting in very dry western regions. It has been postulated that the country’s fresh water resources will be fully utilized within the next twenty to thirty years if the current growth in water demand and use are not curbed or altered [1].

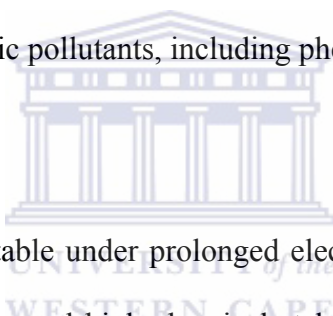
South Africa, on the other hand, has an economy that depends heavily on the mining of mineral and refining of ores. These activities have deleterious effects on the environment, particularly in the rural areas and in historically disadvantaged communities where these mines are often located. The pollution of the underground and other drinking water resources associated with mining operations are major environmental concerns. Though

the South African government is now conscious of the environmental impact of industrial and mine activities, they are hampered by the unavailability of pollution data, coupled with the dependence of the country's economies on revenues from mines. The health problem that concerns phenols and phenol derivative compounds, which are major constituents of wastes from these refineries and ore mines, are that they cause acute toxicity characterised by sweating, cyanosis, lowering of body temperature, decreased respiration, loss of reflex activity and eventually death from respiratory failures in humans [2].

There has been much attention on electro-catalytic remediation of toxic organic pollutants in wastewater, including bio-refractory substances such as phenols and its derivatives [3-7]. The electrochemical processes have the advantage of high efficiency and the possibility that they can be operated essentially under largely similar conditions for a wide variety of wastes [8]. Electro-catalytic oxidative detection or destruction of phenolic compounds, which are used in many chemical and pharmaceutical industries, is a major technique with environmental applications [9-12].

One study [3] showed that electro-oxidation on platinum anode is more efficient for the removal of total organic carbons (TOC) in wastewater than in chemical oxidation treatments, which use large amounts of harmful reagents. However, direct anodic decomposition of phenolic compounds at the metal electrode has been difficult because of electrode fouling (formation of insulating polyphenol film) [8].

Attention is now focused on identifying efficient electrode materials for direct electrochemical incineration processes that will not result in electrodes fouling. Amongst recent attempts has been the use of synthetic diamond electrodes and various doped metal oxide-film electrodes, e.g. PbO_2 , SnO_2 , and TiO_2 . The efficiency of electrochemical oxidation of organic pollutants in wastewater is strongly dependent upon the electro-catalytic properties of the anode materials, including composition, electronic structure, crystallinity and morphology of the film, among other factors [9]. For example PbO_2 and doped SnO_2 anodes exhibit up to five times higher efficiency than a platinum anode for electrochemical oxidation of a wide range of organic substances for oxidative decomposition of several organic pollutants, including phenol and chlorinated phenols [3-7].



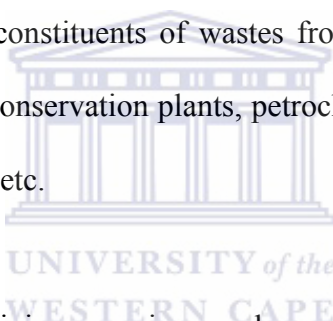
These anode materials are unstable under prolonged electrolysis. Therefore new anodes characterized by high efficiency and high chemical stability are crucial to the future of electro-oxidative detection and removal of pollutants. They may come in the form of either new oxides or new composite materials containing polymers and oxide blends. Recent studies have shown that the electro-catalytic activity and chemical or mechanical stability of oxide electrodes are enhanced by incorporating/ doping other metal ions into the oxides. Apart from metal oxides, polymer supported catalysts are gaining more importance as efficient heterogeneous catalyst in a variety of organic transformations [8].

A significant gap in the literature involves the use of conducting nanostructured polymers as electro-catalysts and that is why this current study was investigated. In this study nanostructured electrodes consisting of organic semiconductor polymers (polyaniline and

its derivatives), will be developed and employed as electro-catalysts for the detection of priority phenolic pollutants (such as Phenol (Ph), 4-Chlorophenol (4-CP), 4-Nitrophenol (4-NP), 2,4-Dinitrophenol (2,4-DNP), 2,4,6-Trichlorophenol (2,4,6-TCP), 4-Chloro-3-methylphenol (4-C3MP), 2,4-Dichlorophenol (2,4-DCP), 2,6 Dinitro-4-methylphenol (2,6-DN4MP), 2,4-Dimethylphenol (2,4-DMP) and Pentachlorophenol (PCP)) in water.

1.1 Rationale and Motivation for the dissertation

Phenols and phenol-derivatives are significant and widespread pollutants in the environment. They are major constituents of wastes from asphalt refineries, petroleum refineries and ore mines, coal conservation plants, petrochemicals, polymeric resins, coal tar distillation, pharmaceutical, etc.



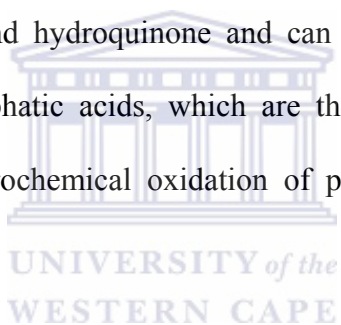
Phenols are generally toxic to living organisms and even at concentrations below 1 $\mu\text{g/L}$ they can affect the taste and the odour of water and fish. On the basis of toxic properties, in the 1970s the US Environmental Protection Agency (EPA) presented a list of eleven priority pollutant phenols characterized by a variety of substituents such as chloro-, nitro- and methyl-groups. EU directive (76/464/CEE) indicates that the maximum admissible individual concentration for organic contaminants in drinking water is 0.1 $\mu\text{g/L}$. The World Health Organisation (WHO) suggest guideline level concentrations lower than 200 $\mu\text{g/L}$ for 2,4,6 Trichlorophenol, 9 $\mu\text{g/L}$ for pentachlorophenol, 10 $\mu\text{g/L}$ for 2-Chlorophenol and 40 $\mu\text{g/L}$ for 2,4-Dichlorophenol. In the EU countries, the determination of phenols in river and drinking water has become of great importance since the 1980s.

The Maximum Admissible Concentration (MAC) was fixed at 0.5 µg/L for the total phenol amount, which only excludes those natural phenols that don't react with chlorine. Incidentally, in South Africa the development of comprehensive environmental policies on pollution from industrial effluents or mining activities is in its infancy and national environmental standards on specific pollutants may not be available. There is therefore need to develop both a method of phenol decontamination and a method of real-time detection of phenol (derivatives) levels in industrial waste streams [9-24].

Technologies available for treatment of phenolic waste are physical, chemical, biological and electrochemical processes. Biological processes have the drawback that the process is inhibited at the generally high concentrations of phenolics associated with industrial wastewater. Chemical processes introduce new chemicals into the waste stream. Since the only reagent is the electron, electrochemical technology appears to be ideal for the treatment of environmental pollution.

Direct and indirect oxidation processes have also been used in the treatment of phenolic pollutants. Indirect oxidation process involves the *in situ* generation of strong oxidants such as hypochlorite/chlorine, ozone, hydrogen peroxide which are utilized for the oxidation of the phenolic compounds. The formation of chlorinated compounds is a drawback of the indirect electrochemical methods [25-40].

In the direct electrochemical process, the pollutants are destroyed by direct electron transfer reactions at the electrode. The efficiency of this direct method of electrochemical oxidation of organic pollutants in wastewater is strongly dependent upon the electrode materials. **Figure 1.1** shows a schematic representation of a Pt/Polymer electrochemical Phenol sensor system. The figure shows that one of two pathways of phenol oxidation may occur at the electrode surface. It is generally considered that the oxidation of phenol begins with electron transfer that leads to phenoxyl radicals. In pathway 1 the phenoxyl radicals results in the formation of polymeric phenols, which leads to poisoning (or fouling) of the electrode surface. In pathway 2 the phenoxyl radicals results in the formation of benzoquinone and hydroquinone and can be further degraded with ring breakage to form various aliphatic acids, which are then further degraded to carbon dioxide and water. The electrochemical oxidation of phenol will be detected by the phenol sensor [41].



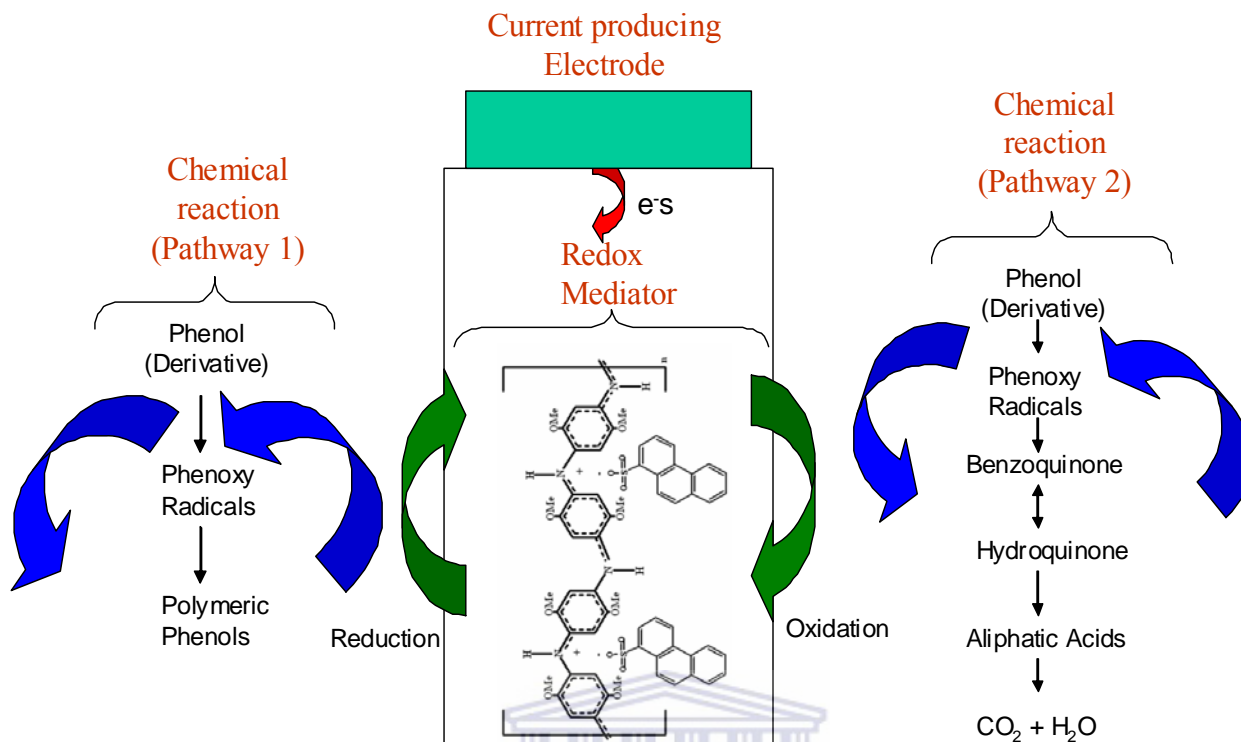


Figure 1.1: A schematic representation of a Pt/Polymer electrochemical Phenol sensor

UNIVERSITY of the
WESTERN CAPE

Diamond (1998) described in Principles of Chemical and Biological Sensors, that a “Chemical Sensor is a small device that, as the result of a chemical interaction or process between analyte and the sensor device, transforms chemical information of a quantitative or qualitative type into an analytical useful signal” [42].

In this study, the use of intrinsic conducting nanostructured polymers as electro-catalyst for electrochemical phenolic sensor devices is proposed, developed and their efficacy assessed.

1.2 Objectives

The aim of this study is to develop polyanilines nanostructured electro-catalysts for phenol and phenol derivative sensor devices in water. The study will have the following objectives:

- (i) Preparation of nanostructured polyanilines supported electro-catalysts:
The preparation of Polyaniline (PANI), Poly (*o*-methoxyaniline) POMA, Poly (2,5 dimethoxyaniline) (PDMA) / Phenanthroline Sulfonic acid (PSA) and Polyaniline (PANI), Poly (*o*-methoxyaniline) POMA, Poly (2,5 dimethoxyaniline) (PDMA) / Anthracene Sulphonic Acid (ASA) nanostructures will be synthesised.
- (ii) Electrochemical [Cyclic Voltammetry (CV), Differential Pulse Voltammetry (DPV) and Square Wave Voltammetry (SWV)] and instrumental [Scanning Electron Microscopy (SEM), Infrared Spectroscopy (FT-IR) and Ultraviolet Spectroscopy (UV-Vis)] physically characterisation of these electro-catalysts:
- (iii) Development of nanostructured polyanilines Pt electrodes
- (iv) The electrochemical characterisation of the electrode systems
- (v) Applications of the electrodes as electrochemical phenol sensor devices.

1.3 Methodology

Processable electrically conducting polymeric nanostructures will be prepared by oxidation polymerisation of aniline, *ortho*-methoxyaniline, 2,5 dimethoxyaniline in acid solutions containing anthracene sulfonic acid (ASA) and phenanthrene sulfonic acid (PSA) as stabilizing surfactants, respectively. Ammonium persulfate (APS) will be used as oxidant. These conducting polymers will be used to construct modified electrodes for phenolic oxidation and sensor devices.

1.4 Synthesis

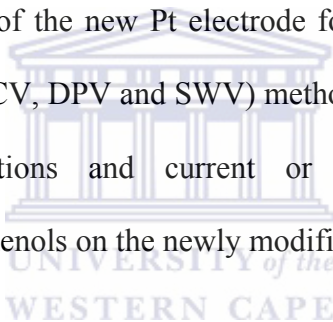
Chemical preparation of the intrinsic, soluble and processable conducting nanostructures will be carried out by modification of different reported methods [16-17]. In this preparation, aqueous solution of dopant acids anthracene sulfonic acid (ASA) and phenanthrene sulfonic acid (PSA) will be reacted with distilled monomers (Aniline, *o*-Methoxyaniline, 2,5 Dimethoxyaniline) in solution, respectively. An aqueous solution of ammonium persulfate (APS) is then added to the monomer/dopant complex under vigorous magnetic stirring for 15-24 hrs at room temperature. The resultant products will then be purified (vacuum filtered and washed 3 times respectively with distilled water, methanol and diethyl ether) and stored for characterisation and application [16-18].

1.5 Characterisation

The characterisation of the conducting polymeric nanostructured powders will be carried out instrumentally using Scanning Electron Microscopy (SEM), Infrared Spectroscopy (FT-IR) and Ultraviolet Spectroscopy (UV-vis) and electrochemically in acid (polymer paste). The modified Pt electrodes will be analysed by Cyclic Voltammetry (CV), Differential Pulse Voltammetry (DPV) and Square Wave Voltammetry (SWV).

1.6 Application

The surface properties of the new Pt electrode for phenol and derivatives, were interrogated by voltammetric (CV, DPV and SWV) methods. This allowed predictions on the evolution of concentrations and current or potential efficiencies during electrochemical oxidation of phenols on the newly modified electrodes [17 -22].



1.7 Outline of the remaining chapters in this thesis

Chapter 2: Literature Review

Theoretical considerations and characterisation methods and tools are reviewed, including: polymers, conducting polymer nanostructured formation, electro-catalysts, sensor devices and phenolic pollutants.

- Chapter 3:** Synthesis and characterisation of the dopants and conducting nanostructured polyanilines.
- Chapter 4:** The polymeric nanostructures were physically characterised by Scanning Electron Microscopy (SEM), Infrared Spectroscopy (FT-IR), Ultraviolet Spectroscopy (UV-vis) and electrochemically characterised via Voltammetry (cyclic, square wave and differential pulse) and includes the results and discussions.
- Chapter 5:** This chapter dealt with the catalytic, electro-catalytic and redox mediator effects from PANI-ASA and PANI-PSA modified nanostructured conducting polymer electrodes for phenol and derivative sensors. The results are then presented and discussed.
- Chapter 6:** These experiments included the development of the catalytic, electro-catalyst sensor devices for detecting different phenolic (derivatives) pollutants using POMA-PSA and POMA-ASA nanophase conducting polymers.
- Chapter 7:** This chapter dealt with the catalytic, electro-catalytic and redox mediator effects from PDMA-ASA and PDMA-PSA modified nanostructured conducting polymer Pt electrodes for phenol and derivative sensors. The results are then presented and discussed.

Chapter 8: General Discussion, Conclusions and Recommendations

Draws conclusions regarding the success of the development of the polyanilines nanostructures as electro-catalysts in sensor devices for phenolic (derivative) pollutants and makes further recommendations for future research.



1.8 References

- [1] M. J. Klink, *The Potential Use of South African Coal Fly Ash as a Neutralization Treatment Option for Acid Mine Drainage*, Published MSc Thesis, University of the Western Cape, RSA (2003)
- [2] J. K. Fawell and S. Hunt, *Environmental Toxicology: Organic Pollutants*, 1st Edition., Ellis Horwood Publishers, England, (1998)
- [3] C. Comninellis and C. Pulgarin, *J. Appl. Electrochem.*, 21 (1991) 703
- [4] R. Kotz, S. Stucki and B. Carcer, *J. Appl. Electrochem.*, 21 (1991) 14
- [5] S. Stucki, R. Kotz, B. Carcer and W. Suter, *J. Appl. Electrochem.*, 21 (1991) 99
- [6] C. Comninellis and C. Pulgarin, *J. Appl. Electrochem.*, 23 (1993) 108
- [7] N. B. Tahar and A. Savall, *J. Appl. Electrochem.*, 29 (1999) 277
- [8] E. Iwuoha, A. Williams-Dottin, L. Hall, A. Morrin, G. N. Mathebe, M. R. Smyth and A. J. Killard, *Pure and Appl. Chem.*, 76 (2004) 789
- [9] B. L. Crowder and M. J. Sienko, *Inorg. Chem.*, 4 (1965) 73
- [10] R. Kotz, S. Stucki and B. Carcer, *J. Appl. Electrochem.*, 21 (1991) 14
- [11] Ch. Comninellis, *Electrochim. Acta*, 39 (1994) 1857
- [12] O. Simond, V. Schaller and Ch. Comninellis, *Electrochim. Acta*, 42 (1997) 2009

- [13] V. S. D. Sucre and A. P. Watkinson, *Can. J. Chem.*, 59 (1981) 52
- [14] S. Palaniappan, A. John, C. A. Amarnath and V. J. Rao, *J. Mol. Cat. A: Chemical*, 218 (2004) 47-53
- [15] P. M. Fedorak and S. E. Hruday, *Wat. Res.*, 20 (1986) 113
- [16] A. R. Hopkins, R. A. Lipeles and W. H. Kao, *Thin Solid Films*, (2004) 447
- [17] Z. Wei, Z. Zhang and M. Wan, *Langmuir*, 18 (2002) 917
- [18] A. Vogel, *Vogel's textbook of quantitative chemical analysis*, 4th Edition, Longman, London, (1978)
- [19] W. Pernkopf, M. Sagl, G. Faflek, J. O. Besenhard, H. Kronberger and G. E. Naauer, *Solid State Ionics*, 176 (2005) 2031
- [20] S. Carrara, V. Bavastrello, D. Ricci, E. Stura and C. Nicolini, *Sens. & Act. B*, 109 (2005) 221
- [21] Y. F. Xing, S. F. Li, A. K. H. Lau, S. J. O'Shea, *J. of Electroanal. Chem.*, 583 (2005) 124
- [22] V. Freger, *Electrochem. Comm.*, 7 (2005) 957
- [23] I. Lelidis and G. Barbero, *Physics Lett. A*, 343 (2005) 440
- [24] G. Bereket, E. Hur and Y. Saihin, *Prog. Org. Coatings*, 54 (2005) 63

- [25] C. Guyon, *Phototransformation des monochlorophenols en phase aqueuse diluee*, Thesis, Universite de Clermont II, France (1993)
- [26] S. Esplugas, P. L. Yue and M. I. Perves, *Wat. Res.*, 28 (1994) 1323 – 1328
- [27]. A. Mills and S. Morris, *J. Photochem. Phobiol., A: Chem.*, 71 (1993) 75 –93
- [28] K. O'Shea and C. Chardona, *J. Org. Chem.*, 59 (1994) 5005 –5009
- [29] J. Qin, Q. Zhang and K. T. Chuang, *Appl. Cat. B: Env.*, 29 (2001) 115 – 123
- [30] S. Hocevar, U. Krasovec, B. Orel, A. S. Arico and H. Kim, *Appl. Cat. B: Env.*, 28 (2000) 113 –125
- [31] O. Koyama, Y. Kamagata and K. Nakamura, *Wat. Res.*, 28 (1994) 895 – 899
- [32] A. Al-Enezi, H. Shaban and M. S. E. Abdo, *Desal.*, 95 (1994) 1 – 10
- [33] F. Wajon, D. H. Rosenblatt and E. P. Burrows, *Environ. Sci. Technol.*, 16 (1982) 396 – 402
- [34] F. Revillon, B. Lassalle, B. Vandewalle and J. Lefebvre, *Anticancer Res.*, 10 (1990) 1067
- [35] J. G. Lin, C. N. Chang, J. R. Wu and Y. S. Ma, *Wat. Sci. Tech.*, 34 (1996) 41 – 48
- [36] J. McGuire, C. F. Dwiggins and P. S. Fedkiw, *J. Appl. Electrochem.*, 15 (1985) 53 – 62

- [37] J. H. Strohl and K. L. Dunlap, *Anal. Chem.*, 44 (1972) 2166 – 2170
- [38] R. S. Eisinger and G. E. Keller, *Envir. Prog.*, 9 (1990) 99 – 104
- [39] O. J. Murphy, G. D. Hitchens, L. Kaba and C. E. Verostko, *Wat. Res.*, 26, No.4, (1992) 443 – 451
- [40] S. Stucki, R. Kotz, B. Carcer, W. Suter, *J. Appl., Electrochem.*, 21 (1991) 99 –
- [41] M. A. Maluleke, *Electromembrane reactors for the decomposition of organic pollutants in potable and wastewaters*, Published PhD. Thesis, University of the Western Cape, RSA (2003)
- [42] D. Diamond, *Principles of Chemical and Biological Sensors*, John Wiley & Sons, Inc (1998)



Chapter 2

Literature Review

2.1 Introduction

A large numbers of industries employ phenol and phenol derivative compounds. These include coal mining, oil refineries, coke plants, paint-, polymer-, pharmaceutical- and other chemical companies [1-3].

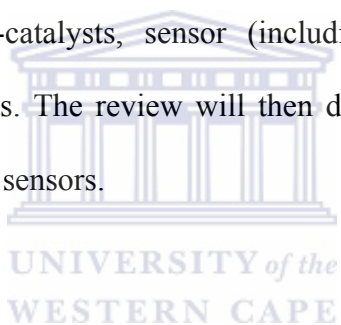
These phenol and derivative compounds, however, are harmful to humans and animals. Phenols are known to produce adverse effects such as reduced growth and reduced resistance against diseases. Therefore the treatment and detection of phenolic compounds are very important in environmental protection due to their toxicity and persistence in the environment [4-5].

Numerous chemical treatment processes [6–9] do exist to degrade phenols, but most of them do not lead to the complete mineralisation of phenols or are either expensive or time consuming. On the other hand, many methods for phenol detection have been developed in recent years, for example, spectroscopic [10], chromatographic [11] and electrochemical detection [12]. These methods are however expensive, need pre-treatment, require skilled operators and cannot be employed at the sampling sites.

Thus the desire to monitor real time phenol concentrations has led to the development of sensors (chemical and biological) for phenol (derivatives) detection. The end result provided us with an inexpensive, portable, miniature and intelligent sensing device to monitor phenol (derivatives) [13].

The intelligent designing of the surface of conventional electrodes, in order to improve their response by combining the intrinsic properties of the modifier (in this case conducting polymers) to a selected electrochemical reaction, has opened numerous possibilities for research.

The focus of this review will be to outline theoretical considerations including: polymers, conducting polymers, electro-catalysts, sensor (including chemical- and biosensor) devices and phenolic pollutants. The review will then describe and discuss the phenol (derivatives) bio- and chemical sensors.



2.2 Polymers

Natural polymers include: DNA, cellulose, etc., but polymeric materials can also be synthesized. The building blocks of any polymer (poly = many in Greek) are the repeating of a large number of the same (mono = one) unit. Each of these units can have a very simple chemical structure, for example (a) polyethylene, or, more complicated as in the case of (b) polyaniline presented in **Figure 2.1**. In both examples the macromolecule is linear, implying if one abstracts from the concrete chemical structure, it can be viewed as a linear chain. One of the most important consequences of such an approach is that many results in polymer physics and chemistry are independent of the chemical structure

of the molecule but rely heavily on the degree of polymerisation (n), or, in other words, the length of molecule.

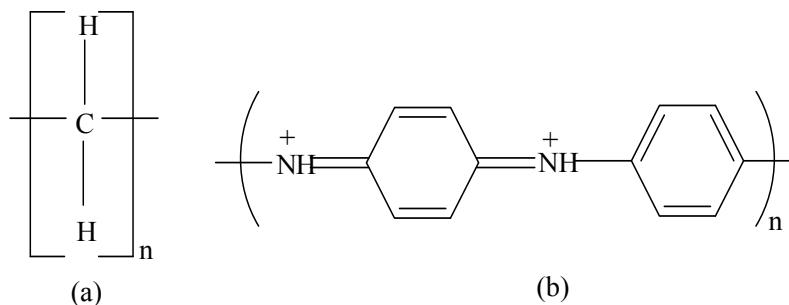


Figure 2.1: Chemical structures of (a) polyethylene and (b) polyaniline

Polymers are one of the most used materials in the modern world. Traditionally, polymers have been used as inactive materials in semiconducting devices due to their chemical inertness, electrical insulation and ease of processing. Their uses and application range from containers to clothing to coatings for metal wires to prevent electric shocks. Since the discovery of conducting polymers (polymers that can conduct electricity) in 1977/8 by the research groups of Shirakawa, MacDiarmid and Heeger, it has generated much more interest in applied science and technology for their unique electrical and physical properties, chemical stability and low cost for various applications [14-19].

2.3 Properties that make polymers conduct electrically

Conducting polymers are characterised by a conjugated structure of alternating single and double bonds, namely organic compounds that have an extended p-orbital system through which electrons can move from one end of the polymer to the other. This

enables the electrons to be delocalised over the whole system and so be shared by many atoms. In a common polymer material, for example polyacetylene, each carbon binds to two other carbons and to one hydrogen atom. The physical chemist would say that the carbon is sp^2 -hybridized and forms 3 σ (sigma)-bonds. However, since carbon has four valence electrons, each carbon atom has one electron left in a non-hybridized p-orbital. These atomic p-orbitals overlap, perpendicular to the polymer backbone, between neighboring carbon atoms to form molecular (π)-orbitals. This results in a conjugated molecular structure with alternating single and double bonds between carbon atoms [20].

2.4 Electronics of electrically conducting polymers (ECPs)

Since, electrically conducting polymers are extensively conjugated molecules, it is believed that they possess a spatially delocalized band-like electronic structure. These bands stem from the splitting of interacting molecular orbitals of the constituent monomer units in a manner reminiscent of the band structure of solid-state semiconductors (**Figure 2.2**) [21-22].

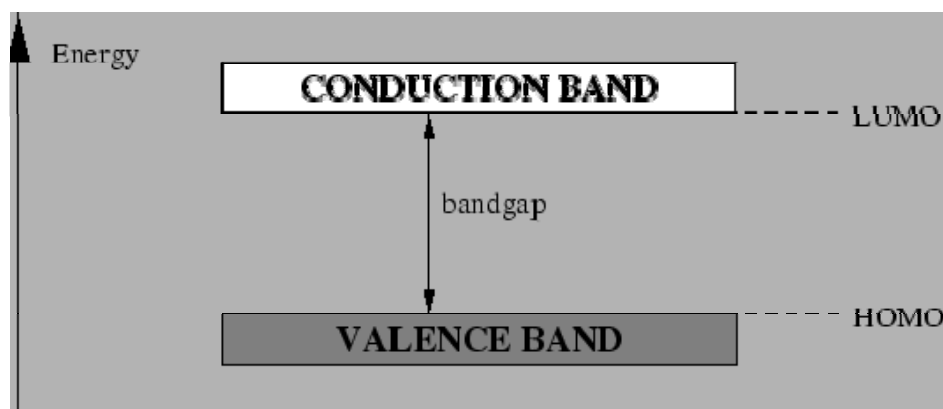


Figure 2.2: Band structure in an electronically conducting polymer

It is generally agreed that the mechanism of conductivity in these polymers is based on the motion of charged defects within the conjugated framework. The charge carriers, either positive p-type or negative n-type, are a result of the products of oxidised or reduced polymers respectively [23-24].

2.5 Conductivity of Electrically Conducting Polymers (ECPs)

The conductivity of a conducting polymer is related to the number of charge carriers and their mobility. Because the band gap of conjugated polymers is usually fairly large, the number of charge carriers is very small under ambient conditions. Consequently, conjugated polymers are insulators in their neutral state and not electrically conducting at this stage. A polymer can be made conductive by oxidation (p-doping) and/or, less frequently, reduction (n-doping) of the polymer either by chemical or electrochemical means, generating the mobile charge carriers [25]

Oxidation of the polymer initially generates a radical cation with both spin and charge. Using solid state physics terminology, this species is referred to as a polaron and comprises both the hole site and the structural distortion which accompanies it. This condition is depicted in **Figure 2.3 A**. The cation and radical form a bound species, since any increase in the distance between them would necessitate the creation of additional higher energy quinoid units. Theoretical treatments of Chung *et al.* [26] and Brédas *et al.* [27] have demonstrated that two nearby polarons combine to form the lower energy bipolaron shown in **Figure 2.3 B**. One bipolaron is more stable than two polarons

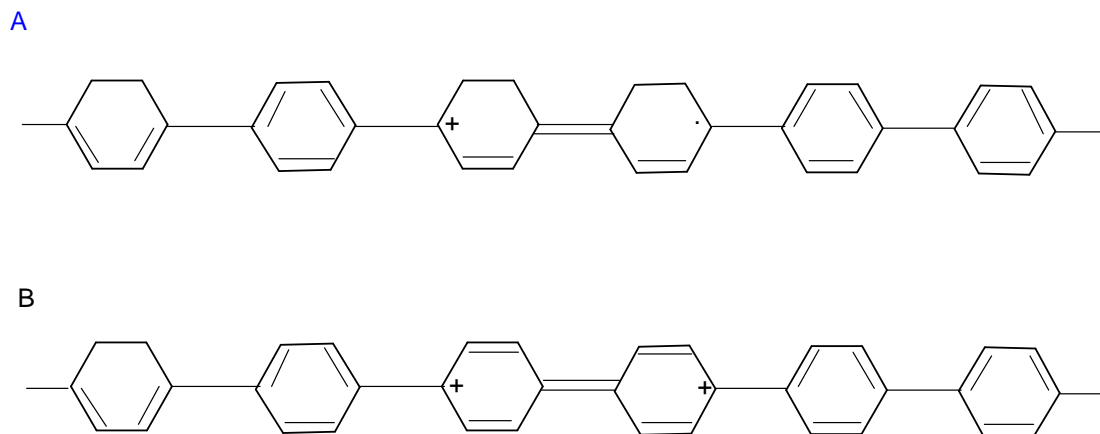


Figure 2.3: Positively charged defects on poly(p-phenylene) A: polaron B: bipolaron [26-27]

despite the coulombic repulsion of the two ions. Since the defect is simply a boundary between two moieties of equal energy -- the infinite conjugation chain on either side -- it can migrate in either direction without affecting the energy of the backbone, provided that there is no significant energy barrier to the process. It is this charge carrier mobility that leads to the high conductivity of these polymers [26-27].

2.6 Doping of Electrically Conducting Polymers

Heeger, MacDiarmid and Shirakawa accidentally discovered in 1977/8 that charge carriers can be introduced in polyacetylene by doping the material, which results in a conductivity increase by several orders of magnitude. This chance discovery occurred when a researcher accidentally added too much catalyst while synthesizing polyacetylene from acetylene gas, resulting in a shiny metallic substance rather than the expected black powder. The importance of this discovery was recognised in 2000 by the awarding of the Noble Prize in Chemistry for the discovery of conducting polymers in 1977 by Heeger, MacDiarmid and Shirakawa. The fundamental process of doping is a

charge-transfer reaction between an organic polymer and a dopant. Doping can be either positive or negative. Positive doping (p-doping) of a conjugated polymer means that an electron has been removed from the valence band (addition of a positive charged “hole”) and negative doping (n-doping) is when an electron is added to the conduction band. Conducting polymers can be doped in a number of different ways, such as chemical and electrochemical doping, photo doping and acid-base doping [28-29].

2.6.1 Classification of dopants

Dopants can be either strong reducing agents or strong oxidizing agents. They may be neutral molecules or inorganic salts, which can easily form ions. Neutral dopants (eg. I_2 , Na) are converted into negative or positive ions with or without chemical modification during the process of doping. Ionic dopants (eg. $LiClO_4$) are either oxidized or reduced by an electron transfer with the polymer and the counter ion remains with the polymer to make the system neutral. Another type of anionic dopant involves the anion derived from the dissociation of the dopant molecule, which neutralizes the positive charge of the polymer during the electrochemical doping process. Organic dopants (eg. Dodecyl benzene sulfonic acid) are anionic dopants, generally incorporated into polymers from aqueous electrolytes during anodic deposition of the polymer. Polymer dopants (polyvinyl sulfonic acid) are functionalized polymer electrolytes containing amphiphilic anions [30].

2.7 Synthesis of Electrically Conducting Polymers (ECP)

There is no singular technique for synthesising electrically conducting polymers. Chemical polymerization is the most widely used technique to synthesize large amounts of conducting polymers and exclude the use of electrodes. Chemical oxidation or oxidative coupling is the oxidation of monomers to a cation radical and their coupling to form dications and the repetition of this process leads to a polymer.

Electrochemical polymerisation on the other hand, use single or dual cell compartments by using a standard three electrode configuration in a supporting electrolyte, which is normally dissolved in an appropriate solvent [31]

Electrochemical polymerization is generally employed by potentiostatic, potentiodynamic, galvanostatic and potential cycling methods methods using a suitable power supply. The electrochemical polymerization technique has received wider attention due to its simplicity, increased reproducibility and the added advantage of obtaining a conducting polymer being simultaneously doped. Also the fact, that a wider choice of cations and anions are available as dopant ions in the electrochemical polymerization process. Photochemical polymerisation (take place in sunlight) utilizes photons to initiate a polymerization reaction using photo sensitizers. Conducting polymers have also been synthesized by other techniques such as metathesis polymerization (Ziegler-Natta polymerization), plasma polymerization, chain polymerization, step growth polymerization, concentrated emulsion polymerization, chemical vapour deposition, solid-state polymerization, etc. However, most of these techniques are time consuming and involve the use expensive chemicals and equipment [32-36].

2.8 Types of Electrically Conducting Polymers (ECPs)

Since the discovery of conducting polyacetylene, there has been much research in conducting polymers and a large number of ECPs have been prepared and investigated so far. Some important and well studied ECPs are polyacetylene (PA), polypyrrole (PPY), polythiophene (PT), polyaniline (PANI), derivatives of polyaniline etc. Some of the ECPs chemical structures are presented in **Figure 2.4**.

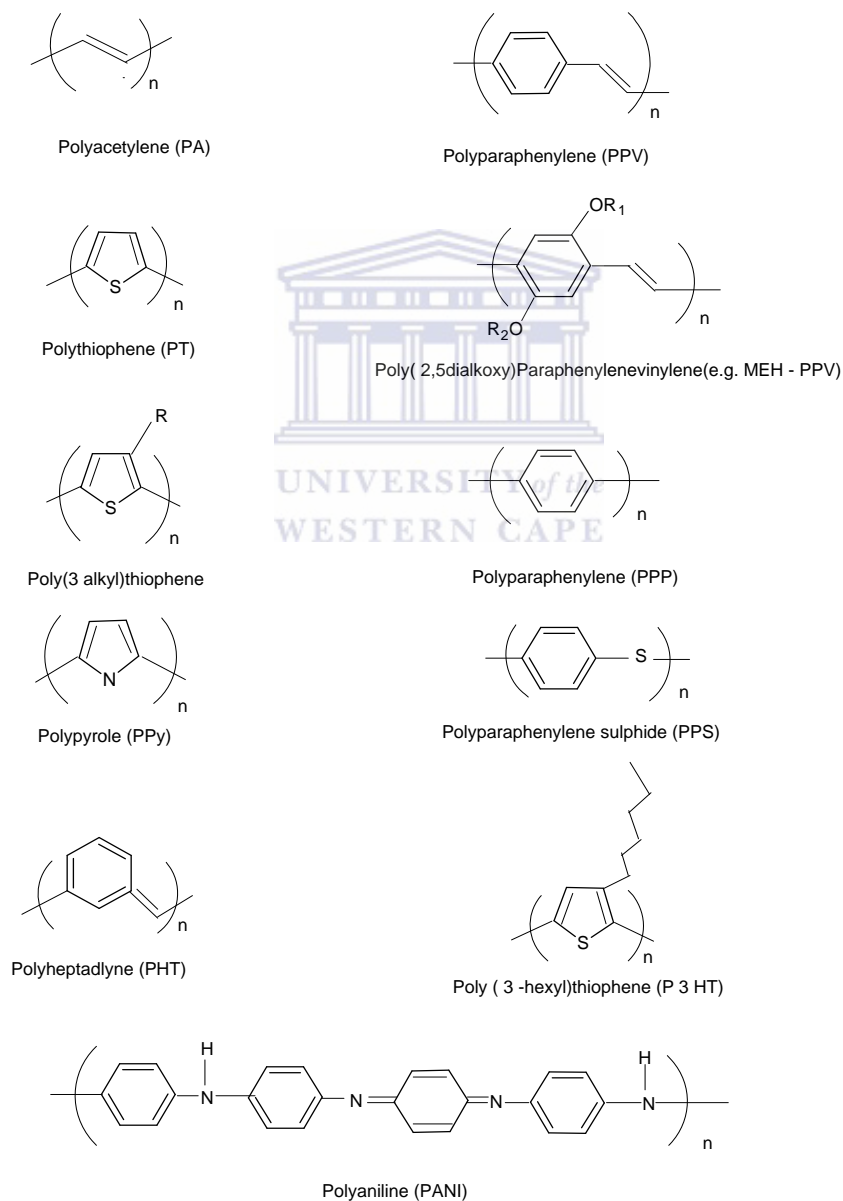


Figure 2.4: Chemical structures of some conjugated polymers [97]

2.9 Polyaniline (PANI) as ECP

Aniline was discovered and designated by Unverdorben as Kristallin, by Runge as Kyanol, by Frische as Aniline (from Spanish anil, indigo) and by Zinin as Benzidam. It was in 1843 when A.W. Hofman established the identity of these four products and Perkin developed the method devised by Bechamp in 1854 for recovering aniline by reducing nitrobenzene with iron filing in the presence of dilute acids into an industrial process in 1857. One way of making dyes from aniline is afforded by oxidation. In 1865 Letheby discovered the anodic oxidation of aniline and in 1891 the practical use of polyaniline was described by Goppelsroede. Willstätter and Green mainly elucidated the chemical constitution of these dyes around the turn of the century [37].

Synthesis of polyaniline is remarkably simple where aniline is chemically or electrochemically oxidized under acidic condition. The chemical structure of polyaniline is in **Figure 2.5**. Because of the oxidation and subsequent dehydrogenation of two molecules of aniline a quinone diimine is formed.

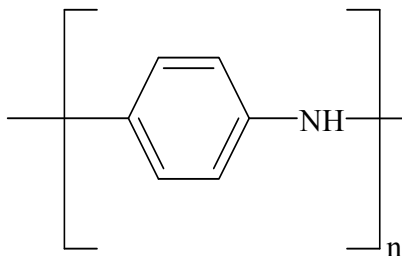


Figure 2.5: Chemical structure of polyaniline

Multiple repetition of this process with simultaneous dehydrogenation affords emeraldine and the nigraniline, which is along-chain molecule consisting of eight benzene rings and paraquinoid groups that are linked in the para position by nitrogen atoms. This converts to pernigraniline and finally aniline black. The electrochemistry of polyaniline was first researched at the end of the last century. The main reasons for the growth in interest during the 1980s were the low cost, relatively easy production process, environmental stability of the conducting forms, the conversion from monomer to polymer is straight forward and simple non-redox doping by protonic acid. The chemical synthesis of PANI is given as a scheme in **Figure 2.6** [37-39].

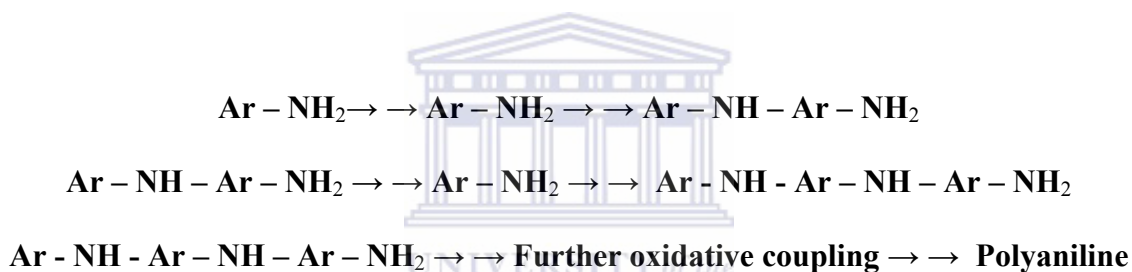


Figure 2.6: Mechanism of chemical oxidation of polyaniline [37-39]

In 1910 Green and Woodhead [40] described a number of well-defined oxidation states for polyaniline as shown as a scheme in **Figure 2.7**. The authors carried out oxidative polymerization studies using mineral acids and oxidants such as persulphate, dichromate and chlorate and determined the oxidation states of each constituent by redox titration using TiCl_3 . The different states range from fully reduced leucoemeraldine via protoemeraldine, emeraldine and nigraniline to fully oxidized pernigraniline. Unlike most other polyconjugated systems, the fully oxidized state of polyaniline is not conducting [37, 39].

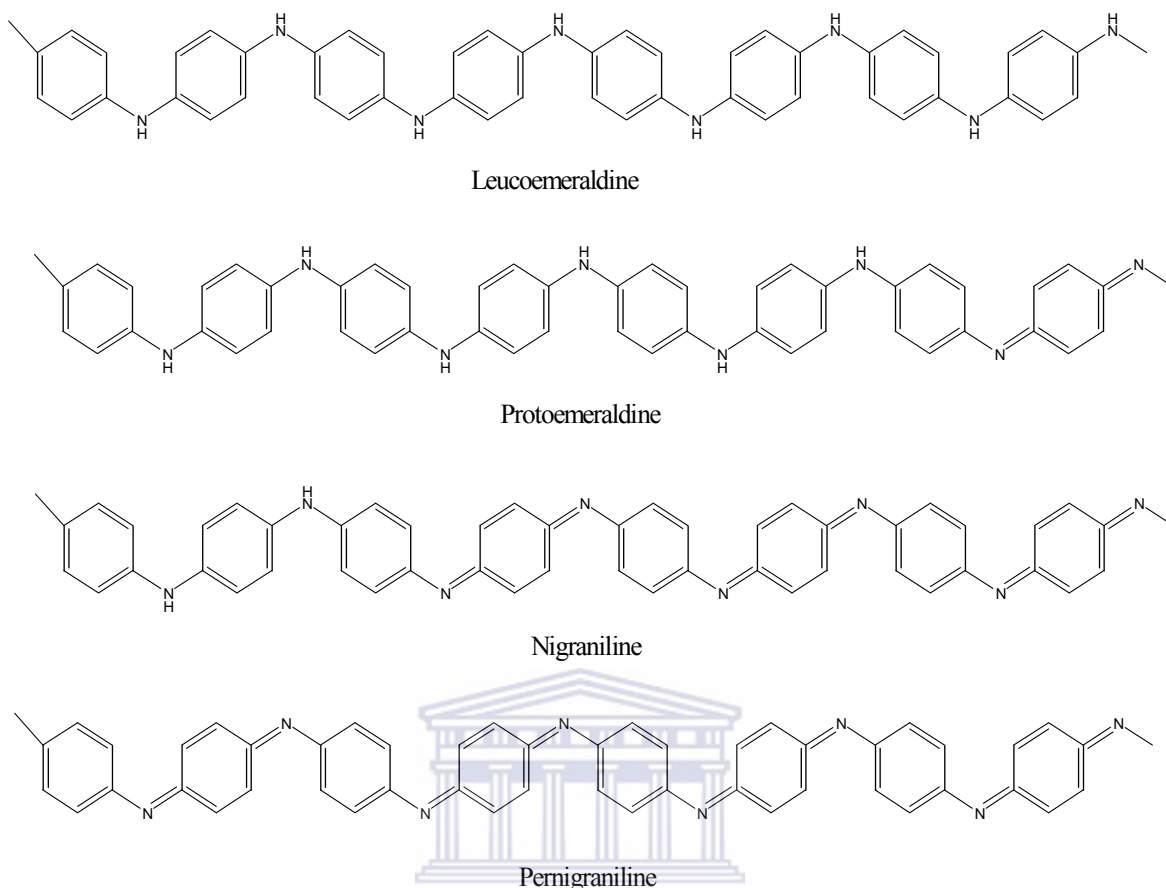
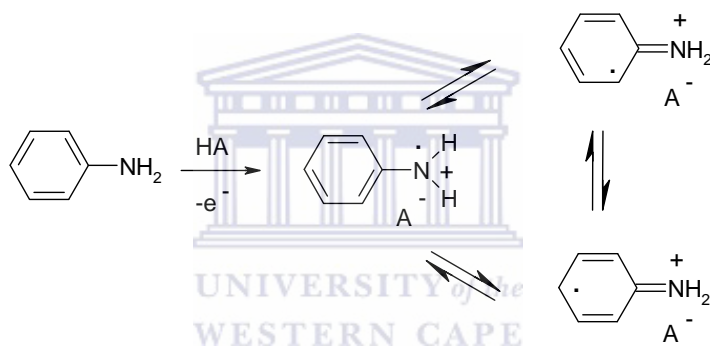


Figure 2.7: Different oxidation states of polyaniline by Green and Woodhead [40]

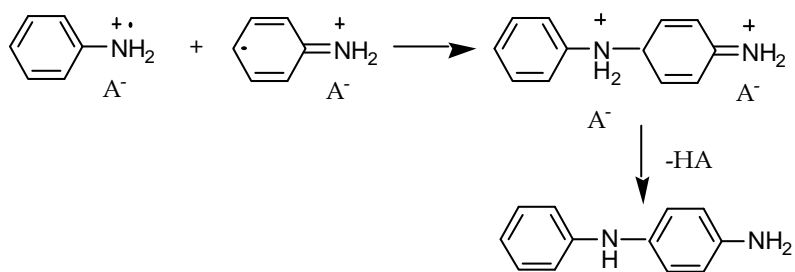
The generally accepted mechanism for the electrochemical polymerisation of aniline is presented as a scheme in **Figure 2.8**. Formation of the radical cation of aniline by oxidation on the electrode surface (step 1) is considered to be the rate-determining step. This is followed by coupling of radicals, mainly (*N*- and *para*- forms), and elimination of two protons. The dimer (oligomer) formed then undergoes oxidation on the electrode surface along with aniline. The radical cation of the oligomer couples with an aniline radical cation, resulting in propagation of the chain. The formed polymer is doped by the acid (HA) present in solution (step 4) [41].

Electrochemical polymerisation is routinely carried out in an acidic aqueous solution of aniline as a low pH is required to solubilise the monomer. Iwuoha *et al.* [42] grew aniline electrochemically on Pt electrode surfaces in HCl using potentiostatic and potentiodynamic techniques, whereby the potentiodynamic techniques showed more homogeneous films. A typical cyclic voltammogram for the electrochemical polymerisation process of aniline on a Pt electrode surface from acidic media is shown in **Figure 2.9** [42].

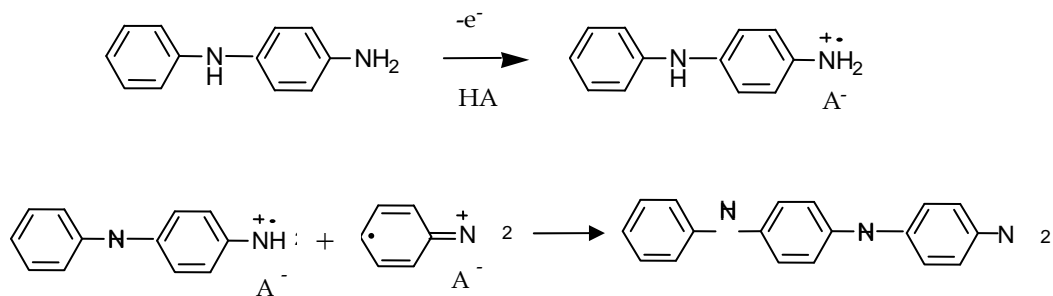
Step 1. Oxidation of monomer



Step 2. Radical coupling and rearomatisation



Step 3. Chain propagation



Step 4. Doping of the polymer

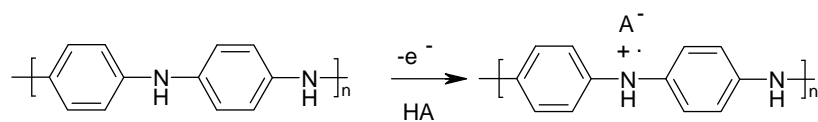


Figure 2.8: Electrochemical polymerisation of aniline [97]

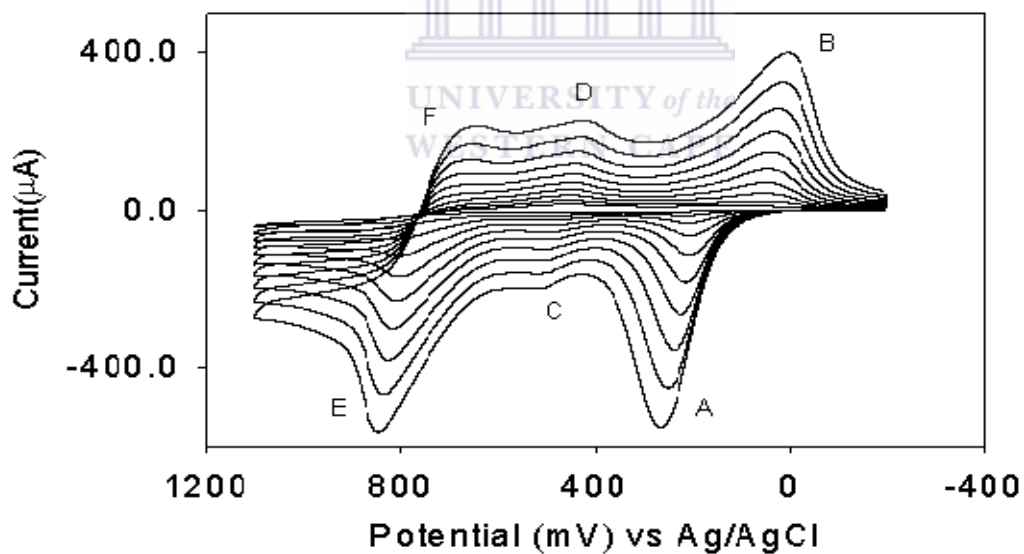


Figure 2.9: Electrosynthesis of a PANI film in HCl (1M) on a Pt electrode surface [43]

Iwuoha *et al.* [42] and Mathebe *et al.* [43] assigned the redox couples as follows: Redox couples A/B and E/F were attributed to intrinsic redox processes of the polymer itself. The redox couple A/B is assigned to the transformation of PANI from the reduced leucoemeraldine (LE) state to the partly oxidized emeraldine state (EM). The redox couple E/F corresponds to transition of the PANI from LE to pernigraniline (PE) state, and is accompanied by the oxidation of aniline monomer. The redox couple C/D is generally attributed to the redox reaction of p-benzoquinone. During the subsequent electrochemical scans, the oxidation of aniline occurred at lower potentials due to the catalytic effect of PANI, which resulted in deposition of polymer on the electrode surface [42-43].

2.10 PANI derivatives Poly(*ortho*-methoxyaniline) [POMA] and Poly(2,5 dimethoxyaniline) [PDMA] as ECPs

O-methoxyaniline (OMA) and 2,5 dimethoxyaniline (DMA) are substituted derivatives of aniline with methoxy ($-\text{OCH}_3$) groups substituted at the *ortho*-position for *o*-methoxyaniline and at positions 2 and 5 for 2,5 dimethoxyaniline respectively (**Figure 2.10**).

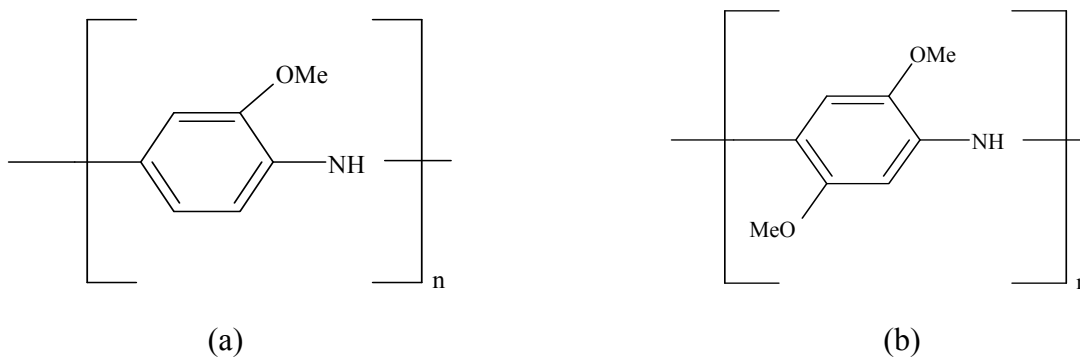


Figure 2.10: Chemical structures of (a) poly(*ortho*-methoxyaniline) and (b) poly(2,5 dimethoxyaniline)

The electrochemical properties of polymerised *ortho*-methoxyaniline (POMA) and 2,5-dimethoxyaniline (POMA) are similar to polyaniline (PANI), but are more soluble in organic solvents. The improved solubility is essentially due to the flexible groups incorporated into the polymer chain torsion in the backbone with departure from planarity effect, as well as the presence of the polar methoxy groups that increases the overall polarity of the polymer chain [44]. Unfortunately substitution of groups in phenyl ring or N-position of polyaniline units results in a decrease of conductivity [45].

Syntheses of poly(*ortho*-aniline) and poly(2,5-dimethoxyaniline) can also be done chemically or electrochemically under acidic condition. The Green and Woodhead [40] notation of well-defined oxidation states for polyaniline as shown in **Figure 2.7**, are also applicable on POMA as demonstrated by Widera *et al.* [46] and PDMA investigated by Huang *et al.* [47]. These authors investigated the polymerisation of OMA (in HCl and HClO₄) and polymerization of DMA (in H₂SO₄) under electrochemical conditions.

2.11 Doping of Electrically Conducting PANI and derivatives

Polyaniline becomes conductive when it is in moderately oxidized state. In particular the emeraldine base is protonated and charge carriers are generated. It holds a special position amongst conducting polymers because its highly conducting doped form can be obtained by two completely different processes- (a) protonic acid doping and (b) oxidative doping.

In protonic acid doping of emeraldine base unit with for example 1M aqueous HCl results in complete protonation of the imine nitrogen atoms to give the full protonated

emeraldine hydrochloride salt (a schematic doping and undoping process is presented in **Figure 2.11**). The same-doped polymer can be obtained by chemical oxidation (p-type doping) of leucoemeraldine base. This actually involves the oxidation of the σ - and π -system rather than just the π -system of the polymer as is usually the case in p-type doping. The reaction with a solution of chlorine in carbon tetrachloride proceeds to give emeraldine hydrochloride. It is this process of “protonic acid doping” that makes polyaniline so unique i.e. no electrons have to be added or removed from the insulating material to make it conducting. [48-51].

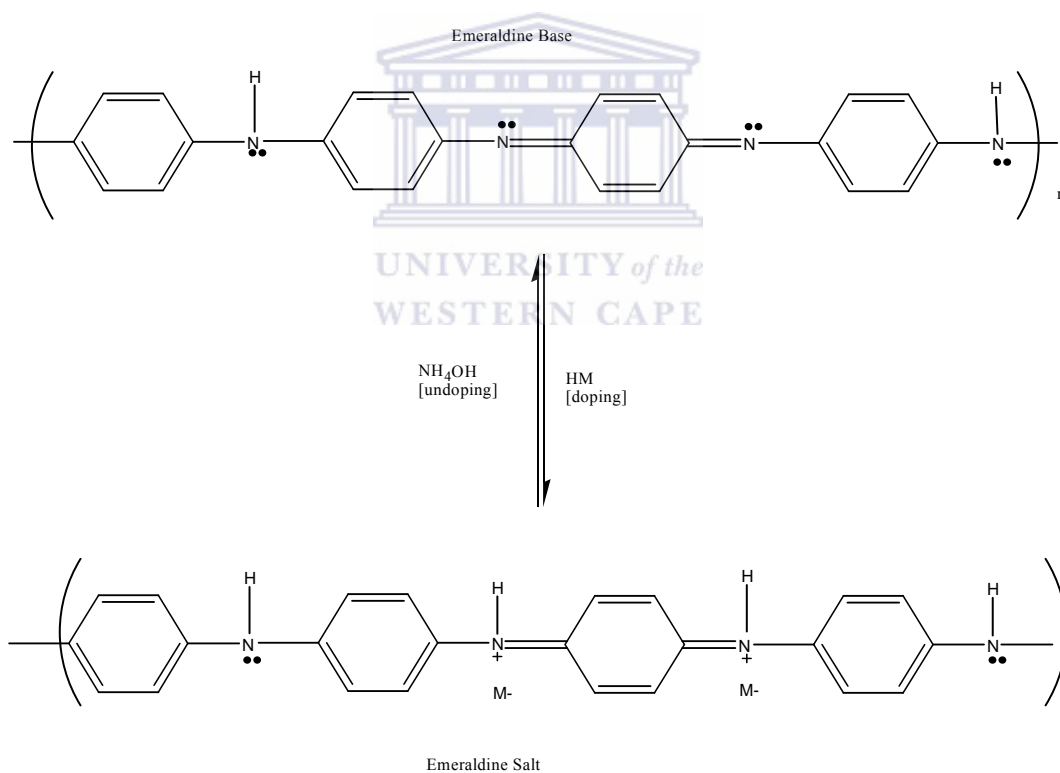


Figure 2.11: Doping and undoping of polyaniline (HM = any protonic acid) [48]

Different functionalised acids have been used as dopants for PANI and its derivatives. These included: para-toluene-sulphonic acid, dodecyl benzenesulphonic acid, camphor-sulphonic acid, poly(styrene) sulphonic acid and m-sulphonic acid [45, 47].

In a study performed by Hung *et al.* [45] with these functionalised acids the results showed that the substituent groups present in the units of the polymer chain caused a decrease in the stiffness of the polymer chain and resulted in better solvation. However, with the substituted aniline they have observed a decrease in conductivity noticed for polymers of substituted anilines with substitution in the phenyl ring or *N*-position. When aniline have two substituted methoxy groups as with 2,5-dimethoxyaniline (DMA), a more soluble polymer of poly(2,5-dimethoxyaniline) (PDMA) is obtained. A conductivity similar to PANI. Huang *et al.* [47] have further indicated in another study that the improvement in the solubility with the use of the dopants can also be attributed to the polar nature of the substituents, which promote compatibility between the polymer and the solvent.

Doping of the polyaniline film with polyvinylsulphonate (PVS) has been carried out by Iwuoha *et al.* [42] and Killard *et al.* [52]. The authors claim that doping enhances the morphology and electrical conductivity of the polymer at non-acidic pH.

A typical cyclic voltammogram for the electropolymerisation process of aniline from acidic media in the presence of PVS is shown in **Figure 2.12**. The oxidation peaks were assigned to the oxidation of leucoemeraldine (LM) to its radical cation, (LM^{•+}) (a), and LM^{•+} to emeraldine (EM) (b). The reduction peaks were assigned to the reduction of EM to its emeraldine radical cation (EM^{•+}) (c) and EM^{•+} to LM (d) [42, 52].

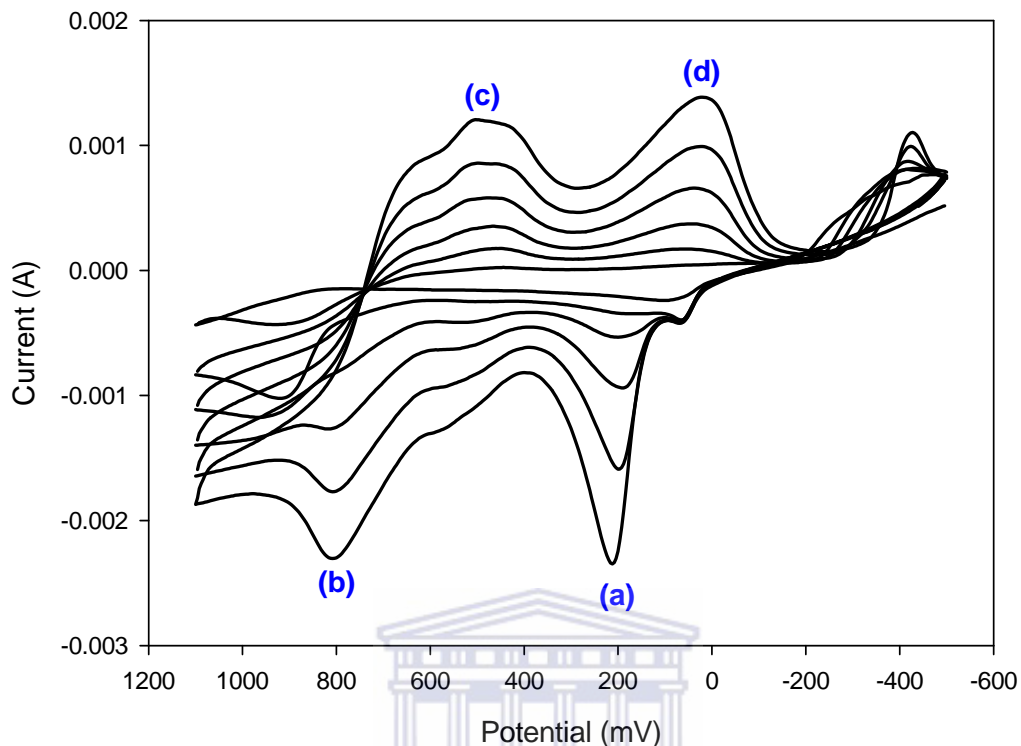


Figure: 2.12: Electrosynthesis of PANI/PVS film in HCl (1 M) on a Pt electrode surface [52]

2.12 Conducting polymer nanostructure

Conducting polymers synthesised in the form of nano-structures are of particular interest since their properties significantly differ from the properties of corresponding macroscopic materials. The change in surface properties is commonly achieved by surrounding a conductive polymer by another material, usually a bulky dopant. This forces the polymer backbone to the inside of the molecule forming all sorts of nano-structured morphology and making the conducting polymer more soluble.

Han *et al.* [53] introduced a bulky dopant into a PANI, which provided the polymer a hydrophobic micro-effect with a controlled electrochemical catalysis, affecting the orientation and solubilisation due to the formation of micelles, thereby greatly improving

the quality of the polymer films. They have further found that the use of camphor sulphonic acid (CSA) increased the conductivity of the PANI film while the use of dodecyl benzenesulphonic acid (DBSA) produced PANI with higher quality and reduced disorder [53].

Mazur *et al.* [54] prepared nano-tubes with PANI and POMA by chemical *in situ* deposition within the pores of polycarbonate membranes.

These structures include nano-micelles, nano-composites, nanotubes, nano-fibres, nano-wires etc. depending on the bulky dopant, which can then be used as electro-catalysts in chemical sensors and biosensors.

2.13 Electro-catalysts

The term electro-catalysis is often used to identify a scientific field at the interface of catalysis and electrochemistry. Trassatti [55] defined electro-catalysis as catalysis of electrode reactions. The catalytic effect in electro-catalysis can be achieved by the action of the electrode material or by the action of species in solution. In the former case one dealt with heterogeneous electro-catalysis and in the latter with homogeneous electro-catalysis.

Similar to heterogeneous catalysis, the effects of the electrode material and its structure on the rate and on the mechanism of electrode reactions are the main topics of interest in heterogeneous electro-catalysis. Heterogeneous catalysis and heterogeneous electro-catalysts are, however not independent disciplines. It has been long realized that liquid phase heterogeneous catalytic systems, where a charge interface is formed, are to be seen as electrochemical systems. Electro-catalytic measurements would be thus advantageous

to the studies in the liquid phase heterogeneous catalysis, since the surface potential is known and/or controlled. Advantages in electro-catalysis are deeply connected to the understanding of mechanism of electrode reactions. The mechanisms and kinetics of electro-catalytic reactions can be studied not only with the help of classic electrochemical methods, such as voltammetry and transient techniques, but also using a number of *in situ* physical characterization techniques. The latter techniques allow the investigation of a surface structure and to identify the reaction products and their concentration [56].

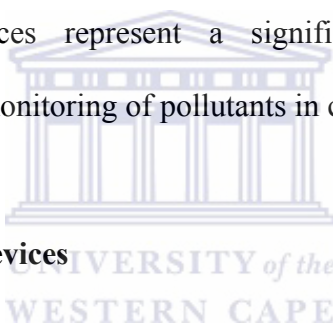
2.14 Development of electro-catalysts

Electro-catalysis involves an electron transfer mediator (for example a conducting polymer) between the target analyte and surface by an immobilized catalyst. Such catalytic action results in faster electrode reactions at lower operating potentials. At the electron transfer mediator modified electrode there is at least three processes that should be considered taking place during electro-catalytic conversion of solution species, these include:

- (i) a heterogeneous electron transfer between the electrode and an electron transfer mediator, and electron transfer within the electron transfer mediator;
- (ii) the diffusion of solution species to the reaction zone, where the electro-catalytic conversion occur and
- (iii) a chemical reaction between solution species and the electron transfer mediator [57].

Various catalytic surfaces have been successfully employed for facilitating the detection of environmentally relevant analytes, with otherwise slow electron transfer kinetics. These include the electro-catalytic determination of hydrazines or nitrosamines at electrodes coated with mixed valent ruthenium films, monitoring of aliphatic aldehydes at palladium modified carbon paste, sensing of nitrite at a glassy carbon electrode coated with an osmium based redox polymer, of nitrate at a copper modified screen printed electrode, monitoring of organic peroxides at cobalt-phthalocyanine containing carbon paste, and of hydrogen peroxide at a copper heptacyano-nitrosylferrate coated electrode [58].

These electro-catalytic surfaces represent a significant breakthrough in sensor development to help with the monitoring of pollutants in contaminated matrices.



2.15 Sensors and Sensor devices

2.15.1 The need for Chemical Sensors

There is an increasing demand to monitor all aspects of our environment in real time which has been brought about by our increasing concerns with pollution, our health and safety. At the same time is there the need to determine contaminants and analytes at lower detection levels and to improve the accuracy and precision at those levels. The desire to monitor everything around us has led to the developing of sensors for a multitude of applications. The end result provided us with a portable, miniature and intelligent sensing device to monitor almost anything we wish at the sample site [59].

2.15.2 Chemical Sensor

A “Chemical Sensor is a small device that, as the result of a chemical interaction or process between analyte and the sensor device, transforms chemical information of a quantitative or qualitative type into an analytical useful signal”.

Hence, a chemical sensor is a device which gives the user information about its environment. **Figure 2.13** illustrates a representation of a chemical sensor making use of a conducting polymer to transfer electrons [13].

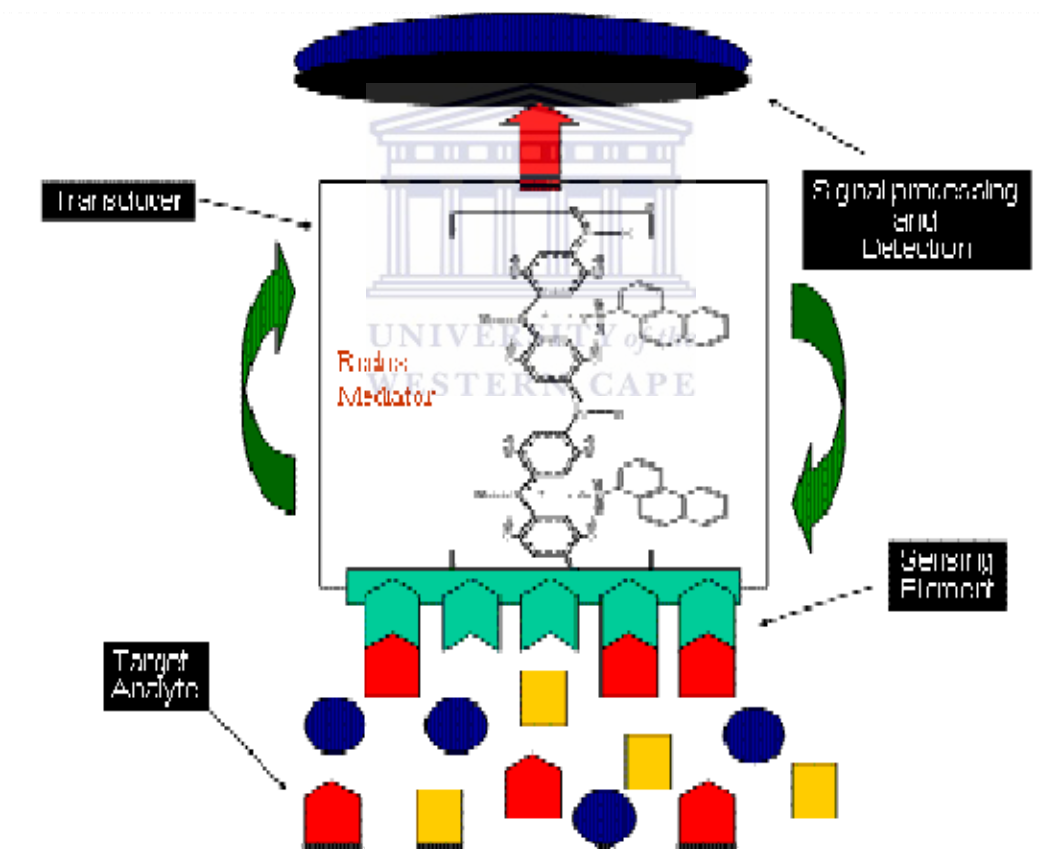


Figure 2.13: Schematic representation of a chemical sensor using a redox mediator [97]

2.15.3 Components of Chemical Sensors

All chemical sensors contain two basic components: a chemical recognition system (receptor) and a transducer [13, 59].

2.15.3.1 Transducers

The physical or chemical changes of the active material that results from the interaction with the analyte, need to be converted into an electrical output signal by an appropriate transducer. These signals from the transducer can be:

- (i) current - an increasing (decreasing) potential is applied to the cell until oxidation (reduction) of the substance to be analysed occurs and there is a sharp rise (fall) in the current to give a peak current. The height of the peak current is directly proportional to the concentration of the electroactive material. If the appropriate oxidation (reduction) potential is known, one may step the potential directly to that value and observe the current (amperometry),
- (ii) a voltage – these involve the measurements of the emf (potential) of a cell at zero current. The emf is proportional to the logarithm of the concentration of the substance being determined (potentiometry) or
- (iii) impedance/conductance - is based on measuring the time dependence of the change in conductivity as a result of the receptor recognition of its complimentary analyte changes (conductimetry).

Chemical layers can be used for importing a high degree of selectivity to electrochemical transducers. Selected transduction parameters and generic device types are summarized schematically in **Figure 2.14** [13, 59].

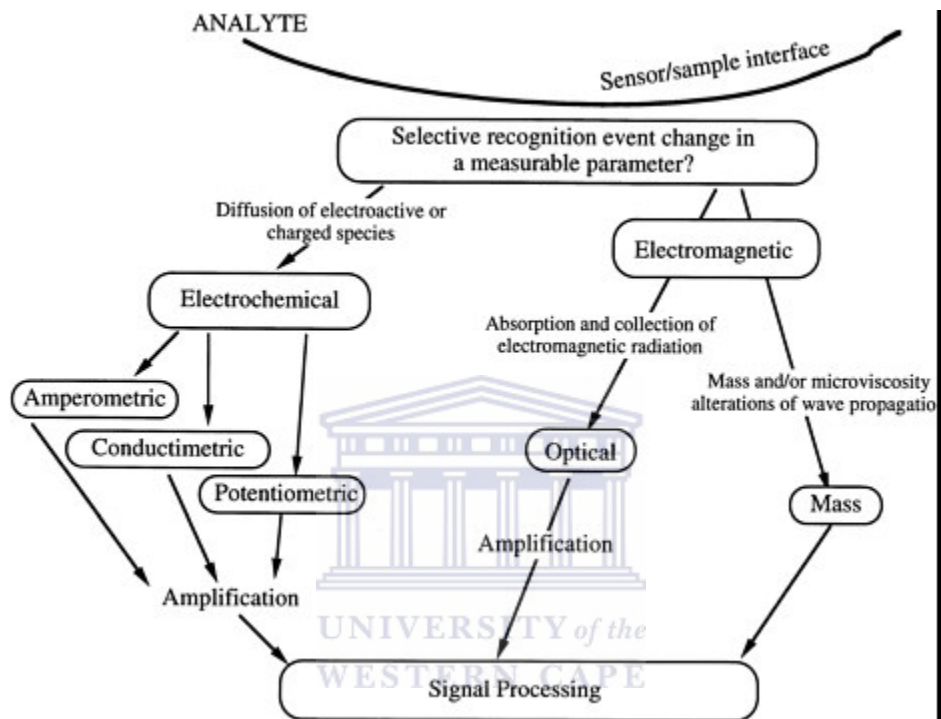
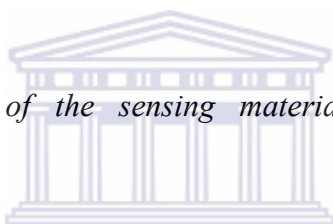


Figure 2.14: Different types of transducers in a chemical sensor [97]

2.15.3.2 Receptors

The operation of a direct-reading, selective chemical sensor is based on the existence of a selective recognition event that results in the change in a measurable parameter. The design of molecular selectivity for analytes typically involves a delicate choice of the sensing chemistry and associated materials. Chemical reactivity can involve a very wide range of chemical phenomena, including:

- ❖ *Recognition of size/shape/dipolar properties of molecular analytes by molecular films, phases, or sites.* These can be bioreceptor sites, structures allowing molecular recognition or host-guest interactions, or ceramic or other materials with templated cavities. The molecular recognition leads to selective, strong binding or absorption of analyte to the sensor material.
- ❖ *Selective permeation of analyte in a thin-film sensor.* If the binding or permeation of analyte is reversible, the sensor film can be re-used (i.e., recycled) in repeated measurements. Irreversible binding of analyte to the sensor, or side reactions with interferants, can stoichiometrically consume the sensor material, shortening its useful lifetime.
- ❖ *Catalytic reaction cycle of the sensing materials,* which results in analyte consumption.



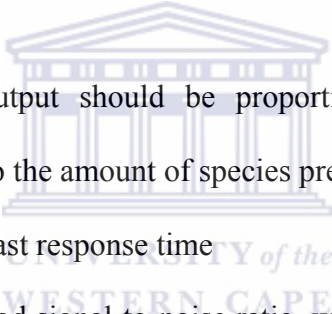
The most important materials-related factor leading to enhancements of direct-reading chemical sensors is the choice of materials employed to elicit stable selectivity of interaction with the target analyte [13, 59].

Chemically modified electrodes (CMEs) provide one approach to the development of these analytical sensor devices. In trace analysis, during the accumulation reaction CMEs pre-concentrate the analyte into a small volume on the electrode, allowing lower concentrations as low, as possible, to be measured in the absence of a pre-concentrated step (adsorptive stripping voltammetry). CMEs can also be applied to electro-analysis because of their own electro-catalytic properties and/or their capacities to immobilize electro-catalytic reagents that improve the sensitivity of the detection step. The majority

of modified electrodes can be obtained by chemi-sorption, covalent bonding and film deposition [13, 59].

2.16 What is the characteristics of an ideal sensor?

Diamond [13] described in Principles of Chemical and Biological Sensors, Dermot Diamond, that the “ideal “ sensor does not exist but that the acceptable characteristics often are a function of the application. Thus, a sensor that performs well for monitoring a particular analyte in a given situation may be totally unsuitable for monitoring the same analyte in a different matrix. The desirable characteristics for a sensor are:

- 
- (i) the signal output should be proportional or bear a mathematical relationship to the amount of species present in the sample
 - (ii) must have a fast response time
 - (iii) must have good signal-to-noise ratio, which determines the limit of the detection
 - (iv) must have adequate selectivity, otherwise the user cannot relate the signal obtained to the target species concentration with any confidence,
 - (v) must be sensitive which determines the ability of the device to discriminate accurately and precisely between small differences in analyte concentrations and
 - (vi) the sensor lifetime which can vary from one measurement to hundreds of measurements depends on factors such as the matrix of the samples analyzed and the polymer composition.

New materials are being investigated for use as a matrix in which to immobilize the receptor molecule. Important contributions are made by polymer technologists who have developed new materials with attractive properties: easily handled as monomers, a wide variety polymerization initiation, rapid setting and good stability in different environments.

2.17 Film Deposition

Chemically sensitive films may be immobilized using a wide variety of techniques. These methods require a solution of the coating material to be prepared in a suitably volatile solvent. Popular procedures involve spraying, droplet evaporation or spin coating. In the spray method the solution is aspirated to generate a finely dispersed aerosol that can be deposited onto the device in a controlled manner. In the droplet evaporation technique a known volume of a particular concentration is directly applied to the electrode and the solvent allowed to evaporate [13].

Spin coating uses a more concentrated and therefore viscous solution that is either drop on the electrode surface while it is rotating or is first applied and then the device is spinned. The most stable films are obtained where the chemically sensitive film is chemically rather than physically bonded to the electrode [13].

2.18 Types of Chemical Sensors

Chemical sensors are normally categorized into groups according to the transducer type [13, 59]:

2.18.1 Electrochemical Sensors

These sensors make use of the development of an electrical charge (potential/current/impedance) at the surface of a solid material when it is placed in a solution containing ions which can exchange with the surface. The magnitude of the electric charge (potential/current/impedance) is related to the number of ions in the solution. Among all the chemical sensors reported in literature, electrochemical sensors are the most attractive because of their remarkable sensitivity, experimental simplicity and low cost.

2.18.2 Optical Sensors

Involves a system in which the reagents are immobilized in or on a solid substrate which changes colour in the presence of a solution of the analyte.

2.18.3 Mass Sensitive (Piezoelectric) Sensors

When a chemical reaction takes place at the surface of a sensor not only is there heat evolved but there is also a change in mass. The mass change is very small but if a sensitive microbalance is used, it can be detected and related to the amount of analyte reacting with the surface.

2.18.4 Heat Sensitive Sensors

When a chemical reaction produces heat and the quantity of heat produced depends on the amounts of the reactants. Hence, the measurement of the heat of the reaction can be related to the amount of a particular reactant.

2.18.5 Biosensors

Biosensors are chemical sensors in which the recognition system uses a biological mechanism or entity (enzyme/substrate, antibody/antigen, receptor/hormone, etc.) as a fundamental part of the sensing process, instead of a chemical process.

In a biosensor the species recognition reagent is often a macromolecule which is immobilized into a membrane or chemically bound to a surface in contact with the analyte solution. A specific chemical reaction then takes place between the reagent and the analyte. A transducer transforms the response measured at the receptor into a detectable signal [13].

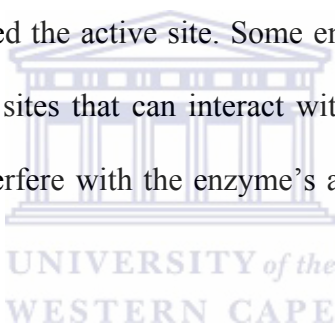
In biosensors the signal is not due to direct oxidation of phenol at the electrode, therefore electrode fouling is far from being as severe as that observed at bare electrode surfaces or even it does not occur at all. Nonetheless, the high cost and the critical storage of the biological components limit the practical application of such biosensors [75].

Various biosensors for the detection of phenol are nowadays described in literature. Some of these sensors include the following:

- (i) An optical biosensor based on the immobilization of tyrosinase into a chitosan film, which catalyses the conversion of phenolic substrates to catechol and then oxidised to quinone [60].
- (ii) The determination of phenol detection using peroxidase-modified graphite electrodes has also been reported. This involves the oxidation of phenolic compounds to phenoxy radicals in the presence of hydrogen peroxide [61].

- (iii) Organic phase biosensors have been developed for the monitoring of phenol in organic phases using silica sol-gel immobilisation of tyrosinase on a glassy carbon electrode [62].
- (iv) Biosensors based on phenol oxidases (tyrosinase and laccase) that catalyse the conversion of certain phenolic compounds to their corresponding quinones on the basis of reduction of molecular oxygen to water have been developed [63].

The above biosensors make use of enzyme to catalyse certain reactions. Enzymes are very specific and can only recognize and bind to one substrate. The binding site for the substrate to the enzyme is called the active site. Some enzymes may have other binding sites, which are called control sites that can interact with other molecules. These other molecules may improve or interfere with the enzyme's ability to recognize and bind its substrate [64].



2.19. The Kinetics of Enzyme Catalysis

An enzyme is essentially a catalyst. In this case an electro-catalyst, and consequently it cannot alter the equilibrium of a chemical reaction. It thus means that enzyme electrodes accelerate the reaction by lowering of the activation energy. In chemical sensors, the electro-catalysts also accelerate rate or cause the reaction to occur by mediating the redox process between the analyte and the electrode surface. The kinetics of this heterogeneous reaction is known to follow the electrochemical Michaelis-Menten kinetics. Hence, the kinetics of the electro-catalysis in chemical sensor is assumed to be the same as the kinetics of the enzyme electrode reactions

This section presents the basic mathematical treatment of enzyme kinetics. The rate of catalysis, V , varies with the substrate concentration, $[S]$, which is the case for many enzymes. This is shown in **Figure 2.15** [64-65].

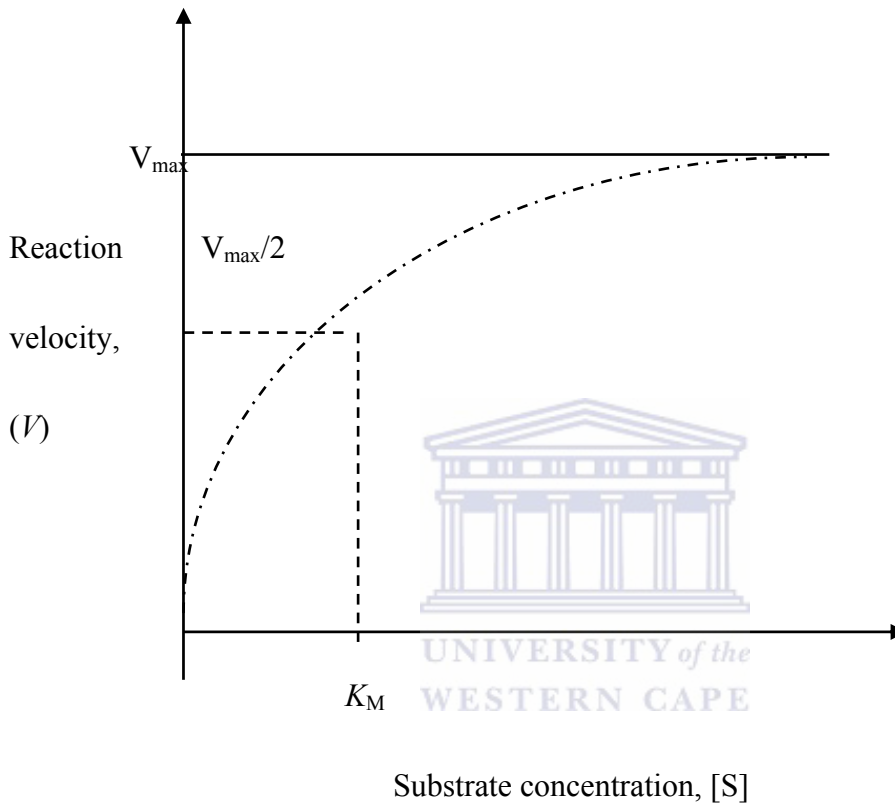


Figure 2.15: Graph of reaction velocity, V , as a function of the substrate concentration, $[S]$, for an enzyme that obeys Michaelis-Menten kinetics

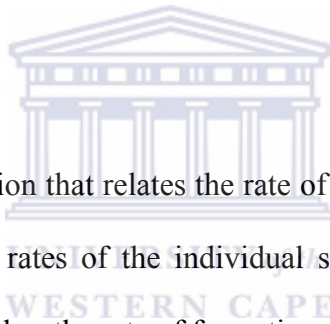
Figure 2.15 indicates that at a fixed concentration of enzyme, V is almost linearly proportional to $[S]$ when $[S]$ is small. On the other hand, at high $[S]$, V is nearly independent of $[S]$.

Using the above data, Michaelis and Menten [64-65], proposed a theory to explain these kinetic characteristics. Assuming that a specific ES complex is a necessary intermediate

in catalysis, where E and S are enzyme and substrate, the model proposed for the kinetic properties of many enzymes are:



In **equation 2.1** an enzyme, E, combines with a substrate S to form an ES complex, with a rate constant k_1 . It is also assumed that none of the product reverts to the initial stage [64-65].



What was needed is an expression that relates the rate of catalysis to the concentration of substrate and enzyme and the rates of the individual steps. We may thus express the reaction rate or velocity, defined as the rate of formation of products as:

$$V = k_3[ES] \quad (2.2)$$

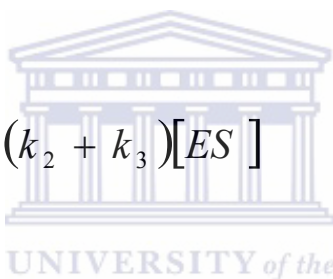
In **equation 2.2** the catalytic rate is equal to the product of the concentration of the ES complex and k_3 . When ES is expressed in terms of known quantities, the rates of formation and breakdown of ES can be written as:

$$\text{Rate of formation: } ES = k_1[E][S] \quad (2.3)$$

$$\text{Rate of breakdown: } ES = (k_2 + k_3)[ES] \quad (2.4)$$

The catalytic rate under steady-state conditions should be considered, since in a *steady state*, the concentrations of intermediates stay the same while the concentrations of starting materials and products are changing. This will occur when the rates of formation and breakdown of the ES complex are equal, so that **equation 2.3** is equal to **equation 2.4**, as follows:

$$k_1[E][S] = (k_2 + k_3)[ES] \quad (2.5)$$



When **equation 2.5** is rearranged, it can be written as [64-65].

$$[ES] = \frac{[E][S]}{(k_2 + k_3)/k_1} \quad (2.6)$$

Equation 2.6 can be simplified by defining a new constant, K_M , called the *Michaelis constant*, so that **equation 2.6** then becomes:

$$K_M = \frac{k_2 + k_3}{k_1} \quad (2.7)$$

When **equation 2.7** is substituted into **equation 2.6**, it then becomes:

$$[ES] = \frac{[E][S]}{K_M} \quad (2.8)$$

When the numerator is examined in **equation 2.8**, it can be deduced that the concentration of uncombined substrate, [S], is very nearly equal to the total substrate concentration. This will only be if the concentration of enzyme is much lower than that of the substrate. Furthermore, the concentration of uncombined enzyme, [E], is equal to the total enzyme concentration, E_T , minus the concentration of the ES complex, as shown in **equation 2.9**.

$$[E] = [E_T] - [ES] \quad (2.9)$$

On substituting **equation 2.9** for [E] into **equation 2.8**, the expression becomes

$$[ES] = ([E_T] - [ES])[S] / K_M \quad (2.10)$$

When **equation 2.10** is solved for [ES], it changes to,

$$[ES] = [E_T] \frac{[S]/K_M}{1 + [S]/K_M}$$

(2.11)

that can also be written as:

$$[ES] = [E_T] \frac{[S]}{[S] + K_M} \quad (2.12)$$

When this expression for [ES] is substituted into **equation 2.2**, we get

$$V = k_3 [E_T] \frac{[S]}{[S] + K_M} \quad (2.13)$$

The *maximal rate*, V_{\max} , is obtained when the enzyme sites are saturated with substrate, in which case [S] is much greater than K_M , so that $[S]/([S] + K_M)$ approaches 1. When this happens, **equation 2.13** changes to [64-65]:

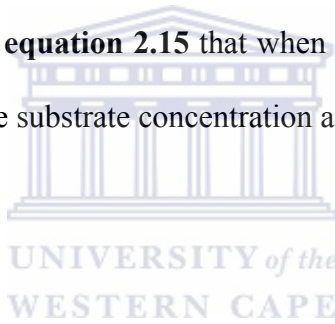
$$V_{\max} = k_3 [E_T] \quad (2.14)$$

Therefore, when **equation 2.14** is substituted into **equation 2.13**, the *Michaelis-Menten equation* is obtained:

$$V = V_{\max} \frac{[S]}{[S] + K_M} \quad (2.15)$$

Equation 2.15 accounts for the kinetic data given in **Figure 2.15**, so that at low substrate concentration, when $[S]$ is much less than K_M , $V = [S] \cdot V_{\max} / K_M$. This means that the rate is directly proportional to the substrate concentration. On the other hand, at high substrate concentration when $[S]$ is much greater than K_M , $V = V_{\max}$. This indicates that the rate is maximal, and independent of substrate concentration.

It can further be deduced from **equation 2.15** that when $[S] = K_M$, then $V = V_{\max}/2$. This indicates that, K_M is equal to the substrate concentration at which the reaction is half of its maximal value.



2.19.1 Determination of V_{\max} and K_M by changing of the substrate concentration

If an enzyme operates according to the scheme given in **equation 2.1**, then the *Michaelis constant*, K_M , and the *maximal rate*, V_{\max} , can be readily derived from rates of catalysis at different substrate concentrations. In order to simplify analysis, the *Michaelis-Menten* equation can be transformed into one that gives a straight line plot. When the reciprocal of both sides of **equation 2.15** is taken, it gives the following equation [64-65]:

$$\frac{1}{V} = \frac{1}{V_{\max}} + \frac{K_M}{V_{\max}} \frac{1}{[S]} \quad (2.16)$$

From **equation 2.16** it is deduced that a plot of $1/V$ versus $1/[S]$ will give a straight line with y-intercept equal to $1/V_{\max}$ and slope equal to K_M/V_{\max} , as shown in **Figure 2.16**.

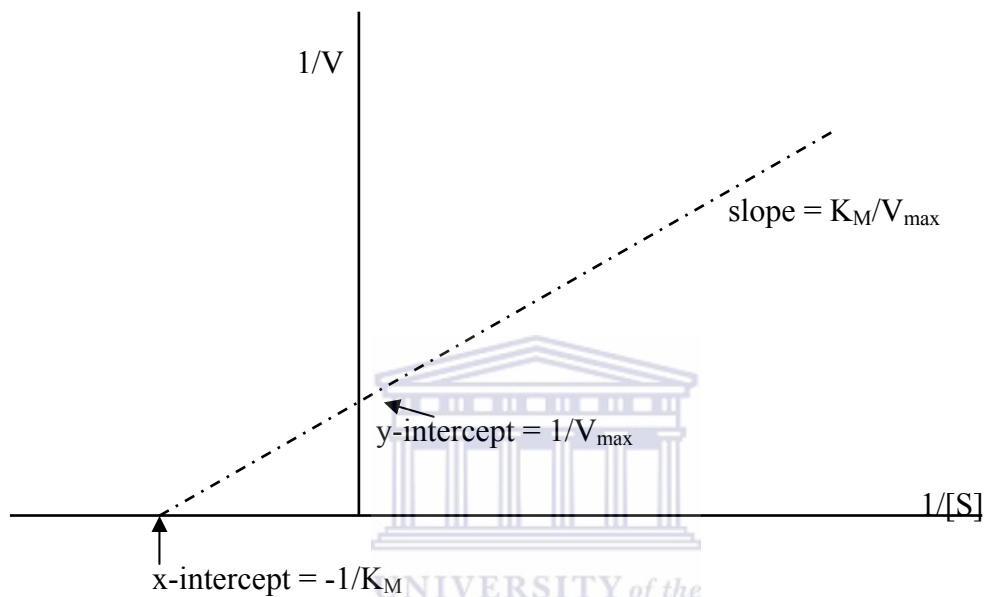


Figure 2.16: A graph of $1/V$ versus $1/[S]$. The slope is K_M/V_{\max} , the y-intercept is $1/V_{\max}$, and the x-intercept is $-1/K_M$.

The linear graph shown in **Figure 2.16** is obtained by using a double reciprocal plot, which is called the Lineweaver-Burk plot. A Lineweaver-Burk graph is also an easy way to test whether you have adherence to Michaelis-Menten kinetics and allows easy evaluation of the critical constants shown in **equation 2.16** [64-65].

The Lineweaver-Burk plot does have one major disadvantage, in that it requires a long extrapolation to determine K_M , with corresponding uncertainty in the results. To

eliminate this disadvantage, alternative ways of plotting the data are sometimes used. If **equation 2.15** is rearranged into the form:

$$V = V_{\max} - \frac{K_M V}{[S]} \quad (2.17)$$

and a graph of $V/[S]$ versus V is plotted, it yields what is called an Eadie-Hofstee plot, as shown in **Figure 2.17** [64-65].

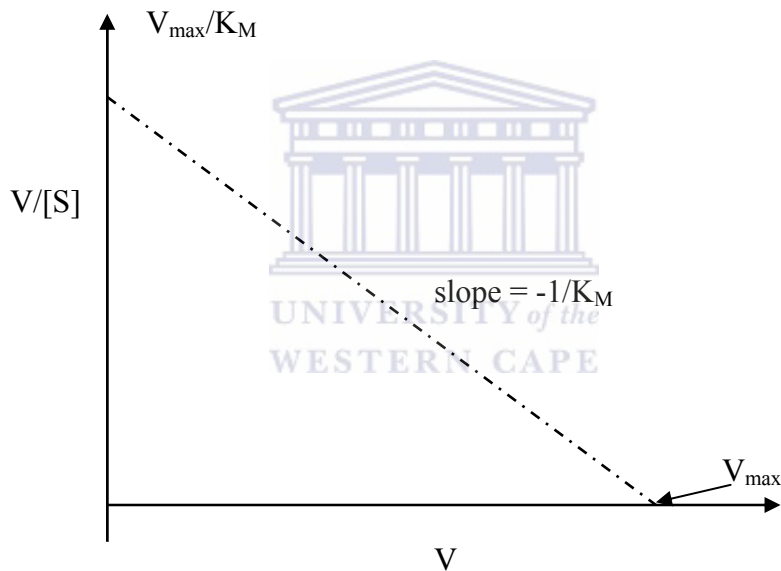


Figure 2.17: An Eadie-Hofstee plot of $V/[S]$ versus V , to obtain V_{\max} at $(V/[S]) = 0$ and K_M from the slope of the line.

The kinetics of the redox mediator chemical sensor is assumed to be the same as the kinetics as the enzyme catalytic reactions. Thus, the same equations will be used to calculate the different parameters (K_M , V_{\max} etc.) for the redox mediator phenol sensor in the study.

2.20 Phenolic pollutants in the environment

Phenols and phenol-derivatives are widely used as raw materials in many chemical, pharmaceutical, petrochemical and related industries. The aqueous effluents from these industries containing phenol compounds are toxic and cause considerable damage and threat to the ecosystems of water bodies and human health [1-3].

What's more it has high oxygen demand and low biodegradability. If released into the environment, they may accumulate in the soil, ground water, or surface water, thus representing an issue of great environmental concern [4-5].

In humans phenols are known to give adverse effects, such as reduced growth, reduced resistance against diseases and taste effects. Their toxicity affects a wide number of organs: primarily lungs, liver, kidneys and the genitor-urinary system. It is therefore important to assess the fate of these compounds in the environment and develop effective methods to detect and remove them from the environment [66].

2.21 Treatment and Reactions of Phenol

Phenols are an environmentally important group of oxygen containing organic compounds. These are aromatic compounds containing one or more hydroxyl groups attached to the aromatic ring. Phenol oxidation is normally used as a model reaction for treatment of aqueous organic waste. Generally phenols are not cathodically reduced.

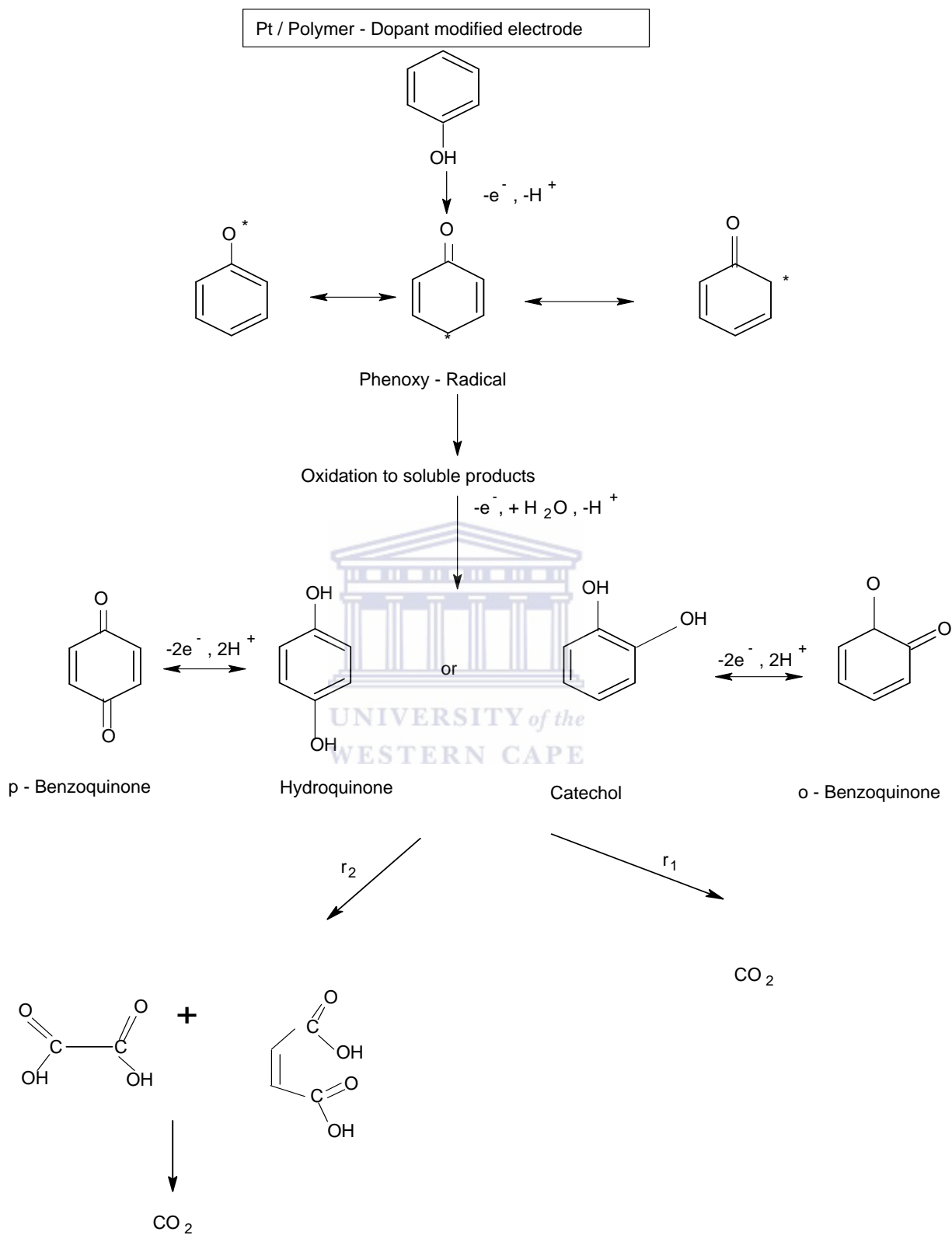


Figure 2.18: The general reaction pathways of phenol oxidation [96]

The general reaction pathways of phenol oxidation are shown in **Figure 2.18** depicting the route to various desired products: carbon dioxide for waste water treatment, quinones for electro-synthesis and the polymeric products for metal coating. The further reactions of the quinones and the ether and quinone type polymer structures are slow reactions with the main products being organic acids.

Numerous chemical treatment processes competes to degrade phenols, but most of them do not lead to the complete mineralisation of phenols.

These processes includes: Decomposition of phenols and removal of total organic carbon (TOC) with ultrasonic amplitude and H_2O_2 [67]; UV photocatalytic oxidation with or without oxidizing agents such as H_2O_2 or ozone [6-7]; Photochemical oxidation with semiconductors for example TiO_2 [8]; Microbial degradation [9]; Activated carbon adsorption and electrosorption methods [68]; Wet oxidation and chemical oxidation by H_2O_2 with Fe^{2+} ions as a catalyst (Fenton method) [69] and by ozone and chlorination treatment [70-71].

Although these technologies can be applied to a wide range of compounds, phenols and simple substitute phenols are frequently used as model pollutants in the study of the performance of different treatment technologies with synthetic wastewaters. The choice of treatment normally depends on the economics as well as ease of control, reliability and treatment efficiency.

2.22 Traditional analytical methods for phenol detection

Various methods are proposed in literature for determining phenols and phenol-derivatives in water. The most used method is based on the evaluation of a phenol “total index” carried out by spectrophotometric analysis of the 4-aminoantipyrine (or 2-nitrophenol) derivatives: the method is subject to interferences and lacks the specificity and sensitivity required by the recent laws. Other methods are based on liquid chromatography coupled to UV, which can be improved by post- and pre-column derivatization reactions [11].

Direct electrochemical detection (at 650 – 900 mV vs. Ag/AgCl) which can allow sensitivities below 0.5 µg/L considered that the detector is not widely diffused and does not allow gradient elution or the use of the usual liquid chromatography solvents [12].

Gas chromatographic methods using both packed and capillary columns are also used with flame ionisation and electron capture detectors often accompanied by derivatization reactions to improve sensitivity. Gas chromatography coupled with mass spectrometry and based on selected ion monitoring are said to provide the most sensitive methods [72].

However, these methods are expensive, some need sample pre-treatment involving separation, extraction and/or adsorption and these can be time-consuming and complex and cannot be taken to the reaction sites.

The EPA has created a list of the 11 most important phenols (**Figure 2.19**) as high priority phenol pollutants that need detection, recovery, removal and destruction.

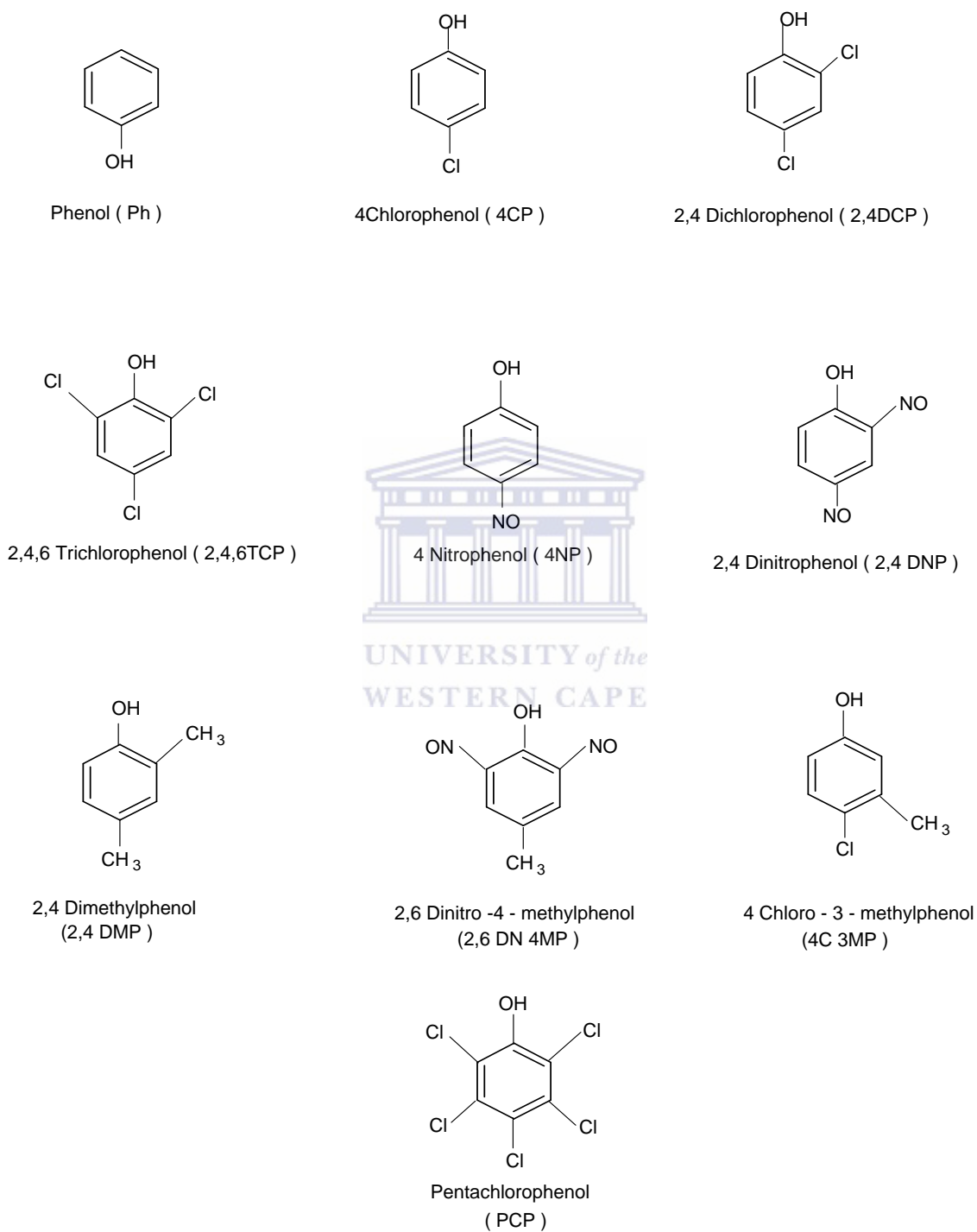


Figure 2.19: Structures of some EPA priority phenols

2.23 Electrochemical Phenol Sensors

Chemical sensors have captured the imagination of the world's scientific and commercial communities by combining the multidisciplinary skills of physicists, chemists, and engineers to provide innovative solutions to analytical problems. They are applicable to clinical diagnostics, food analysis, cell culture monitoring and environmental control. The earliest reported application of electrically conducting polymers has been the use of freestanding polymers as sensor devices. These sensors were designed to detect and measure the level of doping within the same material upon exposure to vapor-phase dopants. This simple sensor also served to inspire the early pursuit of research into sensor applications of ECPs. [73-74].

Several new approaches and different techniques have been investigated in the design and construction of electrochemical phenol chemical and biosensors. Several of these sensor designs are listed below:

Abdullah *et al.* [60] developed an optical biosensor on an immobilised tyrosinase enzyme in a chitosan film for the detection of phenol. They reported on the response characteristics of the biosensor towards different phenolic compounds including: 4-chlorophenol, phenol, *m*-cresol and *p*-cresol.

Wang and Dong [62] constructed an amperometric biosensor in the organic phase by silica sol-gel immobilisation of tyrosinase on a glassy carbon electrode. They found that the biosensor can reach 95% of steady-state current in about 18 s, and that the trend in the sensitivity of different phenols followed the order: catechol > phenol > *p*-cresol.

In another study, Notsu *et al.* [76] determined phenol derivatives using a tyrosinase-modified boron-doped diamond electrode. They concluded that the interference from direct reduction of oxygen at the electrode surface was almost negligible as a result of the overpotential for the oxygen reduction at the boron-doped diamond electrode being greater than those of most conventional electrode materials.

Lindgren *et al.* [61] used amperometric detection of phenols by using peroxidase-modified graphite electrodes. They found that the peroxidase electrodes in their experiments, except chloroperoxidase electrode, were sensitive to all the phenolic compounds.

Sotomayor *et al.* [77] developed a chemical sensor for phenol compounds using a nafion membrane doped with copper dipyriddy complex as a biomimetic catalyst on a glassy carbon electrode. They reported a higher response of dopamine in phosphate buffer (pH 7) with an applied potential of -50mV versus a standard calomel electrode.

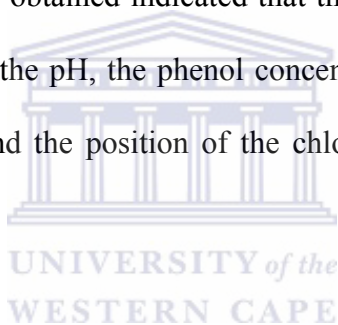
In another study, Rosatto *et al.* [78] prepared $\text{SiO}_2/\text{Nb}_2\text{O}_5$ sol-gel as a support for horseradish peroxidase immobilisation in biosensor preparation for phenol detection. The biosensor response was tested for various phenol substrates and the highest response was observed for 2-amino-4-chlorophenol.

Iwuoha *et al.* [79] took another approach by depositing electrosynthetic poly(phenol) nanofilms on a platinum electrode using a mono-substituted squarate as the electron

transfer mediator.. The synthesis charges of the nonconducting polymers were then recorded at various applied potential for film growth.

Ni *et al.* [80] investigated the voltammetric behaviour of nitrobenzene and nitro-substituted phenols by differential pulse voltammetry and chemometrics based on the compounds reductions at a hanging mercury drop electrode. Linear calibration graphs were obtained in the concentration range of 0.05 – 3 mg/L.

In another study, Ureta-Zañartu *et al.* [81] reported the electro-oxidation of chlorophenols at a gold electrode. The results obtained indicated that the oxidation of chlorophenols at the gold electrode depends on the pH, the phenol concentration, the number of chlorine atoms in the aromatic rings and the position of the chlorine atoms with respect to the phenolic OH.



Lei *et al.* [82] developed the construction, optimisation of performance variables and analytical characterisation of a sensitive and selective microbial amperometric biosensor for measurement of *p*-nitrophenol. The biosensor was able to measure as low as 28 ppb of *p*-nitrophenol selectively without interference from structurally similar compounds such as phenol, nitro-phenols and chlorophenols.

Heras *et al.* [75] reported a chemical sensor with poly(3,4-ethylenedioxythiophene)-poly(styrene sulphonate) composite electrode coating in the electro-oxidation of phenol. They found that electrode passivation was dramatically reduced while incorporating surfactants containing hydrophilic groups into the polymeric structure.

Priyara and Madras [83] studied the kinetics of photo-catalytic degradation of phenols with multiple substituent groups using combustion-synthesised catalyst. The first order kinetic rate constants for the degradation of various phenols were determined. The rate of photo-catalytic degradation followed the order: 4-chloro-3-methyl phenol > 2-chloro-4-methyl phenol > 4-chloro-2-nitro phenol > 4-chloro-2-methyl phenol > 4-chloro-3-nitro phenol > 4-methyl-2-nitrophenol.

Cañizares *et al.* [84] investigated electrochemical oxidation of phenolic wastes with boron-doped diamond anodes. Complete mineralisation was obtained in the treatment of phenols not substituted with chlorine or nitrogen. Chlorinated phenolic compounds were transformed into carbon dioxide and volatile organo-chlorinated compounds and nitro-substituted phenols dealt with the formation of polymeric materials.

In another study, Lui *et al.* [85] developed a renewable phenol biosensor based on a tyrosinase-colloidal gold modified carbon paste electrode. The biosensor showed a sensitive electrochemical response to the reduction of the oxidation product of phenol by oxygen in the presence of immobilised tyrosinase.

Kim and Lee [86] reported an amperometric phenol biosensor based on tyrosinase sol-gel silicate/nafion composite on a glassy carbon electrode. The phenolic compounds were determined by the direct reduction of biocatalytic-liberated quinone species.

Skládal *et al.* [87] studied strains of bacteria for development of phenol sensor using mediator-modified screen-printed electrodes. They found the operational stability was

satisfactory to perform up to 10 consecutive measurements and that the low cost and very simple manufacturing procedure allowed the bacterial sensor to be applied as disposable devices.

The electrochemical oxidation of phenol on a platinum electrode has been investigated by Arslan *et al.* [88] in NaOH and H₂SO₄. A simplified mechanism for the electrochemical oxidation of phenol was proposed, which included a selective oxidation parallel with PtOx formation.

Kane *et al.* [89] developed an amperometric biosensor for the determination of phenolics by complexing horseradish wit a redox osmium polymer on a glassy carbon electrode. The biosensor exhibited a low operating potential, fast response times, high sensitivity and micromolar detection limits for a range of selected phenols.

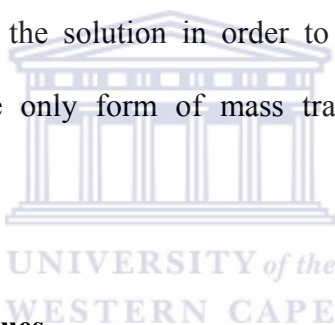
A cobalt (II) phthalocyanine-modified glassy carbon electrode was used as a phenol sensor by Mafatle and Nyokong for detection of cresols, chlorophenols and phenol. They found the modification of the glassy carbon electrode with cobalt (II) phthalocyanine increases the oxidation currents of the phenolic species, increases the stability of the electrode and showed less fouling of the oxidation products of these compounds compare to the unmodified glassy carbon electrode [90].

Önnerfjord *et al.* conducted a study on tyrosinase graphite-epoxy based composite electrodes for detection of phenols. The bioprobe was then electrochemically characterised by hydrodynamic and cyclic voltammetry for catechol and phenol [91].

The above chemical and biosensors all made use of some of the other electrochemical methods and techniques (which is dealt with in the next section) to assess their different parameters for the detection of the analytes.

2.24 Electrochemical Methods and Techniques

It is assumed for all the techniques discussed in this section that the analyte solution is either still or unstirred during the experimental performance, in order to ensure that mass transport by convection is absent. It is also assumed that an excess of ionic electrolyte has been added to the solution in order to ensure that mass transport by migration is also absent. The only form of mass transport remaining that will be considered is diffusion [92].



2.24.1 Voltammetric Techniques

2.24.1.1 Cyclic Voltammetry

Cyclic voltammetry (also called linear scan voltammetry) is an electrochemical technique that is classified under sweep techniques. In cyclic voltammetry the word voltammetry root “voltam-” refers to both potential (“volt-”) and current (“am-”). During any voltammetry experiment the potential of an electrode is varied while we simultaneously monitor the induced current [92].

The basic instrumentation for the cyclic voltammetry analysis requires controlled-potential equipment (potentiostat) and the electrochemical cell which consists of three

electrodes. The analysis is normally carried out using electrochemical analyser (for example BAS 100W, BAS 50W, AMEL7050) connected to a three electrode cell, containing the working electrode, reference electrode and auxiliary electrode.

The working electrode is the electrode at which the reaction of interest takes place. Materials that are used for working electrode include platinum, gold and carbon (carbon can be in the form of graphite, glassy carbon, or diamond). These are materials that are not susceptible to oxidation or reduction.

It is very important that material used as a working electrode should be the material that will not oxidise any ions in solution. The reference electrode provides a stable potential compared to the working electrode. Reference electrodes are used because their potentials are constant. There are different types of reference electrodes and the commonly used ones are saturated calomel electrode (SCE), and silver/silver chloride electrode Ag/AgCl. Auxiliary electrode is usually made of platinum wire. Electrochemical activity of auxiliary electrode does not affect that of the working electrode [92].

In *cyclic voltammetry* the potential is ramped from an *initial potential* (E_i) and at the end of its linear sweep, the direction of the potential scan is reversed, usually stopping at the initial potential. The potential may commence with further additional cycles. The potential at which the change in direction occurs is also known as the *switch potential* (E_λ). The scan rate between E_i and E_λ is the same as that between E_λ and E_i and the values of the scan rate v_{forward} and v_{reverse} are always written with positive numbers. In

Figure 2.20 a voltammogram for a simple solution-phase couple is shown and it is also known as a *cyclic voltammogram* (CV) [92].

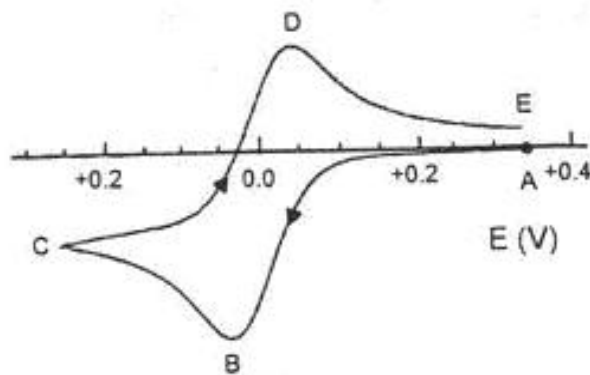
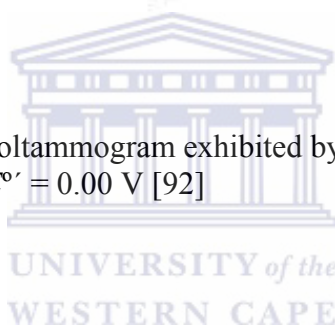


Figure 2.20: A typical cyclic voltammogram exhibited by a species which undergoes a reversible electrochemistry at $E^{\circ} = 0.00$ V [92]



In the CV shown in **Figure 2.20**, a peak is formed in both the forward and reverse sides of the CV. The peaks look similar in shape and the reaction taking place in the reaction vessel is fully reversible, the magnitudes of the peaks will be identical.

Oxidation usually takes place during the forward part of the CV, if scanned from a negative to a positive potential. The reverse part of the CV will then represent reduction taking place, with the potential running from a positive to a negative potential. If the potential is scanned from a negative to a positive value, then reduction would occur during the forward part of the CV scan and oxidation during the reverse CV scan.

For a reversible reaction the CV usually has two peaks, one for each of oxidation and reduction taking place. The potential of the peak (E_p) can be identified and for the

oxidation reaction taking place, the *anodic peak potential* is denoted as $E_{p,a}$. For the reduction reaction taking place, the *cathodic peak potential* is denoted as $E_{p,c}$.

Similarly the current for the anodic reaction ($I_{p,a}$) and the cathodic reaction ($I_{p,c}$) can be identified. In voltammetry the magnitude of the current is proportional to concentration. Thus the equality in size between $I_{p(\text{forward})}$ and $I_{p(\text{reverse})}$ implies a quantitative retrieval of electromodified material, which follows from Faraday's laws [92].

In cyclic voltammetry, the position of both the cathodic and anodic peaks gives us thermodynamic information of the redox couple used. The anodic and cathodic peak potentials also enable you to calculate the *formal electrode potential*, $E^{\circ'}$, as follows:

$$E^{\circ'} = \frac{E_{p,a} + E_{p,c}}{2} \quad (2.18)$$

The formal electrode potential (normally called the formal potential or the formal redox potential) is in concept similar to the standard electrode potential, E^{θ} [93].

(a) Diagnostic Criteria to Identify a Reversible Process

Certain diagnostic tests can be performed for the electrochemical reversibility of a redox couple, when cyclic voltammetry is performed. For a reversible system the following conditions should hold:

- $I_{pc} = I_{pa}$ or $\left| I_{pa} \div I_{pc} \right| = 1$
- The peak potentials ($E_{p,a}$ and $E_{p,c}$) are independent of the scan rate, ν

- The formal potential is positioned midway between $E_{p,a}$ and $E_{p,c}$, so that $(E^{o'} = (E_{p,a} + E_{p,c})/2$
- I_p is proportional to $v^{1/2}$
- The separation between the peak potentials $E_{p,a}$ and $E_{p,c}$ is $59 \text{ mV}/n$ for an n -electron couple at $25 \text{ }^\circ\text{C}$ [93].

The value for the separation peak potential, ΔE_p , arises from the following relationship:

$$\Delta E_p = \frac{2.3 RT}{nF} \quad (2.19)$$

which means that for reversible one-electron processes, the peak-to-peak separation assumes different values as a function of the temperature [93].

WESTERN CAPE

The peak-to-peak separation, ΔE_p , is an important parameter since it relates to the *electrochemical reversibility* of an electrode reaction, i.e. the rate at which electrons are transferred. When the value of ΔE_p is measured, a departure of $10 - 20 \text{ mV}$ from the theoretical value, especially at high scan rates, does not compromise the criterion of reversibility. This is due to the fact that the eventual presence of solution resistance, if not adequately compensated by the electrochemical instrumentation, tends to lay down the forward/reverse peaks system, thereby increasing the relative value of ΔE_p [93].

The chemical meaning of an electrochemical reversible process suggests that no important structural reorganisation accompanies the redox step. This will also be the case for an electrode process in which the rate of electron transfer is higher than the rate of mass transport [93].

When the peak current and potential is determined and the peak of the voltammogram is somewhat broad, it may be difficult to this determine this value. In such a case it is sometimes convenient to report the potential at $I_{p/2}$, called the *half-peak potential*, $E_{p/2}$, which can be determined with the equation [94]:

$$E_{p/2} = E_{1/2} + 1.09 \frac{RT}{nF} = E_{1/2} + \frac{28.0}{n} mV \quad (2.20)$$

Where, **equation 2.20** holds at 25 °C. The value of $E_{1/2}$ is located halfway between E_p and $E_{p/2}$, and a convenient diagnostic for a nernstian wave results in the following equation [94]:

$$\left| E_p - E_{p/2} \right| = 2.20 \frac{RT}{nF} = \frac{56.5}{n} mV \quad (2.21)$$

which also holds at 25 °C.

(b) The Randles-Sevčik Equation

According to the above equation the magnitude of the peak current, I_p , in a cyclic voltammogram is a function of the temperature (T), bulk concentration (c_{analyte}), electrode area (A), the number of electrons transferred (n), the diffusion coefficient (D), and the speed at which the potential is scanned (v), according to the equation in **2.22** [93]:

$$I_p = 0.4463 nFA \left(\frac{nF}{RT} \right)^{1/2} D^{1/2} v^{1/2} c_{\text{analyte}} \quad (2.22)$$

At 25 °C the above **equation. 2.22** changes to ([93-95]):

$$I_p = 2.69 \times 10^5 n^{3/2} A v^{1/2} D^{1/2} c_{\text{analyte}} \quad (2.23)$$

The Randles-Sevčik equation is obeyed if a plot of peak current (I_p) against analyte concentration (c_{analyte}) yields a straight line. It also means that if the electrolyte composition is constant in terms of temperature, solvent, swamping electrolyte, then the Randles-Sevčik equation can be used to determine the concentration of analyte by the construction of a suitable calibration curve. Furthermore, if **equation. 2.23** is used in a plot of I_p (y-axis) against $v^{1/2}$ (x-axis), a straight line should also be obtained that passes through the origin with the slope equal to $(2.69 \times 10^5 \times n^{3/2} \times A \times D^{1/2} \times c_{\text{analyte}})$ as shown in **Figure 2.21** [92].

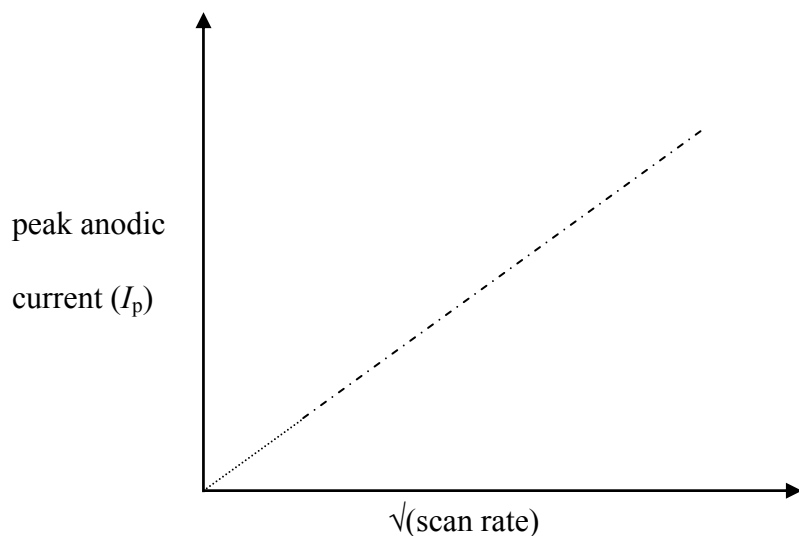


Figure 2.21: A Randles-Sevcik plot of I_p against $v^{1/2}$

The Randles-Sevcik equation also enables the calculation of the other variables listed in **Equations. 2.22** and **2.23**. That is, if the peak current (I_p) at a certain scan rate (v) is measured, knowing the area of the electrode (A), the diffusion coefficient (D) and the concentration (c) of the species under study, one is able to calculate the number of electrons (n) involved in the redox change. Similarly, if the number of electrons (n) is known, one can calculate the diffusion coefficient (D) of the species, and any of the other variables [93].

(c) Brown-Anson Analysis

The linear dependence of peak current (I_p) on the scan rate (v), showed that we have a stationary film immobilise on the electrode, which undergo rapid charge transfer reactions. This is typical of a Nernstian irreversible reaction of a surface confine species.

The surface concentration (Γ^*) of the absorbed species could therefore be estimated from a plot of I_p versus ν in accordance with the Brown Anson model using the equation [93]:

$$I_p = n^2 F^2 \Gamma^* A \nu / 4 R T \quad (2.24)$$

(d) Diagnostic Criteria to Identify an Irreversible Process

The most marked feature of a cyclic voltammogram of a totally reversible system is the total absence of a reverse peak. A typical cyclic voltammetric profile of an irreversible reduction process is shown in **Figure 2.22**. Whereas for the reversible case the value of $E_{p,c}$ is independent of the scan rate, for the irreversible case it is found that $E_{p,c}$ varies with the scan rate.

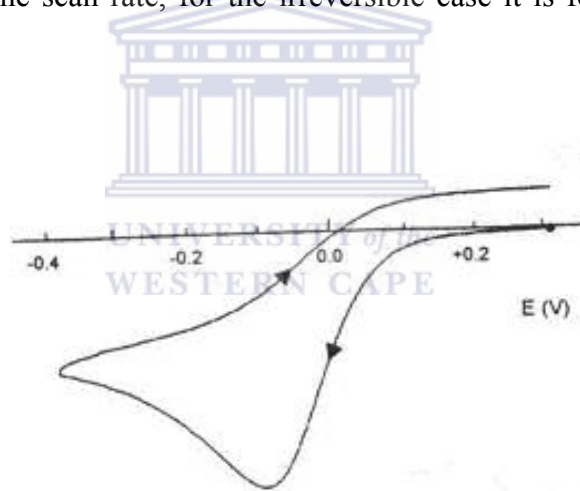


Figure 2.22: A typical cyclic voltammogram for an irreversible electrochemistry process [93]

At $I_{p/2}$, the value of the *half-peak potential*, $E_{p/2}$, can be determined at 25 °C with the equation [93]:

$$\left| E_p - E_{p/2} \right| = \frac{1.857 RT}{\alpha n_\alpha F} = \frac{47.7}{\alpha n_\alpha} (mV) \quad (2.25)$$

where **equation 2.25** is commonly used to calculate the values of $\alpha \cdot n_\alpha$. It often happens that the value of $n = 1$ (or $n_\alpha = 1$), which then enables the calculation of the value of α (transfer coefficient).

For an irreversible process the precise dependence of E_p with scan rate is expressed in the following equation [93]:

$$E_p = E^{o'} - \frac{RT}{\alpha n_\alpha F} \left[0.780 + \ln \left(\frac{D^{1/2}}{k^o} \right) + \ln \left(\frac{\alpha n_\alpha F \nu}{R \cdot T} \right)^{1/2} \right] \quad (2.26)$$

which allows for the calculation of the heterogeneous rate constant, k^o , if the values of $E^{o'}$ and D is known.

The following tests should identify whether an electrochemical process is irreversible:

- There is no reverse peak
- The $I_{p,c}$ is proportional to $\sqrt{\nu}$
- The value of $E_{p,c}$ shifts $-30/\alpha \cdot n_\alpha$ for each decade increase in ν
- $\left| E_p - E_{p/2} \right| = \frac{48}{\alpha \cdot n_\alpha} mV$.

The property of the current for an irreversible process can be expressed by the following equation [93]:

$$I_p = 0.227 n F A C k^o e^{-\frac{\alpha \cdot n \alpha \cdot F}{R \cdot T} (E_p - E^{\circ'})} \quad (2.27)$$

which can be used in a plot of $\ln I_p$ against $(E_p - E^{\circ'})$ that should give a straight line with a slope equal to $(\alpha \cdot n \alpha \cdot F/R.T)$ and the value of the y-intercept equal to $\ln(0.227 \cdot n \cdot F \cdot A \cdot C \cdot k^o)$.

The chemical meaning of an irreversible electrochemical process implies that a large activation barrier to the electron transfer takes place causing breakage of the original molecular frame with the formation of new species [93].

(e) Diagnostic Criteria to Identify a Quasi-reversible Process

A quasi-reversible process refers to one occurring in the transition *zone* between reversible and irreversible behaviour, as shown in **Figure 2.23**. A quasi-reversible process is characterised by determining either the thermodynamic parameter $E^{\circ'}$ (formal potential) or the kinetic parameters α (transfer coefficient) and k^o (rate constant) [93].

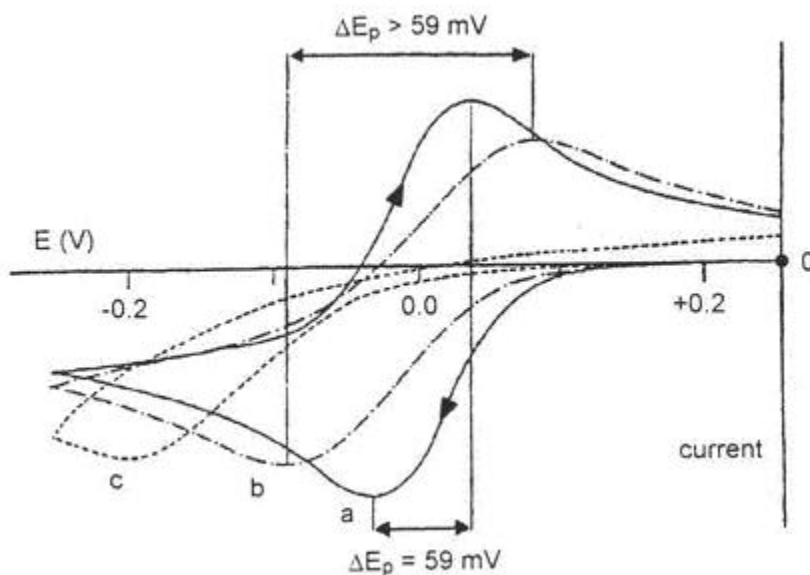


Figure 2.23: Qualitative behaviour of the cyclic voltammograms for a redox process having features of: a) reversibility; b) quasireversibility; c) irreversibility. $A = 0.5$; $E^{\circ'} = 0.00 \text{ V}$, $T = 25 \text{ }^{\circ}\text{C}$

For a quasi-reversible electrochemical process the shape of the peaks and the peak-to-peak separation (ΔE_p) depend, through a complex mathematical function Ψ , from α , k° and ν as shown in the following equation [93].:

$$\Psi = \frac{k^{\circ} \left[\frac{D_{ox}}{D_{red}} \right]^{\alpha / 2}}{\left[D_{ox} \pi \nu \frac{nF}{RT} \right]^{\frac{1}{2}}} \quad (2.28)$$

and with the normal assumptions of $\alpha \approx 0.5$; $D_{\text{ox}} = D_{\text{red}} = D$, the above equation then becomes:

$$\Psi = \frac{k^o}{\left[\frac{\alpha n F v D}{RT} \right]^{1/2}} \quad (2.29)$$

With the use of **equation 2.28** the value of k^o can be calculated from a working curve containing Ψ . Where ΔE_p , is plotted as a function of the parameter, Ψ . If the number of electrons (n) is known, as exchanged per molecule of Ox, measuring the value of ΔE_p at different scan rates, the corresponding value of Ψ can be obtained by using **equation 2.29** [93].

For a quasi-reversible system the following conditions should hold:

- $|I_p|$ increases with $v^{1/2}$ but is not proportional to it
- $\left| \frac{I_{p,a}}{I_{p,c}} \right| = 1$ provided $\alpha_c = \alpha_a = 0.5$
- ΔE_p is greater than $59/n$ mV and increases with increasing v
- $E_{p,c}$ shifts negatively with increasing v .

Furthermore, the chemical meaning of a quasi-reversible electrochemical process suggests that some important structural reorganisation accompanies the redox step, but it doesn't allow the molecular framework to undergo fragmentation [93].

It is possible to identify many side products following their generation at the electrode surface. The advantage of this technique is that, it has an ability to successively oxidize different molecules on different time scales. Changing the scan rate, allows access to different reactions which occur at different time scale. Therefore the mechanisms for the reaction can easily be predicted. The technique however, does have some limitations and therefore must be used with other techniques to prove certain mechanistic pathways [93].

In the following paragraphs two techniques that are particularly useful in the analysis of partially overlapping processes are, i.e. differential pulse voltammetry and square wave voltammetry will be discussed.

2.24.1.2 Square Wave Voltammetry

Square wave voltammetry is a technique whereby a square wave modulation is applied to a constant or nearly constant dc potential, and the current is sampled at the end of successive half cycles of the square wave.

The technique is useful mainly because: the sensitivity is as good as or usually better than any other differential technique, voltammograms are obtained rapidly, background currents are effectively discriminated against, the slope and position of the net current response are largely independent on convective mass transport and the total quantity of charge passed can be very small.

In **Figure 2.24** it is shown that in Osteryoung Square Wave Voltammetry (OSWV), the perturbation of the potential with time consists of an in-phase combination of a staircase

waveform of small and constant step height ($1 < \Delta E_{\text{base}} < 40 \text{ mV}$) with periodic square wave pulses ($1 \leq \Delta E_{\text{SW}} (= \frac{1}{2} \text{ square wave amplitude}) \leq 250 \text{ mV}$). This last perturbation consists of pulses alternating in direction, i.e. succession of forward (reduction or oxidation) and reverse (oxidation and reduction) cycles ($1 \leq \text{frequency SW} \leq 2000 \text{ Hz}$). The overall result obtained is a sequence of equally spaced steps: the forward step of height: $2 \Delta E_{\text{SW}} + \Delta E_{\text{base}}$; the reverse step of height: $-2\Delta E_{\text{SW}}$ [93].

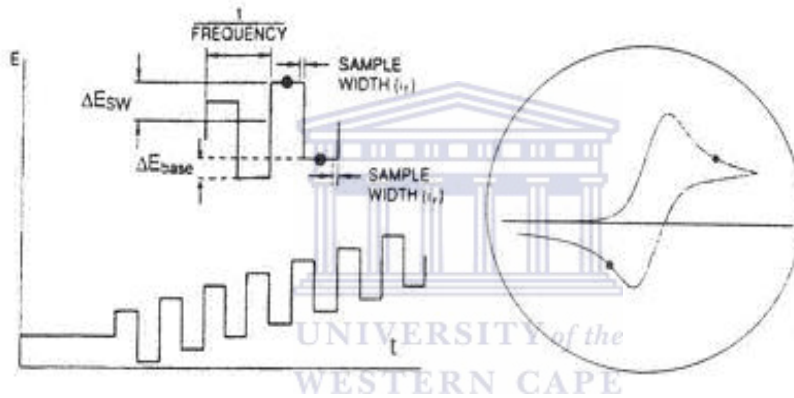


Figure 2.24: Potential-time perturbation on Osteryoung Square Wave Voltammetry [93]

In SWV, the current is sampled at the end of each at the forward and reverse pulse. As a result three curves are produced (**Figure 2.25**): forward current (i_f), the reverse current (i_r) and the net current. For a reversible system, the reverse pulse causes reoxidation of the species produced on the forward pulse back to the original state. This results in anodic current. Thus, the net current at the current-voltage peak is larger than either the forward

or reverse current since it is the difference between them. The peak height is directly proportional to the concentration of the electrochemical species.

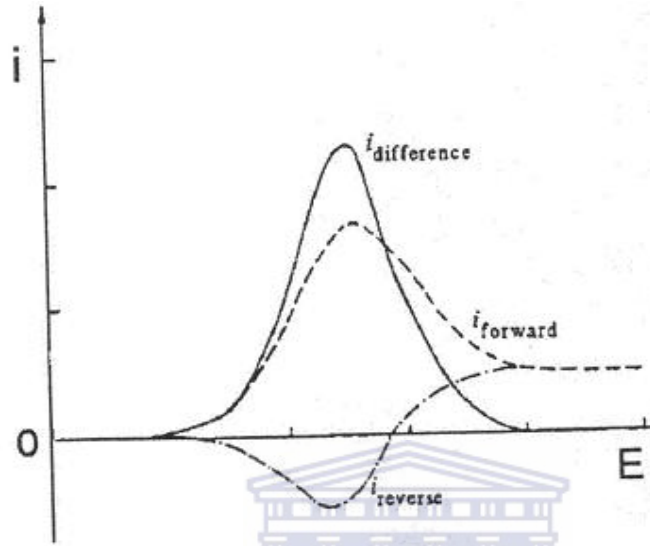


Figure 2.25: Typical Osteryoung Square Wave voltammogram [95]

In SWV, if ΔE_{SW} is small (about $50/n$ mV), it was found that the peak-potential for a *reversible electrochemical process* virtually coincides with the formal electrode potential. In addition to this, in the case of a reversible process the width of the peak at half height, $\Delta E_{p/2}$ is given by the following two equations [93]:

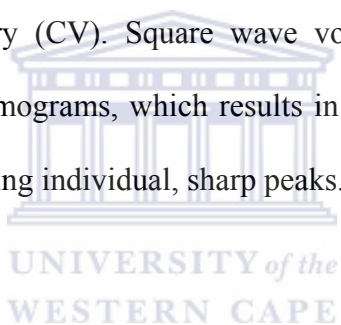
$$\Delta E_{p/2} = 4.90 \frac{RT}{nF} \quad (2.3)$$

or at a temperature of 25 °C:

$$\Delta E_{p/2} = \frac{126}{n} mV \quad (2.31)$$

Therefore, OSWV can be very effectively used in solving almost overlapping processes. In OSWV higher scan rates than in Differential Pulse Voltammetry (DPV) is attained from a few hundreds of mV/s to a few V/s. The value of the scan rate (obtained by the product SW frequency $\times \Delta E_{\text{base}}$) is around 0.2 V/s, a typical value for the scan rate of cyclic voltammetry. This also allows one to compete with the eventual presence of chemical complications coupled to the electron transfers [93].

The technique would largely be utilised in the electrochemical investigations of selective polymeric nano-structures as a way of corroborating redox processes observed in preliminary cyclic voltammetry (CV). Square wave voltammetry can often clear up discrepancies in cyclic voltammograms, which results in the merging from the merging of the redox signals, by producing individual, sharp peaks.



2.24.1.3 Differential Pulse Voltammetry

In Differential Pulse Voltammetry, a series of potential pulses are fixed, but small amplitude (10 – 100 mV) is superimposed on a dc voltage ramp. Two current samples are taken: one is taken immediately before applying the potential pulse, and the second is taken late in the pulse. At potentials well positive of the redox potential, there is no faradaic response to the pulse, so the differential current is zero. At potentials around the redox potential, the differential current reaches a maximum and decreases to zero as the current becomes diffusion controlled. The current response is therefore a symmetrical peak.

The Differential Pulse voltammogram in **Figure 2.26** shows that the perturbation of the potential with time consists in superimposing small constant-amplitude potential pulses ($10 < \Delta E_{\text{pulse}} < 100$ mV) upon a staircase waveform of steps of constant height but they are smaller than the previous pulses ($1 < \Delta E_{\text{base}} < 5$ mV). Some important parameters exist for Differential Pulse Voltammetry (DPV):

- the *pulse amplitude* (ΔE_{pulse}) is the height (in mV) of the applied potential,
- the *pulse width* is the length of the time (in ms) in which the pulse is maintained,
- the *sample width* is the time (in ms) at which the current is measured after the application of the potential pulse,
- the *pulse period* is the time (in ms) needed to make one cycle of variation of potential [93].

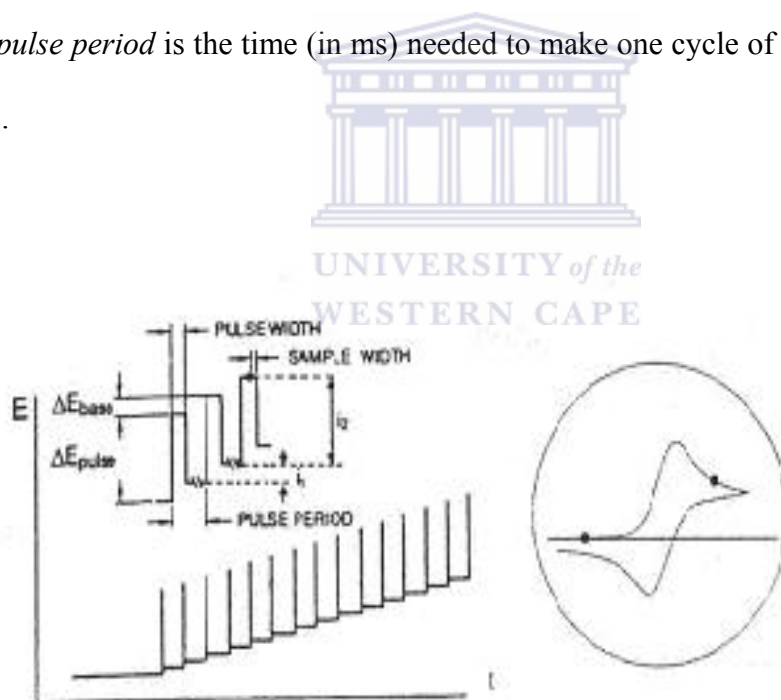


Figure 2.26: Potential-time pulses in Differential Pulse Voltammetry (DPV) [93]

In **Figure 2.26** it is shown that during the pulse period the current is periodically sampled twice, i.e. before the pulse, i_1 , and at the end of the pulse, i_2 , respectively. It also shows that when the two currents are subtracted, i.e. $(i_2 - i_1)$, most of the capacitive currents are eliminated. This ensures that a differential-pulse voltammogram is a plot of the difference $(i_2 - i_1)$ against the potential increase. A typical differential pulse voltammogram is also shown in **Figure 2.27** [93].

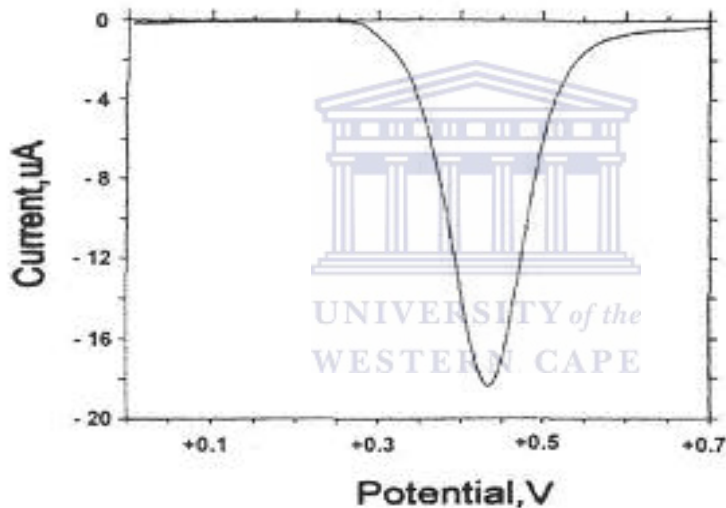


Figure 2.27: A typical voltammogram in Differential Pulse Voltammetry (DPV) [93]

In DPV it is noted that for reversible electron transfers, the peak potential is almost coincident with the formal potential, $E^{\circ'}$, value of the redox couple under study, according to the equation:

$$E_p = E^{\circ'} - \frac{\Delta E_{pulse}}{2} \quad (2.32)$$

but ΔE_{pulse} is usually low at approximately 50 mV.

The width of the peak at half height ($\Delta E_{p/2}$) for a reversible process can be calculated by the equation:

$$\Delta E_{p/2} = 3.52 \frac{RT}{nF} \quad (2.33)$$

or at a temperature of 25 °C the equation becomes:

$$\Delta E_{p/2} = \frac{90.4}{n} (mV) \quad (2.34)$$

Differential pulse voltammetry (DPV) is particularly useful to determine accurately the formal electrode potentials of partially overlapping consecutive electron transfers [93].

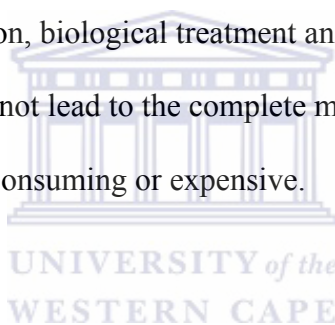
Differential pulse voltammetry can be used in the identification of any species that appears at the surface of the electrode during a scan because each redox species generates an individual symmetrical peak.

Differential pulse voltammetry together with SWV and CV are complimentary methods which could be used for the estimation of the formal potential of redox couples. The formal potential is important for the analysis of the electrochemical behaviour of the conducting polymers and the identification of the redox processes attributed by the phenols.

2.25 Conclusion

Large numbers of industries are characteristics of phenol and phenol derivative compounds as by-products and is expected to be as such well into the future. These phenolic compounds are harmful to all living creatures, including humans. The US Environmental Protection Agency lists 11 phenolic compounds as priority pollutants and is considered to be one of the major water pollutants that need detected, recovered, removed or destroyed.

The treatment processes normally used to treat industrial wastewater containing phenols includes: incineration, adsorption, biological treatment and chemical or electrochemical oxidation, but most of them do not lead to the complete mineralisation of these phenolic compounds, or are either time consuming or expensive.



However, the phenolic compounds must first be detected before it can be treated.

Traditional methods are expensive, some need sample pre-treatment involving separation, extraction and/or adsorption and these can be time-consuming and complex and cannot be taken to the reaction sites.

There is a huge challenge to create a cheap a sensor for phenol and phenolic compounds detection with superior performance for reliable use. In biosensors the signal is not due to direct oxidation of phenol at the electrode, so that electrode fouling is far from being as severe as that observed at bare electrode surfaces or even it does not occur at all.

Nonetheless, the high cost and the critic storage of the biological components limit the practical application of such biosensors.

Electrically conducting nanostructured polymers (e.g. PANI and derivatives) as redox mediator on electrodes for phenolic compounds detection are proposed in this study. Future work into designing out the complexity of the phenolic sensor must be carried out before a cheap, commercial phenolic sensor is viable.



2.26 References

- [1] G. W. Ware, *Reviews of Environmental Contamination and Toxicology*, vol. 126, Springer (Ed.), New York, (1992)
- [2] A. Kaishieva, I. Iliev, R. Kazareva, S. Christov, U. Wollenberger and F. Scheller, *Sens. Act. B*, 33 (1996) 39
- [3] J. Svitel and S. Miertus, *Environ. Sci. Technol.*, 32 (1998) 828
- [4] S. M. Rosatto, L. T. Kubota and G. O. Neto, *Anal. Chim. Acta*, 390 (1999) 65
- [5] R. S. Freire, N. Duran and L. T. Kubota, *J. Braz. Chem. Soc.*, 13 (2002) 456
- [6] S. Esplugas, P. L. Yue and M. I. Perves, *Wat. Res.*, 28 (1994) 1323
- [7] A. Mills and S. Morris, *J. Photochem. Photobiol. A: Chem.*, 71 (1993)
- [8] K. O'Shea and C. Cardona, *J. Org. Chem.*, 59 (1994) 5005
- [9] J. Qin, Q. Zhang and K. T. Chuang, *Appl. Cat. B: Env.*, 29 (2001) 115
- [11] G. Marko-Vagra and D. Barceló, *Chromatographia*, 34 (1992) 146
- [12] E. Nieminen and P. Heikkilä, *J. Chromatogr.*, 360 (1986) 271
- [13] D. Diamond, *Principles of Chemical and Biological Sensors*, John Wiley & Sons, Inc (1998)

- [14] C. Johans, J. Clohessy, S. Fantini, K. Kontturi and V.J. Cunnane, *Electrochem. Commun.*, 4 (2002) 227-230
- [15] A.R. Hopkins, R.A Lipeles and W.H. Kao, *Thin Solid Films*, (2004) 474 – 480
- [16] S. C. Raghavenda, S. Khasim, M. V. N. Ambika-Prasad and A. B. Kulkarn, *Bulletin of Mater. Sci.*, 26 (2004) 733
- [17] M. S. Cho, S. Y. Park, J. Y. Hwang and H. J. Choi, *Mater. Sci. & Engin.*, 24 (2004) 15
- [18] S. Pruneanu, E. Veress, I. Marian and L. Onuciu, *J. Mater. Sci.*, 34 (1999) 2733
- [19] M-K. Park, K. Onishi, J. Locklin and F. Caruso, *Langmuir*, 19 (2003) 8550
- [20] P. Bernier, S. Lefrant and G. Bidan, *Advances in Synthetic Metals – Twenty years of Progress in Science and Technology*, Elsevier, (1999)
- [21] T. Skotheim, Ed.; *Handbook of Conducting Polymers*, volume 1, 2 Marcel Dekker: New York, 1986
- [22] K. Wilbourn and R. W. Murray, *J. Phys. Chem.*, 92 (1988) 3642
- [23] J. E. Frommer and R. R. Chance, *In Encyclopedia of Polymer Science and Engineering*, Vol. 5; Wiley: New York, 1986
- [24] J. Heinze, *Electronically Conducting Polymers: In Topics in Current Chemistry*, Vol. 152; Springer-Verlag: Berlin, 1990
- [25] P. G. Pickup, *J. Chem. Soc. Faraday Trans.*, 86 (1990), 3631

- [26] T. C. Chung, J. H. Kaufman, A. J. Heeger and F. Wudl, *Phys. Rev. B*, 30 (1984), 702
- [27] J. Brédas, R. Chance and R. Silbey, *Phys. Rev. B*, 26 (1982), 5843
- [28] A. G. Macdiarmid, *Synth. Met.*, 125 (2001), 11
- [29] A. J. Heeger, *Synth. Met.*, 125 (2001), 23
- [30] S. Bikas Kar, *Studies on electromechanical sensors and actuators based on conducting polymers*, Unpublished PhD.Thesis University of Pune (India) (2005)
- [31] Y. Cao, A. Andreatta, A. Heeger and P. Smith, *Polymer*, 30 (1989) 2305
- [32] S. A. Chen and C. C. Tsai, *Macromolecules*, 26 (1991) 2234
- [33] Y. Wei, J. Tian, A. G. MacDiarmid, J. G. Masters, A. L. Smith and D. Li, *J. Chem. Soc. Chem. Commun.*, 7 (1994) 552
- [34] P. Beadle, S. P. Armes, P. Cottesfeld, C. Mambourquette, R. Houlton, W. D. Andrew and S. F. Agnew, *Macromolecules*, 25 (1992) 2526
- [35] N. Somnathan and G. Wegner, *Ind. J. Chem.*, 33A (1994) 572
- [36] S. A. Kanhegaokar, *Studies on conducting polymers, synthesis and characterization of conducting polymer blends*, Unpublished PhD.Thesis University of Pune (India) (2004)
- [37] H. Naarmann and P. Strohrriegel, in *Handbook of Polymer Synthesis, Part- B* (Ed: H.R. Kricheldorf), Marcel Dekker, New York (1992)

- [38] J. C. Chiang, A.G. MacDiarmid, *Synth. Met.*, 13 (1986) 193
- [39] R. Kiebooms, R. Menon and K. Lee, in *HandBook of Advance Electronic and Photonic Materials and Devices*, (Ed: H. S. Nalwa), Academic Press, CA, USA 2001, Vol. 8
- [40] A. G. Green and A. E. Woodhead, *J. Chem. Soc.*, 97 (1910) 2388
- [41] G. Zotti, S. Cattarin and N. Comisso, *J. Electroanal. Chem.*, 177 (1988) 387
- [42] E. I. Iwuoha, D. S. de Villaverde, N. P. Garcia, M. R. Smyth and J. M. Pingarron, *Biosens. & Bioelectr.*, 12 (1997) 749-761
- [43] N. G. R. Mathebe, A. Morrin and E. I. Iwuoha, *Talanta*, 64 (2004) 115-12
- [44] D. Concalves, D. S dos Santos, Jr., L. H. C. Mattoso, F. E. Karasz, L. Akcelrud and R. M. Faria, *Synth. Met.*, 90 (1997) 5
- [45] L. Huang, T. Win and A. Gopalan, *Mater. Lett.*, 57 (2003) 1765
- [46] J. Widera, B. Palys, J. Bukowska and K. Jackowska, *Synth. Met.*, 94 (1998) 265
- [47] L. Huang, T. Win and A. Gopalan, *Synth. Met.*, 130 (2002) 155
- [48] M. Trojanowicz, T. K. vel Krawczyk and P. W. Alexander, *Chem. Anal.*, 42 (1997), 199
- [49] P. N. Bartlett and P. R. Birkin, *Synth. Met.*, 61 (1993), 15
- [50] V. Misoska, J. Ding, J. M. Davey, W. E. Price, S. F. Ralph and G. G. Wallace, *Polymer*, 42 (2001), 8571

- [51] J. M. Davey, S. F. Ralph, C. O. Too, G. G. Wallace and A. C. Partridge, *React. Func. Polym.*, 49 (2001), 87
- [52] A. J. Killard, S. Zhang, H. Zhao, R. John, E. I. Iwuoha and Smyth, M.R., *Anal. Chim. Acta*, 400 (1999), 109
- [53] M.G. Han, S.K. Cho, S.G. Oh and S. S. Im, *Synth. Met.*, 126 (2002) 53
- [54] M. Mazur, M. Tagowska, B. Palys and K. Jackowska, *Electrochem. Comm.*, 5 (2003) 403
- [55] S. Trassatti, *Int. J. Hydrogen Energy*, 20 (1995) 835
- [56] A. Wieckowski (Ed.), *Interfacial electrochemistry: theory, experiment and applications*. Marcel Dekker, New York, 1999
- [57] A. Malinauskus, *Synth. Met.*, 107 (1999) 75
- [58] J. Wang, *Electrochemical Sensors For Environmental Monitoring: A Review of Recent Technology Solicitation*, No LV-94-012 (2005)
- [59] R. W. Catrall, *Chemical Sensors*, Oxford University Press Inc., New York 1997
- [60] J. Abdullah, M. Ahmad, N. Karupiah, L. Y. Heng and H. Sidek, *Sens. & Act. B*, 114 (2006) 604
- [61] A. Lindgren, J. Emnéus, T. Ruskas, L. Gorton and G. Marko-Varga, *Anal. Chim. Acta*, 347 (1997) 51
- [62] B. Wang and S. Dong, *J. Electroanal. Chem.*, 487 (2000) 45
- [63] C. Nistor and J. Emnéus, *Waste Management*, 19 (1999) 147

- [64] C. K. Mathews and K. E. Van Holde, *Biochemistry*, Redwood City, California: The Benjamin/Cummings Publishing Company (1990)
- [65] L. Stryer, *Biochemistry*, 2nd edition. San Francisco: W.H. Freeman and Company (1981)
- [66] J. Fu and M. Ji, *Env. Inform. Arch.*, 2 (2004) 983
- [67] J. –G. Lin, C. –N. Chang, J. –R. Wu and Y. –S. Ma, *Wat. Sci. Tech.*, 34 (1996) 41
- [68] J. McGuire, C. F. Dwiggin and P. S. Fedkiw, *J. Appl. Electrochem.*, 15 (1985) 53
- [69] O. Koyama, Y. Kamagata and K. Nakamura, *Wat. Res.*, 28 (1994) 895
- [70] A. Al-Enezi, H. Shaban and M. S. E. Abdo, *Desal.*, 95 (1994) 1
- [71] F. Wajon, D. H. Rosenblatt and E. P. Burrows, *Environ. Sci. Technol.*, 16 (1982) 396
- [72] S. Angelino and M. C. Gennaro, *Anal. Chim. Acta*, 346 (1997) 61
- [73] R. V. Gregoy, T. A. Skotheim, R. L. Elsenbaumer, J. R. Reynolds, in *Handbook of Conducting Polymers* (Eds), Marcel Dekker, New York (1998)
- [74] A. Guiseppi-Elie, G. G. Wallace and Tomakazu Matsue, in *Handbook of Conducting Polymers* (Ed: T.A. Skotheim), Marcel Dekker, New York (1997)
- [75] M. A. Heras, S. Lupu, L. Pigani, C. Pirvu, R. Seeber, F. Terzi and C. Zanardi, *Electrochim. Acta*, 50 (2005) 1685
- [76] H. Notsu, T. Tatsuma and A. Fujishima, *J. Electroanal. Chem.*, 523 (2002) 86

- [77] M. D. P. T. Sotomayor, A. A. Tanaka and L. T. Kubota, *J. Electroanal. Chem.*, 536 (2002) 71
- [78] S. S. Rosatto, P. T. Sotomayor, L. T. Kubota and Y. Gushikem, *Electrochim. Acta*, 47 (2002) 4451
- [79] E. I. Iwuoha, A. R. Williams-Dottin, L. A. Hall, A. Morrin, G. N. Mathebe, M. R. Smyth and A. Killard, *Pure Appl. Chem.*, 76 (2004) 789
- [80] Y. Ni, L. Wang and S. Kokot, *Anal. Chim. Acta*, 431 (2001) 101
- [81] M. S. Ureta-Zañartu, P. Bustos, M. C. Diez, M. L. Mora and C. Gutiérrez, *Electrochim. Acta*, 46 (2001) 2545
- [82] Y. Lei, P. Mulchandani, W. Chen, J. Wang and A. Mulchandani, *Electroanal.*, 15 (2003) 14
- [83] M. H. Priya and G. Madras, *J. Photochem. Photobio. A: Chem.*, 179 (2006) 256
- [84] P. Cañizares, J. Lobato, R. Paz, M. A. Rodrigo and S. Sáez, *Wat. Research*, 39 (2005) 2687
- [85] S. Liu, J. Yu and H. Ju, *J. Electroanal. Chem.*, 540 (2003) 61
- [86] M. A. Kim and W-Y. Lee, *Anal. Chim. Acta*, 479 (2003) 143
- [87] P. Skládal, N. O. Morozova and A. N. Reshetilov, *Biosens. & Bioelectr.*, 17 (2002) 867
- [88] G. Arslan, B. Yazici and M. Erbil, *J. Hazard. Mat. B*, 124 (2005) 37
- [89] S. A. Kane, E. I. Iwuoha and R. Smyth, *Analyst*, 123 (1998) 2001

- [90] T. Mafatle and T. Nyokong, *Anal. Chim. Acta*, 354 (1997) 307
- [91] P. Önnérkjord, J. Emnéus, G. Marko-Varga, L. Gorton, F. Ortega and E. Dominguez, *Biosens. & Bioelectr.*, 10 (1995) 607
- [92] P. Monk, *Fundamentals of Electro-Analytical Chemistry*, Chichester: John Wiley & Sons Ltd (2001)
- [93] P. Zanello, *Inorganic Electrochemistry. Theory, Practice and Application*, Cambridge, UK: The Royal Society of Chemistry (2003)
- [94] A. J. Bard and L. R. Faulkner, *Electrochemical Methods. Fundamentals and Applications 2nd*, New York: John Wiley & Sons, Inc. (2001)
- [95] T. J. Kemp, Southampton Electrochemistry Group In. *Instrumental Methods in Electrochemistry*, Ellis Horwood Ltd: Chichester, (1990)
- [96] M. A. Maluleke, *Electromembrane reactors for the decomposition of organic pollutants in potable and wastewaters*, Published PhD. Thesis, University of the Western Cape, RSA (2003)
- [97] A. Morrin, *Characterisation and optimisation of an amperometric biosensor for use in electrochemical immunosensing*. Report for Transfer to PhD Register. Dublin City University, Ireland (2002)

Chapter 3

Preparation of Dopants and Conducting Nanostructured Polyanilines

3.1 Introduction

The previous chapter reviewed the relevant literature concerning conducting polymers, sensors, phenolic compounds and different phenol sensors. This chapter deals with the syntheses of bulky dopants: anthracene sulfonic acid (ASA), phenanthrene sulfonic acid (PSA) and the incorporation of these dopants into conducting polymers to form soluble conducting polymeric nanostructures.

Several studies have been done in order to improve the solubility of polyaniline. One method is the polymerisation of derivatives of aniline, which include alkyl [1-3], alkoxy [4] and sulfonated anilines [5]. Another technique was to use functionalised protonic acids, mostly sulfonic acids, as dopants. These acids include p-toluene-sulfonic acid [6], benzene-sulfonic acid [6], camphor-sulfonic acid [7], poly(styrene)-sulfonic acid [8], sulfosalicylic acid [9] and phosphoric acid esters [10].

The conducting polymers in this study were prepared via oxidative polymerisation of monomers aniline (ANI), *o*-methoxyaniline (OMA) and 2,5 dimethoxyaniline (DMA) using the bulky dopants, anthracene (ASA) and phenanthrene sulfonic (PSA) acid. The bulky dopants normally increase the surface area of the conducting polymer which significantly differs from the macroscopic properties. The opportunity of increasing the solubility and surface area of the conducting polymers by adding bulky dopants during polymerisation was explored. The increased solubility and surface area will result in improved catalytic efficiency.

3.2 Synthesis of the dopants: Anthracene Sulfonic Acid (ASA) and Phenanthrene Sulfonic Acid (PSA)

3.2.1 Chemicals

The chemical reagents anthracene and phenanthrene were purchased from Sigma-Aldrich and were used as obtained. All other chemical reagents were of analytical grade and were used as obtained without further purification: sulfuric acid (Fluka), fuming sulfuric acid (Fluka) and sodium hydroxide (Sigma-Aldrich). All chemicals were purchased in Cape Town, South Africa.

3.2.2 Synthesis of Anthracene sulfonic acid and phenanthrene sulfonic acid

A 10 mL of fuming H_2SO_4 was diluted with 10 mL H_2SO_4 (6 M) and the mixture was diluted to 100 mL in a volumetric flask. 50 mL of the above solution was added to a round bottom flask that contained 2 g of anthracene or phenanthrene. The contents were heated to boiling in an oil bath (temperature between 120 – 140 °C) fitted with a condenser and thermometer. The mixture was refluxed for 2-3 hours with constant

shaking to immerse reactants into solution. The mixture was then poured into crushed ice for 20 minutes and the unreacted anthracene/phenanthrene was filtered off. 10 mL of a 50% NaOH was added to the mixture and put in a refrigerator to crystallize, to form a white anthracene- or phenanthrene sulfonic salt. The salt was then hydrolysed to form the anthracene/phenanthrene sulfonic acid [11].

3.3 The Preparation of Polyaniline (PANI), Poly(*ortho*-methoxyaniline) (POMA) and Poly(2,5 dimethoxyaniline) (PDMA) with Anthracene Sulfonic Acid (ASA) and Phenanthrene Sulfonic Acid (PSA)

3.3.1 Chemicals

The monomers Aniline, *ortho*-methoxyaniline (*o*-anisidine) and 2,5 dimethoxyaniline were purchased from Sigma-Aldrich and twice distilled under vacuum and polymerised immediately after distillation. Anthracene sulfonic acid and phenanthrene sulfonic acid were chemically synthesised in the laboratory (**Section 3.2**). All other chemical reagents were of analytical grade and were used as obtained without further purification: anthracene (Sigma-Aldrich), phenanthrene (Sigma-Aldrich), hydrochloric acid (Fluka), ammonium persulphate (Fluka), methanol (Fluka), dimethyl ether (Fluka) and ether (Fluka). All chemicals were purchased in Cape Town, South Africa.

3.3.2 Synthesis of polyaniline/Anthracene sulfonic acid nanostructures and polyaniline/Phenanthrene sulfonic acid nanostructures

Aniline (0.2592 mL, 0.142 M) was added into 20 mL of deionised water, whereby anthracene sulfonic acid (0.2592 mg) was added. The mixture was heated for 20 – 30 minutes at 50 °C while vigorously stirred. An aqueous solution of ammonium persulfate (APS) (0.1 M) was added dropwise to the hot solution. The mixture was cooled down to room temperature while continuously stirred for 24 hours. The product was filtered and washed with deionised water, methanol and dimethyl ether 3 times respectively, to remove impurities such as APS, free ASA and unreacted 2,5 dimethoxyaniline. The same procedure was used for the synthesis of poly(2,5 dimethoxyaniline)/Phenanthrene sulfonic acid nanostructures [12].

3.3.3 Synthesis of poly(*ortho*-methoxyaniline)/Anthracene sulfonic acid nanostructures and poly(*ortho*-methoxyaniline)/Phenanthrene sulfonic acid nanostructures

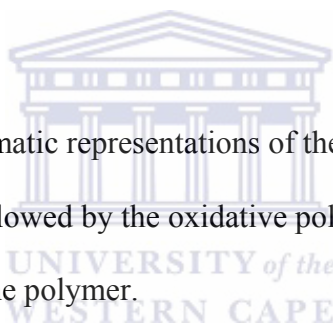
Poly(*ortho*-methoxyaniline)/Anthracene-/Phenanthrene sulfonic acid nanostructures were prepared by adopting a similar procedure as in **Section 3.3.2**. *ortho*-methoxyaniline (0.26 mL) in 20 mL of deionised water and anthracene sulphonic acid (0.2592 mg) were placed in a 100 mL beaker and. The mixture was heated for 30 min at 50 °C while stirring vigorously. An aqueous solution of ammonium persulphate (APS) (0.1 M) was added dropwise to the hot solution. The mixture was cooled down to room temperature while continuously stirred for 24 hrs. The product was filtered and washed with deionised water, methanol and dimethyl ether 3 times respectively, to remove impurities such as APS, free ASA and unreacted 2,5 dimethoxyaniline. The same procedure was used for the synthesis of poly (*ortho*-methoxyaniline)/Phenanthrene

sulfonic acid nanostructures [12 - 13].

3.3.4 Synthesis of poly(2,5 dimethoxyaniline)/Anthracene sulfonic acid nanostructures and poly(2,5 dimethoxyaniline)/Phenanthrene sulfonic acid nanostructures

A 0.0334 g of 2,5 dimethoxyaniline (0.011 M) in 20 mL of deionized water and anthracene sulfonic acid and phenanthrene sulfonic acid (0.2592 g) were placed in a 100 mL beakers respectively. The same procedure was then followed as outlined in **Section 3.3.3** for the synthesis of poly(*ortho*-methoxyaniline)/Anthracene-/Phenanthrene sulfonic acid nanostructures [12 - 13].

Figures 3.1 and **3.2** gives schematic representations of the syntheses of anthracene and phenanthrene sulfonic acids followed by the oxidative polymerisation of the monomer 2,5 dimethoxyaniline to form the polymer.



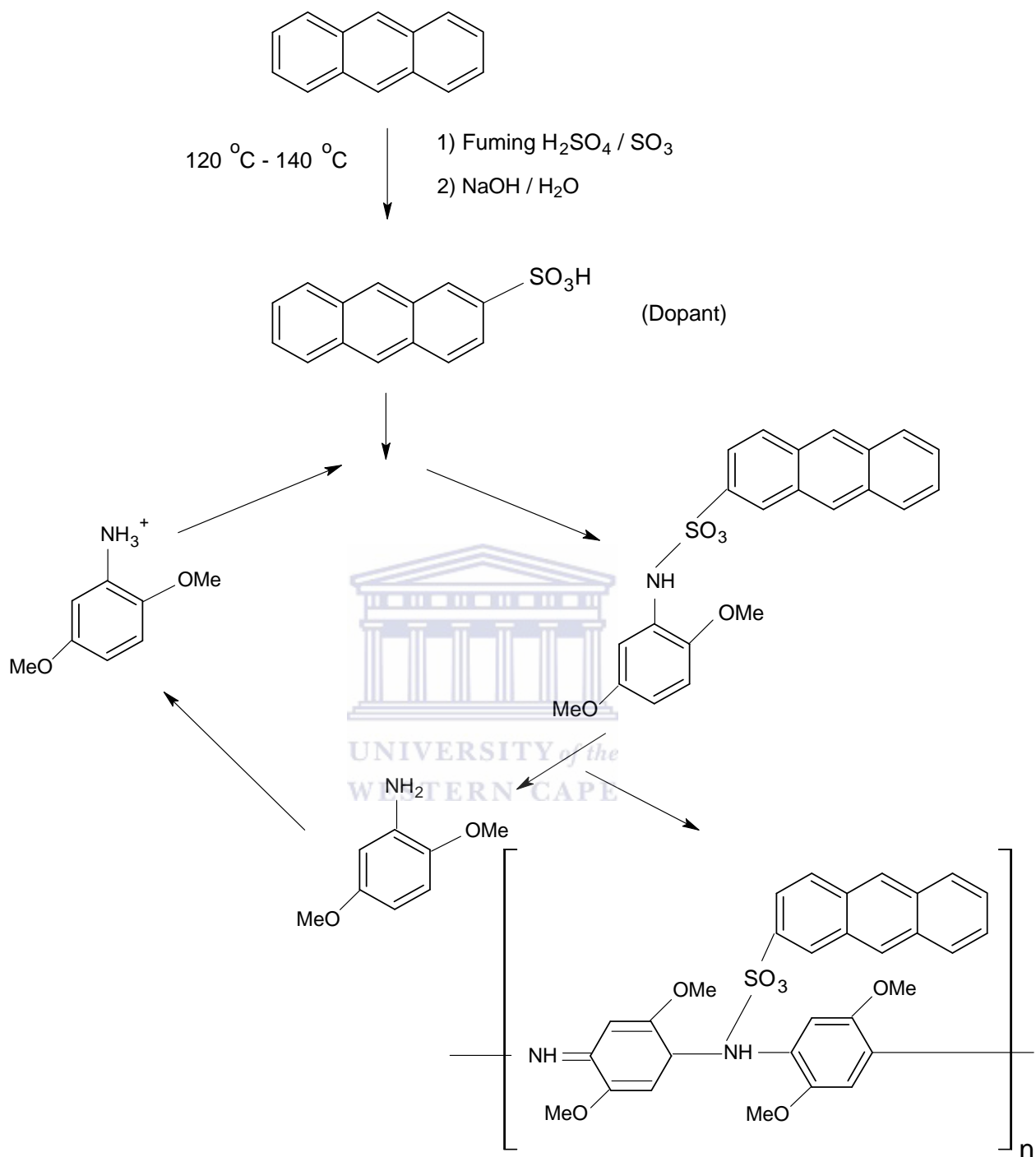


Figure 3.1: Schematic representation of the synthesis and incorporation of anthracene sulphonic acid (ASA) in the polymerisation of 2,5 dimethoxyaniline (DMA)

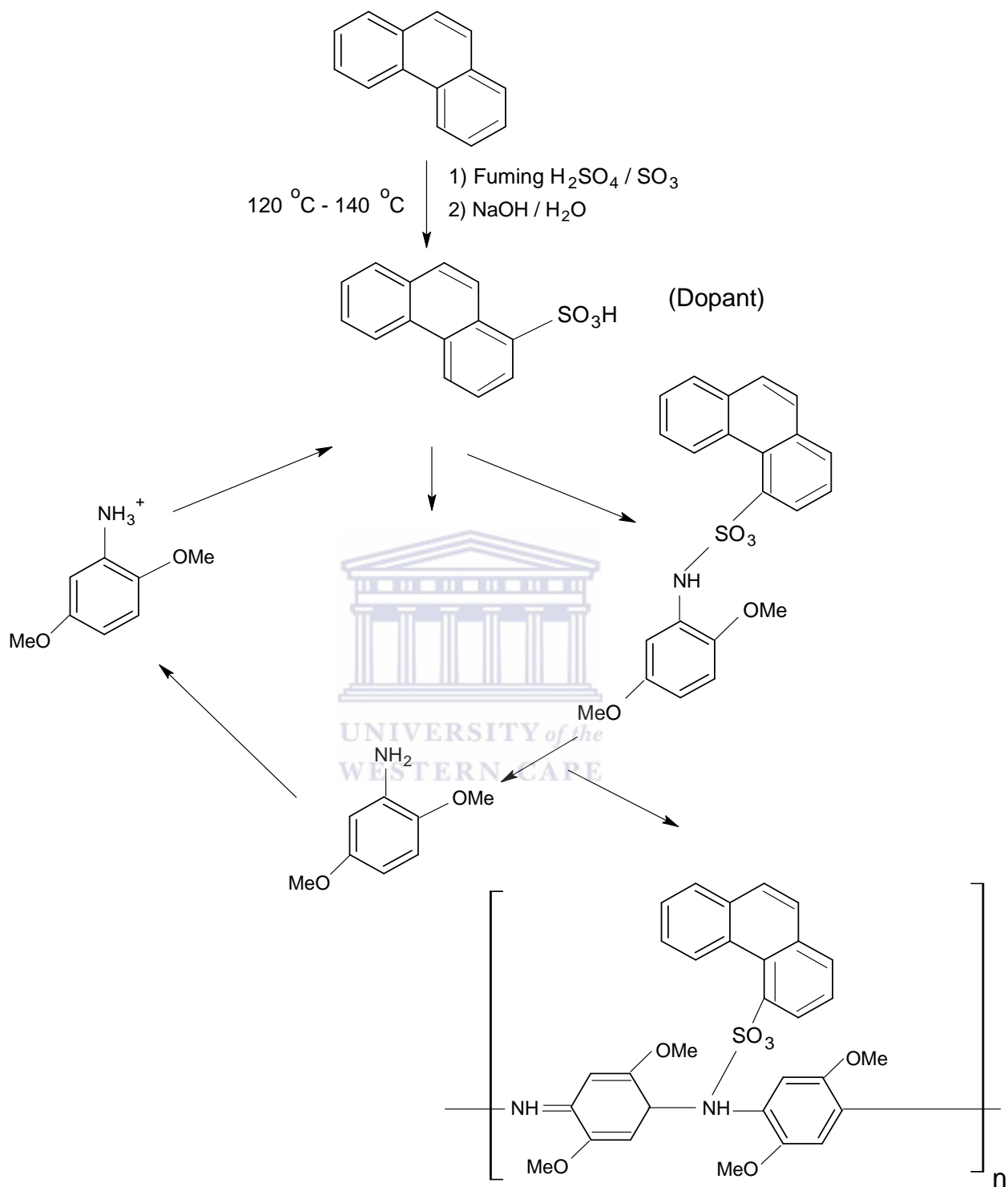


Figure 3.2: Schematic representation of the synthesis and incorporation of phenanthrene sulphonic acid (PSA) in the polymerization of 2,5 dimethoxyaniline (DMA)

3.4. Results and Discussion

The purpose of using a functionalised protonic acid as dopant was so that it would, firstly improve the solubility of the conducting polymer, which will promote the compatibility between the conducting polymer and the solvent as a result of the polar substituents. Secondly, it would increase the surface area when immobilize on an electrode, which will increase the catalytic efficiency [14].

The use of large, bulky protonic acid as dopants was employed to force the insoluble conducting polymer backbone to the inside of the molecule and the soluble dopants sticking out into the solvents [15]. This self-assembly process gives us different morphologies (micelles, tubes, etc.) and sizes (macro, nano, etc.) of the conducting polymers.

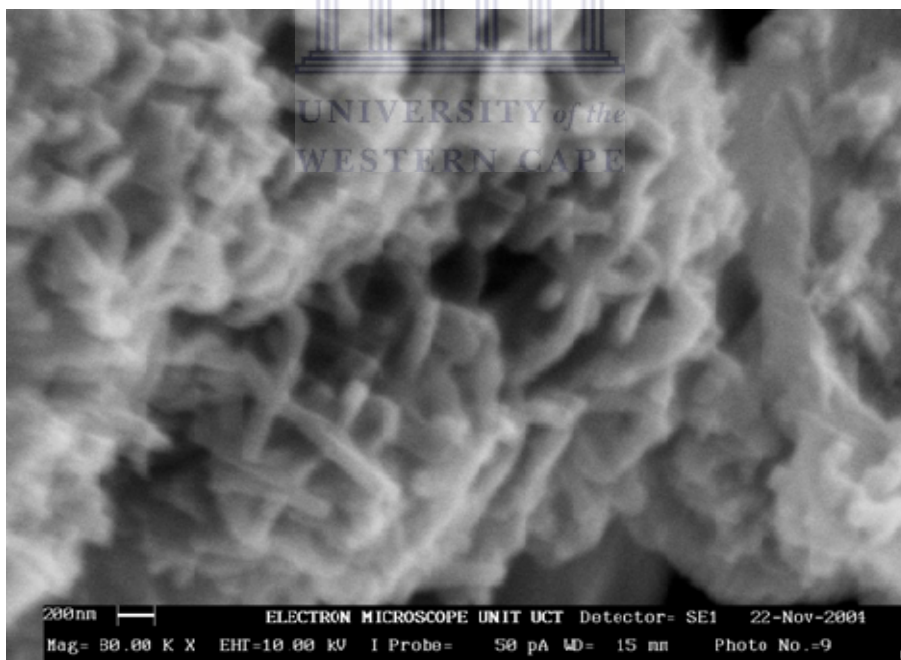


Figure 3.3: SEM micrograph of Polyaniline (PANI) doped with phenanthrene sulfonic acid (PSA)

Figure 3.3 shows a SEM micrograph of polyaniline (PANI) doped with phenanthrene sulfonic acid (PSA). In the micrograph nanostructures (nanotubes or nanofibres) can be seen with diameter between 50 – 100 nm. Nanotubes or nanofibres were also observed when PDMA was doped with PSA (**Figure 3.4**) with observed diameters between 50 and 100 nm [10].



Figure 3.4: SEM micrograph of Poly(2,5 dimethoxyaniline) (PDMA) doped with phenanthrene sulfonic acid (PSA)

However, when POMA was doped with PSA in **Figure 3.5**, micelle (egg-like) structures and disc-like formations with cross sectional diameter in the 100 to 200 nm range were formed. This might be a result of POMA, which is hydrophobic, being forced inside and the bulky groups of phenanthrene sulphonic acid, which is hydrophilic, on the outside in the micelle formation. The flat round, disc-like formations could be the effect of the different isomers of PSA formed during synthesis [16].

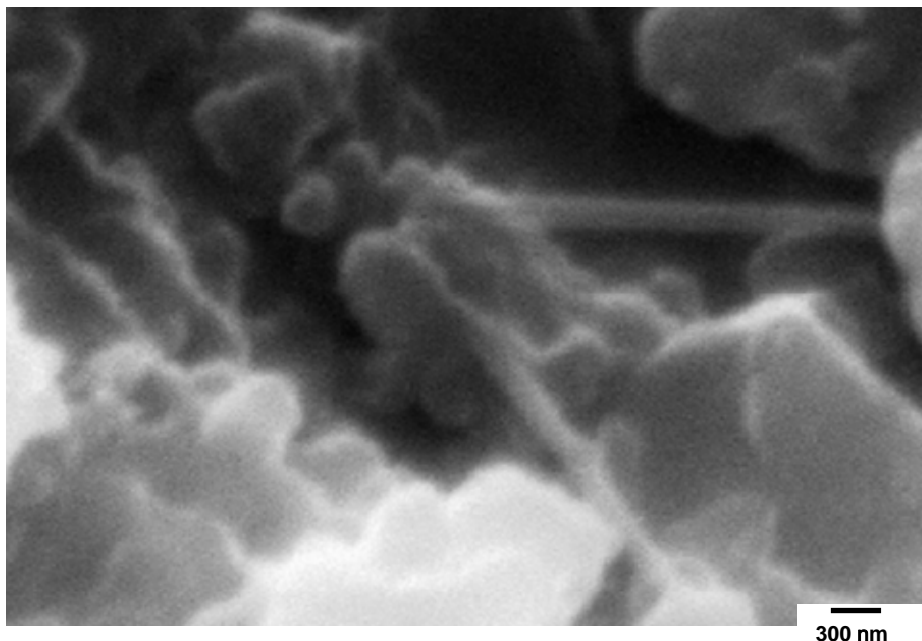


Figure 3.5: SEM micrograph of Poly(*ortho*-methoxyaniline) (POMA) doped with phenanthrene sulfonic acid (PSA)



3.5 Conclusion

Improving the solubility and increasing the surface area with doping the conducting polymers with large, bulky dopants was effective. SEM micrographs showed different nanostructured morphologies for the polymers, which include nanotubes or nanofibres for PANI/PSA and PDMA/PSA and nanosize micelles and disc-like structures for POMA/PSA.

To explore the benefit of increased solubility and surface area on reactivity of the electrode surface area, electrochemical characterisation and electro-catalytic testing were performed on the electrodes prepared on nanostructured conducting polymers.



3.6 References

- [1] A. Ray and A.G. MacDiarmid, *J. Phys. Chem.*, 93 (1989) 495
- [2] E.M. Geniès and P. Noel, *J. Electroanal. Chem.*, 310 (1991) 89
- [3] L.Wang, X. Jing and F. Wang, *Synth. Met.* 41 – 43 (1991) 739
- [4] D. Maccines and L.B. Funt, *Synth. Met.* 25 (1988) 235
- [5] E.M. Geniès and P. Noel, *Synth. Met.*, 55 - 57 (1993) 4192
- [6] A. Kobayashi, X. Xu, H. Ishikawa, M. Satoh and E. Hasegawa, *J. Appl. Phys.*, 72 (1992) 5702
- [7] Y. Coa, P. Smyth and A.J. Heeger, *Synth. Met.*, 48 (1992) 91
- [8] Y. Kang, M.H. Lee and S.B.Rhee, *Synth. Met.*, 52 (1992) 319
- [9] D.C. Trivedi and S.K. Dhavan, *Synth. Met.*, 58 (1993) 309
- [10] A. Proń, J. Laska, J. E. Österholm and P. Smith, *Polymer*, 34 (1993) 4235
- [11] A.I. Vogel, in *Vogel's Text Book of Practical Organic Chemistry*, 5th Ed, Wiley, New York
- [12] Z. Zhang, M. Wan, *Synth. Met.* 128 (2002) 83-89
- [13] Z. Zhang, M. Wan, *Synth. Met.* 132 (2003) 205-212
- [14] W.A.Gazotti, M. dePaoli, *Synth. Met.*, 80 (1996) 263-269

[15] H.J. Qiu and M.X. Wan, *Mater. Phys. Mech.*, 4 (2001) 125 - 128

[16] M.G. Han, S.K. Cho, S.G. Oh, S. S. Im, *Synth. Met.*, 126 (2002) 53-60

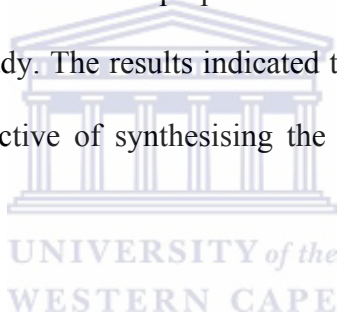


Chapter 4

Characterisation of the Dopants and the Conducting Nanostructured Polyanilines

4.1 Introduction

The previous chapter discussed the preparation and syntheses of the dopants and the polyanilines used in the study. The results indicated that different nanosize polymers were formed. Hence, the objective of synthesising the nanostructure polyanilines was achieved.



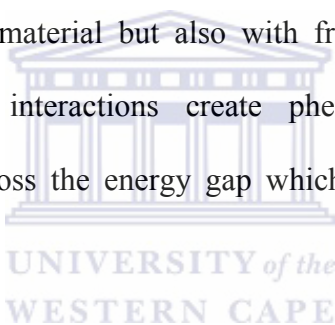
This chapter deals with the characterisation of the dopants anthracene- (ASA), phenanthrene sulfonic acid (PSA) and the conducting polymeric nanostructures used. The conducting polymers were characterised using: FT-IR Spectroscopy, UV/vis Spectroscopy, Scanning Electron Microscopy (SEM) and Electrochemical Spectroscopy including Cyclic Voltammetry.

4.2 Experimental

4.2.1 Fourier Transform Infrared Spectroscopy (FTIR)

FT-IR has provided valuable information regarding the formation of the sulfonic acids and the conducting polymers. The FTIR measurements were recorded as a mixture of KBr (99%) and the polyaniline sample (1%) pellet using a Perkins Elmer, Paragon 1000 PC, FTIR spectrometer. The spectrum was recorded in the wavelength region between 400 – 4000 cm^{-1} .

In conducting polymers, the incident infrared (IR) radiation interacts not only with the vibrational excitations of the material but also with free carriers (dopants) and their electronic structures. These interactions create phenomena such as free-carrier absorptions and excitation across the energy gap which can be detected using FT-IR spectroscopy [1].



4.2.2 Ultraviolet visible Spectroscopy (UV-vis)

UV/vis absorbance measurements were recorded at room temperature on a UV/VIS 920 spectrometer (GBC Scientific Instruments, Australia) using a sample (0.005 g) dissolved in 10 mL dimethyl sulfoxide (DMSO).

The fundamental process of doping is a charge-transfer reaction between an organic polymer and a dopant. When charges are removed from (or added to) a polymer upon chemical doping, geometric parameters, such as bond lengths and angles changed. The charge is localized over the region of several repeated units. Since the localized charges

can move along the polymer chain, they are regarded as charge carriers in the polymer chain. These quasi-particles are classified into polarons and bipolarons according to their charge using UV/vis spectroscopy [2].

4.2.3 *Scanning Electron Microscopy (SEM)*

Scanning electron micrographs were performed using a Hitachi X650 scanning electron microscope. The samples were coated with either carbon or gold.

Scanning Electron Microscopy as its name implies the specimen is traversed by an electron beam. The movement is achieved by scanning (raster) coils in the microscope column controlled by a scan generator. The raster pattern of the primary electron beam is synchronized with the scanning pattern of the Cathode Ray Tube (CRT) yielding a point-by-point translation. This by coupling the deflection coils of the CRT to the scanning coils in the microscope a one-to-one presentation of the area scanned is produced. The signals produced, as a result of the beam being rastered across the specimen surface, are collected by an appropriate detector, amplified and displayed on the CRT. The magnification of the image is the relationship between the length of the scan line on the specimen and that on the CRT [3].

4.2.4 *Electrochemical measurements*

All electrochemical experiments were carried out and recorded with a computer connected to a BAS/50W integrated automated electrochemical workstation (Bioanalytical Systems, Lafayette, IN, USA). Cyclic voltammetry was carried out in an electrochemical cell with Ag/AgCl and platinum wire as reference and auxiliary

electrodes, respectively. A platinum disk electrode was used as working electrode. Alumina micropolish and polishing pads (Buehler, IL, USA) were used for electrode polishing. The method basically consists of measuring the current resulting from an applied triangular potential waveform. The potential is cycled within a given potential range at a constant rate and the current is measured as a function of the potential. The rate can vary from as less than 1 mV/s to hundreds of mV/s. When a high enough potential is applied to the electrode to cause oxidation or reduction of a species in solution, a current arises due to the depletion of the species in the vicinity of the electrode surface. As a consequence, a concentration gradient appears in the solution [4-5].

4.3 Characterisation results and discussion

4.3.1 *Fourier Transform Infrared Spectroscopy (FTIR)*

FT-IR has provided valuable information regarding the formation of the sulfonic acids and PANI, POMA and PDMA polymers doped with the sulfonic acids. The spectra were recorded in the wavenumber regions between 400– 4000 cm^{-1} .

Figure 4.1 shows the FT-IR spectra of Anthracene sulfonic acid (ASA) and Phenanthrene sulfonic acid (PSA) where (—) represents ASA and (...) represents PSA. The spectra reveals a striking resemblance between the two sulfonic acids which suggests the existence of the same basic structure.

A broad band at about 3500 cm^{-1} was seen for ASA as a result of the straight fused benzene rings, which was not seen for the bend PSA fused rings. On the other hand, an absorption peak at 485 cm^{-1} and 885 cm^{-1} was seen for PSA and not observed for ASA.

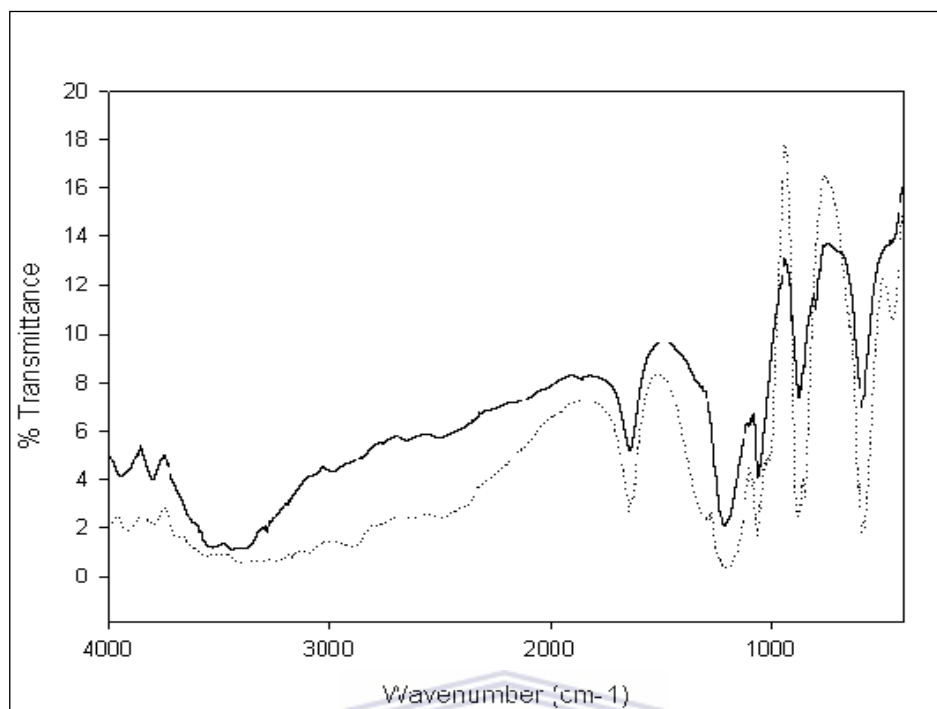


Figure 4.1: FT-IR spectra of (—) Anthracene sulfonic acid (ASA) and (....) Phenanthrene sulfonic (PSA) acid

The presence of the sulfonic acid functionality is seen by the O=S=O stretching vibrations at 1218 (asymmetric) and 1061 cm^{-1} (symmetric) for ASA and 1202 (asymmetric) and 1065 cm^{-1} (symmetric) for PSA.

Other characteristic bands 1639, 876 and 599 cm^{-1} were observed for ASA and 1649, 851 and 594 cm^{-1} for PSA. The strong bands at 1193 cm^{-1} in both ASA and PSA suggesting the presence of SO_3 hydronium sulfonate salts [6-7].

Doping of PANI and its derivatives are known to structurally modify its FT-IR spectra and can also display bands from the dopants used.

Figure 4.2 gives the FT-IR spectra of PANI doped with ASA and PSA. The bands at 1570 cm^{-1} for PANI/ASA and 1595 cm^{-1} for PANI/PSA corresponds to the quinoid rings in the polymer backbone. The corresponding stretching vibration bands for the benzenoid rings occur at 1480 cm^{-1} PANI/ASA and 1495 cm^{-1} for PANI/PSA. The relatively strong bands at 1300 cm^{-1} are assigned to the stretching vibrations of C-N in the quinoid imine units of both polymers [8-10].

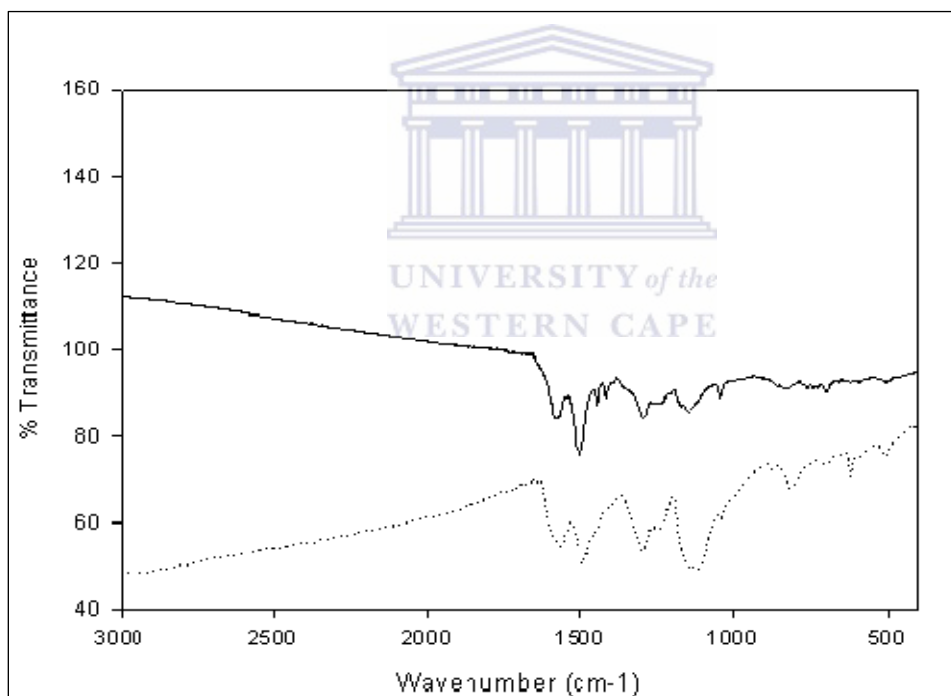
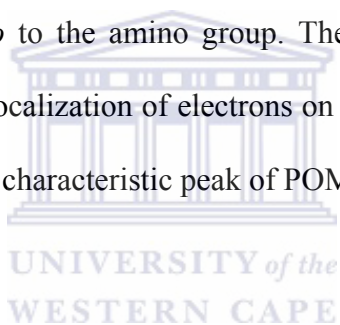


Figure 4.2: FT-IR spectra of (—) PANI-PSA and (.....) PANI-ASA

The bands at 1115 cm^{-1} are assigned to the electronic-like absorption mode of N=Q=N stretching vibrations in the polymer backbones. The bands at 1020 and 505 cm^{-1} for both doped polyanilines are ascribed to the absorption of the $-\text{SOH}_3$ functional group, which

give evidence that polyaniline is doped with ASA and PSA [8-10].

Figure 4.3 display the FT-IR spectra of POMA doped with ASA and PSA, which show similar absorption peaks. The absorption peaks appear almost at the same wavenumbers as that of PANI doped with ASA and PSA, but with small shifts. The band at 1600 cm^{-1} is associated with quinoid structure and 1500 cm^{-1} band with benzoid structure. The shifted quinone imine bands of POMA 1600 cm^{-1} , indicate successful doping with ASA and PSA. The peaks at 800 cm^{-1} in the POMA-ASA and POMA-PSA spectra are characteristic of an *ortho*- or *meta*-substituted aromatic rings and the appearance of the methoxy group which is *ortho* to the amino group. The band at 1170 cm^{-1} is usually considered as a measure of delocalization of electrons on POMA and is referred to as the electronic like band, which is a characteristic peak of POMA conductivity [9, 11, 12].



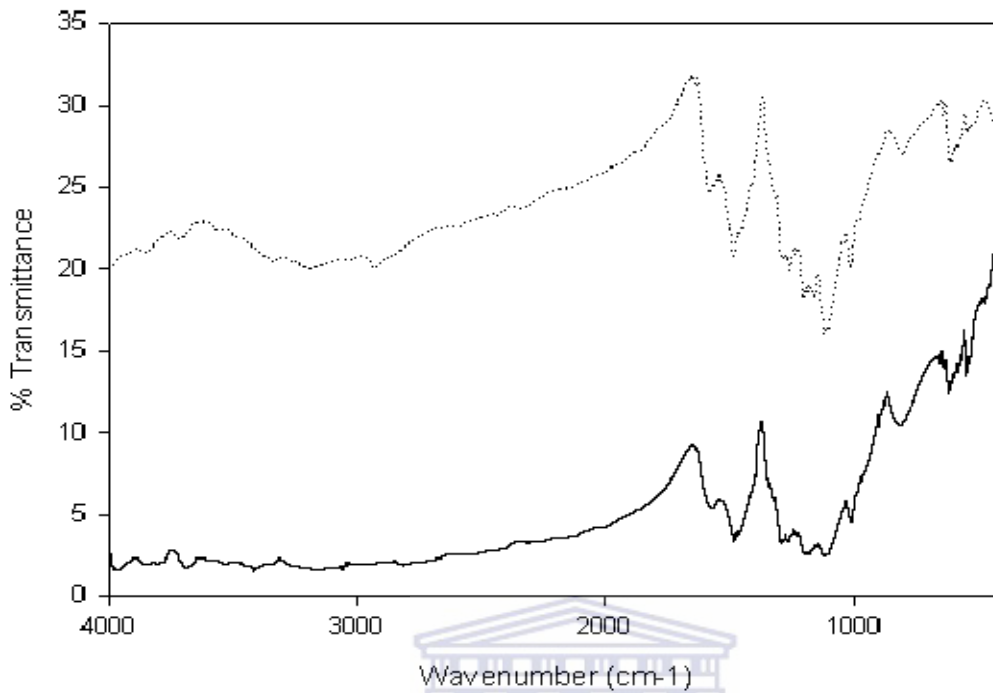


Figure 4.3: FT-IR spectra of (—) POMA-ASA and (....) POMA-PSA

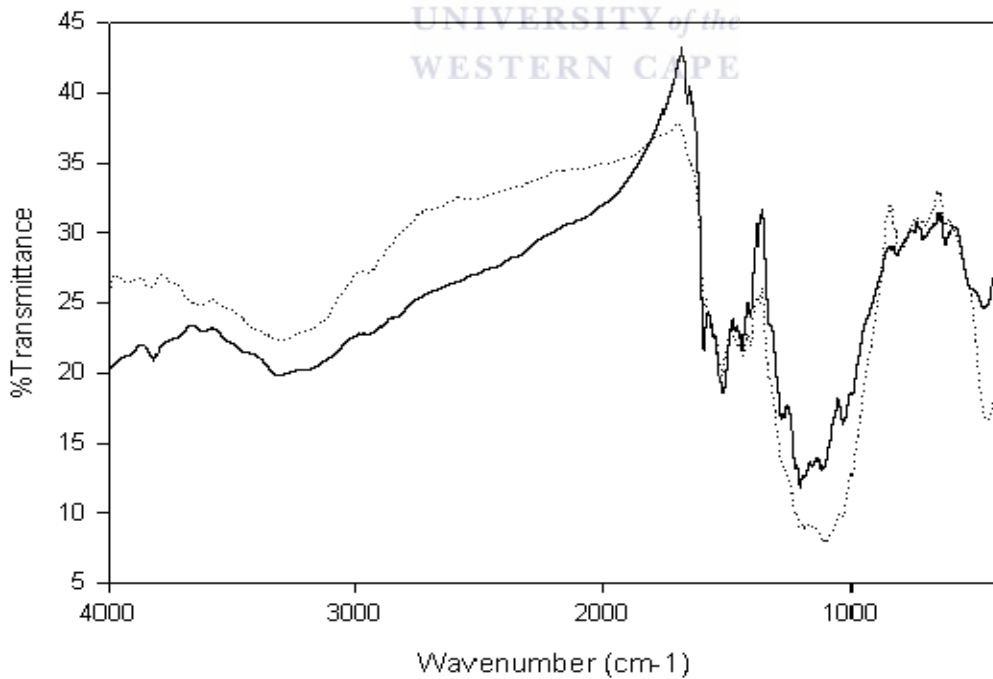


Figure 4.4: FT-IR spectra of (—) PDMA-ASA and (.....) PDMA-PSA

FT-IR spectra of PDMA doped with ASA and PSA are presented in **Figure 4.4**. PDMA-

HCl normally has the major bands at 1594, 1435, 1277, 1115 and 617 cm^{-1} , which are attributed to the stretching vibrations of quinonic-type rings, benzenic-type rings and the characteristic of the p-substituted chains in PANI-HCl polymers, except for a few shifts in the wavenumbers for PDMA/HCl. For PDMA/ASA, the peaks of the quinoid units shift from 1594 and 1152 to 1598 and 1159 cm^{-1} and the stretching vibrations of benzoid ring to 1465 and 1285 cm^{-1} . These shifts suggested changes of environment at the molecular level. The bands at 1115, 1026 and 812 cm^{-1} are revealed to the 1-4 substitution on the benzene ring in PDMA. The absorption band around 1080 cm^{-1} attributed to the presence of S=O stretching bands and confirms the existence of ASA in the polymer complex, suggests the incorporation of ASA into the polymer backbone. FTIR spectrum of PDMA doped PSA have absorptions between 1600 and 1450 cm^{-1} , which are related to the stretching of C-N bonds of benzenic and quinonic rings in the polymer. Absorptions between 1285 and 1154 cm^{-1} related to the asymmetric and symmetric stretching of =C-O-C bonds. The absorption band around 1080 cm^{-1} attributes to the S=O group, also suggests the incorporation of PSA into the polymer backbone [13-14].

4.3.2 Ultraviolet visible Spectroscopy (UV-vis)

UV-vis gives information regarding the sulfonic acids and the doping of PANI, POMA and PDMA with the sulfonic acids. The spectra were recorded in the wavelength regions between 200 – 900 nm.

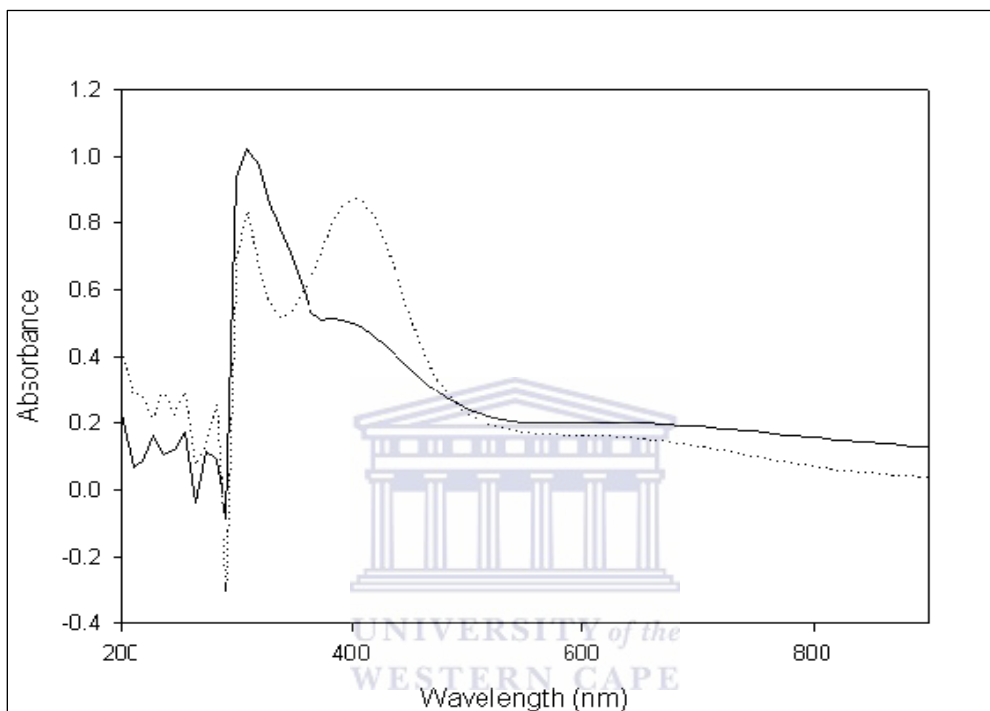


Figure 4.5: UV-visible absorption spectra of the conducting polymers (—) PANI-ASA and (....) PANI-PSA dissolved in DMSO

The doping of PANI with ASA (**Figure 4.5**) have absorption bands at 320 nm, assigned to the $\pi - \pi^*$ transitions of the benzoid structure, at 700 nm due to the exciton absorption of the quinoid structure and at 440 nm due to an intermediate state formed during the electro-oxidation of the leucoemeraldine form of PANI. The band at 450 nm is due to the charged para-coupled phenyl structures and corresponds to phenyl excitons or polarons [18, 19].

Shoulder bands between 200 – 300 nm are assigned to unreacted PANI and ASA in solution. Similar absorption bands were seen for PANI doped with PSA (**Figure 4.5**) with bands at 320 nm, 420 nm and 675 nm [15-17].

The UV-vis absorption spectrum of POMA (**Figure 4.6**) doped with ASA is dominated by 2 absorption bands at 2 selected wavelengths, 350 and 650 nm respectively. The same 2 absorption bands were seen for POMA doped with PSA, but in this case the band at around 650 nm was widened. The same absorption bands were seen for POMA doped with HCl. These bands are associated with π - π^* transition and polaron forms of POMA [15-17].

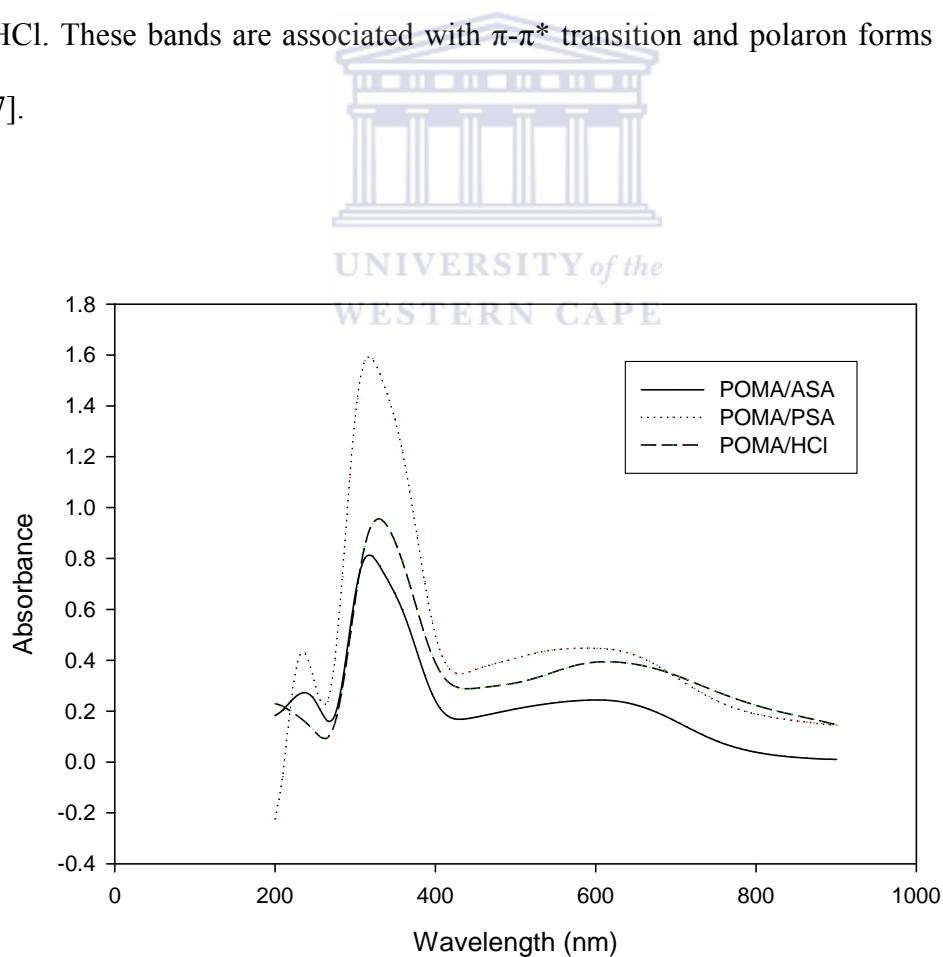


Figure 4.6: UV-visible absorption spectra of the conducting polymers POMA-ASA, POMA-PSA and POMA-HCl dissolved in DMSO

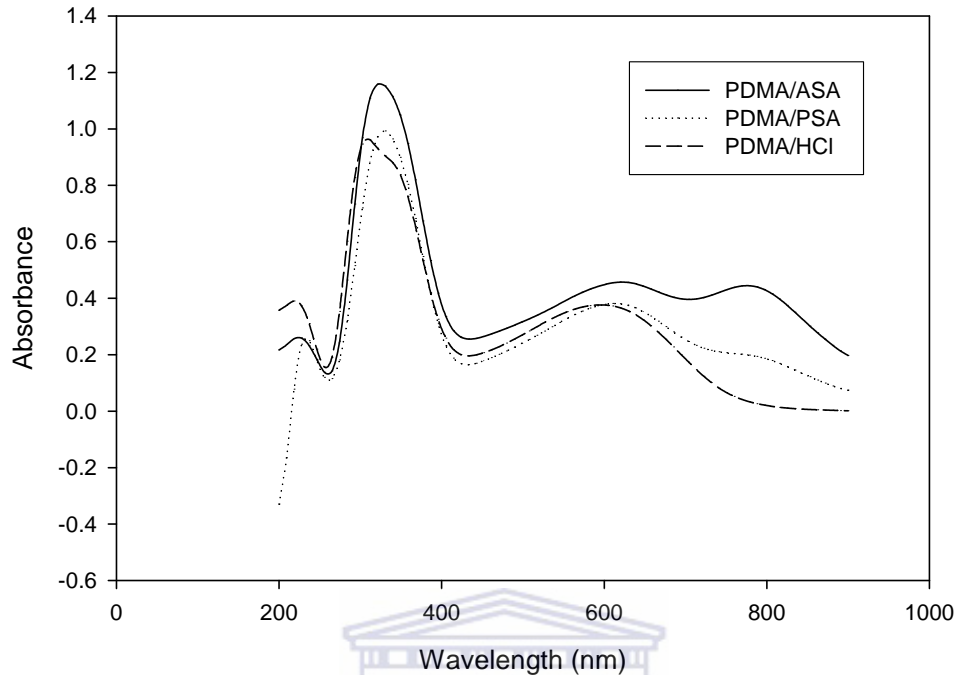


Figure 4.7: UV-visible absorption spectra of the conducting polymers PDMA-ASA, PDMA-PSA and PDMA-HCl dissolved in DMSO

Figure 4.7 shows the UV-visible spectra of the anthracene sulfonated and phenanthrene sulfonated poly(2,5 dimethoxyaniline) polymers in dimethyl sulfoxide (DMSO) in comparison with poly(2,5 dimethoxyaniline) doped with HCl in DMSO. The UV-vis absorption spectra of PDMA doped with ASA showed 3 absorption bands at 3 selected wavelengths, 350, 600 and 800 nm respectively [15-17].

The same 3 absorption bands were seen for PDMA doped with PSA, but in this case the band at around 800 nm was broadened. The band at around 800 nm was not seen for PDMA doped with HCl. The band at 350 nm corresponds to the reduced state (leucoemeraldine) of PDMA. The band at 600 nm corresponds to partial oxidation of

PDMA and can be assigned to represent the intermediate state between leucoemeraldine form containing benzenoid rings and emeraldine form containing conjugated quinoid rings in the backbone of the PDMA (polaron). The emeraldine form transforms into fully oxidized pernigraniline form and characterized by a broadened band at around 800 nm (bipolaron) [20- 21].

4.3.3 Scanning Electron Microscopy (SEM)

The morphology and structure of PDMA, POMA and PANI with the different dopants ASA and PSA were investigated. The effect of the different dopants on the monomer morphologies prepared under the same conditions, was clearly observed in the SEM images. It is generally agreed upon that morphology of the resultant polymers can be as diverse as there are main polymer chains, dopant structure, synthetic routes and conditions [22]. **Figure 4.8** shows SEM micrographs of PDMA with ASA and PDMA with PSA. In micrograph (a) tubes or fibres can be seen when PDMA was doped with ASA with diameter between 200 – 300 nm at 50 000 x magnification. Nanotubes or fibres were also observed when PDMA was doped with PSA (b) with observed diameters between 50 and 100 nm (100 000 x magnification). However, when POMA was doped with ASA in (**Figure 4.9 a**) micelle (egg-like) formations were observed with radius in the 100 to 200 nm range. This might be a result of POMA, which is insoluble in water, being forced inside the molecule. Flat round, disc-like formations were seen (40 000 x magnification) when POMA was doped with PSA (**Figure 4.9 b**), which could be the effect of the different isomers of PSA formed during synthesis [22-24].

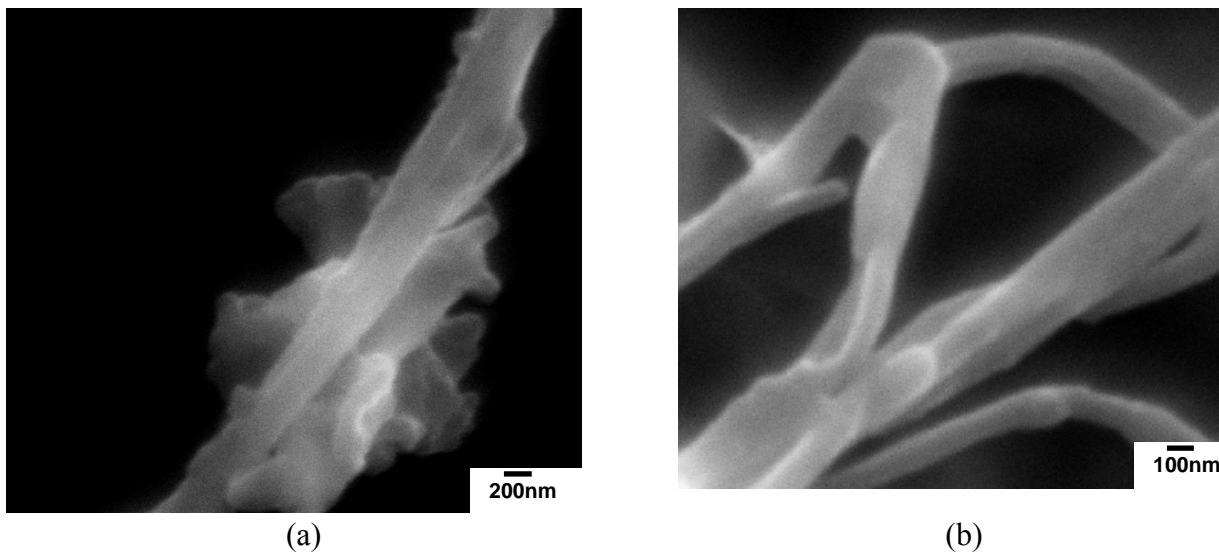


Figure 4.8: SEM images of PDMA/ASA (a) and PDMA/PSA (b) at different magnifications.

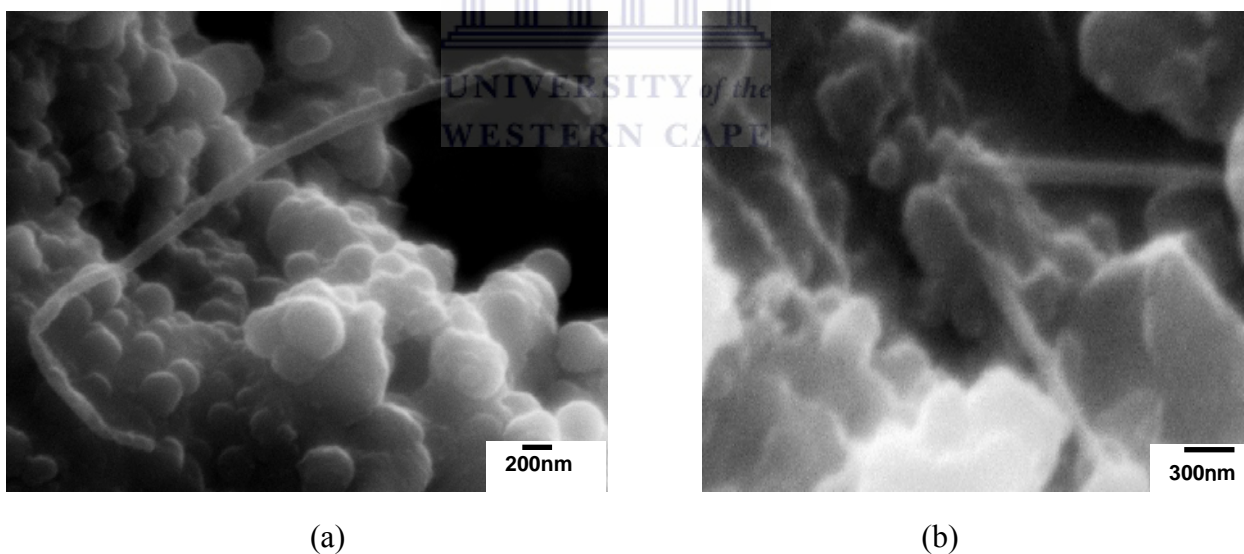
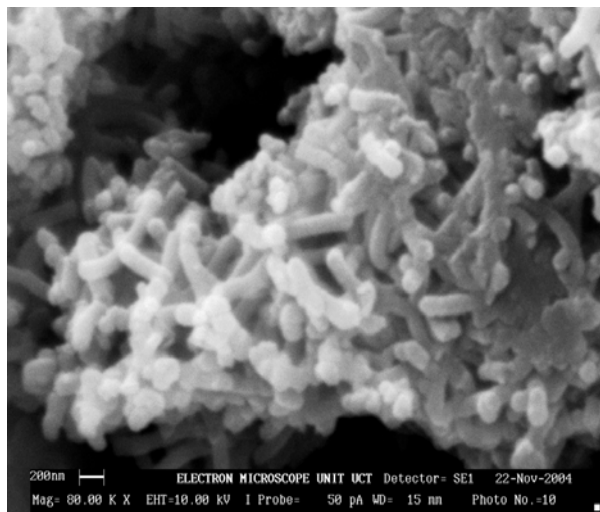
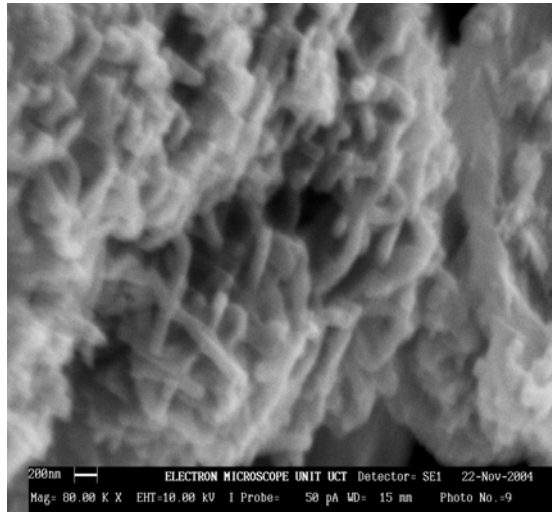


Figure 4.9: SEM images of POMA-ASA (a) and POMA-PSA (b) at different magnifications.



(a)



(b)

Figure 4.10: SEM images of PANI-ASA (a) and PANI-PSA (b) at different magnifications.

When PANI was doped with ASA and PSA (Figure 4.10) nanostructures were also observed. In micrograph (a) tubes or fibres can be seen when PANI was doped with ASA with diameter between 50 – 100 nm at 80 000 x magnification. Nanotubes or fibres were also observed when PANI was doped with PSA (b) with observed diameters between 50 and 100 nm (80 000 x magnification). It is clearly seen that the surface is covered with fibres interconnected with each other showing net-like features [22, 25, 26].

4.3.4 Electrochemical characterisation

The electrochemical behaviour of the polymers PANI, POMA and PDMA doped with the sulfonic acids (ASA and PSA) provided information regarding the electroactivity and the conductivity of the nanostructured polymers.

4.3.4.1 Cyclic Voltammetry (CV) characterisation of the polymers on platinum

Figure 4.11 illustrates multi-scan cyclic voltammograms of PANI-ASA paste on a Pt electrode in HCl (1 M) solution with scan rates 5, 10, 15, 20, 30, 40 and 50 mV/s. Analysis of the voltammograms shows that the peak potentials and corresponding currents vary as the scan rates value varies. This indicates that the polymer nanotubes or fibres are electroactive and the electron transfer processes are coupled to a diffusion process namely, charge transportation along the polymeric nanostructures. Analysis of the cyclic voltammograms established 3 anodic and 3 cathodic peaks.

The redox peaks in the figure have been assigned using Pekmez formalism. The first oxidation peak represents polyleucoemeraldine radical cation (peak a') which is oxidized at more positive potentials to the half oxidized polyemeraldine state (peak b') and then to the pernigraniline radical cation (peak c'). On the reversing potential, the pernigraniline (peak c) is first reduced to the polyemeraldine radical cation (peak b) and finally to the fully reduced polyleucoemeraldine (peak a) [27-29].

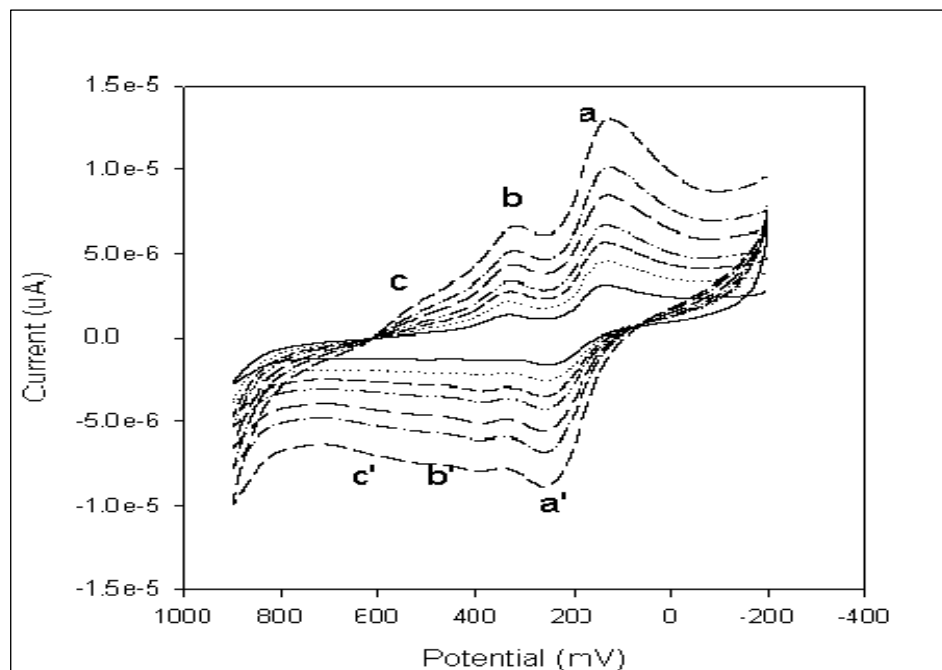


Figure 4.11: Multi-scan cyclic voltammograms (CV) of Pt/PANI-ASA in 1 M HCl at 25 °C

Multi-scan rate voltammograms of PANI/PSA paste on Pt electrode in 1 M HCl with scan rates of 10, 20, 30, 40 and 50 mV/s are shown in **Figure 4.12**. The peak potentials and corresponding currents also varies as the scan rates value varies. This proves that the PANI-PSA nanomaterials are electroactive and that charge transport along the polymer chain was taking place [28].

There are 4 anodic and 4 cathodic peaks in the voltammograms which represents the same redox peaks as in PANI/ASA voltammograms with the inclusion of peaks d and d' that is generally attributed to the redox reaction of *p*-benzoquinone [29].

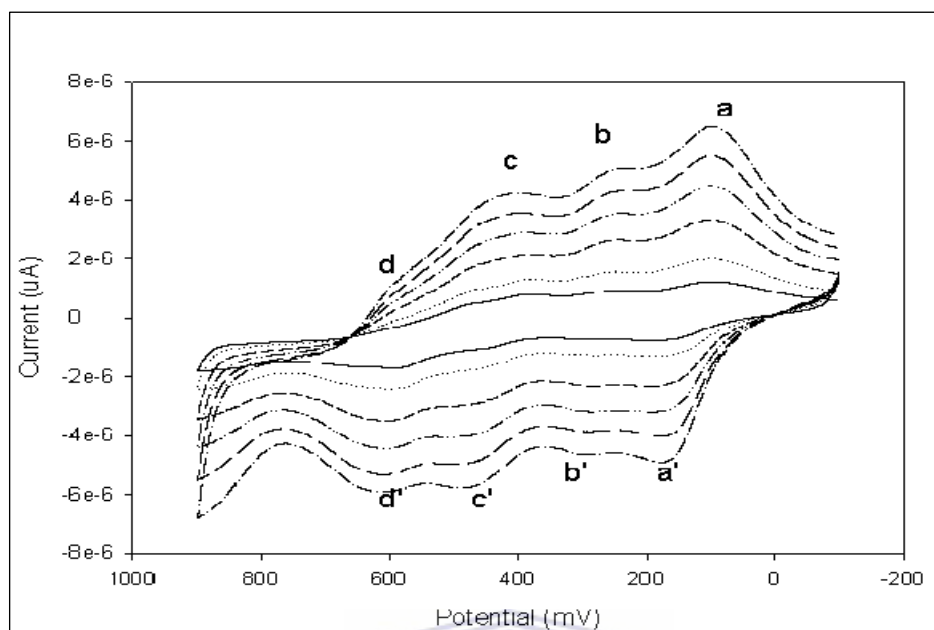


Figure 4.12: Multi-scan cyclic voltammograms (CV) of Pt/PANI-PSA in 1 M HCl at 25 °C

Figure 4.13 illustrates the multi-scan cyclic voltammograms obtained for POMA-ASA paste on a Pt electrode HCl (1 M) at different scan rates. It can be seen that there are 2 anodic and 2 cathodic peaks in the voltammograms. The shift of peak potentials and corresponding currents with scan rates indicated that the polymer nanomicelles are conducting and that hopping of electrons was taking place along the polymer structures. The first oxidation peak (peak b) at +101.7 mV is the emeraldine, which is further oxidized at higher potential to polyemeraldine radical cation at +274.8 mV (peak d). The cathodic peak scan is first reduced to the partly reduced leucoemeraldine radical cation at +216.1 mV (peak c), and then to the fully reduced leucoemeraldine (peak a) at +46.0 mV [30].

The multi-scan rate voltammograms of POMA-PSA paste on Pt electrode in HCl (1M) solution with scan rates 5, 10, 15, 30, 40 and 50 mV/s are shown in **Figure 4.14**. The peak potentials and corresponding currents are also seen to vary as the scan rates value varies. This indicated that the polymer nanomaterial structures are conducting and that diffusion of electrons was taking place along the polymer chain. The first oxidation peak at +113.4 mV is the emeraldine, which is further oxidized at higher potential to polyemeraldine radical cation at +268.9 mV. On the cathodic peak scan, polyemeraldine cation radical at +192.7 mV is reduced to the fully reduced leucoemeraldine at +10.8 mV [31].

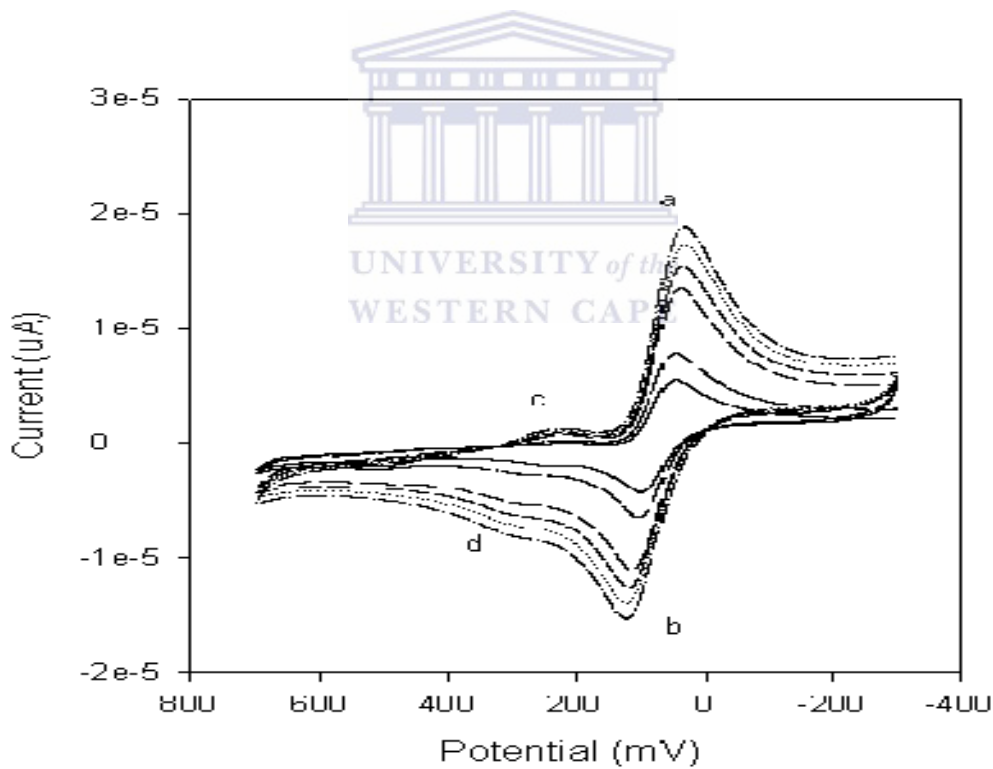


Figure 4.13: Multi-scan cyclic voltammograms (CV) of Pt/POMA-ASA in 1 M HCl at 25 °C

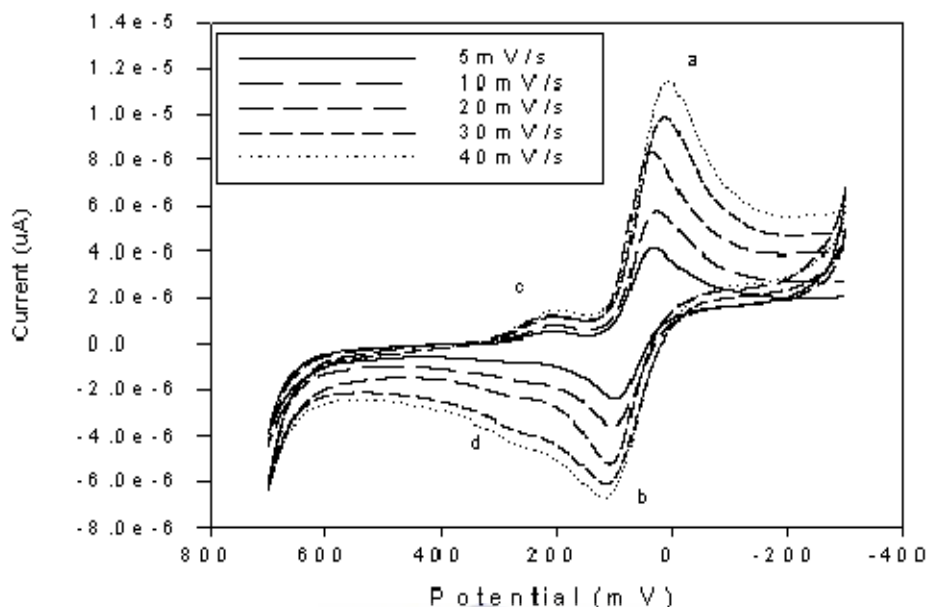


Figure 4.14: Multi-scan cyclic voltammograms (CV) of Pt/POMA-PSA in 1 M HCl at 25 °C

Multi-scan rate voltammograms of PDMA-ASA on Pt electrode in HCl (1 M) with scan rates of 10, 20, 30, 40 and 50 mV/s are shown in **Figure 4.15**. The peak potentials and corresponding currents vary as the scan rates value varies. This confirmed that the polymeric nanowires are electroactive and that charge transport along the polymer chain was taking place [28].

It can be seen that there are 4 anodic and 4 cathodic peaks in the voltammograms. The first oxidation peak (peak a') at +163.3mV is due to the polyemeraldine state, which is further oxidized at higher potential to polyemeraldine radical cation at +268.9 mV (peak b'), which oxidized further to pernigraniline (peak c') at +374.4 mV. For the cathodic scan, pernigraniline cation radical at +336.4mV (peak c) is first reduced to the partly reduced leucoemeraldine radical cation at +239.6mV (peak b), and then to the fully

reduced leucoemeraldine (peak a) at +101.7mV. The redox couple d/d' at approximately +500 mV is generally attributed to the redox reaction of *p*-benzoquinone [29].

The potentials of peaks b and a (reduced forms of the polymers) do not change as the scan rate was increased. This means that a surface bound species (stationary paste) was being used as a working electrode. No charge transfer accompanied the reduction process, only absorption. Peak a', to a small extent, and peaks b', c, c' and d' show increase in peak potential with scan rate. This shows charge transportation along the polymer chain and confirms that the polymer is conducting in its oxidised state [28-29].

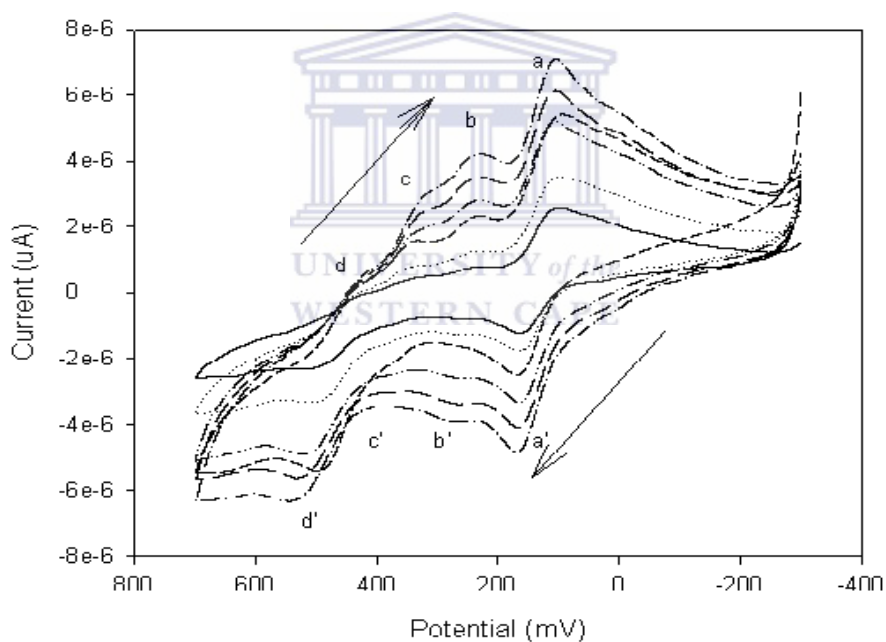


Figure 4.15: Multi-scan cyclic voltammograms (CV) of Pt/PDMA-ASA in 1 M HCl at 25 °C

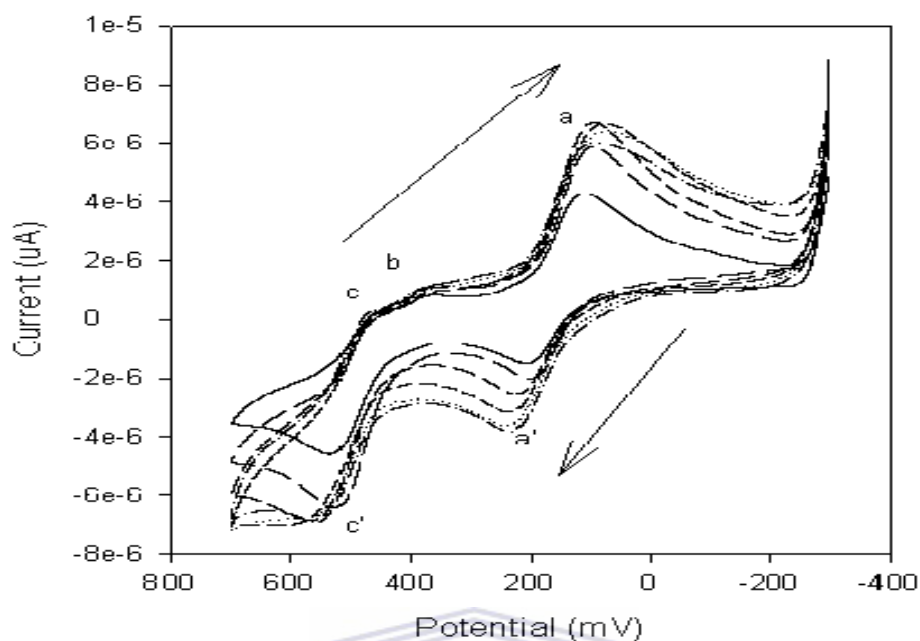


Figure 4.16: Multi-scan cyclic voltammograms (CV) of Pt/PDMA-PSA in 1 M HCl at 25 °C

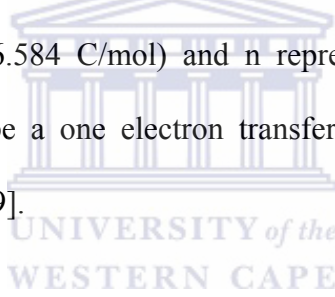
Figure 4.16 illustrates multi-scan voltammograms of PDMA-PSA paste in HCl (1 M) with a Pt electrode with scan rates 5, 10, 15, 30, 40 and 50mV/s. Analysis of the voltammograms shows that the peak potentials and corresponding currents vary as the scan rate value vary. This indicates that the polymer nanowires are electroactive and the electron transfer processes are coupled to a diffusion process namely, charge transportation along the polymeric nanowires. Analysis of the cyclic voltammograms established 2 anodic and 3 cathodic peaks. The first oxidation peak at +224.1 mV is the emeraldine (peak a'), which is further oxidized at higher potential +477.0 mV (peak c'). On the cathodic peak scan, pernigraniline cation radical at +354.0 mV (peak c) is reduced to the fully reduced leucoemeraldine at +119.3 mV (peak a) [22, 28, 29].

4.3.4.2 Kinetic studies of the different polymers on Pt electrode in 1M HCl

The number of electrons transferred was estimated from the CVs and was calculated for each of the polymers: PANI-ASA, PANI-PSA, POMA-ASA, POMA-PSA, PDMA-ASA and PDMA-PSA, using the equation:

$$|E_p - E_{p1/2}| = 2.20 R T / n F = 56.5 / n \quad (4.1)$$

where E_p is the maximum peak potential, $E_{p1/2}$ is half the maximum peak potential, R is the gas constant (8.314 J.(mol. K⁻¹)), T is the absolute temperature (298 K) of the system, F is the Faraday constant (96.584 C/mol) and n represents the number of electrons transferred. It was found to be a one electron transfer system for all the conductive nanostructured polymers [28-29].



The linear dependence of peak current on the scan rate for the various polymers, showed that we have a stationary paste of conducting electro-active polymers immobilized on the electrode, which undergo rapid charge transfer reactions. This is typical of a Nernstian reversible reaction of a surface confined species. The surface concentration (Γ^*) of the absorbed electroactive species could therefore be estimated from a plot of I_p versus v in accordance with the Brown Anson model [32-34] using the equation:

$$I_p = n^2 F^2 \Gamma^* A v / 4 R T \quad (4.2)$$

where I_p represents the peak current, A is the surface area of the electrode (0.0177 cm^2), v is the scan rate (V/s), Γ^* is the surface concentration of the absorbed electro-active species, and F , R , T are the same as in **equation 4.1**. The surface concentrations were seen to decrease in PANI > POMA > PDMA (**Table 4.1**), which was due to the substituted methoxy groups in POMA and PDMA. On the other hand, the surface concentrations of polymers doped with PSA were higher than those doped with ASA, which was a result of the bulky angular PSA group compared with the bulky linear ASA group [32-34].

There is a direct correlation between the bulkiness of the polymer substituents, the efficiency of the electron-hopping and the rate of electron diffusion along the polymer chain. The Randel-Sevčik equation of analysis of voltammetric data was used to determine the rate of charge transport coefficient (D_e) along the different polymer chains. The Randel-Sevčik behaviour of the cyclic voltammetric peak currents has been used to evaluate D_e from the slope of the straight line obtained from the I_p versus $v^{1/2}$ [32-34]

Conducting nano-structured Polymer	Surface conc. Γ^* (mol/cm ²)	Diffusion coeff. (D_e) cm ² /s	Standard rate constant (k^0) cm/s
PANI-ASA	8.093×10^{-3}	3.48×10^{-6}	1.2×10^{-3}
PANI-PSA	4.29×10^{-3}	7.0983×10^{-7}	6.042×10^{-4}
POMA-ASA	4.629×10^{-2}	1.0994×10^{-8}	2.9255×10^{-5}
POMA-PSA	9.679×10^{-2}	5.4114×10^{-9}	8.8875×10^{-7}
PDMA-ASA	1.231×10^{-2}	2.429×10^{-7}	1.557×10^{-4}
PDMA-PSA	2.960×10^{-2}	2.008×10^{-9}	5.593×10^{-5}

Table 4.1: Kinetic parameters for the conducting nanostructured polymers

The diffusion coefficient was seen to decrease in PANI > POMA > PDMA (**Table 4.1**) which was caused by the substituted methoxy groups that increases the inter-chain distance between the polymer units and thus impede electron-hopping across the units. The diffusion coefficient of polymers doped with ASA was faster than those doped with PSA. This was due to the steric hindrance emanating from the bend bulky PSA that increased the inter-chain separation and decreased frequency electron-hopping, compared to straight bulky ASA. These findings were further confirmed by calculation of the standard rate constant (k^0), which was better along PANI > POMA > PDMA (**Table 4.1**) [32-34].

4.4. Conclusion

It can be concluded that nanostructured conducting polyaniline (PANI), poly(*ortho*-methoxyaniline) (POMA) and poly(2,5 dimethoxyaniline) (PDMA) doped with anthracene sulfonic acid (ASA) and phenanthrene sulfonic acid (PSA) can be synthesised chemically.

All polymers studied exhibited quinoid and benzoid bands typically of polyaniline FTIR-spectra which confirmed the polymers were formed. The presence of the sulfonate functionality suggested that the ASA and PSA groups were incorporated into the polymer backbones.

Furthermore, UV-vis bands and shifts also showed that ASA and PSA were incorporated into the polymer backbones.



SEM micrographs showed different nano-structured morphologies for the polymers, which include nano-tubes/fibres (PANI-ASA and PANI-PSA), nano-micelles or nano-sheets (POMA-ASA and POMA-PSA) and nano-wires (PDMA-ASA and PDMA-PSA).

Cyclic voltammetric characterisation of the polymer pastes showed distinctive redox peaks, which prove that the polymer films on the Pt electrode were electroactive and conductive and exhibit reversible electrochemistry.

Thus, applying appropriate potential, the conductive nanostructured polymers can be stabilised at required oxidation states.

These results support the view that conducting nanostructured polymers could prove promising for developing novel electro-catalysts for use in sensor devices.



4.5. References

- [1] B. Schrader, *Infrared and Raman Spectroscopy – Methods and Applications*, VCH, (1995)
- [2] G. Zerby, *Modern Polymer Spectroscopy*, Wiley-VCH, (1999)
- [3] M. T. Postek Jn. and Ladd Research Ind. Inc., *Scanning Electron Microscopy: A student's handbook* (1980)
- [4] A. Ivaska, *Electroanalysis* 3 (1991) 247
- [5] C. E. D. Chidsey and R.W. Murray, *Science* 231 (1986) 25
- [6] R. T. S. Muthu Lakshmi, J. Meier-Hack, K. Schlenstedt, H. Komber, V. Choudhary and I. K. Varma, *React. Funct. Polym.*, (2005) Article in Press
- [7] S. Saravanan, C. Joseph Mathai, M. R. Anantharaman, S. Venkatachalam and P. V. Prabhakaran, *J. Phys. Chem. Solids* (2006) Article in Press
- [8] J. Widera, B. Palys, J. Bucowska and K. Jackowski, *Synth. Met.*, 94 (1998) 265
- [9] F. Cataldo and P. Maltese, *European. Polym. J.*, 38 (2002) 1791
- [10] L. Zang and M. Wan, *Thin Solid Films* 477 (2005) 24
- [11] V. Patil, S. R. Sainkar and P. P. Patil, *Synth. Met.*, 140 (2004) 57
- [12] S. Patil, J. R. Mahajan, M. A. More and P. P. Patil, *Mater. Chem and Phys.*, 58 (1999) 31-36

- [13] M. G. Han, S. K. Cho, S. G. Oh and S. S. Im, *Synth. Met.*, 126 (2002) 53-60
- [14] W. A. Gazotti and M. de Paoli, *Synth. Met.*, 80 (1996) 263-269
- [15] Z. Zhang, Z. Wei, L. Zhang and M. Wan, *Acta Materiala*, 53 (2005) 1373
- [16] Y. Wei, W. W. Focke, G. E. Wnek and A. Ray, A.G MacDiarmid, *J. Phys. Chem.*, (1989) 93, 495
- [17] M. Karakisia, M. Sakac, E. Erdem and U. Akbulut, *J. of Appl. Electrochem.*, 27 (1997) 309
- [18] M. R. Fernandes, J. R. Garcia, M. S. Schultz and F. C. Nart, *Thin Solid Films* 474 (2005) 279
- [19] A. Malinauskas and R. Holze., *Synth. Met.*, 97 (1998) 31
- [20] L. Huang, T. Wen and A. Gopalan, *Synth. Met.*, 130 (2002) 155-163
- [21] L. Huang, T. Wen and A. Gopalan, *Mater. Chem. & Phys.*, 77 (2002) 726-733
- [22] M. Wan, Z. Wei, Z. Zhang, L. Zhang, K. Huang and Y. Yang, *Synth. Met.*, 135 – 136 (2003) 175 – 176
- [23] S. Patil, J. R. Mahajan, M. A. More and P. P Patil, *Mater. Science & Engin.*, B87 (2001) 134 – 140
- [24] M. Mazur, M. Tagowska, B. Palys and K. Jackowska, *Electrochem. Commun.*, 5 (2003) 403 - 407

- [25] A. R. Hopkins, R. A. Lipeles and W. H. Kao, *Thin Solid Films* (2004) 474 – 480
- [26] P. Sbaite, D. Huerta-Vilca, C. Barbero, M. C. Miras and A. J. Motheo, *European Polym. J.*, 40 (2004) 1445 - 1450
- [27] E. I. Iwuoha, D. S. de Villaverde, N. P. Garcia, M. R. Smyth and J. M. Pingarron, *Biosens. and Bioelectr.* 12 (1997) 749-761
- [28] N. G. R. Mathebe, A. Morrin and E. I. Iwuoha, *Talanta* 64 (2004) 115-12
- [29] A.J Bard and L.R Faulkner, *Electrochemical Methods: Fundamentals and Applications*, 2nd ed., Wiley, New York (2001)
- [30] J. C. Chiang, and A. G. MacDiarmid, *Synth. Met.*, 13 (1986) 193
- [31] A. G. MacDiarmid, J. C. Chiang, A. F. Ritcher and A. J. Epstein, *Synth. Met.*, 18 (1987) 285
- [32] P. Monk, *Fundamentals of Electro-Analytical Chemistry*, Chichester: John Wiley & Sons Ltd (2001)
- [33] P. Zanello, *Inorganic Electrochemistry. Theory, Practice and Application* Cambridge, UK: The Royal Society of Chemistry (2003)
- [34] T. J. Kemp, and Southampton Electrochemistry Group In., *Instrumental Methods in Electrochemistry*, Ellis Horwood Ltd: Chichester, (1990)

Chapter 5

The Catalytic, Electro-catalytic and Redox Mediator Effects of Nanostructured PANI-ASA and PANI-PSA Modified Electrodes as Phenol (and phenol derivatives) Sensors

5.1 Introduction

In the previous chapter we discussed the preparation and characterisation of the different conducting and electro-active nanostructured polymers. The results indicated that the monomers (aniline, *ortho*-methoxyaniline and 2,5 dimethoxyaniline) can be polymerised in the presence of bulky dopants (ASA and PSA) to give us conducting and electro-active nanostructured polymers.

This chapter deals with the catalytic effect that the polymers (PANI-ASA and PANI-PSA) have as redox mediators (electron shuttles) for the oxidation of phenol and its derivatives using electrochemical means which includes Differential Pulse Voltammetry (DPV), Square Wave Voltammetry (SWV) and Cyclic Voltammetry (CV).

These methods are widely used in liquid electrochemistry for determining concentrations of chemical species, which are based on the oxidation or reduction of chemical species on the electrode. This study reports only on a sweep of the oxidation detection of phenol and its derivatives.

Section 5.2 gives a description on the experimental procedure, which includes construction of the chemical sensor and the determination of phenol and derivatives.

Section 5.3 discusses the results and **Section 5.4** draw conclusions about the experiments.

5.2 Method

5.2.1 Chemicals

The chemical reagents Phenol (Ph), 2,4 Dichlorophenol (2.4-DCP), 4-Chloro-3-methylphenol (4-C3MP), 2,4,6 Trichlorophenol (2.4.6-TCP), 2,6 Dinitro-4-methylphenol (2.6-DN4MP), 4-Nitophenol (4-NP), 4-Chlorophenol (4-CP), Pentachlorophenol (PCP), 2,4 Dinitrophenol (2.4-DNP), 2,4 Dimethylphenol (2.4-DMP), acetone and methanol were purchased from Sigma-Aldrich and were used as obtained. Hydrochloric acid (Fluka), sulfuric acid (Fluka) and 30% H₂O₂ (Fluka) were of analytical grade and were used as obtained without further purification. All chemicals were purchased in Cape Town, South Africa.



5.2.2 Construction of Phenol (derivative) Chemical sensor

Prior to use, a platinum disc electrode was first etched for about 5 minutes in a hot 'Piranha' solution {1:3 (v/v) 30% H₂O₂ and concentrated H₂SO₄}. It was then polished on aqueous slurries of 1, 0.3 and 0.05 micron alumina powder. After thorough rinsing with deionized water followed by acetone, the electrodes were cleaned electrochemically by cycling it between -200 and 1500 mV in 0.05 M H₂SO₄ at a scan rate of 10 mV/s for 10 min or until the CV characteristics for a clean Pt electrode were obtained. The redox mediator was formed by dissolving 0.001 g of polymer in 0.1 mL of methanol (MeOH), whereby, a 10 µL of the polymer (PANI-PSA or PANI-ASA) solution was put on top of a Pt-disk electrode and the MeOH solvent was allowed to evaporate. The dried modified electrode (Pt/PANI-PSA or Pt/PANI-ASA) was then characterised in 1 M HCl (pH 0 – 1) at different scan rates using Cyclic Voltammetry (CV).

5.2.3 Determination of Phenol and Phenol derivatives

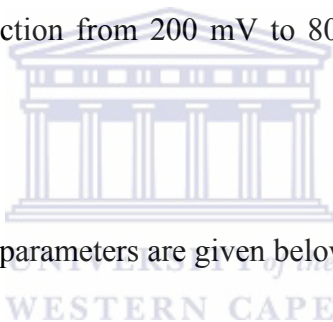
The chemosensor (Pt/PANI-PSA or Pt/PANI-ASA) was placed in 1 mL 1 M HCl (pH 0 -1) solution to which 10 - 20 μ L additions of 0.002 M Phenol (and phenol derivatives) were added. Differential Pulse Voltammetry (DPV) and Square Wave Voltammetry (SWV) were performed after each addition of the phenol (derivatives) up to maximum concentration. The increase or decrease in current due to the phenol (derivatives) oxidation was recorded.

The assumptions that were made for the determination of the chemosensor include:

- (i) that the conducting polymers are uniformly distributed throughout the polymer matrix;
- (ii) the conducting polymer does not form aggregates;
- (iii) it is assumed for all the techniques that the analyte solution is either still or unstirred during the experimental performance, in order to ensure that mass transport by convection is absent;
- (iv) that an excess of ionic electrolyte has been added to the solution in order to ensure that mass transport by migration is also absent;
- (v) the only form of mass transport remaining that will be considered is diffusion and;
- (vi) that the catalytic current is equal to the absolute value of the difference between starting current (no addition) and actual current (after addition) of the analyte response.

5.2.4 *Experimental conditions*

A BAS/50W integrated automated electrochemical workstation (Bioanalytical Systems, Lafayette, IN, USA) was used for all electrochemical experiments. The cell volume was kept at 1 mL for all electrochemical (DPV, SWV and CV) investigations. The conducting nanostructured polymers were adhered on the Pt-disk working electrode. As described in **Section 5.2.2** a standard Ag/AgCl electrode was used as a reference electrode and a Pt-wire as counter electrode. The electro-catalytic properties of these conducting polymers were investigated in acid medium (1 M HCl). Potential scans were carried out in the positive direction from 200 mV to 800 mV, first oxidizing and then reducing.



The values of all experimental parameters are given below (**Table 5.1, 5.2 and 5.3**).

Parameter	Value
Initial Potential	200 mV
High Potential	800 mV
Sensitivity	10 μ A
Scan rate	10 mV/s
Frequency	5 Hz
Amplitude	50

Table 5.1: Parameters for differential pulse voltammetry (DPV) experiments

Parameter	Value
Initial Potential	200 mV
High Potential	800 mV
Sensitivity	10 μ A

Table 5.2: Parameters for square wave voltammetry (SWV) experiments

Parameter	Value
Initial Potential	-200 mV
High Potential	1200 mV
Low Potential	-200 mV
Scan Rates	2 – 70 mV/s
Sensitivity	10 – 100 μ A

Table 5.3: Parameters for cyclic voltammetry (CV) experiments

5.3 Results and discussion

5.3.1 The potentials of the modified electrodes

Figure 5.1 represents the formal potentials (E°) of the different Pt/polymer modified electrodes in 1 M HCl, before addition of the different analytes used in the study. From the graph it is clear that the Pt/PANI-ASA (+494.7 mV) modified electrode has the highest formal potential and Pt/PDMA-PSA (+75.7 mV) has the lowest formal potential. It can also be seen that the highest formal potential are for PANI doped polymers followed by POMA doped polymers and then the PDMA doped polymers. The formal potentials are seen to decrease with more substituted monomers (PANI > POMA > PDMA). The PSA doped polymer has smaller formal potentials for PANI and PDMA compared with ASA doped. However, ASA doped POMA have a smaller formal potential compare with PSA doped POMA.

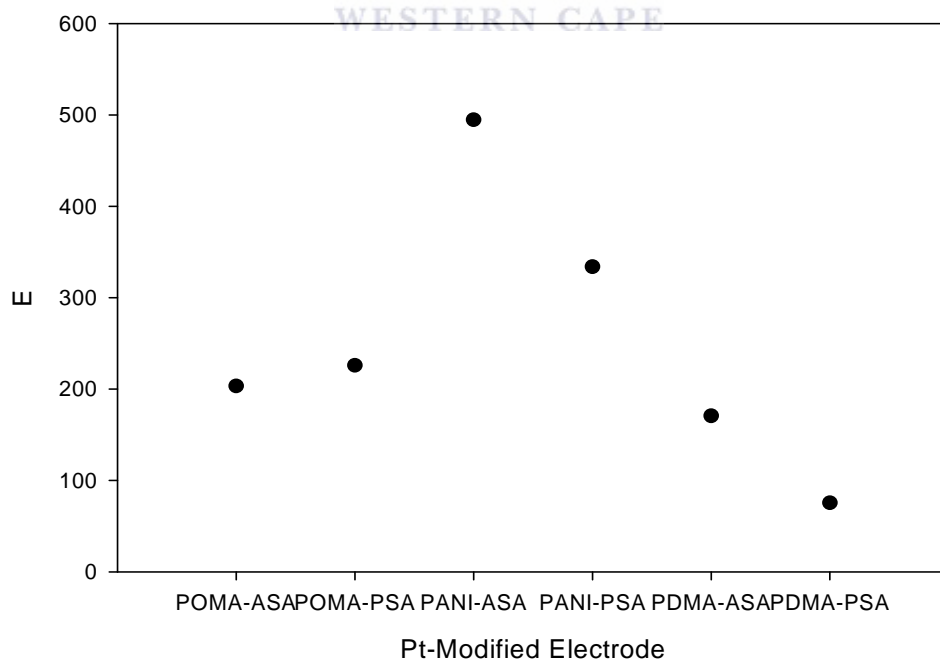


Figure 5.1: The formal potentials ($E = E^{\circ}$) of the different Pt/Polymer modified electrodes in 1 M HCl before the addition of the phenol (derivatives)

5.3.2 Electrochemical behaviour of the Pt/PANI-ASA electrode

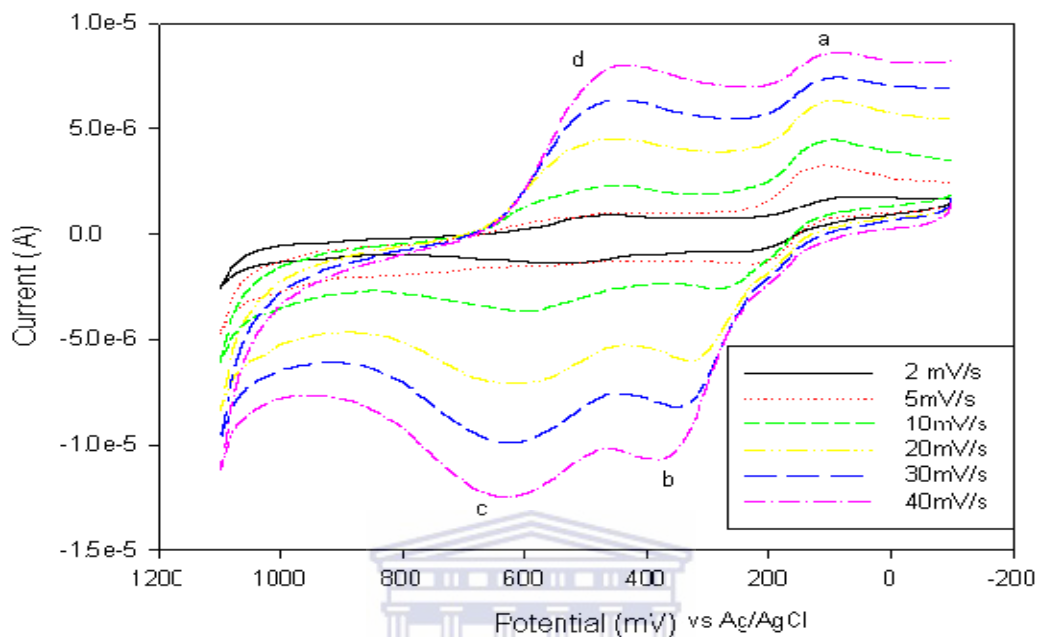


Figure 5.2: Characterisation of Pt/PANI-ASA on Pt electrode in 1 M HCl at scan rates 2, 5, 10, 20, 30, and 40 mV/s.

Multi-scan rate voltammograms of PANI-ASA on a Pt electrode in 1 M HCl with scan rates of 2, 5, 10, 20, 30 and 40 mV/s are shown in **Figure 5.2**. The peak potentials and corresponding currents vary as the scan rate value varies. This showed that the polymeric nanostructure was electro-active and that charge transport (electron shuttling) along the polymer chain was taking place. Pt/PANI-PSA in a 1 M HCl electrolyte solution also displayed similar oxidation-reduction responses indicating that the modified electrode is electro-active [1-3].

5.3.3 *The difference in shift potentials of Pt/PANI-ASA and Pt/PANI-PSA electrodes with phenol (derivatives) addition*

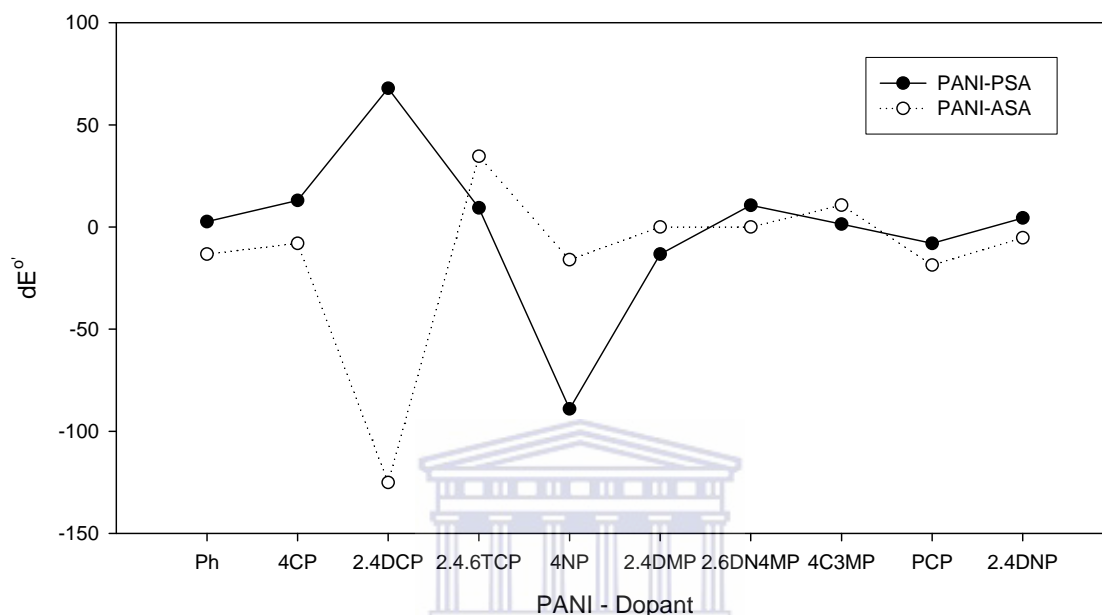


Figure 5.3: The shift in formal potentials ($dE^{\circ} = \Delta E^{\circ}$) of the different Pt/PANI-dopant modified electrodes in 1 M HCl before and after the addition of 20 μ L of phenol (derivatives)

The difference in shift formal potential (ΔE°) between the PANI-ASA and PANI-PSA modified electrodes before and after the addition of 20 μ L of analyte is presented in **Figure 5.3**. The shift in formal potentials for the Pt/PANI-dopant modified electrodes showed very similar trends for most of the phenolic compounds used. The ΔE° was seen to be highest for Pt/PANI-PSA modified electrode except when 2,4,6-TCP, 4-NP, 2,4-DMP and 2,6-DN4MP were used. The lowest ΔE° for Pt/PANI-ASA was 2,4-DCP and for Pt/PANI-ASA was when 4-NP was added. These shifts in formal potential suggested that some kind of catalytic reactions were taking place at the surface of the Pt/PANI-dopant modified electrodes [4].

5.3.4 Electrochemical behaviour of Phenol (Ph) at the Pt/PANI-ASA and Pt/PANI-PSA electrodes

An increase in oxidation current was first observed at a potential of about +330 mV, when phenol (0.002 M) was added to the Pt/PANI-PSA modified electrode in the electrochemical cell, after which a decrease in current was seen beyond 7.7×10^{-5} M suggesting saturation of the conducting polymer (**Figure 5.4**). Small negligible shifts in anodic peak potentials were also observed. Electro-catalysis of the phenol was verified with these results [5].

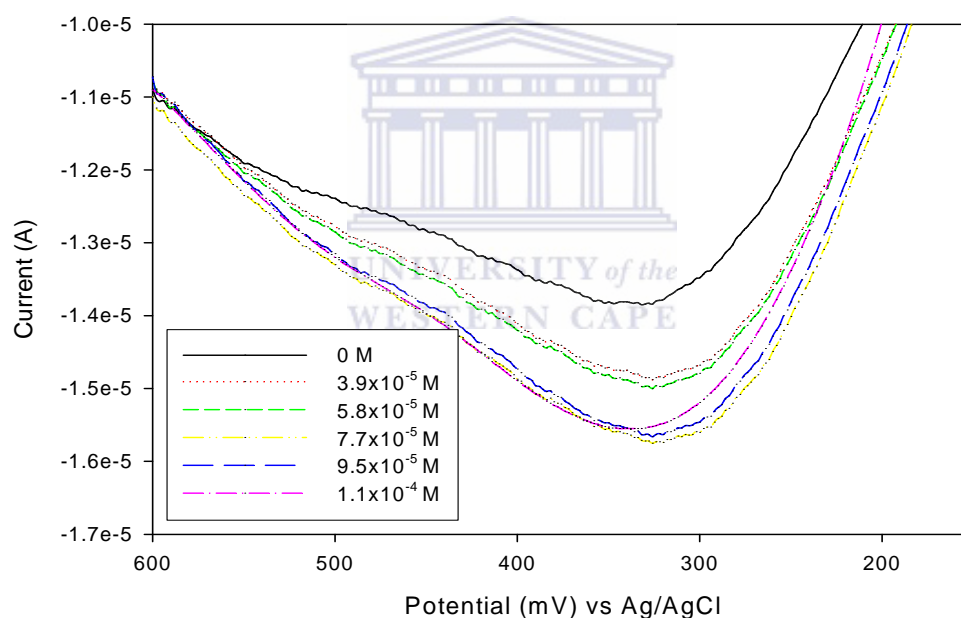


Figure 5.4: Differential pulse voltammograms of Pt/PANI-PSA chemosensor responses to 0, 20, 30, 40, 50 and 60 μ L addition of Phenol (0.002 M) in 1M HCl (1mL) at a scan rate of 10 mV/s and a frequency of 5 Hz

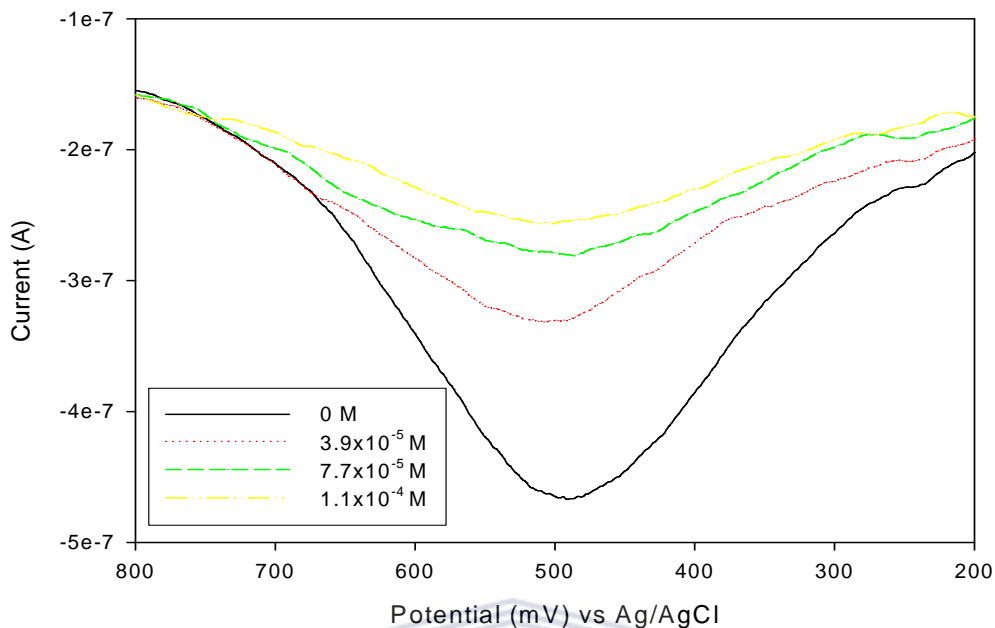


Figure 5.5: Differential pulse voltammograms of Pt/PANI-ASA chemosensor responses to 0, 20, 40 and 60 μL addition of Phenol (0.002 M) in 1 M HCl (1 mL) at a scan rate of 10 mV/s and a frequency of 5 Hz

A decrease in anodic current was observed with the Pt/PANI-ASA as a chemosensor for phenol at a potential of +495 mV (**Figure 5.5**). The decrease in current can be explained to poisoning of the electrode by formation of a non-conducting poly(phenol) on top of the conducting polymer, which hampered the electron-mediating capability of the conducting polymer [6].

5.3.5 *Electrochemical behaviour of 4-ChloroPhenol (4-CP) at the Pt/PANI-ASA and Pt/PANI-PSA electrodes*

Figure 5.6 and **5.7** reports the anodic DPV and SWV responses of Pt/PANI-PSA and Pt/PANI-ASA as a chemosensor for 4-CP, respectively, under anaerobic conditions. The oxidation peak currents decreased with the addition of the 4-CP to the different electrochemical cells, which was a resultant of a non-conducting film formed on top of the conducting polymer, forming a barrier to the transfer of electrons between the conducting polymer (electrode surface) and the 4-CP [7].

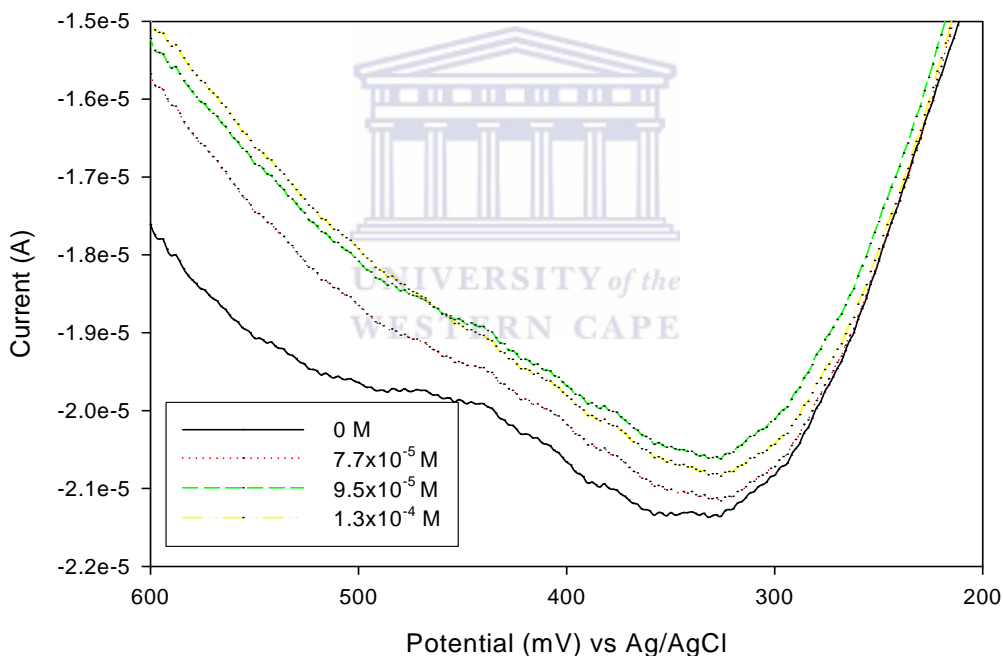


Figure 5.6: Differential pulse voltammograms of Pt/PANI-PSA chemosensor responses to 0, 40, 50 and 70 μL addition of 4-CP (0.002 M) in 1 M HCl (1 mL) at a scan rate of 10 mV/s and a frequency of 5 Hz

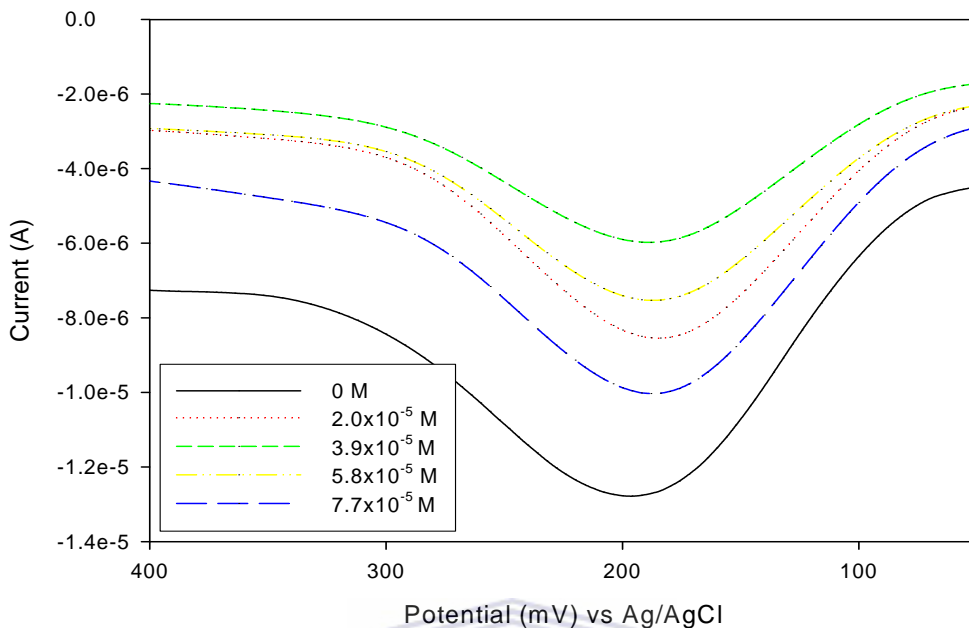
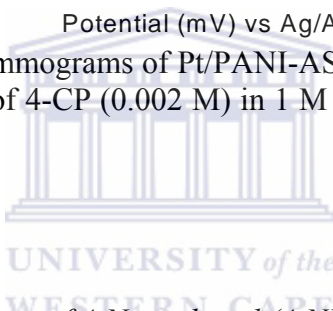


Figure 5.7: Square wave voltammograms of Pt/PANI-ASA chemosensor responses to 0, 10, 20, 30 and 40 μL addition of 4-CP (0.002 M) in 1 M HCl (1 mL) at a scan rate of 10 mV/s and a frequency of 5 Hz



5.3.6 Electrochemical behaviour of 4-Nitrophenol (4-NP) at the Pt/PANI-ASA and Pt/PANI-PSA electrodes

Figure 5.8 and **5.9** contains the oxidation DPV and SWV currents of Pt/PANI-PSA and Pt/PANI-ASA as a chemosensors for 4-NP, respectively. Similar results were obtained in **Section 5.3.4** when 4-CP was added to the modified electrodes. Electrode fouling was faster than electron transferred resulting in the 4-NP not being oxidized, but rather the adsorption of a non-conducting poly(4-nitrophenol) film [8].

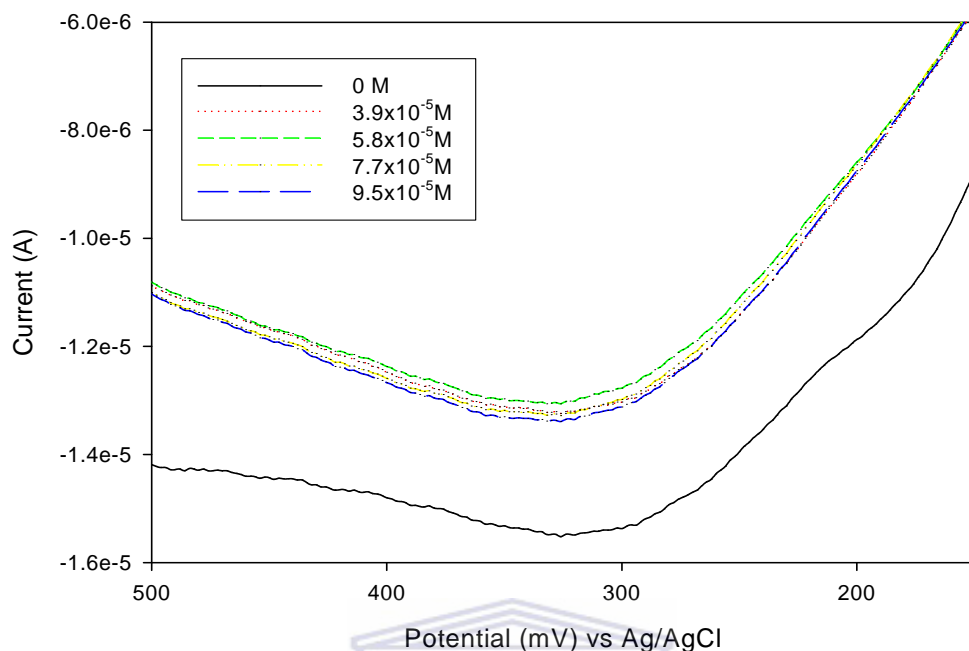


Figure 5.8: Differential pulse voltammograms of Pt/PANI-PSA chemosensor responses to 0, 20, 30, 40 and 50 μ L addition of 4-NP (0.002 M) in 1 M HCl (1 mL) at a scan rate of 10 mV/s and a frequency of 5 Hz

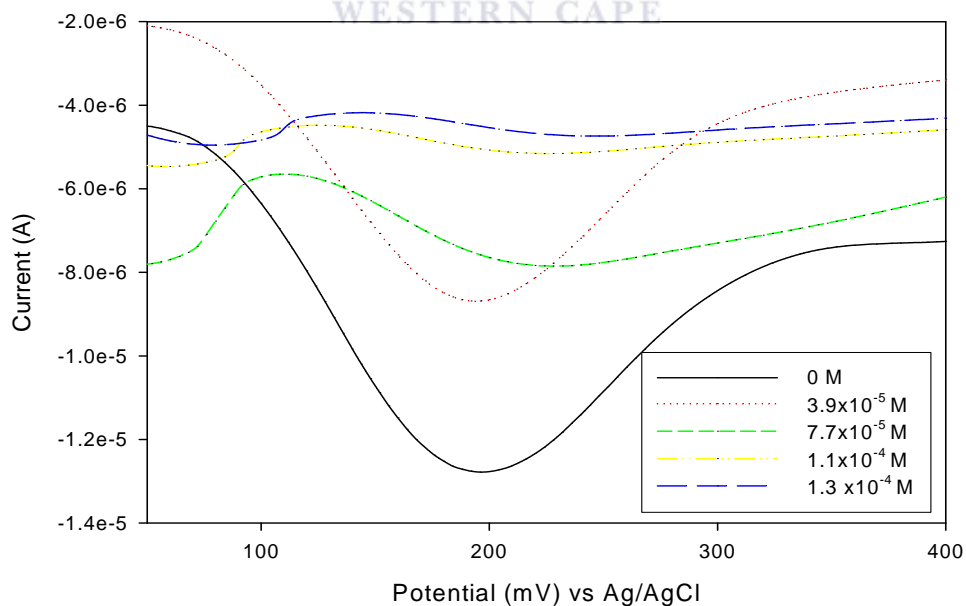


Figure 5.9: Square wave voltammograms of Pt/PANI-ASA chemosensor responses to 0, 20, 40, 60 and 70 μ L addition of 4-NP (0.002M) in 1 M HCl (1 mL) at a scan rate of 10 mV/s and a frequency of 5 Hz

5.3.7 Calibration curves of the Pt/PANI-PSA chemosensors for Phenol (derivatives)

Figure 5.10 reports the calibration curves of the Pt/PANI-PSA chemo-sensor towards Ph, 2,4-DCP, PCP and 4-C3MP. The calibration curve for Ph was linear for the concentration range 2.0×10^{-5} M – 1.1×10^{-4} M, after which a negative departure from linearity was observed, reasonably due to adsorption/precipitation of reaction intermediates or of final products onto the electrode. The Pt/PANI-PSA chemosensor also exhibited good responses to 2,4-DCP, PCP and 4-C3MP. These calibration curves also displayed non-linear responses of current with concentration and was modelled according to the Michaelis-Menten equation [9].

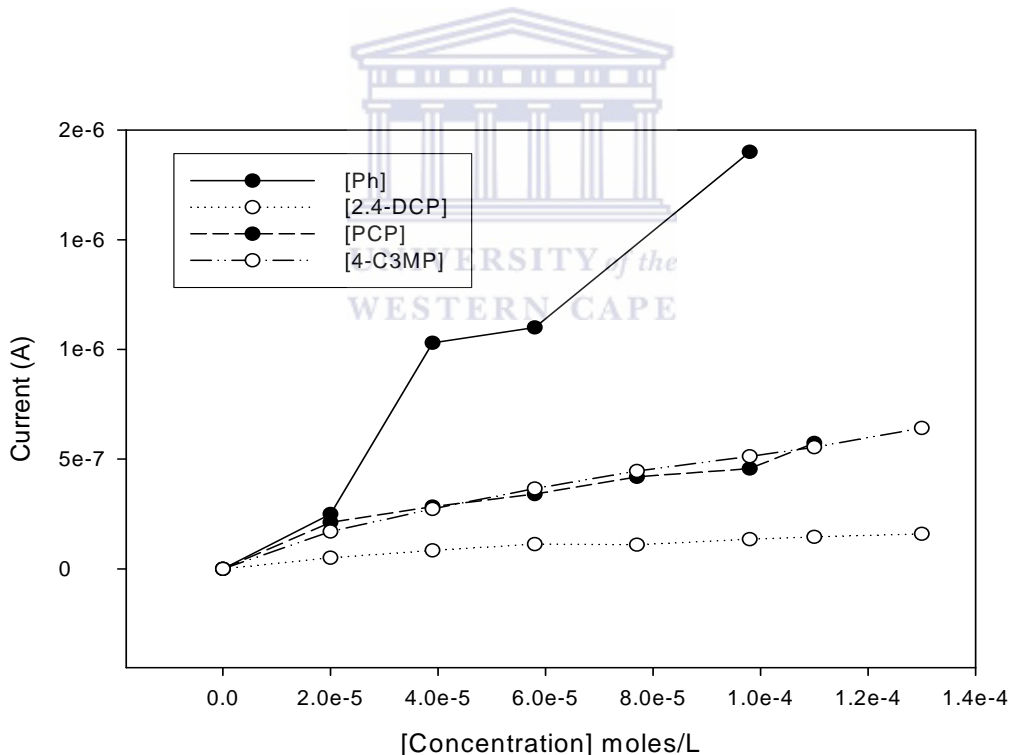


Figure 5.10: Calibration curves of the Pt/PANI-PSA modified electrode for Ph, 2,4-DCP, PCP and 4-C3MP

5.3.8 Pt/PANI-PSA chemosensor kinetic parameters for phenol (derivatives) detection

The kinetic parameters of Pt/PANI-PSA for some phenol (derivative) compounds are listed in **Table 5.4**. The sensitivity for phenolic compounds which is normally dependent on the solubility of phenolic compounds in the immobilisation matrix [10], followed the order Ph > 4-C3MP > PCP > 2.4-DCP. The apparent Michaelis- Menten constant (K'_m) gives information, in this case, on the PANI-PSA towards Phenol (derivatives) kinetics for the Pt/PANI-PSA electrode [11] and decreases in the order 2.4-DCP > 4-C3MP > PCP > Ph. The k'_{cat} followed the order Ph > 4-NP > 4-C3MP > PCP > 2.4-DCP, which suggests faster reaction rate and higher currents for Pt/PANI-PSA as a chemosensors for Ph compare to Pt/PANI-PSA as a chemosensors for 2.4-DCP. A high detection limit was observed for the Pt/PANI-PSA as Phenol (derivatives) chemosensor at an estimated signal to noise (S/N) ratio of 3 [12].

Analyte	Sensitivity (mA/M)	K'_m (μ M)	k'_{cat} (nmol.cm ⁻² .s ⁻¹)	Detection Limit (M)
Phenol	15.8	106.9	0.989	2.83 x 10 ⁻³
4-CP	nd	nd	nd	nd
4-NP	nd	nd	nd	nd
2.4-DCP	1.1	142.1	0.093	9.214 x 10 ⁻³
2.4.6-TCP	nd	nd	nd	nd
2.4-DNP	nd	nd	nd	nd
2.4-DMP	nd	nd	nd	nd
PCP	4.5	119.4	0.315	5.209 x 10 ⁻³
4-C3MP	4.7	136.6	0.376	2.080 x 10 ⁻³
2.6-DN4MP	nd	nd	nd	nd

nd = not detected

Table 5.4: Kinetic parameters of the Pt/PANI-PSA chemosensor for various phenol (derivatives).

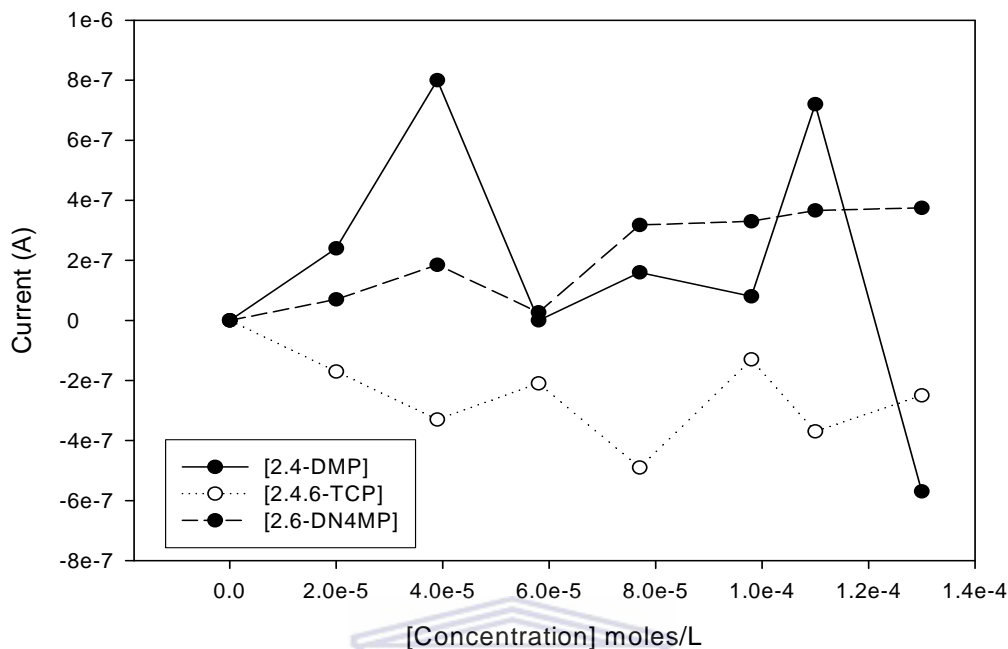


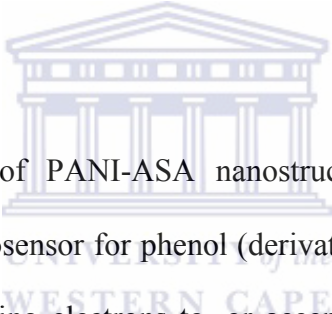
Figure 5.11: Calibration curve of the Pt/PANI-PSA modified electrode for 2.4 DMP, 2.4.6-TCP and 2.6-DN4MP

Figure 5.11 depicts the electrochemical responses obtained when aliquots of 2.4-DMP, 2.4.6-TCP and 2.6-DN4MP were added to a Pt/PANI-PSA modified electrode in an electrochemical cell containing 1 M HCl (1 mL). These calibration curves did not show any significant trends and could not be modelled to any electrochemical fitting equation yet. The same calibration curve trends were seen when phenol (derivatives) were added to the Pt/PANI-ASA chemo-sensor (**Appendix A: Table A1 and A2**).

5.4 Conclusions

The starting potentials for the polymer modified electrodes were relatively low (+495 to +75 mV vs Ag/AgCl) compared to conventional direct electrochemical detection (+650 to +900 mV vs Ag/AgCl) [13].

The Pt/PANI-ASA and Pt/PANI-PSA modified electrodes were seen to exhibit redox properties in aqueous solution with 1 M HCl as the supporting electrolyte. Hence, the PANI-ASA and PANI-PSA nanostructured conducting polymers adhered on the Pt-electrodes were electro-active and that charge propagation was taking place along the polymer chain.



However, the performances of PANI-ASA nanostructured conducting polymer as transfer mediators in the chemosensor for phenol (derivative) system suggested that they were incapable of either donating electrons to, or accepting electrons from the phenol oxidation products. This was due to the fact that the linear ASA group in PANI-ASA was adsorbed too tightly on the Pt-electrode, compared to the bulky PSA group in PANI-PSA, thereby attributing to impeding electron transfer.

On the other hand, it appears that the Pt/PANI-PSA chemo-sensor system involving PANI-PSA as an electron mediator is more sensitive than its PANI-ASA counterpart for certain phenolic compounds. The Pt/PANI-PSA electrode was seen to electrically catalyse the oxidation of Ph, 2,4-DCP, PCP and 4-C3MP.

5.5 References

- [1] A. J Bard and L.R. Faulkner, *Electrochemical Methods: Fundamentals and Applications*, 2nd ed., Wiley, New York (2001)
- [2] E. I. Iwuoha, D. S. de Villaverde, N. P. Garcia, M. R. Smyth and J. M. Pingarron, *Biosens. and Bioelectr.* 12 (1997) 749-761
- [3] N. G. R. Mathebe, A. Morrin and E. I. Iwuoha, *Talanta* 64 (2004) 115-12
- [4] S. Brahim, A. M. Wilson, D. Narinesingh, E. Iwuoha and A. Guiseppi-Elle, *Microchim. Acta*, 143 (2003) 123-137
- [5] A. Morrin, R. M. Moutloali, A. J. Killard, M. R. Smith, J. Darkwa and E. I. Iwuoha, *Talanta*, 64 (2004) 30
- [6] T. Mafatle and T. Nyokong, *Analyt. Chim. Acta*, 354 (1997) 307 – 314
- [7] E. I. Iwuoha, A. R. Williams, L. A. Hall, A. Morrin, G. N. Mathebe, M. R. Smith and A. Killard, *Pure Appl. Chem.*, 76 (2004) 789
- [8] P. Önnarfjord, J. Emnéus, G. Marko-Varga, L. Gorton, F. Ortega and E. Dominguez, *Biosens. & Bioelectr.*, 10 (1995) 607
- [9] B. Wang and S. Dong, *J. Electroanal. Chem.*, 487 (2000) 45
- [10] A. Lindgren, J. Emnéus, T. Ruzgaz, L. Gorton and G. Marko-Varga, *Anal. Chim. Acta*, 347 (1997) 51

[11] M. A. Kim and W-Y. Lee, *Anal. Chim. Acta*, 479 (2003) 143

[12] S. Liu, J. Yu and H. Ju, *J. Electroanal. Chem.*, 540 (2003) 61

[13] E. Nieminen and P. Heikkilä, *J. Chromaogr.*, 360 (1986) 271



Chapter 6

The Catalytic, Electro-catalytic and Redox Mediator Effects of Nanostructured POMA-ASA and POMA-PSA Modified Electrodes as Phenol (and phenol derivatives) Sensors

6.1 Introduction

In the previous chapter we discussed the catalytic, electro-active and redox mediator effects of PANI-ASA and PANI-PSA modified nanostructured conducting polymer Pt electrodes as phenol (derivatives) electrochemical sensors.

The results indicate that the Pt/PANI-ASA and Pt/PANI-PSA chemosensors were not completely successful. The performances of most of the PANI/ASA and some of the PANI/PSA as electron transfer mediators in the phenol (derivative) system suggested that it was incapable of either donating or accepting electrons. This chapter deals with the catalytic effect that the polymers (POMA-ASA and POMA-PSA) have as redox mediators (electron shuttles) for the oxidation of phenol and its derivatives using electrochemical means.

6.2 Methods

The description of the experimental procedure, which includes the construction and assumptions of the chemical sensor for the determination of phenol and derivatives are the same as outline in **Chapter 5**.

Section 6.3 discusses the results and **Section 6.4** draw conclusions about the experiments.

6.3 Results and discussion

6.3.1 Electrochemical behaviour of the Pt/POMA-ASA electrode

Multi-scan rate voltammograms of POMA-ASA on Pt electrode in 1 M HCl with scan rates of 5, 10, 20, 30, 40 and 50 mV/s are shown in **Figure 6.1**. The peak potentials and corresponding currents vary as the scan rate values vary. These results suggest that the polymeric nanostructure is electro-active and possesses the potential for under going both oxidation and reduction reactions. Pt/POMA-PSA in a 1 M HCl electrolyte solution also displayed similar oxidation-reduction responses indicating that the modified electrode is electro-active [1-3].

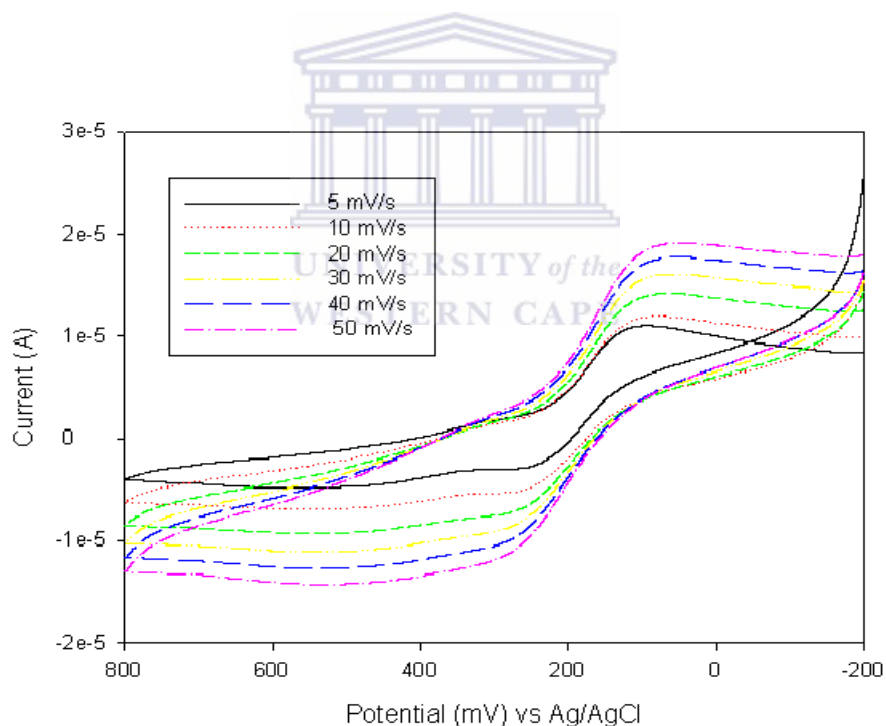


Figure 6.1: Characterisation of Pt/POMA-ASA on Pt- electrode in 1 M HCl at scan rates 5, 10, 20, 30, 40 and 50 mV/s.

6.3.2 The shift in formal potentials (ΔE°) of Pt/POMA-ASA and Pt/POMA-PSA electrodes with phenol (derivatives)

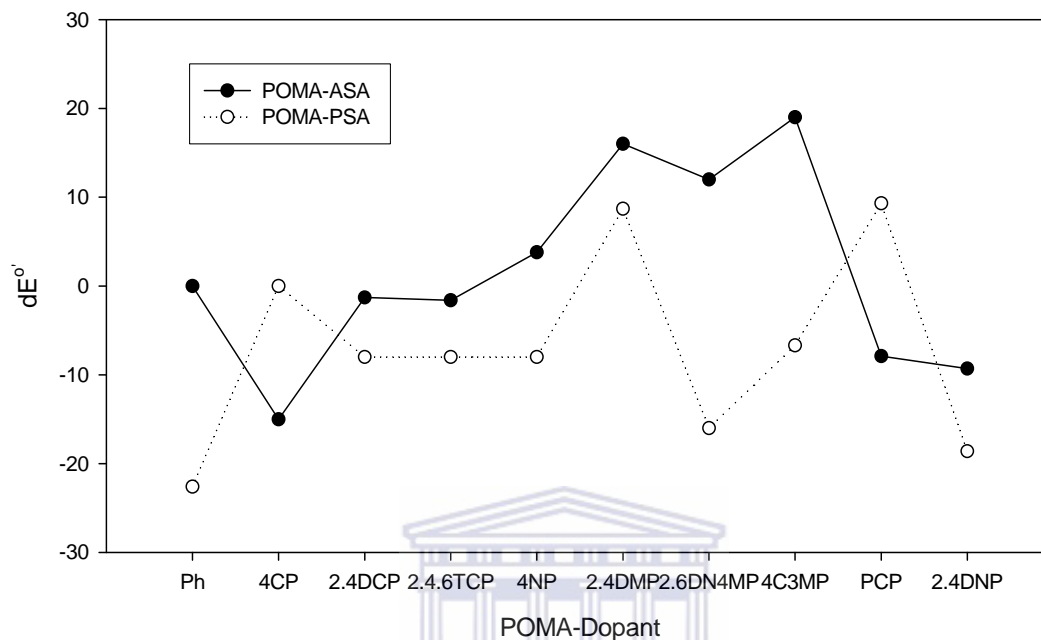


Figure 6.2: The shift in formal potentials ($dE^{\circ} = \Delta E^\circ$) of the different Pt/POMA-dopant modified electrodes in 1M HCl before and after the addition of the phenol (derivatives)

The shift in the formal potential of Pt/POMA-ASA and Pt/POMA-PSA modified electrodes in 1 M HCl before and after addition of 20 μ L of phenol (derivatives) are presented in **Figure 6.2**. When the phenolic compounds were added to the Pt/POMA-ASA electrode the formal potential before and after addition of the phenolic compounds showed both positive and negative shifts. The shift in peak potentials before and after phenolic compounds that were added to the Pt/POMA-PSA electrode, showed mostly negative formal potentials. These results showed that some catalytic activity was taken place at the surfaces of these modified electrodes [4].

Also, that the difference in the potentials for the oxidation of the phenolic species are a result of the electron-donating and electron-withdrawing abilities of the substituents [5].

6.3.3 Electrochemical behaviour of Phenol (Ph) at the Pt/POMA-ASA and Pt/POMA-PSA electrodes

Figure 6.3 contains the anodic DPV responses of Pt/POMA-ASA chemosensor for phenol in cell solution containing 1 ml HCl (1 M) alone and the additions of several 0.002 M of Phenol under anaerobic conditions. A decrease in peak current at around +230 mV was observed as the phenol was added to the Pt/POMA-ASA chemosensor. The decrease in current can be explained to fouling of the electrode by dimeric and polymeric products [5]

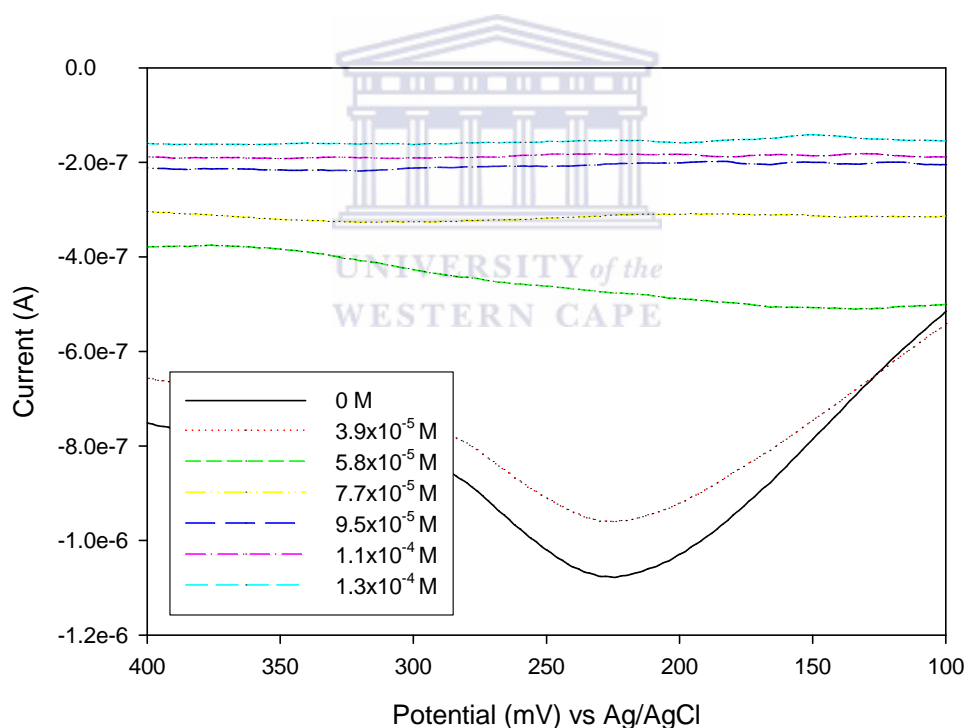


Figure 6.3: Differential pulse voltammograms of Pt/POMA-ASA chemosensor responses to 0, 20, 30, 40, 50, 60 and 70 μ L addition of Phenol (0.002 M) in 1 M HCl (1 mL) at a scan rate of 10 mV/s and a frequency of 5 Hz

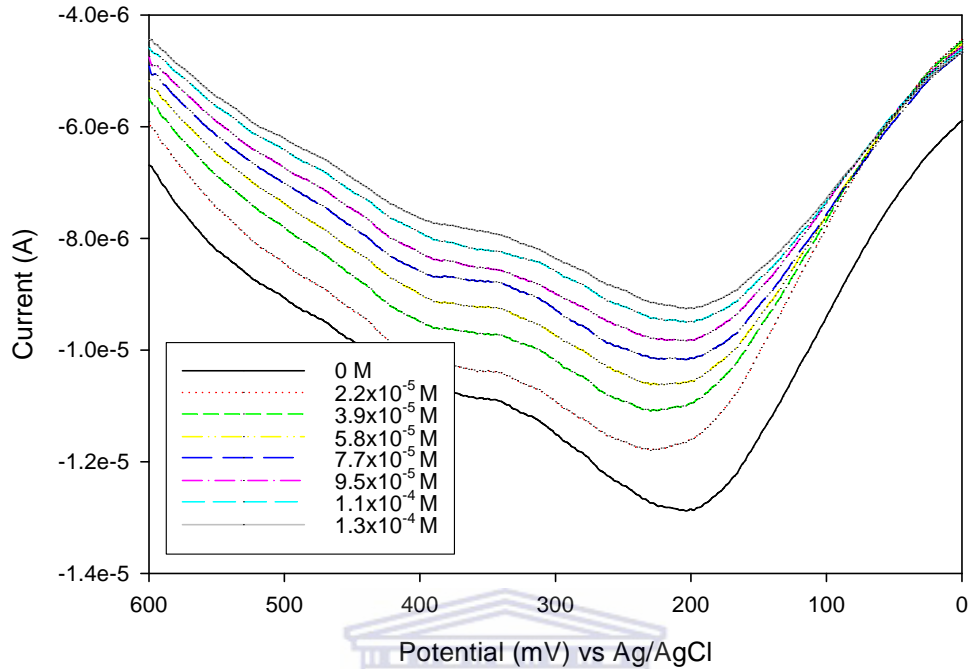


Figure 6.4: Differential pulse voltammograms of Pt/POMA-PSA chemosensor responses to 0, 10, 20, 30, 40, 50, 60 and 70 μL addition of Phenol (0.002 M) in 1 M HCl (1 mL) at a scan rate of 10 mV/s and a frequency of 5 Hz

UNIVERSITY of the
WESTERN CAPE

The DPV responses of Pt/POMA-PSA chemosensor for phenol in 1 M HCl (1 mL) are shown in **Figure 6.4**. There was a decrease of current around +200 mV when phenol was added to the Pt/POMA-PSA chemosensor. The current was seen to get smaller at high concentrations which could be attributed to the formation of a non-conducting poly(phenol) film formed on top of the POMA-PSA conducting polymer [6].

6.3.4 Electrochemical behaviour of 4-ChloroPhenol (4-CP) at the Pt/POMA-ASA and Pt/POMA-PSA electrodes

The same trends in catalytic DPV anodic responses were observed when 4-chlorophenol was added to Pt/POMA-ASA (**Figure 6.5**) and Pt/POMA-PSA chemosensors (**Figure 6.6**) in a 1 mL HCl (1 M) solution. There was a decrease in current when 4-CP was added to Pt/POMA-ASA and Pt/POMA-PSA chemosensors. This decrease in catalytic current was a result of the electron withdrawing of the chlorine groups, which made it difficult for the free radicals to form, therefore resulting in a formation of a non-conducting poly(4-CP) on top of the conducting polymers [7].

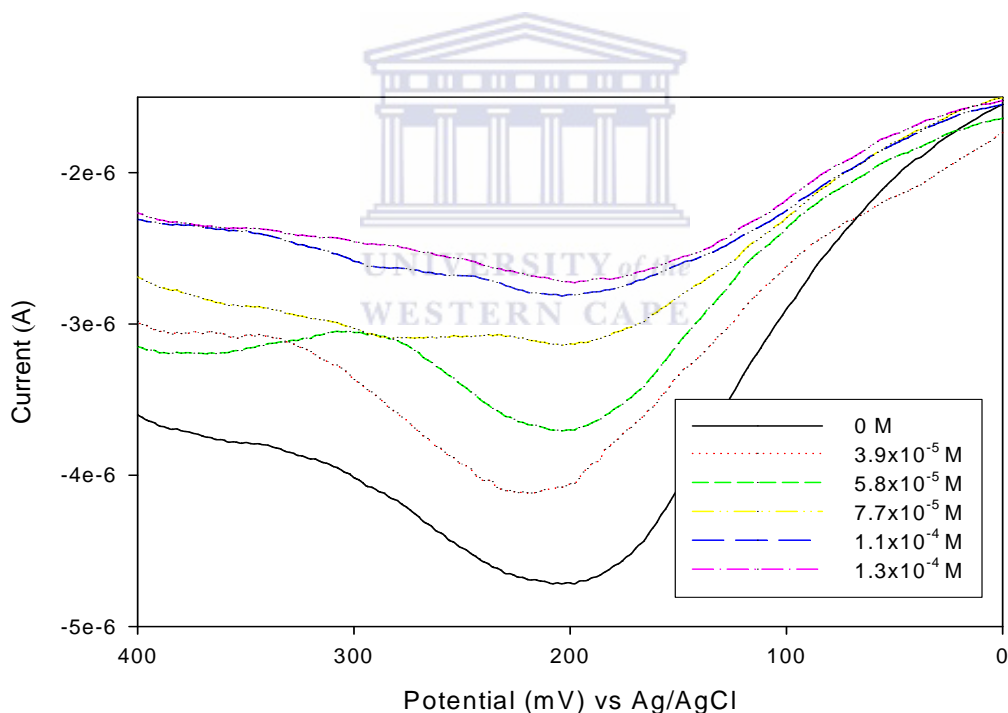


Figure 6.5: Differential pulse voltammograms of Pt/POMA-ASA chemosensor responses to 0, 20, 30, 40, 60 and 70 μ L addition of 4-CP (0.002 M) in 1 M HCl (1 mL) at a scan rate of 10 mV/s and a frequency of 5 Hz

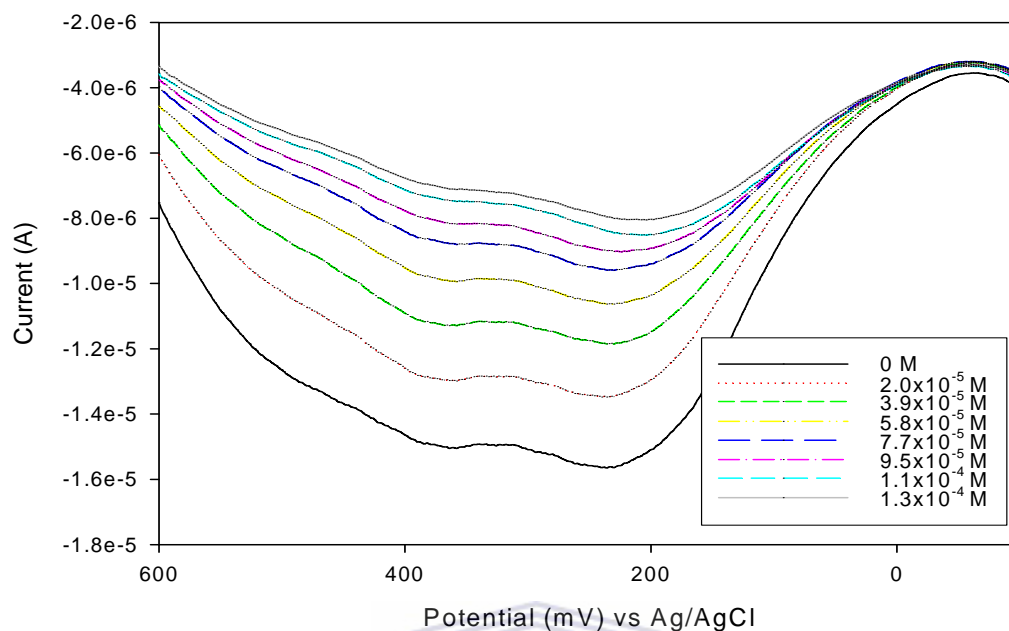


Figure 6.6: Differential pulse voltammograms of Pt/POMA-PSA chemosensor responses to 0, 20, 30, 40, 50, 60 and 70 μL addition of 4-CP (0.002 M) in 1 M HCl (1 mL) at a scan rate of 10 mV/s and a frequency of 5 Hz

6.3.5 Electrochemical behaviour of 4-Nitrophenol (4-NP) at the Pt/POMA-ASA and Pt/POMA-PSA electrodes

Figure 6.7 represents the DPV anodic responses when 4-Nitrophenol was added to the Pt/POMA-ASA chemosensor in 1 mL HCl (1 M) under anaerobic conditions. An increase in the oxidation current was observed when 4-NP was added to the Pt/POMA-ASA chemo-sensor. The increase in catalytic current was due to the catalytic oxidation of the 4-NP to its different oxidation products [8]. However, a decrease in anodic responses of Pt/POMA-PSA chemosensor was found (**Figure 6.8**) when 4-NP was added to the electrochemical cell. This decrease in catalytic current could be a result of steric hindrance of the bend fused PSA groups in the POMA-PSA polymer minimizing the oxidation of 4-NP [5].

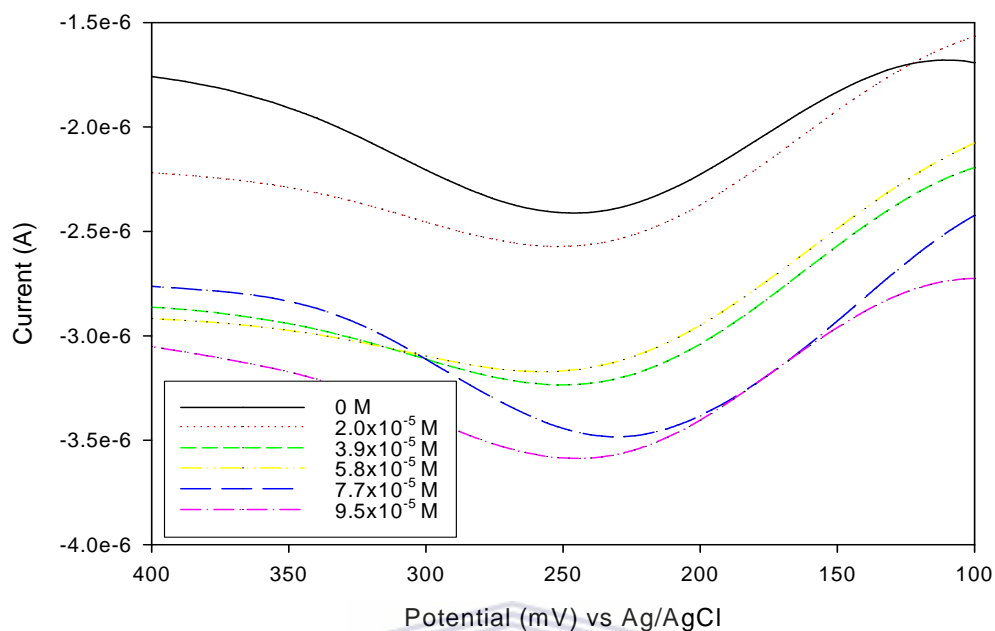


Figure 6.7: Differential pulse voltammograms of Pt/POMA-ASA chemosensor responses to 0, 10, 20, 30, 40 and 50 μL addition of 4-NP (0.002 M) in 1 M HCl (1 mL) at a scan rate of 10 mV/s and a frequency of 5 Hz

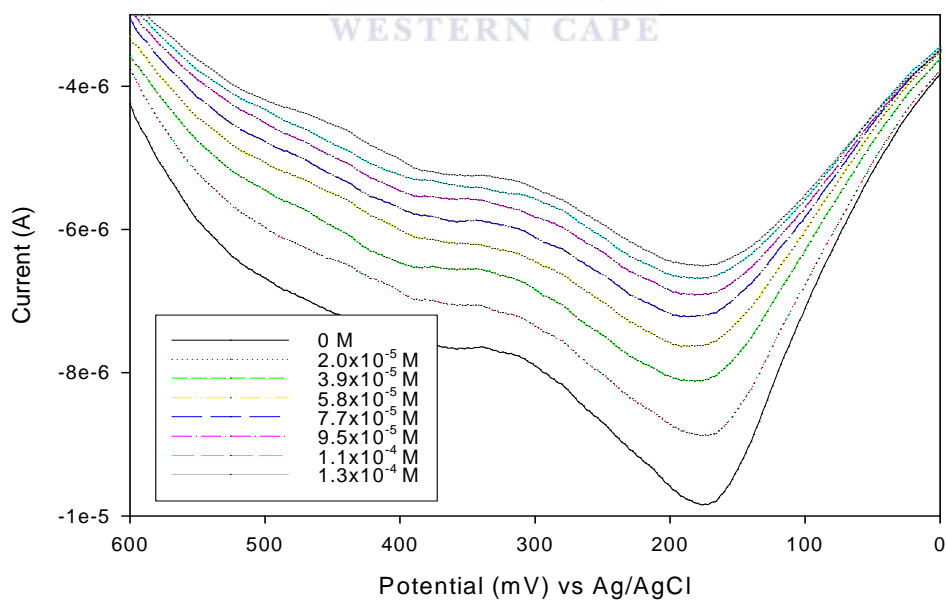


Figure 6.8: Differential pulse voltammograms of Pt/POMA-PSA chemosensor responses to 0, 20, 30, 40, 50, 60 and 70 μL addition of 4-NP (0.002 M) in 1 M HCl (1 mL) at a scan rate of 10 mV/s and a frequency of 5 Hz

6.3.6 Calibration curves of the Pt/POMA-ASA and Pt/POMA-PSA chemosensors for Phenol (derivatives)

The response characteristics of the Pt/POMA-ASA and Pt/POMA-PSA chemosensors as a function of phenolic compounds were studied in this section. The calibration curve was a measure of the absolute value of the difference between the peak current with no addition and when the phenolic compounds were added versus the concentration.

The calibration curves obtained for the Pt/POMA-ASA chemosensor for Ph, 4-CP and 4-NP are depicted in **Figure 6.9**. The chemosensor was first stabilised with the first additions of Ph and 4-CP after which an increase in current was noticed at low concentrations. Leveling off of the current was observed at higher concentrations which may be a result of fouling of the chemosensor surface by the oxidation products [9].

This is in contrast with the linear calibration curve of Pt/POMA-ASA as a chemosensor for 4-NP in 1 M HCl as electrolyte. A decrease in current was observed when 4-NP was added to the electrode until a plateau was reached at high concentrations. The same trend was seen when 2,4-DCP and 2,4,6-TCP (**Figure 6.10**) were added to the chemosensor. This was a result of the inhibiting effect of the phenolic compounds on the chemosensor.

No significant trends were seen when 2,4-DNP, 2,4-DMP, PCP and 4-C3MP and

2,6-DN4MP was added to the Pt/POMA-ASA chemosensor (**Figure 6.11**).

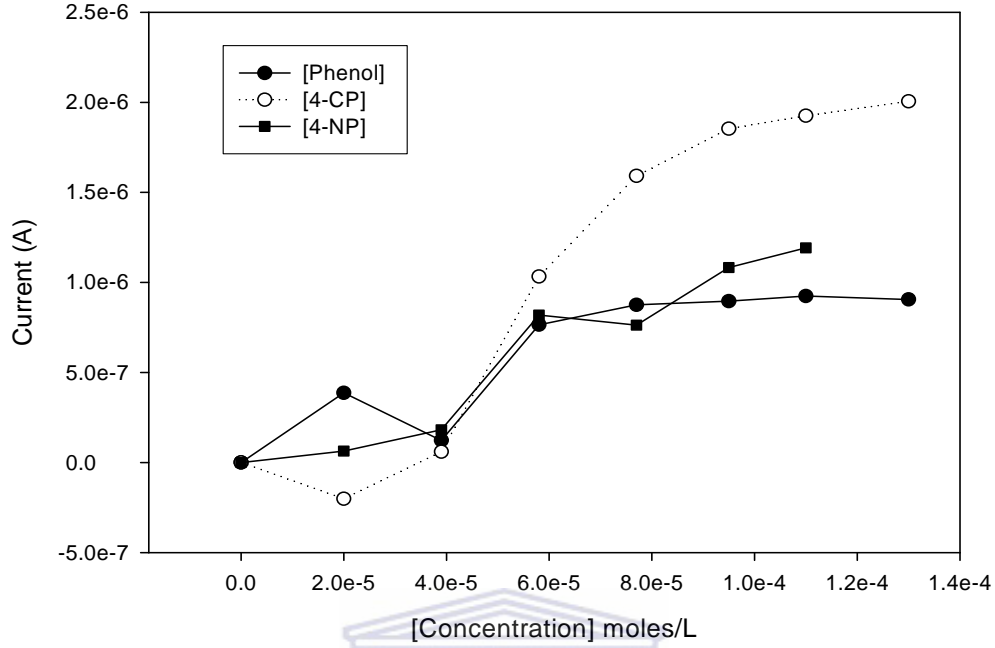


Figure 6.9: Calibration curves of the Pt/POMA-ASA modified electrode for Ph, 4-CP and 4-NP

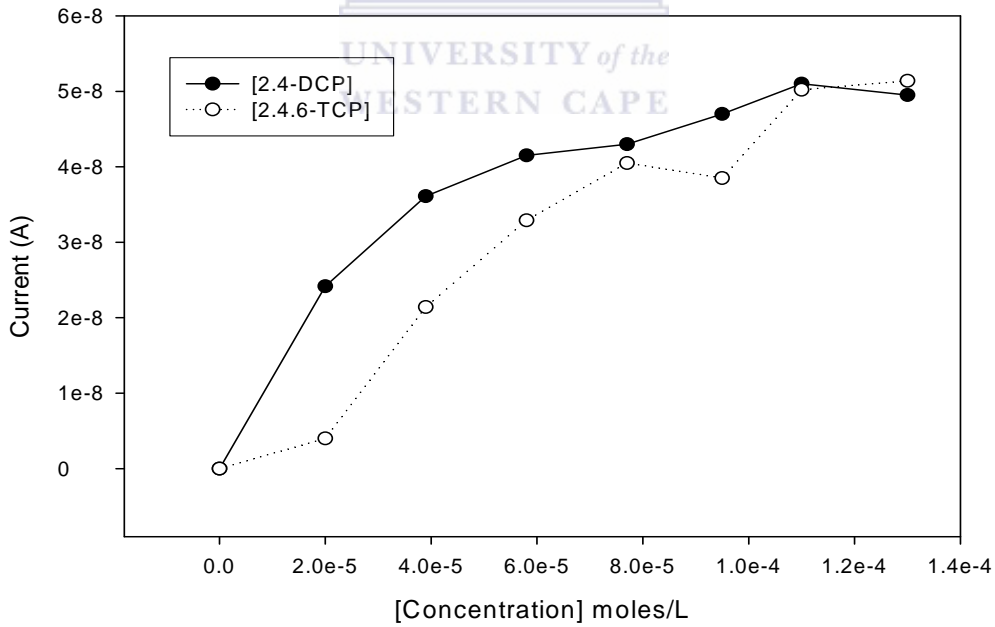


Figure 6.10: Calibration curves of the Pt/POMA-ASA modified electrode for 2.4-DCP and 2.4.6-TCP

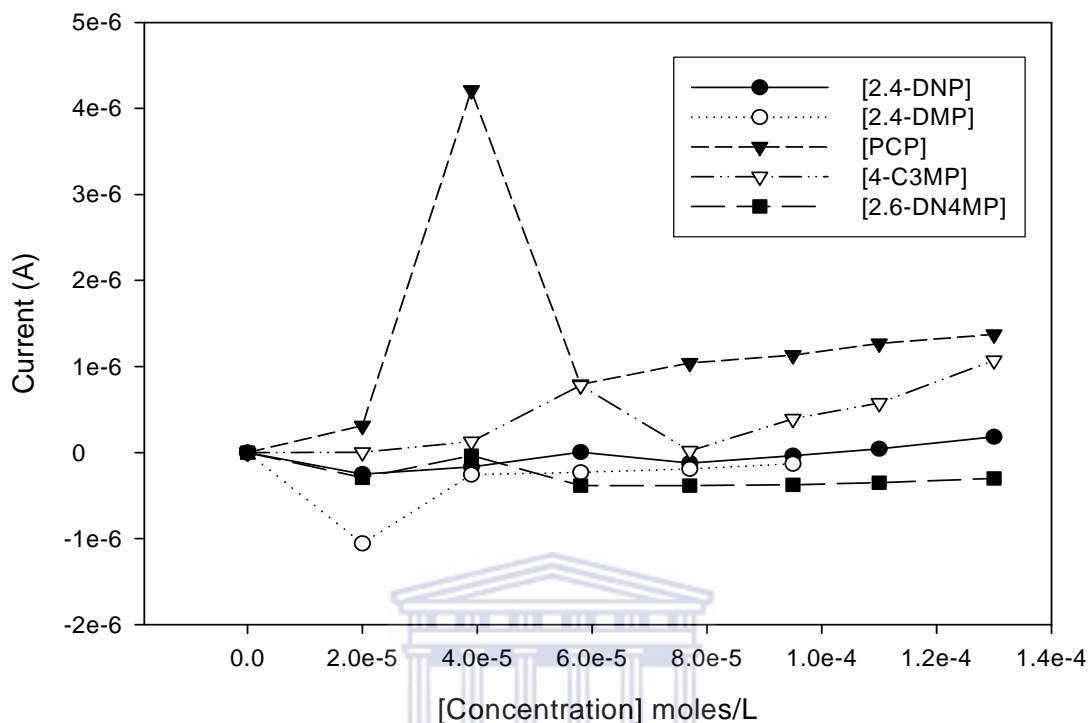


Figure 6.11: Calibration curves of the Pt/POMA-ASA modified electrode for 2,4- DNP, 2,4.-DMP, PCP and 4-C3MP and 2,6-DN4MP

The calibration curves obtained for the Pt/POMA-PSA as a chemosensor for Ph, 4-CP and 4-NP are shown in **Figure 6.12**. An increase in the current responses was noted as the concentrations of phenol and 4-nitrophenol are increased up to 1.1×10^{-4} M. The curves increased to a maximum at this concentration. The 4-chlorophenol sensors first stabilized for the first two additions before an increase was noticed. These calibration curves showed that catalytic oxidation processes was taking place.

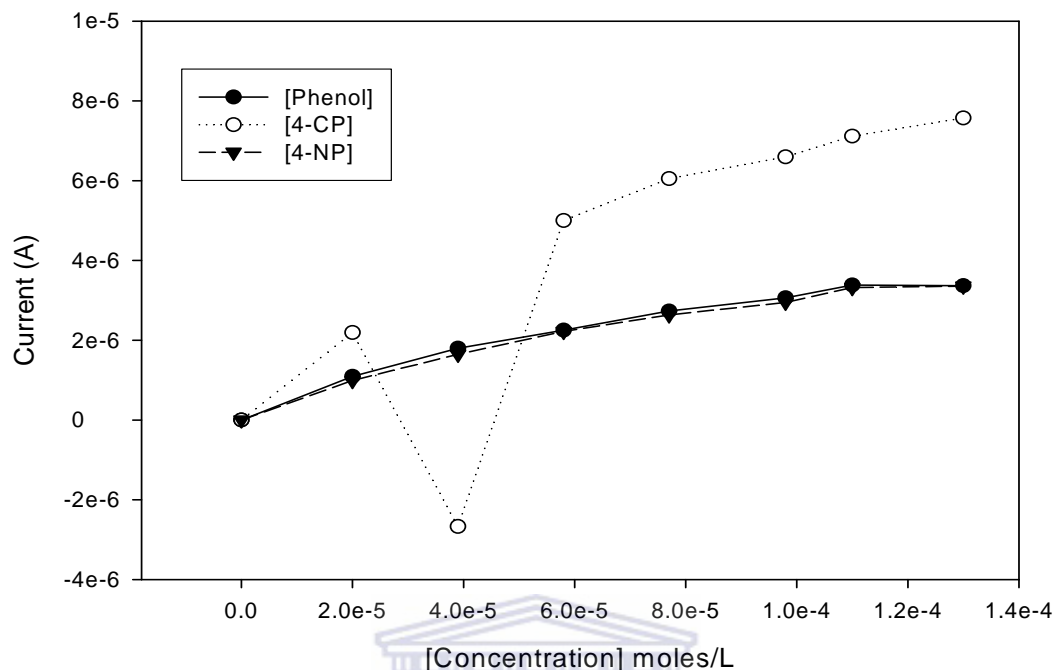


Figure 6.12: Calibration curves of the Pt/POMA-PSA modified electrode for Ph, 4CP and 4NP

Figure 6.13 represents the Pt/POMA-PSA chemosensor calibration curves in 1 M HCl when 2,4-DCP, 2,4-DNP, 2,4-DMP, 2,4,6-TCP, PCP and 4-C3MP were added. An increase in current responses was detected as the concentration of the phenolic compounds was increased. A maximum current was reached where the activity of the chemosensor is decreased at high concentrations of the phenolic compounds, which was probably due to the competition for active sites on the chemosensor surface. The Pt/POMA-PSA chemosensor exhibited good responses to all the tested phenolic compounds over a wide concentration range (**Appendix A: Table A3 and A4**) [5].

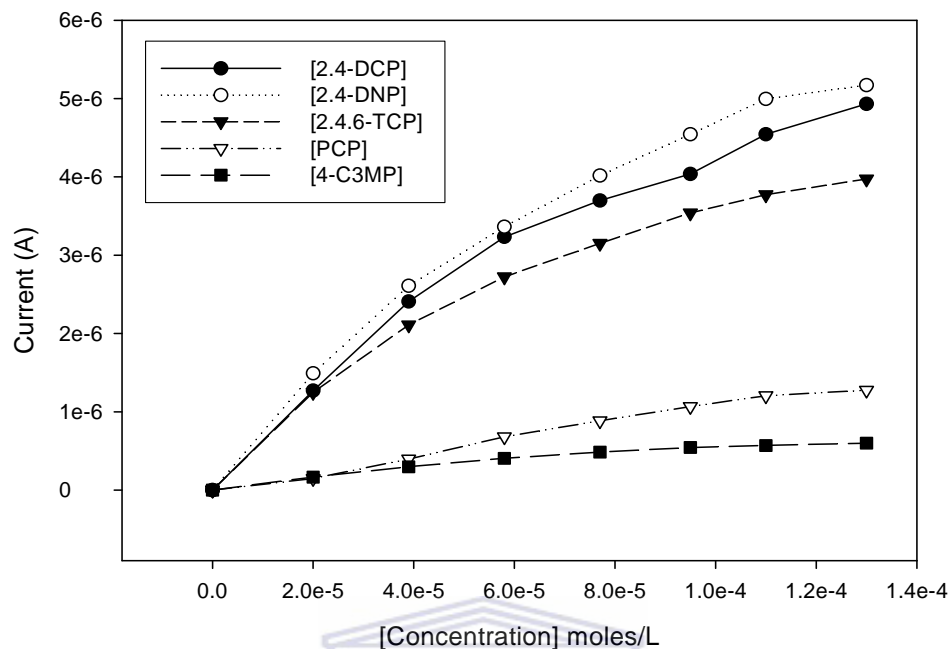


Figure 6.13: Calibration curves of the Pt/POMA-PSA modified electrode for 2,4-DCP, 2,4-DNP, 2,4,6-TCP, PCP and 4-C3MP

6.3.7 Chemosensor Kinetic Parameters for Phenol (derivative) detection

Since they have all the same trend, the kinetic parameters of the Pt/POMA-PSA nanostructured polymer for phenol and derivatives, are displayed in **Table 6.1**. The kinetic modeling of the chemosensor results was based on the assumption that the Pt/POMA-PSA sensing layer was a thin homogeneous film in which the phenol (derivatives) oxidation charge is propagated along the polymer chain by electron reactions involving the reduced and oxidized form of the conducting nanostructured polymers. The calibration curves all displayed non-linear responses of current with phenol (derivative) concentration and was modelled according to the Michaelis-Menten equation [2, 10].

Analyte	Sensitivity (mA/M)	K'_m (μM)	k'_{cat} ($\text{nmol.cm}^{-2}.\text{s}^{-1}$)	Detection Limit (M)
Ph	28	120.7	1.979	6.810×10^{-4}
4-CP	229	26.4	3.541	7.399×10^{-5}
4-NP	28.4	116.8	1.943	4.699×10^{-4}
2,4-DCP	49	75.8	2.166	3.266×10^{-4}
2,4,6-TCP	41	77.7	1.844	3.597×10^{-4}
2,4-DNP	52	77.2	2.351	2.165×10^{-4}
2,4-DMP	8.6	104.3	0.522	1.081×10^{-3}
PCP	11.5	104.7	0.705	9.523×10^{-4}
4-C3MP	5.7	95.4	0.329	4.217×10^{-4}
2,6-DN4MP	nd	nd	nd	nd

nd = not detected

Table 6.1: Kinetic parameters of the Pt/POMA-PSA chemosensor for various phenol (derivatives)

The sensitivities (measured by the slope of the calibration curves), which is generally dependent on the solubility of phenolic compounds in the immobilization matrix, followed the order 4-CP > PCP > 2,4-DNP > 2,4DCP > 2,4,6TCP > 4-NP > Ph > 2,4 DMP > 4-C3MP. Thus indicating that the electron-withdrawing phenolic compounds is more soluble in the POMA-PSA matrix than the electron donating phenolic compounds [11].

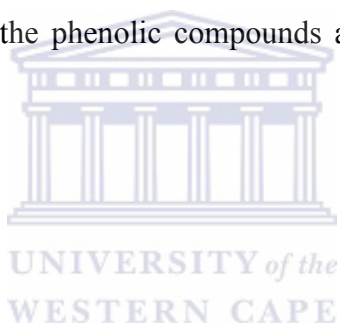
The Michaelis-Menten constant (K'_m) in this case predicts the ease with which a phenolic molecule partition into the POMA-PSA polymer film and followed the order Ph > 4-NP > PCP > 2,4-DMP > 4-C3MP > 2,4,6-TCP > 2,4-DNP > 2,4-DCP > 4-C3MP. This means that Ph stays longer in the solvent medium than 4-C3MP, with the result that the sensor requires a large amount of the Ph to saturate its activity [10].

The apparent turnover rate constant (k'_{cat}) gives us an idea of the total phenolic compounds concentration in the POMA-PSA film and the maximum current of the sensor

at saturation. The k'_{cat} followed the order 4-CP > 2,4-DNP > 2,4-DCP > Ph > 4-NP > 2,4,6-TCP > PCP > 2,4-DMP > 4-C3MP, which suggest faster reaction rate and higher currents for Pt/POMA-PSA as a chemosensor for 4-CP compared to Pt/POMA-PSA as a chemosensor for 4-C3MP. A high detection limit was observed for the Pt/POMA-PSA as a chemosensor for phenol (derivatives) at an estimated signal to noise (S/N) ratio of 3 [12].

The voltammetric responses obtained by the Pt/POMA-PSA modified electrode obtained in the presence of phenolic compounds is proposed to be representative of the catalytic current results from the redox mediation reactions of the POMA-PSA conducting polymer and the oxidation of the phenolic compounds as schematically represented in

Figure 6.13.



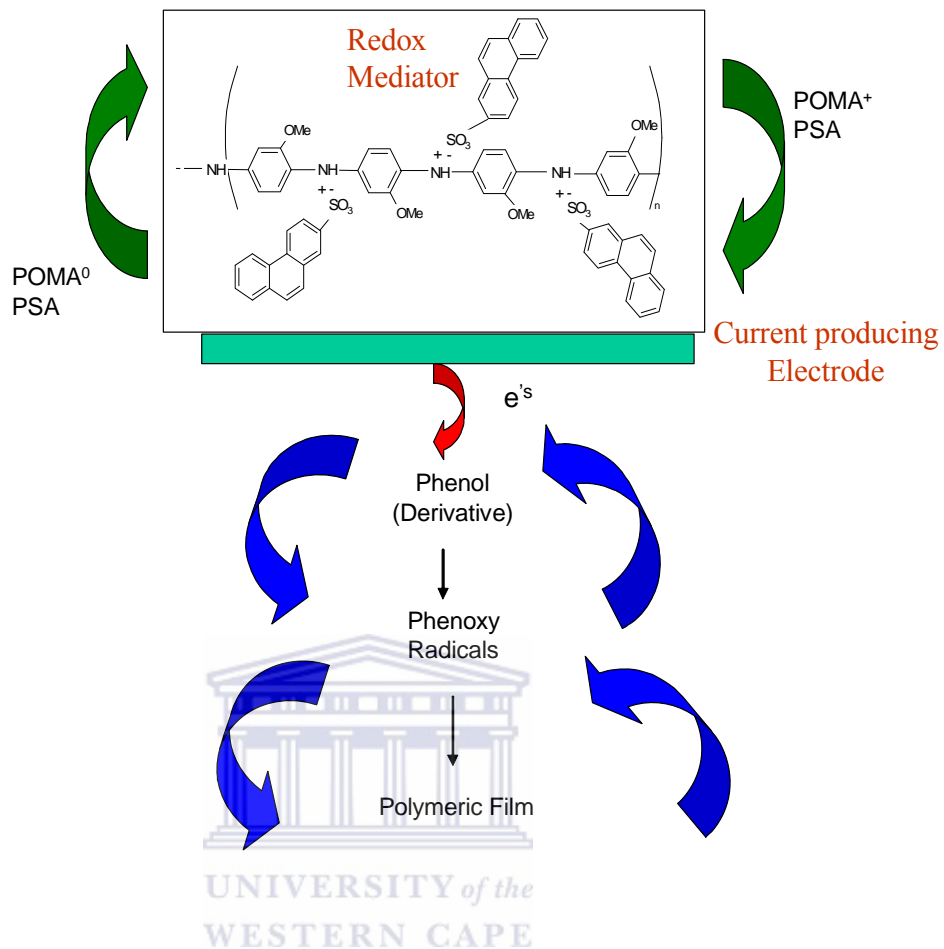


Figure 6.14: Reaction scheme outlining the role of the POMA-PSA as a redox mediator in the oxidation of phenol for the Pt/POMA-PSA chemosensor

The diagram shows that the phenol is oxidised to phenoxy radicals as the reaction proceeds and that a non-conducting poly(phenol) film formed, which leads to the poisoning of the electrode [13]. However, this formation of the non-conducting poly(phenol) film with increasing concentrations and decreasing current (normally we have an increasing current with increasing concentration) allows for the development of an unconventional Pt/POMA-PSA chemosensor for Phenol (derivatives).

6.4 Conclusions

The Pt/POMA-ASA and Pt/POMA-PSA modified electrodes both exhibited redox properties in aqueous solutions with 1 M HCl as the supporting electrolyte. The POMA-ASA and POMA-PSA conducting polymers performances as redox electron transfer mediators in the Pt/POMA-ASA and Pt/POMA-PSA chemosensor for phenol (derivatives) systems suggested that they were capable of either donating or accepting electrons. The nature of the substituent attached to the phenol influenced both the transfer abilities of the electrons and the solubility into the polymer film, which has a major impact on the chemosensor. However, after the formation of the phenolic radicals an insulating film formed, which gradually prevents movement of electrons with increasing phenolic compound concentration and results in the passivation of the electrode surface. It is likely that these species remain strongly adsorbed on, or even trapped inside the polymer films. Hence, a reverse Pt/POMA-ASA and Pt/POMA-PSA chemosensors were proposed.

6.5 References

- [1] A. J. Bard and L. R. Faulkner, *Electrochemical Methods: Fundamentals and Applications*, 2nd ed., Wiley, New York (2001)
- [2] E. I. Iwuoha, D. S. de Villaverde, N.P. Garcia, M.R. Smyth and J.M. Pingarron, *Biosens. and Bioelectr.* 12 (1997) 749-761
- [3] N. G. R. Mathebe, A. Morrin and E. I. Iwuoha, *Talanta*, 64 (2004) 115-12
- [4] S. Brahim, A. M. Wilson, D. Narinesingh, E. Iwuoha and A. Guiseppi-Elle, *Microchim. Acta*, 143 (2003) 123-137
- [5] T. Mafatle and T. Nyokong, *Anal. Chim. Acta*, 354 (1997) 307 – 314
- [6] E. I. Iwuoha, A. R. Williams, L. A. Hall, A. Morrin, G. N. Mathebe, M. R. Smith and A. Killard, *Pure Appl. Chem.*, 76 (2004) 789
- [7] S. A. Kane, E. I. Iwuoha and M. R. Smyth, *Analyst* 123 (1998) 2001
- [8] Y. Lei, P. Mulchandani, W. Chen, J. Wang, A. Mulchandani, *Electroanal.*, 15 (2003) No. 14
- [9] J. Wang and M. S. Lin, *Anal. Chem.*, 61 (1989) 2809
- [10] I. E. Iwuoha, L. Ingrid, M. Edna and Ó. F. Ciárin, *Anal. Chim. Acta*, 69 (1997) 1674
- [11] M. A. Kim and W-Y. Lee, *Anal. Chim. Acta*, 479 (2003) 143 – 150
- [12] Z. Wen and T. Kang, *Talanta* 62 (2004) 351
- [13] M.S. Ureta-Zañartu, P. Bustos, C. Berrios, M. C. Diez, M. L. Mora and C. Gutiérrez, *Electrochim. Acta*, 47 (2002) 2399 – 2406

Chapter 7

The Catalytic, Electro-catalytic and Redox Mediator Effects of Nanostructured PDMA-ASA and PDMA-PSA Modified Electrodes as Phenol (and phenol derivatives) Sensors

7.1 Introduction

The previous chapter discussed the catalytic, electro-active and redox mediator effects of Pt/POMA-ASA and Pt/POMA-PSA modified nanostructured conducting polymer electrodes as phenol and derivative sensors. The results showed that POMA-ASA and POMA-PSA immobilised on Pt exhibited redox responses, but was not successful as a conventional chemosensor construction. However a reverse chemosensor was proposed.

This chapter deals with the catalytic effect that the polymers (PDMA-ASA and PDMA-PSA) have as electron shuttles for the oxidation of phenol and its derivatives using electrochemical means.

7.2 Methods

The description of the experimental procedure, which includes construction and the assumptions of the chemical sensor for the determination of phenol and derivatives are the same as outline in **Chapter 5**.

Section 7.3 discusses the results and **Section 7.4** draw conclusions about the experiments.

7.3 Results and discussion

7.3.1 Electrochemical behaviour of the Pt/PDMA-ASA electrode

Multi-scan rates voltammograms of PDMA-ASA on Pt electrode with scan rates 10, 20, 30, 40 and 50 mV/s are shown in **Figure 7.1**. It can be seen that the peak potential and corresponding peak currents vary as the scan rate value vary, which suggested that the polymeric nanostructure on the Pt is electroactive and that charge transport along the polymer structure was taking place. The potentials of peaks a and b' do not change as the scanrates was increased. This means that the PDMA-ASA was bound to the Pt electrode.

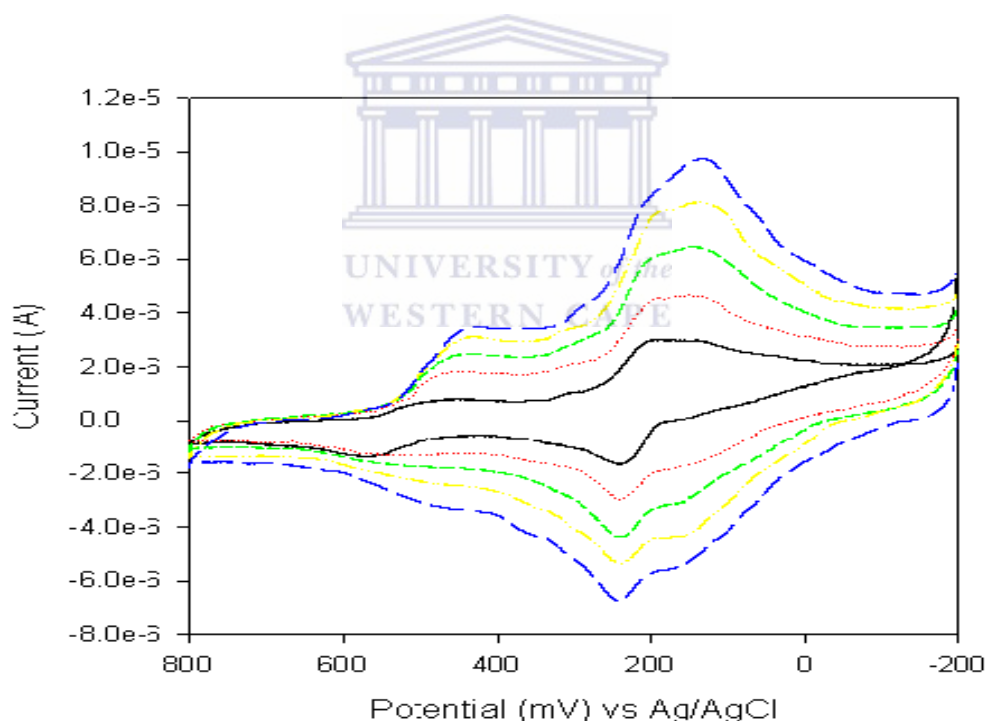


Figure 7.1: Characterisation of PDMA-ASA on Pt electrode in 1 M HCl at scan rates 10, 20, 30, 40 and 40 mV/s.

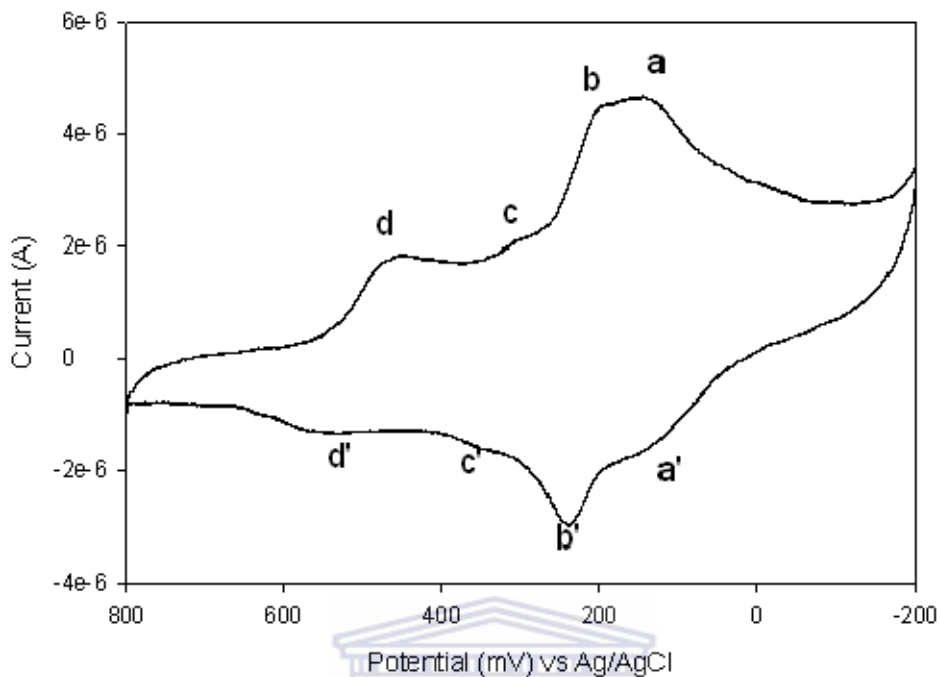


Figure 7.2: Characterisation of PDMA-ASA on Pt electrode in 1 M HCl at a scan rate of 20 mV/s

It is clear from **Figure 7.2** (single scan rate) that there are 4 anodic and 4 cathodic peaks in the voltammograms. The first oxidation peak (peak a') is due to the polyemeraldine state, which is further oxidized at higher potential to polyemeraldine radical cation (peak b'), which oxidized further to pernigraniline (peak c').

For the cathodic scan, pernigraniline cation radical (peak c) is first reduced to the partly reduced leucoemeraldine radical cation (peak b), and then to the fully reduced leucoemeraldine (peak a). The redox couple d/d' is attributed to the redox reaction of p-benzoquinone. The Pt/PDMA-PSA was also found to be electro-active [1-4].

7.3.2 The shift in potentials (ΔE°) of Pt/PDMA-ASA and Pt/PDMA-PSA electrodes with phenol (derivatives)

The difference in the shift potentials (ΔE°) of the Pt/PDMA-ASA and Pt/PDMA-PSA electrodes before and after 20 μL additions of phenol (and derivatives) were added to 1 mL HCl (1 M) are illustrated in **Figure 7.3**.

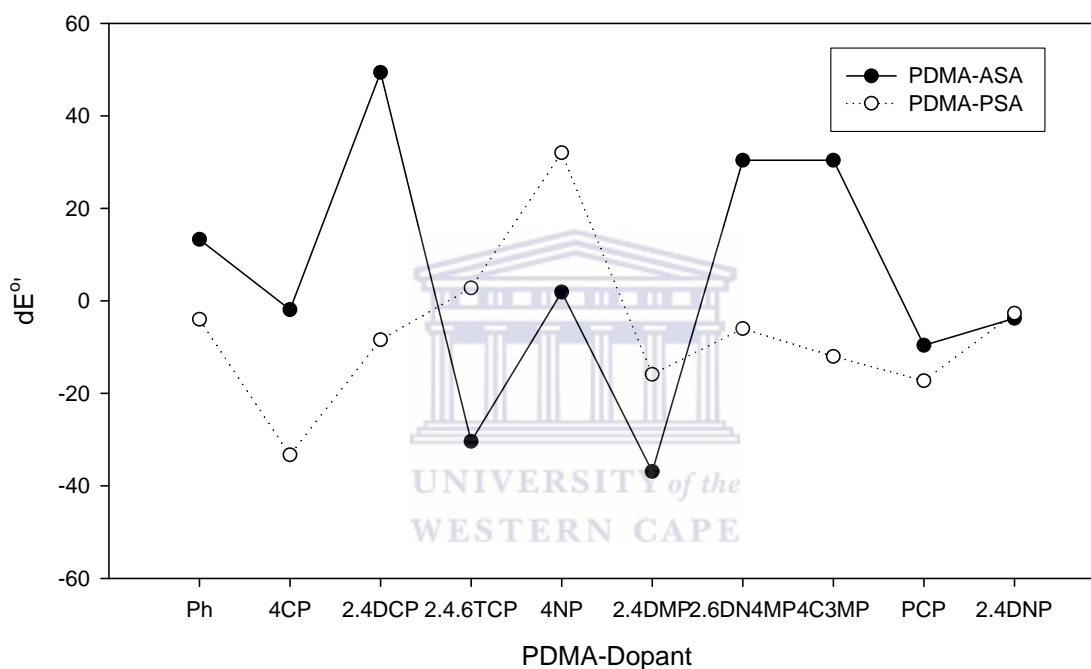


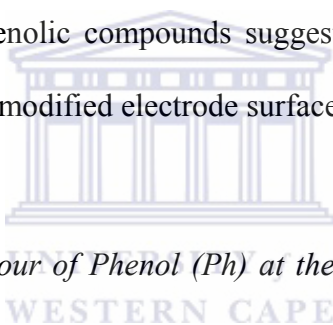
Figure 7.3: The shift potentials difference ($dE^\circ = \Delta E^\circ$) with Pt/PDMA-ASA modified electrodes in 1M HCl before and after 20 μL addition of the phenol (derivatives)

From the graph (**Figure 7.3**) the difference in the shift of potential (ΔE°) before and after 20 μL addition of 2.4-DCP (+49.4 mV) was seen to be the highest followed by 2.6-DN4MP (+30.4 mV) and 4-C3MP (+30.4 mV) with the Pt/PDMA-ASA modified electrode. The lowest ΔE° 's were seen for 2.4-DMP (-36.9 mV), 2.4.6-TCP (-30.4 mV)

and PCP (-9.6 mV). Intermediate ΔE° 's were observed for Ph (+13.3 mV), 4-CP (-1.9 mV), 4-NP (+1.9 mV) and 2,4-DNP (-3.8 mV).

The shift in potential was the biggest for 4-NP (+32.0 mV) followed by 2,4,6-TCP (2.8 mV) and 2,4-DNP (-2.7 mV) respectively for Pt/PDMA-PSA modified electrodes. The intermediate potential shifts included Ph (-4.0 mV), 2,6-DN4P (-6.0 mV), 2,4-DCP (-8.0 mV), 4C3MP (-12.0 mV), 2,4-DMP (-15.9 mV) and PCP (-17.3 mV). The lowest potential shift was seen for 4-CP (-33.3 mV).

The different substituents on the phenol compound, whether electron-withdrawing or electron-donating, showed different shifts in formal potentials. The results in shift of potentials with addition of phenolic compounds suggested that some kind of catalytic activity was taking place at the modified electrode surface [5-7].



7.3.3 *Electrochemical behaviour of Phenol (Ph) at the Pt/PDMA-ASA and Pt/PDMA-PSA electrodes*

The electrochemical detection of phenol was performed using differential pulse voltammetry (DPV) because of its more sensitive nature than the cyclic voltammetry (CV) technique [8].

The nanostructured Pt/PDMA-ASA modified electrode show low background current before the addition of 0.002 M phenol. Upon addition of the phenol to the electrochemical cell under anaerobic conditions (**Figure 7.4**), there was a small initial increase in current response followed by a big increase in the 1 M HCl solution. The increase in current with phenol concentration was seen to be linear at a potential of approximately +130 mV. The enhanced current may be as a result of the electron transfer

of o-quinone to the Pt/PDMA-ASA electrode surface or the catalytic reactions of phenols to form o-quinone or both [5-6].

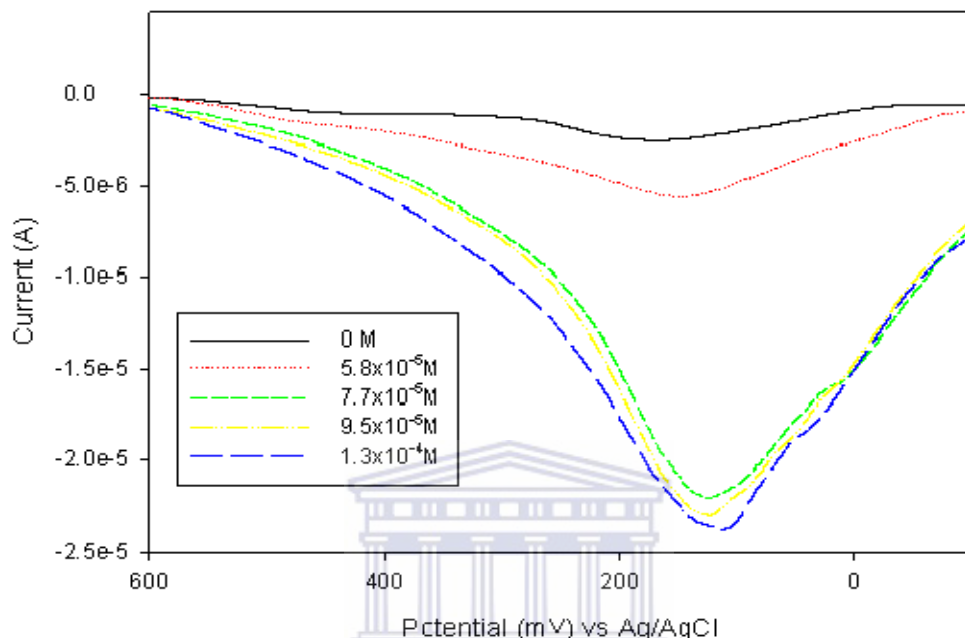


Figure 7.4: Differential pulse voltammograms of Pt/PDMA-ASA chemosensor responses to 0, 30, 40, 50 and 70 μL addition of Phenol (0.002 M) in 1 M HCl (1 mL) at a scan rate of 10 mV/s and a frequency of 5 Hz

There was no remarkable shift in the differential pulse peak potential on addition of phenol to Pt/PDMA-PSA (**Figure 7.5**). An increase in the catalytic current was observed at a potential of +75 mV, which is a result of the most conducting emeraldine state of PDMA, upon addition of phenol. The increase in current can be explained as resulting from the formation of the phenol oxidation products. A decrease of catalytic current was observed around +250 mV, which was attributed to the less conducting pernigraniline state of PDMA not being able to oxidise phenol [9].

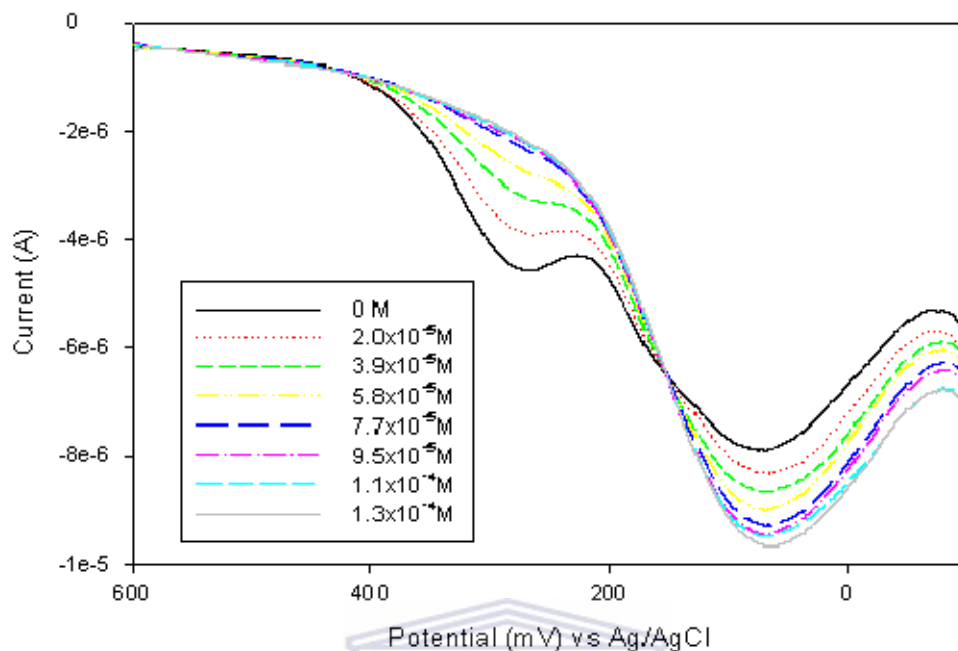
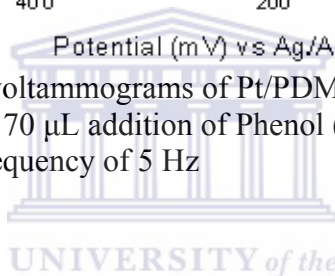


Figure 7.5: Differential pulse voltammograms of Pt/PDMA-PSA chemosensor responses to 0, 10, 20, 30, 40, 50, 60 and 70 μL addition of Phenol (0.002 M) in 1 M HCl (1mL) at a scan rate of 10 mV/s and a frequency of 5 Hz



7.3.4 Electrochemical behaviour of 4-ChloroPhenol (4-CP) at the Pt/PDMA-ASA and Pt/PDMA-PSA electrodes

Differential Pulse Voltammograms of Pt/PDMA-ASA modified electrode in 1 M HCl with the addition of 4-Chlorophenol (0.002 M) are given in **Figure 7.6**. There was at first a rapid increase in current response following addition of increasing concentrations of 4-CP in 1 M HCl solution, after which a maximum current was reached, followed by a decreased again. The increase in current was due to the oxidation of 4-CP into its different oxidation products. When the maximum current was reached the Pt/PDMA-ASA chemosensor for 4-CP reached its saturation point. This was as a result of oxidation products formed on the active sites poisoning the electrode attributed to slow surface fouling by the reaction products or insulating 4-CP film on the Pt/PDMA-ASA electrode.

The observations imply that the activity of the electrode is decreased at high concentrations of 4-CP, probably due to competition for active sites on the electrode surface [5, 10]

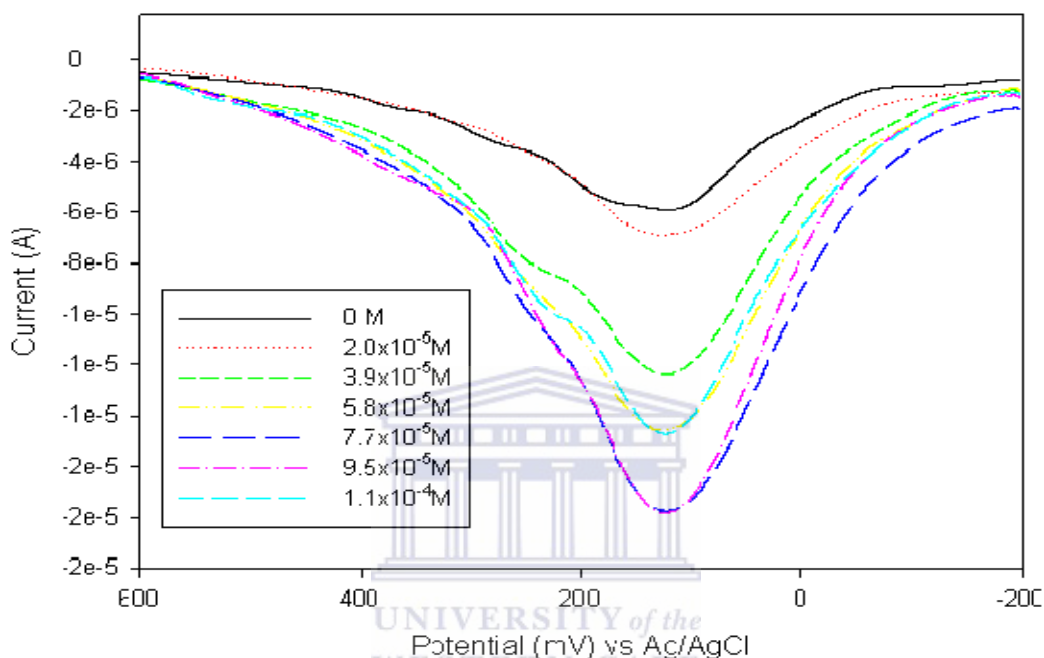


Figure 7.6: Differential pulse voltammograms of Pt/PDMA-ASA chemosensor responses to 0, 10, 20, 30, 40, 50 and 60 μL of 4-Chlorophenol (0.002 M) in 1 M HCl (1 mL) at a scan rate of 10 mV/s and a frequency of 5 Hz

The same phenomenon was seen when 4-CP was added to the Pt/PDMA-PSA modified electrode (**Figure 7.7**) as when Ph was added to Pt/PDMA-PSA. There was a negative shift in potential (+95 mV) with the increase in 4-CP concentration, confirming catalytic reactions taking place. A steady increase in current was also observed with an increase in 4-CP addition, which suggested the oxidation of 4-CP into its products. A decrease of current with increased 4-CP concentration was also observed at about +290 mV, which was attributed by the to the less conducting pernigraniline state of PDMA [9].

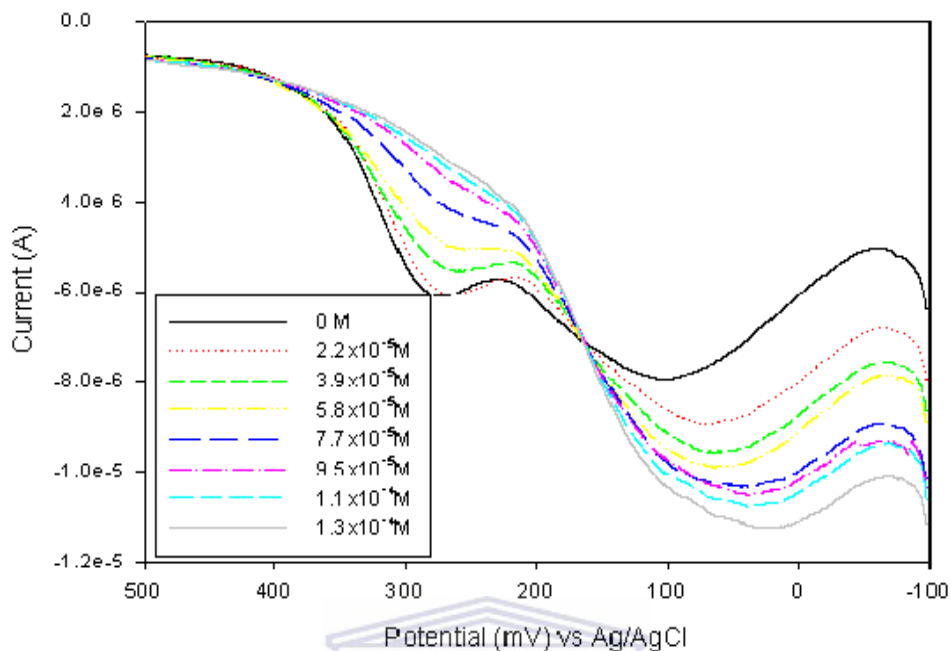


Figure 7.7: Differential pulse voltammograms of Pt/PDMA-PSA chemosensor responses to 0, 10, 20, 30, 40, 50, 60 and 70 μL of 4-Chlorophenol (0.002 M) in 1 M HCl (1 mL) at a scan rate of 10 mV/s and a frequency of 5 Hz

7.4.5 Electrochemical behaviour of 4-Nitrophenol (4-NP) at the Pt/PDMA-ASA and Pt/PDMA-PSA electrodes

The electrochemical behaviour of Pt/PDMA-ASA with 4-Nitrophenol can be seen in **Figure 7.8** using differential pulse voltammetry. An increase in current was seen for the first addition of 4-NP after which a decrease of current was noticed on subsequent additions as expected on the basis of literature reports. This decrease in current is normally observed when a non-conducting polyphenol (in this case poly 4-Nitrophenol) film formed on top of the conducting polymer electrode which hampered the flow of electron transfer. Therefore, a decrease of current was observed after the first addition of 4-Nitrophenol [11].

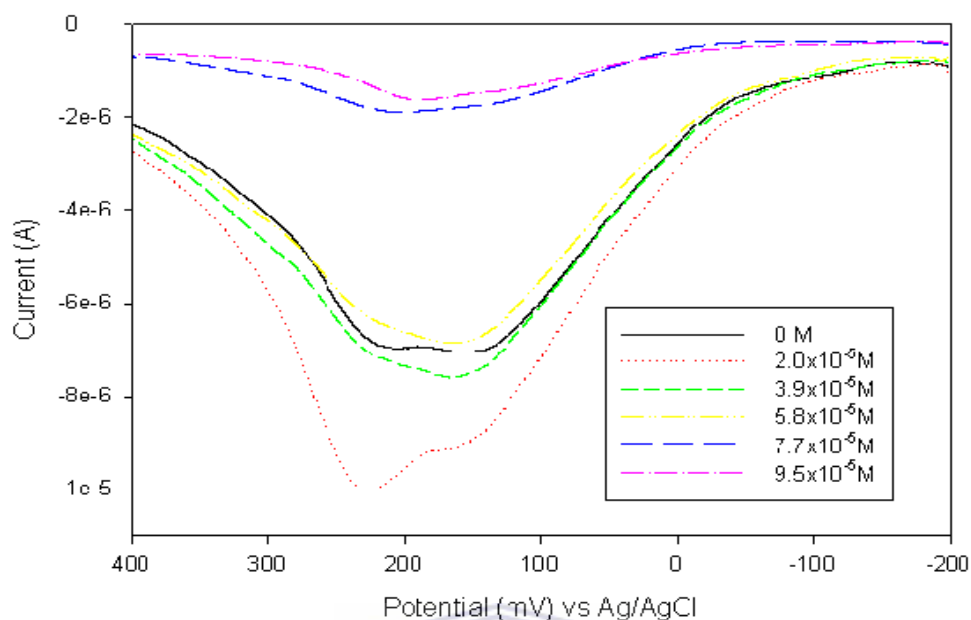


Figure 7.8: Differential pulse voltammograms of Pt/PDMA-ASA chemosensor responses to 0, 10, 20, 30, 40 and 50 μL of 4-Nitrophenol (0.002 M) in 1 M HCl (1 mL) at a scan rate of 10 mV/s and a frequency of 5 Hz

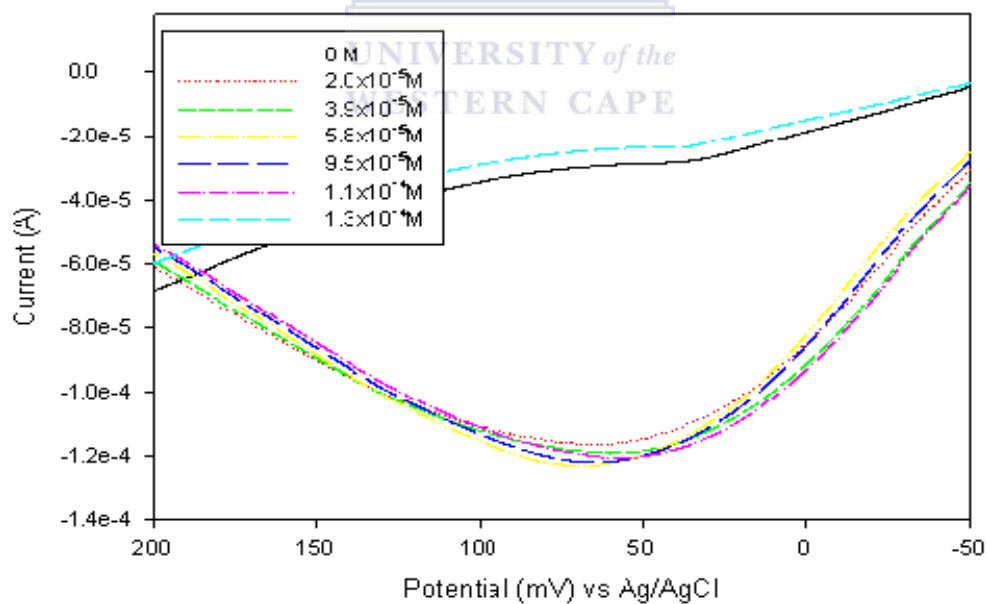


Figure 7.9: Square wave voltammograms of Pt/PDMA-PSA chemosensor responses to 0, 10, 20, 30, 50, 60 and 70 μL of 4-Nitrophenol (0.002 M) in 1 M HCl (1 mL) at a scan rate of 10 mV/s and a frequency of 5 Hz

Figure 7.9 represents the square wave voltammograms when different concentrations of 4-NP were added to a Pt/PDMA-PSA modified electrode in 1 M HCl. At first there was a huge increase in current suggesting oxidation of the 4-NP followed by a very small increase, whereby saturation was reached and then a huge decrease in current.

7.4.6 Calibration curves of the Pt/POMA-ASA and Pt/POMA-PSA chemosensors for Phenol (derivatives)

The response characteristics of the Pt/PDMA-ASA and Pt/PDMA-PSA chemosensors as a function of phenolic compounds were studied in this section.

The calibration curves obtained for the Pt/PDMA-ASA chemosensor for Ph, 4-CP and 4-NP are illustrated in **Figure 7.10**. The chemosensors was stabilised with the first additions of Ph, 4-CP and N-CP after which an increase in current was noticed at low concentrations. Leveling off of the current were observed at higher concentrations which may be a result of fouling of the chemosensor by the oxidation products [12].

An increase in current was observed when 2,4-DNP, 2,4-DMP and 4-C3MP were added to the Pt/PDMA-ASA electrode (**Figure 7.11**) until a plateau was reached at high concentrations. No significant trends were seen when 2,4 DNP, 2,4. DMP, PCP and 4C3MP and 2,6DN4MP were added to the Pt/PDMA-ASA chemosensor (**Figure 7.12**).

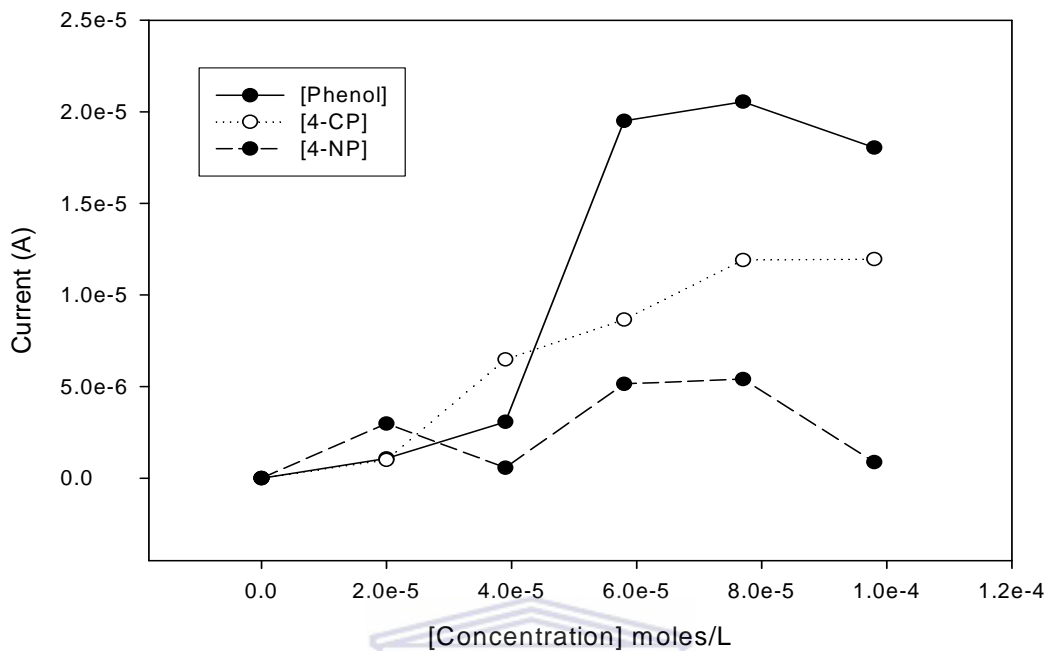


Figure 7.10: Calibration curves of the Pt/PDMA-ASA modified electrode for Ph, 4-CP and 4-NP

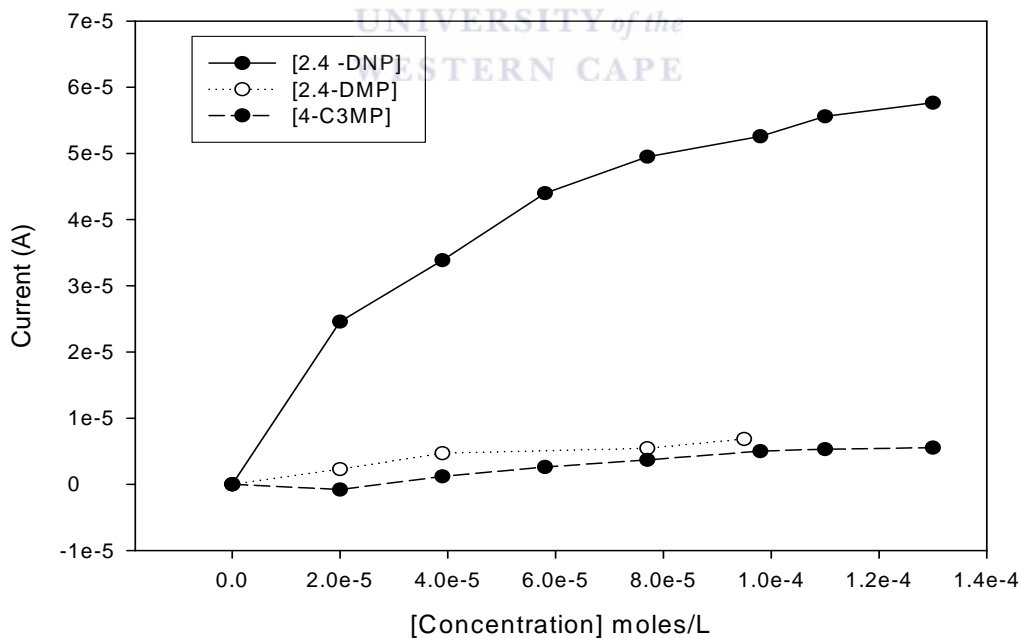


Figure 7.11: Calibration curves of the Pt/PDMA-ASA modified electrode for 2.4-DNP, 2.4DMP and 4-C3MP

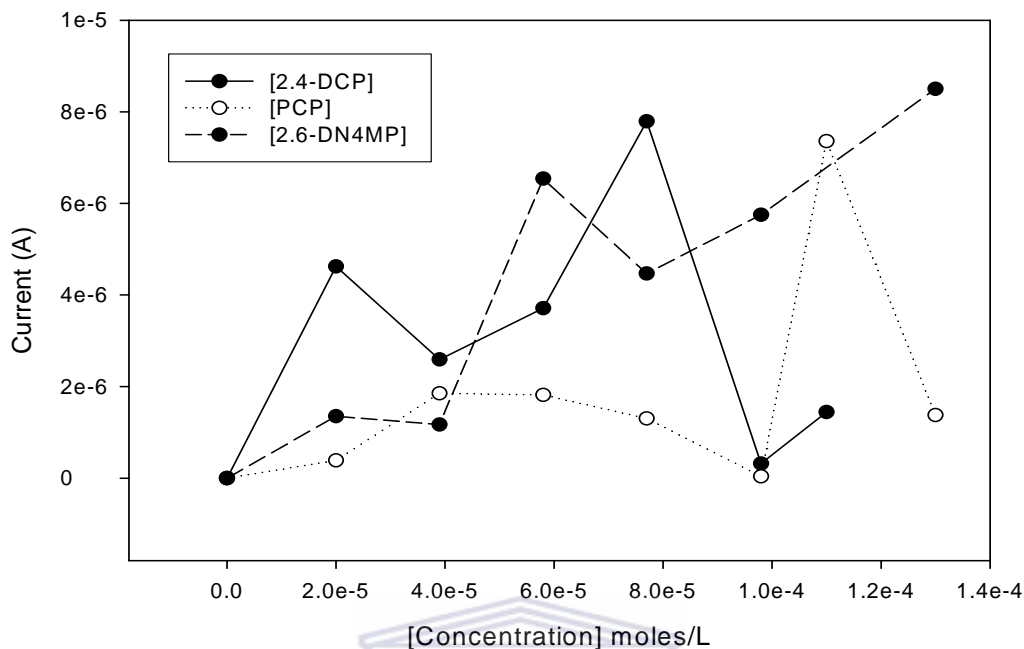


Figure 7.12: Calibration curves of the Pt/PDMA-ASA modified electrode for 2,4-DCP, PCP and 2,6-DN4MP

Figure 7.13 represents the Pt/PDMA-PSA chemosensor calibration curves in 1 M HCl when 4-CP, 2,4-DCP, 2,4-DNP, 2,4-DMP and 2,4,6-TCP were added to the electrochemical cell. An increase in current responses was detected at low concentration of the phenolic compounds. A maximum current was reached where the activity of the chemosensor is decreased at high concentrations of the phenolic compounds, which was probably due to the competition for active sites on the chemosensor surface [5].

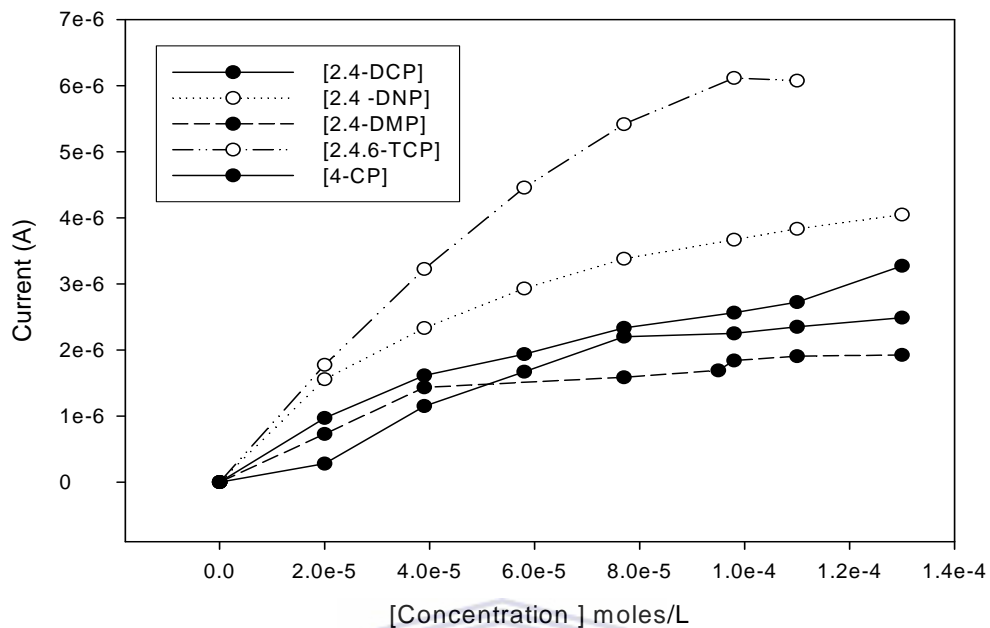


Figure 7.13: Calibration curves of the Pt/PDMA-PSA modified electrode for 4-CP, 2,4-DCP, 2,4-DNP, 2,4-DMP and 2,4,6-TCP

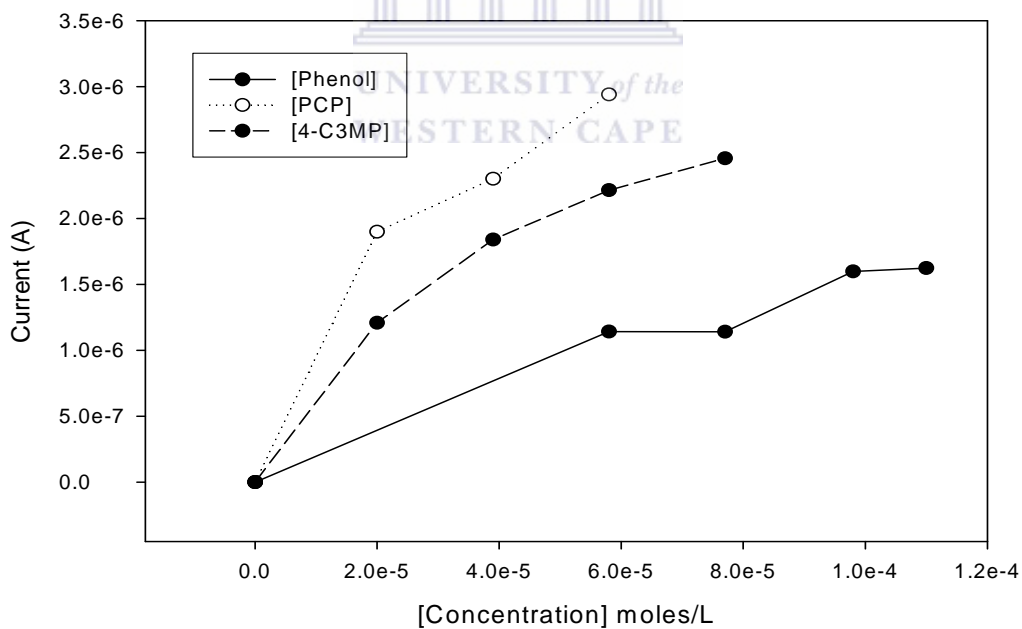


Figure 7.14: Calibration curves of the Pt/PDMA-PSA modified electrode for 2,4-DCP, PCP and 2,6-DN4MP

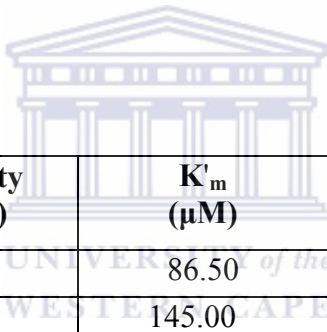
The calibration curves obtained for the Pt/PDMA-PSA chemosensor for Ph, PCP and 4-C3MP are shown in **Figure 7.14**. An increase in the current responses was noted as the concentrations of the analytes were increased. The curves increased to a maximum after which a linear curve was formed. These calibration curves showed that catalytic oxidation processes was taking place. The Pt/PDMA-PSA chemosensor exhibited good responses to all the tested phenolic compounds over a wide concentration range (**Appendix A: Table A5 and A6**).

7.3.7 Chemosensor Kinetic Parameters for Phenol (derivatives) detection

The kinetic parameters of the Pt/PDMA-PSA nanostructured polymer for phenolic compounds, since they have all the same trend, are displayed in **Table 7.1**. The calibration curves all displayed non-linear responses of current with phenolic compound concentration and was modelled according to the Michaelis-Menten paradigm [13-16]. The sensitivities, measured by the slope of the calibration curves, followed the order 2.4.6-TCP > PCP > 2.4-DNP > 2.6DN4MP > 2.4.6TCP > 4-CP > 2.4-DCP > 4-C3MP > Ph > 2.4-DMP. Thus indicating that the electron-withdrawing phenolic compounds are more soluble in the PDMA-PSA matrix than the electron donating phenolic compounds [15].

The Michaelis-Menten constant (K'_m) in this case predicts the ease with which an analyte interact with the polymer and followed the order 2.4-DMP > 4-CP > 2.4-DCP > 2.4.6-TCP > Ph > 2.4-DNP > 2.6-DN4MP > 4-C3MP > PCP. This means that 2.4-DMP stays longer in the solvent medium than PCP, with the result that the sensor requires a large amount of the 2.4-DMP to saturate its activity [13].

The apparent turnover rate constant (k'_{cat}) of the chemo-sensor is directly proportional to the total analyte concentration in the sensing nanostructured polymer and it therefore determines the maximum current, realizable from the sensor at saturation concentration of the analyte. The k'_{cat} followed the order 2.4.6-TCP > 2.4-DNP > 4-CP > PCP > 2.4-DCP > 2.6-DN4MP > 2.4-DMP > Ph > 4-C3MP, which suggests faster reaction rate and higher currents for Pt/PDMA-PSA as a chemosensor for 2.4.6-TCP compare to Pt/PDMA-PSA as a chemosensor for 4-C3MP. A high detection limit was observed for the Pt/PDMA-PSA electrode as a chemosensor for phenol (derivatives) at an estimated signal to noise (S/N) ratio of 3 [14].



Analyte	Sensitivity (mA/M)	K'_m (μ M)	k'_{cat} (nmol.cm ⁻² .s ⁻¹)	Detection Limit (M)
Phenol	13.65	86.50	0.691	2.089 x 10 ⁻³
4-CP	22.54	145.00	1.916	1.434 x 10 ⁻²
4-NP	nd	nd	nd	nd
2.4-DCP	20.50	121.50	1.458	2.526 x 10 ⁻³
2.4.6-TCP	63.00	97.05	3.58	7.152 x 10 ⁻⁵
2.4-DNP	42.00	80.43	1.978	6.347 x 10 ⁻⁴
2.4-DMP	6.00	320.80	1.127	3.708 x 10 ⁻³
PCP	48.00	6.13	1.721	6.089 x 10 ⁻⁴
4-C3MP	17.70	18.3	0.1897	1.045 x 10 ⁻³
2.6-DN4MP	31.00	79.19	1.437	7.89 x 10 ⁻⁴

nd = not determined

Table 7.1: Kinetic parameters of the Pt/PDMA-PSA chemosensor for various phenol (derivatives)

The voltammetric responses obtained by the Pt/PDMA-PSA modified electrode obtained in the presence of phenolic compounds is proposed to be representative of the catalytic current results from the redox mediation reactions of the PDMA-PSA conducting polymer and the oxidation of the phenolic compounds as schematically represented in **Figure 7.15**.

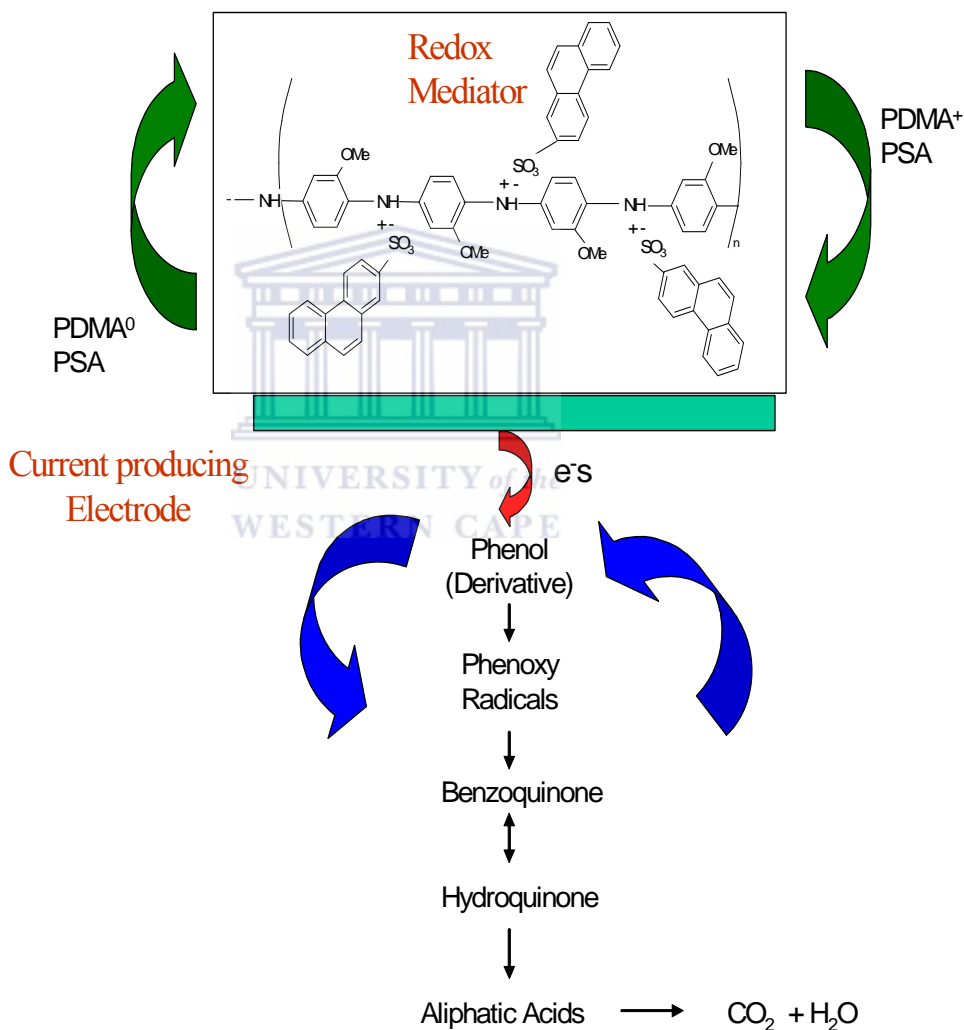


Figure 7.15: Reaction scheme outlining the role of the PDMA-PSA as a redox mediator in the oxidation of phenol for the Pt/PDMA-PSA chemosensor

The diagram shows that the phenol is firstly oxidised to phenoxy radicals, which is further converted to benzoquinone and hydroquinone, as the reaction proceeds the aliphatic acids were formed and then eventually converted to carbon dioxide and water [17].

7.4 Conclusions

The PDMA-ASA and PDMA-PSA nanostructured conducting polymers immobilised on Pt electrodes exhibited redox properties in aqueous solutions with 1 M HCl as the supporting electrolyte. The PDMA-ASA and PDMA-PSA conducting polymers in the Pt/PDMA-ASA and Pt/PDMA/PSA electrodes as a chemosensor system for phenol (derivatives) suggested that they were capable of mediating the electron-transfer between the electrode and the phenolic compounds.

When the phenolic compounds were added to the Pt/PDMA-ASA and Pt/PDMA-PSA modified electrodes system an increase in current, with addition of phenolic compounds was detected (for most of the compounds) until the polymer modified system was completely saturated, after which a decreased in current were observed. These results confirmed that electro-catalytic reactions were taking place at the polymer electrode surface. The Pt/PDMA-PSA/Phenol (derivative) chemo-sensor system was also seen to display low over potential between +60.00 and -60.00 mV, where less interference of co-oxidation and co-reduction of compounds are normally experienced.

The nature of the substituent (electron-donating or electron-withdrawing) attached to the phenol influenced both the transfer abilities of the electrons and the solubility into the polymer film has a major impact on the chemosensor sensitivities and detection limits.

Voltammetric responses obtained by the Pt/PDMA-PSA modified electrode obtained in the presence of phenolic compounds is proposed to be representative of the catalytic current resulting from the redox mediation reactions of the PDMA-PSA conducting polymer, where the phenol (derivatives) is firstly oxidised to phenoxy radicals, which is further converted to benzoquinone and hydroquinone, as the reaction proceeds the aliphatic acids were formed and then eventually converted to carbon dioxide and water.



7.5 References

- [1] P. Zanello, *Inorganic Electrochemistry. Theory, Practice and Application*
Cambridge, UK: The Royal Society of Chemistry (2003)
- [2] E. I. Iwuoha, D. S. de Villaverde, N. P. Garcia, M. R. Smyth and J. M. Pingarron,
Biosens. and Bioelectr. 12 (1997) 749-761
- [3] N. G. R. Mathebe, A. Morrin and E. I. Iwuoha, *Talanta* 64 (2004) 115-12
- [4] S. Brahim, A. M. Wilson, D. Narinesingh, E. Iwuoha and A. Guiseppi-Elle,
Microchim. Acta, 143 (2003) 123-137
- [5] T. Mafatle and T. Nyokong, *Anal. Chim. Acta*, 354 (1997) 307 – 314
- [6] K. I. Ozoemena and T. Nyokong, *Electrochim. Acta*, 51 (2006) 5131 – 5136
- [7] P. N. Mashazi, K. I. Ozoemena, D. M. Maree and T. Nyokong, *Electrochim. Acta*, 51
(2006) 3489 – 3494
- [8] A. Morrin, R. M. Moutloali, A. J. Killard, M. R. Smith, J. Darkwa and E. I. Iwuoha,
Talanta 64 (2004) 30
- [9] S-S. Chen, T-C. Wen and A. Gopalan, *Synth. Met.*, 132 (2003) 133 - 143
- [10] M.S. Ureta-Zañartu, P. Bustos, C. Berrios, M. C. Diez, M. L. Mora and C. Gutiérrez,
Electrochim. Acta, 47 (2002) 2399 – 2406
- [11] M. Aránzazu Heras, S. Lupu, L. Pigani, C. Pirvu, R. Seeber, F. Terzi, C. Zanardi;
Electrochim. Acta 50 (2005) 1685 – 1691

- [12] J. Wang and M.S. Lin, *Anal. Chem.*, 61 (1989) 2809
- [13] I. E. Iwuoha, L. Ingrid, M. Edna and Ó. F. Ciárin, *Anal. Chim. Acta*, 69 (1997) 1674
- [14] M. A. Kim and W-Y. Lee, *Anal. Chim. Acta*, 479 (2003) 143 – 150
- [15] Z. Wen and T. Kang, *Talanta* 62 (2004) 351
- [16] E. I. Iwuoha, A. R. Williams-Dottin, L. A. Hall, A. Morrin, G. R. Mathebe, M. R. Smyth and A. Killard, *Pure Appl. Chem.*, 76 (2004) 789 – 799
- [17] M. A. Maluleke, *Electromembrane reactors for the decomposition of organic pollutants in potable and wastewaters*, Unpublished PhD. Thesis, University of the Western Cape, RSA (2003)



Chapter 8

General discussions, conclusions and recommendations

8.1 Introduction

This study has been directed towards the development of a chemical sensor for the detection of EPA priority phenols using conducting, electro-active nanostructured polyanilines.

The aim of the study was to see whether aniline and its derivatives (*ortho*-methoxyaniline and 2,5 dimethoxyaniline) when polymerised in the presence of bulky dopants (Anthracene sulfonic acid (ASA) and Phenanthrene sulfonic acid (PSA)), will constitute in conducting, electro-active nanostructured polymers, which will then be used as electro-catalysts for the oxidative detection of phenol and its derivatives.

This chapter deals with a summary of the discussion and conclusions of the results presented in the study and make further recommendations for phenol chemical sensor research.

The approach taken involved the preparation of dopants and conducting nanostructures polyanilines (8.2); the characterisation of the dopants and the conducting polyaniline nanomaterials (8.3); the electro-catalytic and redox mediator effects of PANI-ASA and PANI-PSA modified Pt electrodes as phenol (and phenol derivatives) sensors (8.4); the electro-catalytic and redox mediator effects of POMA-ASA and POMA-PSA modified Pt electrodes as phenol (and phenol derivatives) sensors (8.5); the electro-catalytic and

redox mediator effects of PDMA-ASA and PDMA-PSA modified Pt electrodes as phenol (and phenol derivatives) sensors (8.6); the comparison of the polymers as redox mediators for phenol (and phenol derivatives) sensors (8.7); recommendation for further study (8.8) and output from the thesis (8.9) which includes: contribution at conferences (8.9.1), papers published (8.9.2) and papers prepared for publication (8.9.3).

8.2 The preparation of dopants and conducting nanostructured polyanilines

The purpose of doping the polyaniline (derivatives) (Chapter 3) was to promote the compatibility between the conducting polymer and the solvent as a result of the polar substituents and to increase the surface area when immobilized on an electrode, which will then increase the catalytic efficiency. Large, bulky protonic acid dopants were employed to force the insoluble conducting polymer backbone to the inside of the molecule and the soluble dopants sticking out into the solvents making the insoluble conducting polymer more soluble.

Improving the solubility and increasing the surface area with doping the conducting polymers with large, bulky dopants was effective. SEM micrographs showed different nanostructured morphologies for the polymers, which includes: nanotubes or nanofibres for PANI/PSA and PDMA/PSA and nanosized micelles and disc-like structures for POMA/PSA.

8.3 The characterisation of the dopants and the conducting polyaniline nanomaterials

The conducting polyanilines were characterized (**Chapter 4**) using: FT-IR Spectroscopy, UV/vis Spectroscopy, Scanning Electron Microscopy (SEM) and Electrochemical Spectroscopy including Cyclic Voltammetry. It was concluded that nanostructured polyaniline (PANI), poly(*ortho*-methoxyaniline) (POMA) and poly(2,5 dimethoxyaniline) (PDMA) doped with anthracene sulfonic acid (ASA) and phenanthrene sulfonic acid (PSA) can be synthesised chemically.

All polymers studied exhibited quinoid and benzoid bands typically of polyaniline FTIR-spectra which confirmed the polymers were formed. The presence of the sulfonate functionality suggested that the ASA and PSA groups were incorporated into the polymer backbones.

Furthermore, UV-Vis bands and shifts also showed that ASA and PSA were incorporated into the polymer backbones.

SEM micrographs showed different nanostructured morphologies for the polymers, which includes: nanotubes or nanofibres of PANI-ASA and PANI-PSA with diameters between 50 – 100 nm, nanomicelles and nanosheets of POMA-ASA and POMA-PSA respectively, with radii in the 100 to 300 nm range, nanowires of PDMA-ASA with diameter between 200 – 300 nm and nanowires of PDMA-PSA with observed diameters between 50 and 100 nm.

Cyclic voltammetric characterisation of the polymer pastes showed distinctive redox peaks, which prove that the polymer films on the Pt electrode were electro-active and conductive and exhibit reversible electrochemistry. Hence, the polymers polyaniline

(PANI), poly(*ortho*-methoxyaniline) (POMA) and poly(2,5 dimethoxyaniline) (PDMA) doped with anthracene sulfonic acid (ASA) and phenanthrene sulfonic acid (PSA) were nanostructured, electro-active and conductive.

8.4 The electro-catalytic and redox mediator effects of PANI-ASA and PANI-PSA modified Pt electrodes as phenol (and phenol derivatives) sensors

The catalytic effect that the conductive, electro-active nanostructured polymers (PANI-ASA and PANI-PSA) has as redox mediators when immobilized on a Pt electrode for the oxidation of phenol and its derivatives using Differential Pulse Voltammetry (DPV), Square Wave Voltammetry (SWV) and Cyclic Voltammetry (CV) were investigated (**Chapter 5**).

The starting potentials for the polymer modified electrodes were seen to be relatively low compared to conventional direct electrochemical detection.

The Pt/PANI-ASA and Pt/PANI-PSA modified electrodes were seen to exhibit redox properties in aqueous solution with 1 M HCl as the supporting electrolyte. Hence, the PANI-ASA and PANI-PSA nanostructured conducting polymers adhered on the Pt-electrodes were electro-active and that charge propagation was taking place along the polymer chain.

However, the performances of PANI-ASA nanostructured conducting polymer as transfer mediators in the chemosensor for phenol (derivatives) system suggested that they were incapable of either donating electrons to, or accepting electrons from the phenol and oxidation products.

On the other hand, it appears that the Pt/PANI-PSA chemosensor system involving PANI-PSA as an electron mediator is more sensitive than its PANI-ASA counterpart for

certain phenolic compounds. The Pt/PANI-PSA electrode was seen to electro-catalytically catalyse the oxidation of Ph, 2,4-DCP, PCP and 4-C3MP.

8.5 The electro-catalytic and redox mediator effects of POMA-ASA and POMA-PSA modified Pt electrodes as phenol (and phenol derivatives) sensors

The catalytic effect that the conductive, electro-active nanostructured polymers (POMA-ASA and POMA-PSA) have as electron shuttles when immobilized on a Pt electrode for the oxidation of phenol and its derivatives using electrochemical means were undertaken (**Chapter 6**).

The Pt/POMA-ASA and Pt/POMA-PSA modified electrodes both exhibited redox properties in aqueous solutions with 1 M HCl as the supporting electrolyte. The nature of the substituent attached to the phenol influenced both the transfer abilities of the electrons and the solubility into the polymer film, which has a major impact on the potential of the modified electrode.

The POMA-ASA and POMA-PSA conducting polymers performances as redox electron transfer mediators in the Pt/POMA-ASA and Pt/POMA/PSA phenol chemosensor system suggested that they were capable of either donating or accepting electrons from the phenol. However, after the formation of the phenolic radicals an insulating film formed, which gradually prevented movement of electrons with increasing concentration of the phenolic compound and results in the passivation of the electrode surface. It is likely that these species remain strongly adsorbed on, or even trapped inside the polymer films. Hence, a reverse chemosensor was proposed for the detection of phenolic compounds.

8.6 The electro-catalytic and redox mediator effects of PDMA-ASA and PDMA-PSA modified Pt electrodes as phenol (and phenol derivatives) sensors

The catalytic effect that the conductive, electro-active polyanilines (PDMA-ASA and PDMA-PSA) have as electron mediator when immobilised on a Pt electrode for the oxidation of phenol and its derivatives using electrochemical means were investigated (**Chapter 7**).

The PDMA-ASA and PDMA-PSA nanostructured conducting polymers immobilised on Pt electrodes exhibited redox properties in aqueous solutions with 1 M HCl as the supporting electrolyte. The PDMA-ASA and PDMA-PSA conducting polymers in the Pt/PDMA-ASA and Pt/PDMA/PSA phenol (derivatives) chemosensor system suggested that they were capable of mediating the electron-transfer between the electrode and the phenolic compounds.

When the phenolic compounds were added to the Pt/PDMA-ASA and Pt/PDMA/PSA modified electrodes system an increased in current with addition of phenolic compounds was detected (for most of the compounds) until the polymer modified system was completely saturated, after which a decrease in current was observed. These results confirmed that electro-catalytic reactions were taking place at the polymer electrode surface. The Pt/PDMA-PSA phenol (derivatives) chemosensor system was also seen to display low over potential between +60.00 and -60.00 mV (vs Ag/AgCl), where less interference of co-oxidation and co-reduction of compounds are normally experienced.

The nature of the substituent (electron-donating or electron-withdrawing) attached to the phenol influenced both the transfer abilities of the electrons and the solubility into the polymer film has a major impact on the chemosensor sensitivities and detection limits.

Voltammetric responses obtained by the Pt/PDMA-PSA modified electrode obtained in the presence of phenolic compounds is proposed to be representative of the catalytic current results from the redox mediation reactions of the PDMA-PSA conducting polymer, where the phenol (derivatives) is firstly oxidised to phenoxy radicals, which is further converted to benzoquinone and hydroquinone, as the reaction proceeds the aliphatic acids were formed and then eventually converted to carbon dioxide and water. Hence, the Pt/PDMA-PSA chemosensor was successfully applied for the detection of phenolic compounds.

8.7 The comparison of the polymers as redox mediators for phenol (and phenol derivatives) sensors

All the Pt conducting, electro-catalytic nanostructured modified electrodes were seen to exhibit redox properties in aqueous solution with 1 M HCl as the supporting electrolyte. The Pt/conducting, electro-catalytic, nanostructured polymer as electrochemical chemosensor for phenol (derivatives) system was also seen to display lower over potential compared to conventional direct electrochemical detection.

The performances of PANI-ASA nanostructured conducting polymers as transfer mediators in the chemosensor for phenol (derivatives) system suggested that they were incapable of either donating electrons to, or accepting electrons from the phenol and oxidation products. However, it appears that the Pt/PANI-PSA chemosensor system involving PANI-PSA as an electron mediator is more sensitive than its PANI-ASA counterpart for certain phenolic compounds.

The POMA-ASA and POMA-PSA conducting polymers performances as redox electron transfer mediators in the Pt electrodes as chemosensor system suggested that they were capable of either donating or accepting electrons from the phenol.

However, after the formation of the phenolic radicals an insulating film formed, which gradually prevents movement of electrons with increasing phenolic compound concentration and results in the passivation of the electrode surface. Hence, a reverse chemosensor was proposed for the detection of phenolic compounds.

The PDMA-ASA and PDMA-PSA conducting polymers in the Pt electrodes as phenol (derivatives) chemosensor system suggested that they were also capable of mediating the electron-transfer between the electrode and the phenolic compounds.

When the phenolic compounds were added to the modified electrodes systems an increase in current with addition of phenolic compounds was detected (for most of the compounds) until the polymer modified system was completely saturated, after which a decrease in current were observed. The Pt/PDMA-PSA chemosensor was successfully applied for the detection of phenolic compounds.

These results showed that the rate of electron transferred (PDMA > POMA > PANI), solubility and chemical structure (methoxy groups in POMA and PDMA) played significant roles in the construction of the electrochemical sensor.

8.8 Recommendations for future work

The following aspects of the development of a chemical sensor for the detection of EPA priority phenols using conducting, electro-active, nanostructured polyaniline and its derivatives need further investigation:

- ❖ More experimental work needs to be done on optimisation of the Pt/polymer for phenol (derivatives) chemosensor. That includes: using different ratios of polymer and dopants, using different pH's and different temperatures.
- ❖ How long is the Pt/polymer phenol (derivatives) chemosensor stable?
- ❖ What are the interferences and selectivities of other compounds on the potential of the Pt/polymer phenol (derivatives) chemosensor?

8.9 Output from this thesis

8.9.1 Contributions at conferences

- ❖ **M.J. Klink**, V.S. Somerset, M. Sekota, P.G.L. Baker, and E.I. Iwuoha. (2005). Preparation and spectroelectro-chemical reactivities of novel polyaniline nanotubes. Paper presented at the 5th International Kenya Chemical Society Conference, Kenyatta University, 22 – 26 August 2005, Nairobi, Kenya.
- ❖ **M.J. Klink**, V. Somerset, P. Baker, M. Sekota and E.I. Iwuoha. (2005). Spectroelectrochemical Reactivities Of Novel Polyaniline Nanotube Pesticide Biosensors. Paper presented at the 2nd International Workshop on Biosensors for Food Safety and Environmental Monitoring, Université Hassan II-Mohammedia, Faculté des Sciences et Techniques, 10 – 12 November 2005, Agadir, Morocco.

- ❖ **M.J. Klink**, V.S. Somerset, S.E. Mavundla, M. Sekota, P. Baker, E. Iwuoha. Electrochemical Properties of Novel Polyaniline Nanotubes and Nanomicelles. Paper presented at the East and Southern Africa Environmental Chemistry Workshop (ESAECW) and the Sixth Theoretical Chemistry Workshop in Africa (TCWA); University of Namibia, 5 – 9 December 2005, Windhoek, Namibia.
- ❖ **M.J.Klink**, V.S.Somerset, I. M. Michira, M.Sekota, R.O. Akinyeye, A. Al-Ahmed, P.Baker, E.Iwuoha. Conductive polymers as mediator for phenol and derivative detection. Paper presented at the South African Chemical Institute (SACI); University of Kwazulu-Natal, 4 – 8 December 2006, Durban, South Africa.



8.9.2 *Papers published*

- ❖ Polyaniline-mercaptobenzothiazole biosensor for organophosphate and carbamate pesticides. Vernon S. Somerset , **Michael J. Klink**, Mantoa M. C. Sekota, Priscilla G.L. Baker and Emmanuel I. Iwuoha, *Analytical Letters* 39, 1 - 16 (2006)
- ❖ Electrochemical and Spectroscopic Properties of Fly Ash-Polyaniline Matrix Nanorod Composites. Emmanuel I. Iwuoha, Siphon E Mavundla, Vernon S Somerset, Leslie F Petrik, **Michael J Klink**, Mantoa Sekota and Priscilla Baker *Microchimica Acta* 155, 453-458 (2006)
- ❖ Acetylcholinesterase-polyaniline biosensor investigation of organophosphate pesticides in selected organic solvents. Vernon S. Somerset , **Michael J. Klink**, Mantoa M. C. Sekota, Priscilla G.L. Baker and Emmanuel I. Iwuoha, *J. Env. Science & Health: Part B* 42:3, 297-304 16 (2006)

8.9.3 *Papers prepared for publication*

- ❖ *Electrochemical Properties of Novel Polyaniline Nanotubes and Nanomicelles.*
M.J.Klink, V.S.Somerset, S.E.Mavundla, M.Sekota, P.Baker, E.Iwuoha
- ❖ *Electrochemical Properties and Characterization of Novel Poly(2,5 dimethoxyaniline) Nanotubes.* M.J. Klink, M. Sekota, V.S. Somerset, I.N. Michira, P. Baker, E. Iwuoha
- ❖ *Novel Phenol (derivative) Sensor based on Poly (2,5 dimethoxyaniline)-Phenanthrene Sulphonic Acid (PDMA-PSA) Nanostructured Conducting Polymer as a Redox Mediator.* M.J. Klink, V.S. Somerset, R. Akinyeye, I.N. Michira, A. Al-Ahmed, M. Sekota, P. Baker, E. Iwuoha
- ❖ *The electro-catalytic and redox mediator effects of nanostructured PDMA-ASA and PDMA-PSA modified electrodes as phenol and phenol derivatives sensors.*
M.J. Klink, V.S. Somerset, R. Akinyeye, I.N. Michira, A. Al-Ahmed, M. Sekota, P. Baker, E. Iwuoha
- ❖ *The electro-catalytic and redox mediator effects of nanostructured POMA-ASA and POMA-PSA modified electrodes as phenol and phenol derivatives sensors.*
M.J. Klink, V.S. Somerset, R. Akinyeye, I.N. Michira, A. Al-Ahmed, M. Sekota, P. Baker, E. Iwuoha

Appendix A

Concentration (M)	Phenol	4-CP	4-NP	2,4-DCP	2,4-DNP
0.0000	0.0000	0.0000		0.0000	0.0000
2.0000e-5		0.0000	0.0000	1.8900e-6	0.0000
3.9000e-5	1.3450e-7	2.5610e-6	3.6187e-6	3.5800e-6	0.0000
5.8000e-5		-1.1390e-6	3.6252e-6	3.5490e-6	
7.7000e-5	1.8700e-7	1.1003e-6	3.6506e-6	3.6970e-6	-1.8500e-8
9.8000e-5		-1.5100e-6	3.6784e-6	3.5530e-6	
1.1000e-4	2.1100e-7			3.5720e-6	3.6000e-9
1.3000e-4				3.6690e-6	-1.2000e-8
Concentration (M)	2,4-DMP	2,4,6-TCP	PCP	4-C3MP	2,6-DN4MP
0.0000		0.0000	0.0000		0.0000
2.0000e-5	0.0000	2.3720e-7		0.0000	-6.4580e-6
3.9000e-5	-5.0400e-8	2.8680e-7	5.1340e-6	-1.9300e-8	-2.5270e-6
5.8000e-5	-5.1200e-8	2.8470e-7		-6.0500e-8	-7.6910e-6
7.7000e-5	-6.2200e-8	3.0690e-7	4.7220e-6	-1.0570e-7	-6.9080e-6
9.8000e-5	-1.8750e-7	3.4440e-7		-5.5100e-8	-1.0470e-6
1.1000e-4		3.2700e-7	3.9970e-6	-6.5600e-8	
1.3000e-4			4.8660e-6		

Table A1: Catalytic currents (A) versus concentrations (M) of the Pt/PANI-ASA modified electrode for phenol (derivatives)

Concentration	phenol	4-CP	4-NP	2,4-DCP	2,4-DNP
0.0000	0.0000	0.0000	0.0000	0.0000	0.0000
2.0000e-5	2.5000e-7	-1.6000e-7	-1.4698e-5	-5.0100e-8	-1.9800e-6
3.9000e-5	-1.0300e-6	-9.3000e-7	-1.2418e-5	-8.3900e-8	3.0900e-6
5.8000e-5	-1.1000e-6	-3.2000e-7	-1.2258e-5	-1.1280e-7	-1.9800e-6
7.7000e-5	-9.0000e-7	1.6000e-7	-1.2448e-5	-1.0990e-7	-2.2000e-6
9.8000e-5	-1.9000e-6	6.9000e-7	-1.2578e-5	-1.3490e-7	-2.2000e-6
1.1000e-4	-1.7900e-6	-6.0000e-8	-1.2758e-5	-1.4510e-7	-2.6400e-6
1.3000e-4	-1.6900e-6	4.8000e-7	-1.3061e-5	-1.5910e-7	-2.7200e-6
Concentration	2,4-DMP	2,4,6-TCP	PCP	4-C3MP	2,6-DN4MP
0.0000	0.0000	0.0000	0.0000	0.0000	0.0000
2.0000e-5	2.4000e-7	-1.7000e-7	-2.1200e-7	-1.7000e-7	-7.0000e-8
3.9000e-5	8.0000e-7	-3.3000e-7	-2.8300e-7	-2.7300e-7	-1.8500e-7
5.8000e-5		-2.1000e-7	-3.4100e-7	-3.6600e-7	-2.6900e-8
7.7000e-5	1.6000e-7	-4.9000e-7	-4.1900e-7	-4.4600e-7	-3.1800e-7
9.8000e-5	8.0000e-8	-1.3000e-7	-4.5700e-7	-5.1300e-7	-3.3000e-7
1.1000e-4	7.2000e-7	-3.7000e-7	-5.7300e-7	-5.5400e-7	-3.6600e-7
1.3000e-4	-5.7000e-7	-2.5000e-7		-6.4200e-7	-3.7500e-7

Table A2: Catalytic currents (A) versus concentrations (M) of the Pt/PANI-PSA modified electrode for phenol (derivatives)

Concentration	phenol	4-CP	4-NP	2.4-DCP	2.4-DNP
0.0000	0.0000	0.0000	0.0000	0.0000	0.0000
2.0000e-5	3.8700e-7	-2.0100e-7	-6.4000e-8	-2.4170e-8	-2.5000e-7
3.9000e-5	1.2300e-7	5.9200e-8	-1.8200e-7	-3.6100e-8	-1.6600e-7
5.8000e-5	7.6500e-7	1.0320e-6	-8.1900e-7	-4.1500e-8	6.0000e-9
7.7000e-5	8.7500e-7	1.5910e-6	-7.6300e-7	-4.3000e-8	-1.2300e-7
9.8000e-5	8.9590e-7	1.8530e-6	-1.0830e-6	-4.7000e-8	-3.7000e-8
1.1000e-4	9.2410e-7	1.9250e-6	-1.1920e-6	-5.1000e-8	4.3000e-8
1.3000e-4	9.0500e-7	2.0050e-6		-4.9500e-8	1.8300e-7
Concentration	2.4-DMP	2.4.6-TCP	PCP	4-C3MP	2.6-DN4MP
0.0000	0.0000	0.0000	0.0000	0.0000	0.0000
2.0000e-5	-1.0577e-6	-4.0000e-9	3.1100e-7	4.0000e-9	-2.9200e-7
3.9000e-5	-2.5600e-7	-2.1400e-8	4.2110e-6	1.2800e-7	-3.7400e-8
5.8000e-5	-2.3000e-7	-3.2900e-8	7.9100e-7	7.8000e-7	-3.8400e-7
7.7000e-5	-1.9000e-7	-4.0500e-8	1.0420e-6	2.0000e-8	-3.8400e-7
9.8000e-5	-1.3100e-7	-3.8500e-8	1.1320e-6	3.9100e-7	-3.7400e-7
1.1000e-4		-5.0200e-8	1.2670e-6	5.7600e-7	-3.5000e-7
1.3000e-4		-5.1400e-8	1.3740e-6	1.0720e-6	-3.0100e-7

Table A3: Catalytic currents (A) versus concentrations (M) of the Pt/POMA-ASA modified electrode for phenol (derivatives)

Concentration	phenol	4-CP	4-NP	2.4-DCP	2.4-DNP
0.0000	0.0000	0.0000	0.0000	0.0000	0.0000
2.0000e-5	1.0900e-6	2.1900e-6	9.8800e-7	1.2700e-6	1.4900e-6
3.9000e-5	1.8000e-6	-2.6700e-6	1.6470e-6	2.4100e-6	2.6090e-6
5.8000e-5	2.2500e-6	5.0000e-6	2.2180e-6	3.2330e-6	3.3630e-6
7.7000e-5	2.7300e-6	6.0490e-6	2.6320e-6	3.6990e-6	4.0160e-6
9.8000e-5	3.0620e-6	6.5960e-6	2.9480e-6	4.0370e-6	4.5450e-6
1.1000e-4	3.3830e-6	7.1130e-6	3.3182e-6	4.5440e-6	4.9960e-6
1.3000e-4	3.3670e-6	7.5720e-6	3.3540e-6	4.9320e-6	5.1710e-6
Concentration	2.4-DMP	2.4.6-TCP	PCP	4-C3MP	2.6-DN4MP
0.0000	0.0000	0.0000	0.0000	0.0000	0.0000
2.0000e-5	1.5500e-7	1.2480e-6	1.4800e-7	1.6600e-7	9.2100e-3
3.9000e-5	2.8900e-7	2.1100e-6	3.9700e-7	2.9800e-7	1.8710e-5
5.8000e-5		2.7220e-6	6.8100e-7	4.0700e-7	2.3490e-5
7.7000e-5	7.2100e-7	3.1510e-6	8.8500e-7	4.8500e-7	2.7690e-5
9.8000e-5	8.1100e-7	3.5390e-6	1.0670e-6	5.4500e-7	3.4120e-5
1.1000e-4	8.9100e-7	3.7710e-6	1.2040e-6	5.6900e-7	4.0430e-5
1.3000e-4	1.1470e-6	3.9720e-6	1.2750e-6	5.9900e-7	4.0820e-5

Table A4: Catalytic currents (A) versus concentrations (M) of the Pt/POMA-PSA modified electrode for phenol (derivatives)

Concentration	phenol	4-CP	4-NP	2,4-DCP	2,4-DNP
0.0000	0.0000	0.0000	0.0000	0.0000	0.0000
2.0000e-5	1.0760e-6	-9.8800e-7	-2.9840e-6	4.6240e-6	2.4580e-5
3.9000e-5	-3.0750e-6	-6.4770e-6	-5.6800e-7	-2.5900e-6	3.3860e-5
5.8000e-5	-1.9513e-5	-8.6570e-6	5.1480e-6	3.7090e-6	4.3980e-5
7.7000e-5	-2.0553e-5	-1.1907e-5	5.4050e-6	-7.7920e-6	4.9490e-5
9.8000e-5	-1.8054e-5	-1.1957e-5	8.7100e-7	3.2000e-7	5.2570e-5
1.1000e-4	-2.1353e-5	-8.8170e-6	3.1530e-6	-1.4400e-6	5.5590e-5
1.3000e-4	-2.2833e-5				5.7650e-5
Concentration	2,4-DMP	2,4,6-TCP	PCP	4-C3MP	2,6-DN4MP
0.0000	0.0000	0.0000	0.0000	0.0000	0.0000
2.0000e-5	-2.2900e-6	-1.6989e-5	3.8700e-7	-8.1000e-7	-1.3500e-6
3.9000e-5	-4.6900e-6	-1.5559e-5	1.8540e-6	1.1900e-6	1.1700e-6
5.8000e-5	-5.4400e-6	-1.0999e-5	-1.8160e-6	2.6100e-6	6.5400e-6
7.7000e-5	-6.8400e-6	-5.4800e-7	1.3031e-6	3.6900e-6	4.4700e-6
9.8000e-5	-8.5400e-6	-1.3259e-5	-3.8000e-8	5.0100e-6	5.7500e-6
1.1000e-4	-1.5440e-5	-13.0690e-4	-7.3570e-6	5.3000e-6	
1.3000e-4	-1.8320e-5		-1.3790e-6	5.5400e-6	8.5000e-6

Table A5: Catalytic currents (A) versus concentrations (M) of the Pt/PDMA-ASA modified electrode for phenol (derivatives)

Concentration	phenol	4-CP	4-NP	2,4-DCP	2,4-DNP
0.0000	0.0000	0.0000	0.0000	0.0000	0.0000
2.0000e-5	-4.3500e-6	-9.7100e-7	2.2000e-7	-2.8000e-7	-1.5580e-6
3.9000e-5	-7.7000e-7	-1.6140e-6	-8.8110e-5	-1.1500e-6	-2.3300e-6
5.8000e-5	-1.1420e-6	-1.9360e-6	-9.0310e-5	-1.6700e-6	-2.9300e-6
7.7000e-5	-1.1410e-6	-2.3330e-6	-9.0310e-5	-2.2000e-6	-3.3780e-6
9.8000e-5	-1.5980e-6	-2.5630e-6	-9.4710e-5	-2.2500e-6	-3.6680e-6
1.1000e-4	-1.6240e-6	-2.7230e-6	-9.3610e-5	-2.3500e-6	-3.8310e-6
1.3000e-4	-1.8120e-6	-3.2730e-6	-9.2210e-5	-2.4900e-6	-4.0460e-6
Concentration	2,4-DMP	2,4,6-TCP	PCP	4-C3MP	2,6-DN4MP
0.0000	0.0000	0.0000	0.0000	0.0000	0.0000
2.0000e-5	-7.2900e-7	-1.7740e-6	-1.8990e-6	1.8080e-6	-1.2090e-6
3.9000e-5	-1.4320e-6	-3.2240e-6	-2.3010e-6	1.6600e-6	-1.8390e-6
5.8000e-5	-1.5860e-6	-4.4540e-6	-2.9400e-6	8.5300e-7	-2.2140e-6
7.7000e-5	-1.6890e-6	-5.4140e-6	-1.8990e-6	6.4400e-7	-2.4550e-6
9.8000e-5	-1.8400e-6	-6.1140e-6	-1.9750e-6	4.1200e-7	-4.7100e-7
1.1000e-4	-1.9040e-6	-6.0740e-6	-2.1350e-6	3.2400e-7	-8.0600e-7
1.3000e-4	-1.9250e-6	-7.1640e-6	-2.1350e-6	3.7700e-7	-2.4290e-6

Table A6: Catalytic currents (A) versus concentrations (M) of the Pt/PDMA-PSA modified electrode for phenol (derivatives)



UNIVERSITY *of the*
WESTERN CAPE



UNIVERSITY *of the*
WESTERN CAPE